Investigation of some medicinal plant molecules as inhibitors against mycobacterial Flavin Dependent Thymidylate Synthase (Thy X) using computational and molecular approaches

A thesis submitted in partial fulfilment of the requirements for the degree of Doctor of Philosophy

By

Ms. Nilakshi Barua

Registration No: 005 of 2010

School of Science

Department of Molecular Biology and Biotechnology

Tezpur University

Tezpur- 784028, Assam, India

September, 2013

Abstract

The battle between humankind and *Mycobacterium tuberculosis*, the etiological agent of tuberculosis dates back to antiquity. Tuberculosis (TB) still remains a major international health problem which is likely to become even more alarming in the coming years due partly to TB deaths in HIV-infected patients and partly to the emergence of multidrug resistant strains of *Mycobacterium tuberculosis*. The World Health Organization (WHO) declared TB a global emergency in 1993. The first line drugs used against combating *Mycobacterium tuberculosis* includes isoniazid, rifampicin, ethambutol, pyrazinamide and streptomycin. The second line of antituberculosis chemotherapeutic agents comprises of fluoroquinolones, ethionamide, cycloserine, paraminosalicylic acid, capreomycin, kanamycin and amikacin. In view of the alarming global assessment of the disease in the context of the emerging threats from the phenomena of Multi Drug Resistance (MDR) and Extensive Drug Resistance (XDR) against the conventional first and second line of drugs, there is an urgent need for discovering/developing new antimycobacterial agents.

Plants have been the corner stone of medicinal therapies for thousands of years, and continue to be an essential part of health care throughout the world. In the nineteenth century, before the advent of the pharmaceutical industry, all medicinal preparations were derived directly from nature, mostly from plants. Drug researchers have shifted their focus towards synthetic drugs in the wake of development of synthetic chemistry during the 1970s and the 1980s, limiting plant derived drugs developed in this period. However, in the 1990s the renewed interest in phytochemistry encouraged the major pharmaceutical industries to start plant screening programme.

The systematic study of the mechanisms of a large number of natural products by means of traditional assay based methods is a costly and time-consuming process due to the difficulty in extraction, synthesis, and activity testing. Therefore, *in silico* virtual screening is expected to be an alternative

approach for low-cost and rapid analysis of the plant derived natural products and efficient search for their targets. Ligand-protein docking is a popular virtual screening technology in rational drug design which could be utilized to identify ligands as well as the potential protein targets and can be readily extended to study the structural and molecular mechanics of the binding between them.

Another most widely used virtual screening approach in rational drug design is Quantitative Structure Activity Relationship (QSAR) studies. QSAR is based on statistical analysis of the relationship between certain biological activities of a molecule against quantitative attributes of the structure of the molecule. The resultant statistical model of QSAR may be used to predict the antimycobacterial activity of a molecule, even before its synthesis, or to explore virtual modifications at the structural levels for enhanced antimycobacterial activity of an existing molecule by its quantitative attributes calculated from its structure.

In the present study the experiments were carried out using *M. smegmatis as a surrogate in vitro model* for the detection of compounds which are inhibitory to the growth of *Mycobacterium tuberculosis*. *M. smegmatis* offers technical benefits like shorter generation time and negligible risk to laboratory workers in comparison to pathogenic *M. tuberculosis*.

In the present work the *in silico* approach enabled the generation of a hypothesis about possible *drug-target* interactions implicating plant derived natural products and a potential target- the Thy X protein in *M. tuberculosis* using the *M. smegmatis* model system target. The absence of this enzyme in human makes it an important candidate for future drug target. The *thyX* encoded ThyX (EC 2.1.1.148) protein catalyzes the methylation of deoxyuridine 5'-monophosphate (dUMP) to deoxythymidine 5'- monophosphate (dTMP) in the *de novo* pathway of nucleotide biosynthesis. Subsequently for validation of the hypothesis, molecular and biochemical approaches were followed . In the first step, the *thy x* gene of *M. smegmatis* was cloned and expressed in an expression vector. In the second step, inhibition of the enzymatic activity of the purified target protein by selected natural products has been studied through enzmye assays.

The advent of nanotechnology has generated nanoparticles (1-100nm), as an alternative source for antibacterial agents. The high surface to volume ratio endows nanoparticles with an increased potential to interact with pathogens. Carbon nanotubes (CNTs) are promising candidates to alleviate the problem of resistance in various microbial strains. The preliminary study on the activity of few selected functionalized multiwall carbon nanotubes (MWCNTs) as well as few selected nanocomposites as potential antimycobacterial agents have also been studied, in this work.

Chapter I , the Introduction, presents the problem of tuberculosis caused by *M. tuberculosis*, the requirement of new drugs due to the emergence of resistance against the conventional chemotherapeutic agents and various new approaches to drug discovery. Traditional knowledge has been highlighted as a potent source of antimycobacterial secondary metabolites.

Chapter II includes the Review of Literature, and presents comprehensive review on the contemporary work on antimycobacterial drug discovery, various *in silico* approaches like QSAR and molecular docking. The chapter concludes with the review on the enzyme Flavin dependent tymidylate synthase (Thy X) .

Chapter III is on Materials and Methods which discusses in details the different techniques used in the study which include microbiological, *in silico*, biochemical and molecular methods methods used in carrying out the various experiments.

Chapter IV is on the Results and Discussions. The chapter presents the results in details along with a critical analysis of the results. The QSAR analysis identified the molecular descriptors of chalcone molecules endowing their antimycobacterial activity. The flavonoid molecules of the seven plants exhibiting antimycobacterial activity were selected and subjected to virtual screening using molecular docking against Thy X leading to the identification of hit 16 molecules. The Thy X enzyme of *M.smegmatis* ATCC 14468 has been cloned, overexpressed and purified in order to validate the in silico driven hypothesis

of binding of these 16 selected molecules to the enzyme. The antimycobacterial activity of nanocomposites has also been explored.

Chapter V is on the conclusions of the work and also proposes future works in which could be done in the presented work.

The final part of the thesis contains the references and appendices.

DECLARATION BY THE CANDIDATE

I hereby declare that the thesis **"Investigation of some medicinal plant molecules as inhibitors against mycobacterial Flavin Dependent Thymidylate Synthase using computational and molecular approaches."**, submitted to **Department of Molecular Biology and Biotechnology, Tezpur University**, Tezpur, Assam in partial fulfilment for the award of the degree of Doctor of Philosophy in Molecular Biology and Biotechnology and it has not been previously considered for the award of any degree, diploma, associateship, fellowship or any other similar title or recognition from any University, Institute or other organizations.

Nilakshi Barua

Date: 27/09/2013 (Nilakshi Barua)

Place: Tezpur, Assam Department of Molecular Biology and Biotechnology

Tezpur University

TEZPUR UNIVERSITY
(Central University established by an Act of Parliament)
NAPAAM, TEZPUR-784028
DISTRICT: SONITPUR ASSAM, INDIA

Dr. A.K. Buragohain, *PhD. DIC (London)*
Professor

Phone: +91-3712- 275403(O)
+91-9954115220(M)
Fax: +91- 3712- 267005 (O)
E-mail: alak@tezu.ernet.in

CERTIFICATE OF THE SUPERVISOR

This is to certify that the thesis entitled **"Investigation of some medicinal plant molecules as inhibitors against mycobacterial Flavin Dependent Thymidylate Synthase using computational and molecular approaches."** submitted to the School of Science, Tezpur University in partial fulfilment for the award of the degree of Doctor of Philosophy in **Molecular Biology and Biotechnology** is a record of research work carried out by **Ms.Nilakshi Barua** under my supervision and guidance.

All help received by her from various sources have been duly acknowledged.

No part of this thesis has been submitted elsewhere for award of any other degree.

A.K. Buragohain

Date: 27/09/2013

(Alak K. Buragohain)

Place: Tezpur, Assam

TEZPUR UNIVERSITY

(Central University established by an Act of Parliament)

NAPAAM, TEZPUR-784028

DISTRICT: SONITPUR ASSAM, INDIA

Phone: +91-3712- 267004(O), Fax: +91- 3712- 267005 (O) , Email: adm.tezu.ernet.in

---

Certificate of the External Examiner and ODEC

This is to certify that the thesis entitled **"Investigation of some medicinal plant molecules as inhibitors against mycobacterial Flavin Dependent Thymidylate Synthase using computational and molecular approaches."**, submitted to **Department of Molecular Biology and Biotechnology, School of Science ,Tezpur University** in partial fulfillment for the award of the degree of **Doctor of Philosophy** in **Molecular Biology and Biotechnology** has been examined by us

on_____ and found to be satisfactory.

The committee recommends for the award of the degree of Doctor of Philosophy.

Supervisor **External Examiner**

Date: **Date:**

ACKNOWLEDGEMENT

First and foremost, I would like to thank my supervisor, Professor A.K. Burgohain, Department of MBBT, for his guidance, support, inspiration and for all the invaluable advice and Experience he has provided throughout my PhD. I would also like to thank Professor R.C. Deka, Dept. of Chemical sciences , Dr. S.K. Ray and Dr. R. Doley, Department of MBBT, for the constant motivation and guidance.

I would also like to convey my sincere thanks to the Head of Department, Department of MBBT. I would like to offer my special thanks to all the faculty members of the Department of MBBT for their help and support.

Furthermore, I would like to acknowledge Dr. K.K. Hazarika , Dr. N.K. Bordoloi, Mr. P. Mudoi, Mr. S. Kakati and Mr. D. Deka for their constant support.

I would also like to convey my sincere gratitude to Dr. N. Chakraborty , NIPGR, Professor N. Karak, Department of Chemical sciences, Tezpur University and Dr. G. A. Ahmed , Department of Physics, Tezpur University for their constant help and support.

I would also like to thank Pubalee ba and Iftikar, Dept. of Chemical sciences ,for all the in silico analyses. I sincerely thank friend Juanli, Dept. of Mathematics her help in the statistical analyses.

My special thanks goes to my hard working seniors, lab mates and friends , Susmita ba, Lipika, Shubhendu, Bhaskar, Yutika, Sudhir da, Jyoti da, Deboshree ba, Rajeev, Atlanta, Abid, Sujata, Rocktotpal and Sanchita ba for helping me throughout the work and to learn the techniques and details of my work. I would also like to thank all the Research scholars of the Department of MBBT for their constant help and support.

I would like to extend my gratitude to Dept. of Chemical sciences, Dept. of Physics, Tezpur University, DRL (Defence research laboratory), Tezpur and NIPGR, New Delhi , for their support in the completion of the work.

I acknowledge the financial support received from Tezpur University, U.G.C., DST-FIST, DBT and CSIR.

My deepest gratitude goes to my family. My father and mother showed me the joy of intellectual pursuit since my childhood. I would like to thank my husband, Pritom for his dedication, love and persistent confidence in me.

Last but not the least I thank 'God' the Almighty, for bestowing me the courage to face life.

Nilakshi Barua

Contents

LIST of TABLES

List of Figures

Abbreviations

**	QSAR Descriptor
X	Electronegativity
°C	Degree Celsius
μ	Chemical Potential
μg	Micro gram
μM	Micro Molar
1D	One Dimensional
2D	Two Dimensional
3D	Three Dimensional
4D	Four Dimensional
Å	Angstrom
ADME-TOX	Absorption Distribution Metabolism Excretion-Toxicity
AIDS	Acquired immunodeficiency syndrome
ATCC	American Type Culture Collection
BCG	Bacille of Calmette and Guerin
bp	Base pair
C	Cytosine
C. dactylon	*Cynodon dactylon* L.
C. odorata	*Chromonaela odorata* L.
DFT	Density Functional Theory
DMEM	Dulbecco's Modified Eagle Media
DMSO	Dimethyl sulfoxide
DOTS	Directly Observed Therapy shortcourse
E	Total Energy
ETH	Ethambutol
FBS	Fetal Bovine Serum
FTIR	Fourier Transform Infra Red
G	Guanine
G. max	*Glycine max* L.
H	Hour
HCl	Hydrochloric Acid
HIV	Human immunodeficiency virus
HBPEA	Hyper Branched Polyester-amide
HPLC	High Pressure Liquid Chromatography
IC	Inhibitory Concentration
INH	Isoniazid
KBr	Potassium bromide
KCl	Potassium Choride
KH2PO4	Potassium Dihydrogen Phosphate
L. inermis	*Lawsonia inermis* L.

M	Molar
M. smegmatis	*Mycobacterium smegmatis*
M. *tuberculosis*	*Mycobacterium tuberculosis*
mA	Milli ampere
MALDI-TOF	Matrix-assisted laser desorption/ionization-time of flight
MDR-TB	Multi Drug Resistant Tuberculosis
mg	Milligram
MIC	Minimum Inhibitory Concentration
M. pudica	*Mimosa pudica L.*
ml	Milliliter
mM	Milli Molar
MR	Molar Refractivity
MS	Mass Spectroscopy
MTT	[3-(4,5-Dimethylthiazol-2-yl)-2,5-Diphenyltetrazolium Bromide]
MVD	Molegro Virtual Docker
N	Normality
N	No of electrons
η	Chemical Hardness
Na2HPO4	Disodium Hydrogen Phosphate
NADH	Nicotinamide Adenine Dinucleotide
NaOH	Sodium Hydroxide
nm	Nanometer
OADC	Oleic Acid – Albumin- Dextrose- Catalyst
PBS	Phosphate Buffer Saline
PDB	Protein Data Bank
POA	Pyrazinoic Acid
P. oreintalis	*Platycladus orientalis* L.
P. fulgens	*Potentilla fulgens* L.
PZA	Pyrazinamide
QSAR	Quantitative Structure Activity Relationship
RIF	Rifampicin
S	Svedberg Unit
SE	Standard Error
SEM	Scanning Electron Microscope
TB	Tuberculosis
TK	Traditional Knowledge
UV-VIS	Ultra Violet- Visible Spectrophotometry
WHO	World Health Organization
XDR-TB	Extensively Drug Resistant Tuberculosis
λ	Absorption
ω	Electrophilicity Index

Chapter I
Introduction

1.1 The *Mycobacterium complex*

The *M. tuberculosis* complex includes *M. tuberculosis*, *M. africanum*, *M. canettii*, *M. bovis*, and *M. microti*. These species are closely related sharing >99% identity at the nucleotide level for some loci but they differ significantly in morphology, biochemistry, host range, and disease patterns in experimental animals [1].

Although humans are reported to be the only natural hosts for *M. tuberculosis*, experimental animal models exist. In contrast, *M. bovis* exhibits a broad host range, producing tuberculosis in several mammals including human and cattle and has been a major cause of human tuberculosis prior to pasteurization of milk. Infection by *M. canettii* appears to be rare; however, in parts of Africa, *M. africanum* causes more cases of tuberculosis in comparison to *M. tuberculosis* [2]. The pathology and course of the diseases caused by *M. tuberculosis*, *M. bovis*, and *M. africanum* in humans are similar. *M. microti* infects voles and is avirulent in humans and mice. The attenuated *M. bovis* derived BCG and *M. microti* are potent live tuberculosis vaccines [3].

TB has claimed the maximum number of lives compared to any other disease [4]. Long generation time, fastidious growth requirements and high risk of contagion of *M. tuberculosis* present a tremendous challenge to the biomedical researchers. The genus *Mycobacterium* comprises of more than 150 species and most of the species are non-Pathogenic. However, *M. tuberculosis*, *M. leprae*, and *M. ulcerans*, the etiological agents of tuberculosis, leprosy, and Buruli ulcers, respectively are highly

successful pathogens which may be attributed to their ability to establish residence and proliferate inside host macrophages [5, 6].

1.2 *Mycobacterium smegmatis* as the model organism

M. smegmatis with a generation time of approximately 2 to 3 hours [7] was discovered by Lustgarten in 1884[8, 9]. It was first isolated from the smegma and forms colonies on solid media within 3 to 4 days [10]. It is an acid fast bacillus with an approximate size of 3.0 to 5.0μm. The relatively less risk and the ease of genetic manipulation with respect to *M. smegmatis*,makes it an attractive model for investigating different aspects of the virulent forms of *Mycobacterium* including *M. tuberculosis*. The similarity between *M. smegmatis and M. tuberculosis* in eliciting hypoxia response has been reported [11, 12, 13,14]. A comparative study of the *M. smegmatis* and *M. bovis* BCG models for the discovery of *M. tuberculosis* inhibitors indicated lesser sensitivity of the *M. smegmatis* model. However, it is pertinent to point out that the screening of bacteriostatic drug takes longer period of 14 days in *M. bovis* BCG model as compared to 4 days in *M. smegmatis* because of the slow growth rate of the former [14]. The efficacy of the *M. smegmatis* model as a screening organism for anti-tubercular drug can be appreciated from the identification of TMC207, a diarylquinoline, which is currently undergoing clinical trials as one of the potent anti-tubercular drugs using the high-throughput screen in *M. smegmatis* [15]. The assay of the sensitivity profiles of *M. smegmatis*, *M. phlei* and *M. fortuitum* as well as Multi Drug Resistant (MDR) clinical isolates of *M. tuberculosis* against anti-TB drugs isoniazid and rifampicin have also revealed that the profile of *M. smegmatis* is similar to that of the MDR *M. tuberculosis*. *M. smegmatis* exhibited 100% specificity and 78% sensitivity *vis-à-vis* the MDR *M. tuberculosis*. These results highlight the utility of *M. smegmatis* as an avirulent and fast growing organism for primary screening of anti-tubercular molecules in order to forward shortlisted compounds for advanced screening against MDR *M. tuberculosis* [16]. The conserved molecular pathways common to both *M. smegmatis* and *M. tuberculosis* has been reported [17, 18]. In the context of the above, *M. smegmatis* has been usd as a surrogate system in the present study to explore the common

mycobacterial biology with a view to identify potential target for inhibition through shortlisted ligand molecules and to understand the possible mechanism of drug-target interaction which may be extended to *M.tuberculosis* in the long run.

1.3 Tuberculosis- an emerging threat

The battle between humankind and *M. tuberculosis*, the etiological agent of tuberculosis (TB), dates back to about 9,000 years as evident from the studies on a Neolithic settlement in the Eastern Mediterranean [19,20] . Historically the disease had been referred to as 'consumption,' 'wasting away,' 'king's evil,' 'lupus vulgaris,' 'the white plague' or 'phthisis based on its clinical manifestations [21, 22].

Notorious amongst all the infectious diseases afflicting mankind since antiquity, the incidence of TB and mortality due to this dreaded disease had been significantly reduced with the improvement in the living conditions and sanitation, introduction of TB chemotherapy in the 1950s and widespread use of BCG vaccine [23]. However, TB has re-emerged in recent years and the emergence of drug-resistant TB is particularly alarming. Non-compliance of patients to the current therapy of TB due to prolonged therapy and significant toxicity has lead to the emergence of Mutli Drug Resistant (MDR, strains which are resistant two at least two frontline drugs like rifampin and isoniazid) and Extensively Drug Resistant (XDR, strains which are resistant to isoniazid and rifampin, plus any one fluoroquinolone and at least one of three injectable second-line drugs like amikacin, kanamycin, or capreomycin) strains of *M. tuberculosis*. Chemotherapy of TB is also limited to small number of antibiotics due to the intrinsic tolerance of *M. tuberculosis* to most of the commercially available antibiotics .

Several fatal outbreaks of MDR-TB have already occurred [24] making MDR-TB a significant threat to the treatment and control of the disease especially in some parts of the world where the incidence of MDR-TB is as high as 14% [24]. In 2011, an estimated 8.7 million new cases of TB (13% co-infected with HIV) was reported. 1.4 million people died from the deadly infection. The high mortality rate in

women, with 300 000 deaths among HIV-negative women and 200 000 deaths among HIV-positive women in 2011 has made TB the highest killer disease in women [25]

The burden of TB is highest in Asia and Africa with 40% of the world's TB cases reported from India and China together. The African Region has the highest rates of cases and deaths per capita and constitutes 24% of the world's TB cases. Globally, 3.7% of the new cases and 20% of previously treated cases are estimated to have been caused by the multi drug resistant strains of *M tuberculosis* in 2011. The highest percentage of TB patients with MDR-TB is reported in Eastern Europe and central Asia [25].

Immunocompromised individuals due to HIV infection are particularly susceptible to infection of *M tuberculosis*. In the African Region 80% of the TB cases are reported among individuals infected with HIV. An estimated 0.5 million cases and 64 000 deaths have been reported among children (aged less than 15) in 2011[25].

TB has claimed the maximum number of lives compared to any other disease [4]. Long generation time, fastidious growth requirements and high risk of contagion of *M. tuberculosis* present a tremendous challenge to the biomedical

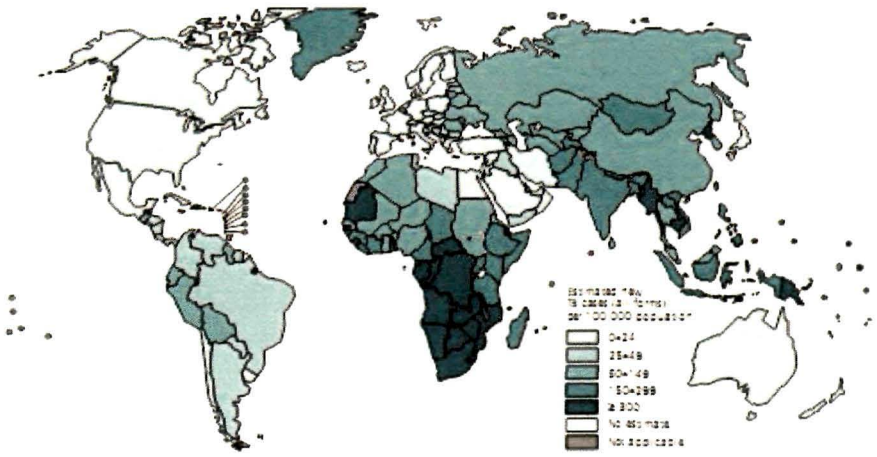

Fig1.1: Estimated TB incidences in 2011

(Source: Global TB Report, WHO, 2012.)

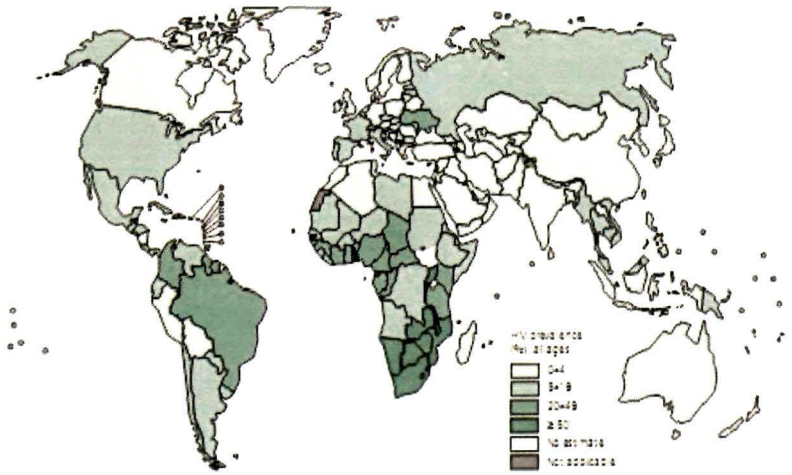

Fig 1.2: Estimated HIV prevalance in new TB cases in 2011

(Source: Global TB Report, WHO, 2012.)

researchers. The genus *Mycobacterium* comprises of more than 150 species and most of the species are non-Pathogenic. However, *M. tuberculosis, M. leprae*, and *M. ulcerans*, the etiological agents of tuberculosis, leprosy, and Buruli ulcers, respectively are highly successful pathogens which may be attributed to their ability to establish residence and proliferate inside host macrophages [5, 6].

1.4 The Genome and proteome of *M. tuberculosis*

The collaborative project featuring the Sanger Centre and the *Institut Pasteur* determined the complete sequence of *M. tuberculosis*. The *M. tuberculosis* genome comprises of 4411529 bp and possesses an average G+C content of 65.6%. Bioinformatics tools enabled the identification of 50 genes encoding stable RNA species and 3924 genes encoding proteins accounting for 91% of the potential coding capacity [27] with gene density at one gene per 1.1 kb. The protein-coding genes were classified into 11 broad groups. Similar to the *Escherichia coli* and *B. subtilis* genomes, about 51% of the coding sequences has arisen from gene duplication events [26, 27].

The abundance of amino acids such as Gly, Ala, Pro and Arg, which are encoded by G+C rich codons, reflect the high G+C content of the genome [28]. A significant portion of the genome relates to genes involved in lipid metabolism which endows *Mycobacteria* with the characteristic mycobacterial cell envelope containing unusual lipids, glycolipids, mycolic acids and polyketides. However, most of the encoded enzymes are involved in fatty acid degradation. The presence of about 100 genes encoding enzymes that could catalyse individual steps of the classical L-oxidation cycle in addition to the *FadA/FadB* proteins indicate the possibility of existence of an alternative lipid oxidation pathway . These enzymes might be involved in the degradation of the host vacuolar or cellular membranes lipids required for the energy metabolism [27, 28].

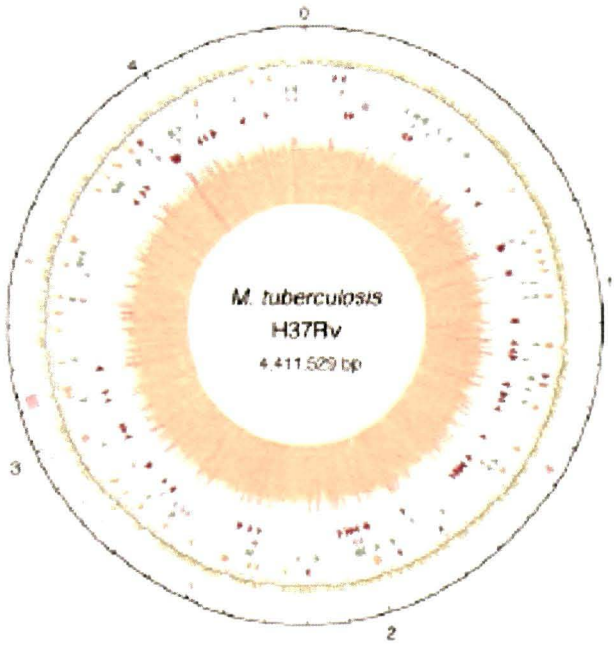

Fig1.3: The genome of M. tuberculosis H37Rv.

(Source: Cole et al., 1998)

Recent genomic analyses have shed new light on the evolutionary lineage within the *Mycobacterium* complex. Studies on the distribution of a series of DNA deletions (regions of difference', RD) among closely related *Mycobacteria* [1, 29] have argued that *M. tuberculosis*, with the fewest regions deleted, is the most ancestral of all organisms comprising the complex. *M. bovis*, with the most regions deleted is on the other hand is the most evolved species. *M. africanum* and *M. microti* share intermediate positions in this new evolutionary scenario. These studies contradict the belief that *M. tuberculosis* evolved from the broad-range *M. bovis* as an unintended consequence of the domestication of cattle However, the fact that *M. bovis* possesses a broader host range could not be explained in a process dominated by the loss of DNA [30,31].

Sequencing and analysis o f the genomes of 259 globally diverse strains of the *M. tuberculosis* complex (MTBC), suggest that MTBC strains emerged in Africa about 70,000 years ago[32]. Comparative study of the evolutionary history of *M. tuberculosis* with a corresponding analysis of ~5,000 human mitochondrial genomes representing the major human haplogroups, revealed close coevolution of MTBC strains with present humans as these humans migrated out of Africa and colonized different regions globally. Abrupt increase in human density during the Neolithic Demographic Transition, around 10,000 years ago, helped in the successful spread of this pathogen,thus, pointing to human demography as a strong selective force. However, an another recent study by Pepperell et al. , 2013, argues against the codivergence of human and MTBC populations [33, 34].

In contrast to the previous assumption that *M. tuberculosis* posses a remarkably stable genome, recent high-density oligonucleotide array analysis demonstrated the existence of polymorphism. An average of 2.9 deletions per strain in 15 of 16 clinical *M. tuberculosis* isolates had been detected [35]. The comparison of the genomes of the virulent laboratory strain H37Rv and the clinical isolate CDC1551 exhibited over 1000 single nucleotide polymorphisms and 74 large sequence polymorphisms (LSP; insertions or deletions unique to one strain relative to the other) [36].

1.5 Host-Pathogen Interaction

M. tuberculosis is a slow-growing facultative intracellular pathogen and is transmitted predominantly by the inhalation of infected aerosol droplets. Once *M. tuberculosis* gains entry to the lungs, the primary site of infection, it is rapidly engulfed by the alveolar macrophages. However, it survives in the macrophage by utilizing the strategies employed by the intracellular parasites including inhibition of phago-lysosome fusion[37], modification of the phagolysosome to facilitate survival and replication of the parasite [38, 39], preferentially using the uptake pathways that do not lead to phagolysosomal fusion [40], resistance to the lysosomal contents

[41], inactivation of enzymes in lysosome [42,43] and escape into the cytoplasm [44, 45].

The replication of the bacteria recruits macrophages, epitheloid cells and lymphocytes thus leading to the formation of the granulomas [46]. Granulomas are involved in the sequestering the pathogen from the adaptive immune system. A persistent infection is developed by the establishment of equilibrium between the growth of the harbored *M. tuberculosis* and the protective immune response. Subsequently, macroscopic nodules called 'tubercles' are formed due to the development of fibrosis within the granuloma and in the surrounding parenchyma.

The histological hallmark of TB lesions is cavitation and the formation of caseum, a liquid containing the highly contagious bacilli. Disruption of immune responses results in uncontrolled growth of *M. tuberculosis*, leading to symptomatic disease causing fever, cough, followed by weight loss. Progression of the disease leads to necrosis of the lungs causing the spread to other organs, like the central nervous system and the bone [47, 48].

The molecular details of the host immune response against TB are still poorly understood. Infected macrophages initiate the host immune response by secretion of interleukin-12(IL-12) which in turn activates and recruits T lymphocytes to the site of infection. Subsequently, CD4+ and CD8+T cells secrete type I cytokines, most importantly interferon-γ (IFNγ) and tissue necrosis factor-α (TNF-α) after recognition of the mycobacterial antigens presented by phagocytes in association with Class II and Class I major histocompatibility complex (MHC) molecules. In addition to the generation of reactive oxygen radicals, nitric oxide, and iron chelators (lipocalins), which serve as bacteriostatic and bactericidal molecules by the activated macrophages, the T cells produce perforin and granulysin that contribute to microbicidal activity [49, 50]. The host immune response may restrict bacterial replication and progression of the active disease. However *M. tuberculosis* can also remain dormant for many months or years, and may cause the disease later in life by

the process called 'reactivation'. Reactivation is a poorly understood process. It has been observed that immunosuppression may lead to reactivation of infection . Reports have also shown that *M. tuberculosis* evades the potent host immune response by the recruitment of mesenchymal stem cells (MSCs) to the site of infection. The MSCs suppress the T-cell responses by producing nitric oxide [51].

The clinical outcome of infection with *M. tuberculosis* may be different [52], which may include development of symptoms within the first 1–2 years of infection and is termed as 'primary disseminated TB'. This type of outcome of the infection represents the majority of pediatric cases. Alternatively, *M. tuberculosis* infection may become chronic by slow progression and exhibiting the clinical symptoms after more than 2 years of infection. However, in 90% of cases, the infection may remain latent and the infected individual remains totally asymptomatic. These two latter groups of infected individuals comprise the reservoir of *M. tuberculosis*. The host and microbial factors which influence the rate of progression of *the M. tuberculosis* infection to clinical disease are poorly understood [53].

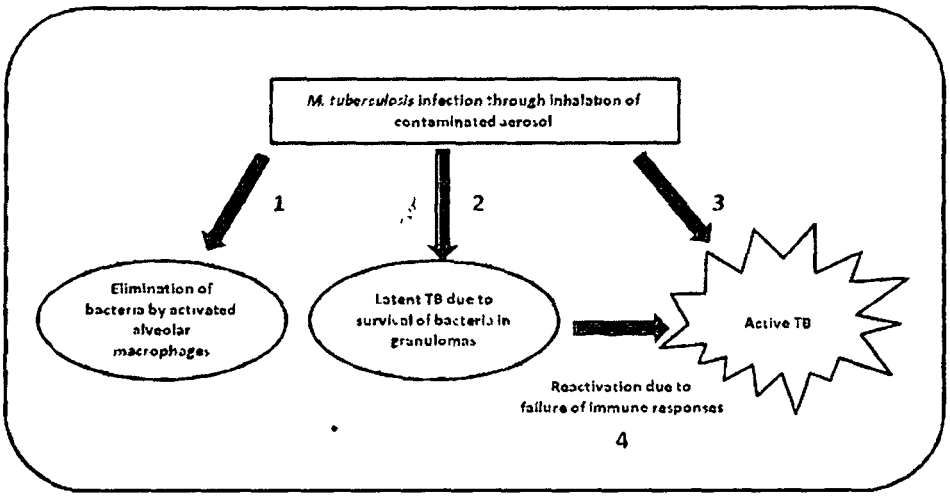

Figure 1.4: Pathogenesis of Tb infection and disease

1.6 Chemotherapy of TB

Streptomycin was discovered by Albert Schatz and Selman Waksman from *Streptomyces griseus* in 1944 and marked the advent of modern TB chemotherapy [54]. In 1946, para-aminosalicylic acid (PAS) was discovered as an effective TB drug by Lehmann from Sweden followed by the discovery of the highly active TB drug isoniazid (INH) in 1952. Discovery of INH was based on the nicotinamide activity against tubercle bacilli in the animal model and is a major milestone in the chemotherapy of TB because it is highly active, inexpensive, and without significant side effects [55] . This was followed by the discovery of pyrazinamide (PZA) in 1952, ethionamide (ETH)/Prothionamide (PTH) in 1956 and Ethambutol (EMB) was discovered in 1961 [56, 57, 58] .Many other antituberculosis drugs such as cycloserine [59];kanamycin [60] and its derivative amikacin; viomycin [61]; capreomycin [62] ; and rifamycins [63] and its derivative rifampin (RIF) [64].Most of the drugs used today in TB chemotherapy were discovered in the 1950s and 60s which is termed as the golden era of TB drug discovery. The broad-spectrum quinolone drugs, developed in 1980s, are used as the second-line drugs for drug-resistant TB strains [65, 66].

The current strategy to contain TB is through a multi-drug therapy (MDT) of the first-line drugs to reduce drug resistance and to increase drug efficacy [67]. The therapy consists of RIF, INH and PZA together with an introductory phase of ETH and/or streptomycin [68, 69, 70, 71] for the initial two months followed by the continuation of the phase which involves treatment with RIF and INH, the two most potent first-line drugs.

The six month therapy is administered via DOTS (Directly Observed Therapy shortcourse) to ensure adherence to the prescribed drug regimen and to reduce the emergence of drug resistant strains of *M tuberculosis* [72]. However, the prolonged therapy leads to patient noncompliance that defeats the therapy and complicated further through emergence of the multi-drug resistant form of TB (MDR-Tb).

1.7 Mechanism of Action of the TB Drugs

The TB drugs can be divided into two categories *viz.*, the bacteristatic and thebactericidal drugs. The bacteristatic drugs include EMB and PAS, whereas the bactericidal drugs include INH, RIF, SM, and FQ (fluoroquinolones) [73].Ethambutol (ETH) is known to inhibit arabinosyl transferases, mainly the embB gene product, involved in cell-wall biosynthesis directly effecting the polymers arabinogalactan (AG) and lipoarabinomannan (LAM) [74, 75].Isoniazid (INH) inhibits InhA, a nicotinamide adenine dinucleotide (NADH)-specific enoyl-acyl carrier protein (ACP) reductase. InhA is involved in fatty acid synthesis. The prodrug is activated by KatG, a catalase-peroxidase hemoprotein [76]. The active moiety of Pyrinizamide (PZA) ,*viz.*, pyrazinoic acid (POA), has been shown to inhibit various functions at acid pH in *M. tuberculosis* [77, 78].PZA has been reported to diffuse into the *M. tuberculosis* cell and then is converted to POA by the enzyme pyrazinamidase (PZAase), also called nicotinamidase. A portion of the POA exits the cell and becomes protonated in the acidic pH. The protonated POA re-enters the cell and disrupts the membrane potential. The POA and protonated POA accumulate and lower the intracellular pH which may lead to inactivation of many pathways which include the fatty acid synthase and affect membrane transport function. However, the mechanism of action of POA is poorly understood and it is widely accepted that POA may not inhibit a specific target, but rather it inhibits mycobacterial growth by cellular acidification [79,80].Rifampin (RIF) targets the essential rpoB gene product β -subunit of bacterial DNA dependent RNA polymerase activity thus, inhibiting the transcription [81].Streptomycin greatly inhibit bacterial growth by targeting the 30S ribosomal subunit thus limiting protein synthesis.

1.7.1 Mechanism of Action of the first-line drugs

Mutations in the genes *embA* or in *embB* lead to the resistance to the drug ethambutol. Mutations in the target gene(*inhA*) and in the activating enzyme KatG

cause resistance to INH . Target-specific mutants resistant to PZA have not been isolated. However, PZA-resistant mutations are usually found in the enzyme PZAase [82] .Mutations in the RIF-resistant determining region (RDR), a 81 bp stretch of the rpoB gene leads to resistance to Rifampin [83].

MDR-Tb has developed as a result of ineffective drug therapies and failure to adhere to the treatment regimen [84] .Strains exhibiting a combined resistance to INH and RIF are defined as MDR-strains [85]. The WHO reported 3.7% of new cases and 20% of previously treated cases to have MDR-TB. India, China, the Russian Federation and South Africa have been reported to have almost 60% of the world's MDR-TB cases. The highest proportion of MDR TB patients are in eastern Europe and central Asia. Almost 80% of TB cases among people living with HIV reside in Africa [25].

The problem of TB has become so grave that the WHO declared TB a global emergency in 1998 and launched the DOTS-Plus project in 1999 for the management of MDR-TB.

1.7.2 Mechanism of Action of th Second-line drugs

The second-line drugs of TB include aminoglycosides (kanamycin and amikacin), fluroquinolones (ofloxacin and ciprofloxacin), polypeptides (capreomycin, viomycin and enviomycin), D-cycloserine and thionamides (ethionamide and prothionamide); out of which, aminoglycosides and fluroquinolones are the most potent among all the second-line drugs [86].

Since the isolation of nalidixic acid, first quinolone drug, during manufacture of quinine in the early 1960s , [87, 88] many fluroquinolones (FQ) derivatives have been evaluated for their antibacterial activity. FQ include ciprofloxacin, ofloxacin, levofloxacin, and sparfloxacin which are highly active against *M. tuberculosis* [89]. FQ target DNA synthesis by inhibiting the DNA gyrase A and B subunits. FQ drugs are being used as second-line drugs to treat

MDR-TB.However, strains are becoming resistant to FQ [90] by mutations in the GyrA or GyrB subunit [91,92].

Aminoglycosides target protein synthesis by binding to the 30s ribosomal subunit. The mechanism of action of polypeptides are yet to be elucidated. D-cycloserine, an inhibitor of alanine racemase, is an analog of D-alanine. The enzyme alanine racemase is involved in the synthesis of peptidoglycan in cell wall biosynthesis [84] .

The MDR-TB therapy is comparatively longer in comparison to the period of treatment with respect to the drug susceptible TB and the drugs too have more side-effects and are less efficacious [84, 93, 94]

The emergence of Extensively drug-resistant TB, or XDR-TB was first reported by the Centers for Disease Control and Prevention, in March 2006. Strains that are resistant to RIF, INH- the most potent first line and to the 3 or more of the second-line drugs, one or more fluroquinolones and one or more of the injectable antibiotics (capreomycin and/or any aminoglycosides) [94] are defined as XDR strains. The therapy for treatment of the XDR-TB is comparatively toxic and less effective. XDR-TB has been reported from 84 countries; the average proportion of MDRTB cases with XDR-TB is 9.0%.13 out of 68 (19.1%) countries and territories have reported more than 10 XDR-TB cases in a single year since 2007. Among them, the proportion of MDR-TB cases with XDR-TB was highest in Azerbaijan, Belarus , Estonia, Latvia , Lithuania and Tajikistan [25].

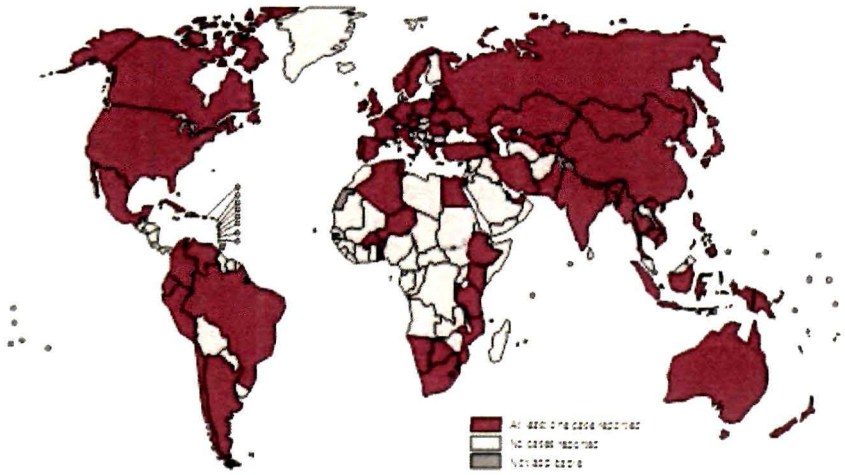

Fig1.5: Countries that had notified at least one case of XDR-TB by the end of 2011

(Source: Global TB Report, WHO, 2012.)

Recently, the emergence of totally drug resistant TB (TDR-Tb) [95] has been reported.The intrinsic tolerance of *M. tuberculosis* to most of the commercially available antibiotics due to the presence of the highly hydrophobic cell wall [96,27, 97].Since 1972, no new classes of drugs have been approved for the treatment of TB by the US Food and Drug Administration [98].

In view of the emergence of MDR, XDR and TDR strains of *M. tuberculosis* , there is an urgent need to identify new drugs with novel mechanism of action as well as new drug targets to tackle the problem of TB [99].

1.8 Drug Development

New drugs for TB need to be less toxic and more efficacious with short treatment regimen in order to overcome the drawbacks of the current therapy. The new drugs should also be able to eradicate latent *M. tuberculosis* [100] and should

not interfere with antiretroviral drugs (ARVs) used for the treatment of HIV. Currently a number of candidate molecules are in the pipeline.

1.8.1 TB drugs in the pipeline

There are a number of potential TB drugs in the pipeline which are briefly stated below.

1) **LL3858**

It is in the phase 1 clinical trial and a fixed dose combination with the first line anti TB drugs is also being developed. The mechanism of action of this pyrrole derivative is not yet elucidated [101].

2) **PA-824**

PA-824 has exhibited activity against the fully susceptible and the MDR strains and also has greater activity than isoniazid and moxifloxacin *in vitro* and in mice. It has also shown comparable activity to the combination therapy with rifampicin and isoniazid. The chemical entity is in the phase I clinical trials [102].

3) **TMC207**

It inhibits the ATP synthase and has exhibited activity against the nonreplicating bacteria. It is also under the phase II clinical trials.

4) **OPC 67683**

This chemical entity is a 6-nitro-2,3-dihydroimidazo[2,1-b] oxazole exhibiting *in vitro* activity against both drug susceptible and resistant strains of *M. tuberculosis*. It does not demonstrate any cross resistance to the presently available anti-TB drugs. It inhibits the methoxy-mycolic acid and keto-mycolic acid synthesis pathways [103, 104].

5) **Moxifloxacin**

Moxifloxacin is a fluoroquinolone which targets DNA gyrase. This drug candidate has reached the phase III clinical trials [105,106]. It exhibits very low interaction with thecytochrome P450 enzymes which are involved in the metabolism of some of the ARVs(Anti-retrovirals) [107] .

6) **SQ109**

Currently the ethambutol analogue SQ109 is being studied and has given the status of orphan drug by the U.S. Food and Drug Administration (USFDA) and European Medicines Agency [108].

1.9 TB Vaccines

Mycobacterium bovis– bacillus Calmette-Gu´erin (BCG) was first used in humans 90 years ago. The TB vaccine has been administered to an estimated 3.5 billion people. However evidences show that it does not reliably prevent the pulmonary form of the disease in adults. Therefore, there is an urgent requirement of an effective vaccine that could prevent a TB epidemic. The preparation of a successful vaccine solely depends on the fundamental understanding the disease pathogenesis which currently requires more exploration [109].

1.10 Drug Targets-the essential and the conserved genes

Minimal gene set is defined as the number of genes required to sustain cellular life under favorable conditions without external stress. The gene products of the minimal gene set are critical for cellular life processes and include essential enzymes which are involved in DNA replication, DNA recombination and repair, transcription, translation, cell division, cell membrane and cell wall synthesis, bioenergetics and macromolecule synthesis and therefore considered as excellent drug targets [99]. It is important to ensure that the gene product selected as a drug target is essential for the survival of the bacteria under all growth conditions and is absent in the eukaryotic genome for broad-spectrum antibiotic development [110]. The identification of such potent drug targets in bacteria has been greatly accelerated with the advent of *in silico screening* and comparative genomics approach [111,112,113,114].

1.10.1 Flavin-dependent thymidylate synthase (Thy x)

Understanding of the molecular and biochemical mechanisms of *drug - target* interaction constitutes an important component in forwarding a candidate molecule effective against potent pathogen. Recently it was discovered that *M.tuberculosis* posseses a flavin-dependent thymidylate synthase (FDTS or ThyX) in addition to the conventional ThyA (thymidylate synthase)[115].The Thy A and the ThyX enzymes are involved in the catalysis of the conversion of 2′-deoxyuridine-5′-monophosphate (dUMP) to dTMP in the presence of R- N^5, N^{10} methylene-5,6,7,8-tetrahydrofolate (CH_2THF)[115]. Thy A lacks a cofactor and in the reductive methylation reaction catalyzed by Thy A , CH2THF donates a methylene group as well as acts as the reductant forming the product 7,8-dihydrofolate (DHF) [116].In this mechanism, dihydrofolate reductase (DHFR ; E C 1.5.1.3) reduces DHF to generate tetrahydrofolate (THF). THF is methylated by serinehydroxymethyl transferase (SHMT; EC 2.1 .2. 1) to regenerate CH_2THF On the other hand, in the reaction catalyzed by ThyX , CH2THF acts only as a methylene group donor and therefore results in the production of THF in place of DHF.

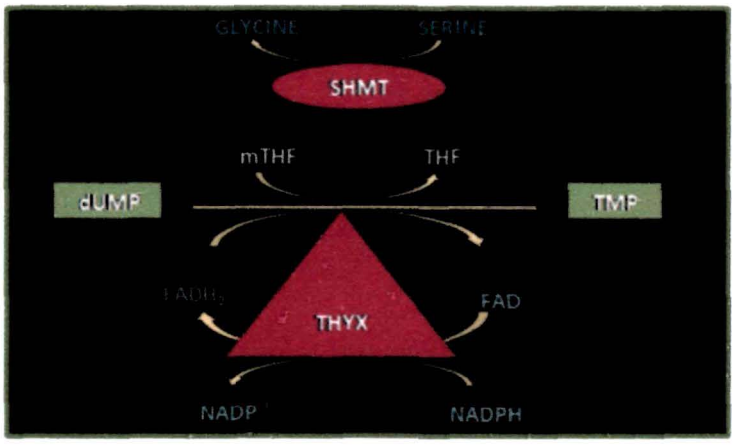

Fig1.6: ThyX converts dUMP to TMP using mTHF, NADPH, and FAD as cofactors. mTHF is regenerated by serine hydroxymethyltransferase (SHMT)

In ThyX catalysis, the cofactor FAD functions as the reductant. A critical step in the Thy X catalysis is reduction of FAD by transfer of electron from reduced pyridine nucleotides (NADH or NADPH) [117, 118]. It has been reported that organisms that lack the gene for TS also lack the gene for DHFR. Thy X is a potential target for new anti-bacterial drugs since the thyX gene is rare in eukaryotes and is absent in humans [119, 120,]. Transposon site hybridization (TraSH) experiments indicate that the *Mycobacterium* thyX is an essential gene for optimal growth of the pathogen [121, 122] .

Important human pathogens,*viz.*,*Helicobacter pylori*, *Bacillus anthracis*, and the *Mycobacteria* have been reported to posses the *thy x* gene. The expression of the thy x gene has been shown to be altered in different growth conditions of *M. tuberculosis* [122, 123]. However, neither sequence nor structural similarity have been identified between the homodimeric ThyA and homotetrameric ThyX proteins [124, 125, 126]. Existence of ThyX in organisms lacking ThyA shows a sporadic phylogenetic distribution indicating lateral gene transfers [117].

1.11 Targeted Screening

After a target has been validated as being crucial for the survival of the pathogen, screening for compounds which specifically inhibit its function is performed. Screening assays can be generally divided into three types *viz.*, the cell based assays, functional cell-free assays, and the binding assays. In cell-based assays, the effect of the inhibitor is studied on the cell growth, alteration of the expression level of the target protein or activity of a suitable marker. The functional cell-free assay involves measuring of an enzymatic activity and binding assays which on the other hand depend on the formation of a ligand-receptor complex[127] . The function of an unknown gene may be studied by binding assays. However, whole-cell assays can determine the permeability of the drug trough the highly hydrophobic cell wall of *M. tuberculosis* [112]. Additional information like the mechanism of action of the compounds [128],identification of related targets in mammals, ADME-TOX values of the drug to mammalian cells and rational drug design (RDD) could be

studied using bioinformatics approach[129]. Before a promising drug candidate for the treatment of TB is approved by the FDA for clinical use, it has to undergo the clinical trials for validation of its efficacy and safety.

1.12 Plants and Traditional Knowledge

Plants have been the corner stone of medicinal therapies for thousands of years, and continue to be an essential part of health care throughout the world [130, 100].In the nineteenth century, before the advent of the pharmaceutical industry, all medicinal preparations were derived directly from nature, mostly from plants. Drug researchers have shifted their focus towards synthetic drugs in the wake of development of synthetic chemistry during the 1970s and the 1980s, limiting plant derived drugs developed in this period. However, in the 1990s the renewed interest in phytochemistry encouraged the major pharmaceutical industries to start plant screening programme.

Currently, 60% of the world population and 80% of the population in developing countries depend on traditional medicines- mostly plant derived drugs for their primary health care needs [131,132]. In India 70% of the population is still dependent on traditional plant based medicines [133] .

North East India is one of the 'biodiversity hotspots' of the world comprising of the states of Arunachal Pradesh, Assam, Manipur, Meghalaya, Mizoram, Nagaland, Sikkim and Tripura [134, 135]. The region therefore has enormous possibilities for drug discovery exploration.

1.13 *In silico* tools for virtual screen

The systematic study of the mechanisms of a large number of natural products by means of traditional assay based methods is a costly and time-consuming process due to the difficulty in extraction, purification, synthesis, and activity testing [136]. Therefore, Computer aided drug design (CADD) is fast emerging as an alternative

approach for low-cost and rapid analysis of the plant derived natural products and efficient search for their targets.

CADD approaches can be categorized into structure-based drug design (SBDD), ligand-based drug design (LBDD) and sequence-based approaches.Introduction of databases of crystal structure of ligands with the biomolecular target in the post-genomic era has enabled "structure-based drug design" (SBDD) and the efficient optimization of leads(Jorgensen,2004). SBDD has contributed to the introduction of approximately 50 compounds into clinical trials and to numerous drug approvals [137, 138].

LBDD tools which include quantitative structure-activity relationship (QSAR), pharmacophore modeling,molecular field analysis and 2D or 3D similarity assessment, are used in the absence of three-dimensional (3D) structures of potential targets. LBDD tools can provide insights into the interactions between drug targets and ligands, thus can be used to construct predictive models that are suitable for lead discovery and optimization [139,140]. The sequence-based approaches are used to compare and analyze multiple to identify potential targets from the sequence in order to conduct lead discovery [141, 142].Currently, drug discovery and development requires combinational and hierarchical strategies which employ multiple computational approaches [140].

Ligand-protein docking is a popular virtual screening technology in rational drug design which could be utilized to identify the ligands as well as the potential protein targets and can be readily extended to study the structural and molecular mechanics of the binding between ligand and the target [143].*In silico* tools such as molecular docking [144],pharmaco phore [145] , structure-activity relationship (SAR) and quantitative structure activity relationship (QSAR) [146] ,machine learning [147], and combination methods [148] have been widely used for lead discovery against individual targets [149]. Identification of compounds/molecules with favorable pharmacokinetics and toxicological properties in drug discovery require the Absorption, Distribution, Metabolism, Elimination and Toxicity (ADMETOX)

studies. The ADME TOX profile defines the success of a drug. Currently computational ADMET studies lead molecules using standard *in silico* tools help in saving time and expenditure by enabling the screening of large numbers of undesirable molecules in a relatively very short period of time [150].

Another most widely used virtual screening approach in rational drug design is Quantitative Structure Activity Relationship (QSAR). QSAR is based on statistical analysis of the relationship between certain biological activities of a molecule *vis-a-vis* the quantitative attributes of the structure of the molecule. The resultant statistical model of QSAR may be used to predict the antimycobacterial activity of a molecule even before its synthesis, or to explore virtual modifications at the structural levels for enhanced antimycobacterial activity of an existing molecule by its quantitative attributes calculated from its structure [151].QSAR is essentially dependent on the information content of the training set (TS) of molecules (statistical sample) and the analyzis, extraction, quantification and representation of this information as QSAR studies correlate information on molecular structure with information on molecular properties [152].

QSAR modeling can be classified as local, pharmacophore-based and global. Local QSAR (2D-QSAR) is an extension of Hammett's equation to biological systems (Hansch's analysis) ,considers a limited chemical space and are usually easily interpretable and predictive. 2D-QSAR modeling are mainly used in the lead optimization step, by modifying type and position of small substituents on a large common chemical scaffold recognized to bear a specific bioactivity. The pharmacophore-based QSAR models explore the chemical and biological space based on the common mechanistic interpretation of drug interaction [152]. The global QSAR models are based on different similarity search algorithms (including 3D-pharmacophore search). The global models consider a very large number of compounds which possess considerably different and (apparently) unrelated chemical structure[152, 153].

1.14 Nanocomposites as antimycobacterial agents

Emergence of drug resistant tuberculosis has prompted the development of alternative strategies to treat bacterial diseases [154].Among the different strategies nanoscale materials have emerged as novel antimicrobial agents. In vitro as well as in animal model studies present nanoparticles and nanosized carriers for antibiotics delivery as more effective for treating infectious diseases, including antibiotic-resistant infections [155]. Nanoparticles poise to play as important tools in biotechnology and medicine, as well as for studying biological systems. The appearance of new mechanical, chemical, electrical, optical, magnetic, electro-optical, and magneto-optical properties of the nanoparticles that are different from their bulk properties can be attributed to the high surface area to volume ratio [156,157].Appropriate functionalization will enable the selective application of nanoparticles. Recently, antibacterial properties of nanomaterials have become increasingly attractive, including silver nanoparticles (Ag NPs) [158], silver nanorods [159], copper nanoparticles [160] and carbon nanotubes. Carbon nanotubes (CNTs) are graphene sheets are rolled into a tube and have been explored for their potential application as the antimicrobial materials in the last few years [161, 162, 163, 164] . The microbial adsorption capacity of CNTs so far reported is higher than any other commercially available adsorbent media [165].The first report on antibacterial activity of single-walled carbon nanotubes (SWCNTs) and multi-walled carbon nanotubes (MWCNTs) was by Kang et al. [166,167,168]. In the present study we investigate the antimycobacterial activity of nanocomposites.

1.15 Objectives

The work embodied in this thesis proceeded with the following objectives in view of the the urgent requirement to identify potential new molecules as drugs to cure tuberculosis described in the preceding introduction.

1. Virtual screening of some important natural products (ligand) to identify probable target protein of *Mycobacterium*.

2. Determination of Minimum Inhibitory Concentration (MIC) values of the selected molecules, through in vivo studies.

3. QSAR (Quantitative Structure Activity Relationship) to predict the antimycobacterial activity of the selected molecules.

4. Validation of the in silico driven hypothesis through cloning, expression and inhibition assay of the target enzyme.

5. Determination of antimycobacterial activity of some selected nanocomposites.

Chapter II

REVIEW OF LITERATURE

2.1 Global burden of TB

Mycobacterium tuberculosis was identified by Robert Koch in 1882 as the causative agent of tuberculosis (TB). About one seventh of the total deaths in Europe and one third of all deaths among the younger population at that time were attributed to TB [169].

TB is a contagious disease that is caused by *Mycobacterium* complex which includes *M. tuberculosis, M. bovis, M. africanum, M. microti, and M. canetti.* The TB bacillus is a thriving pathogen infecting 2 billion persons around the world and claiming approximately 2-3 million lives per day globally. TB is most frequent in the developing countries and in the countries with higher incidence of HIV infection and the frequency of TB has multiplied several folds in these countries [169].

Most species of *Mycobacterium* are non-pathogenic environmental bacteria intimately related to the groups of the soil bacteria Streptomyces and Actinomyces. Only a few species are very successful pathogens *viz.*, *M. tuberculosis, M. leprae,* and *M. ulcerans,* the causative agents of tuberculosis, leprosy, and Buruli ulcers, respectively [5,6].These species are able to establish and multiply within the host cells, *viz.*, the macrophages despite the antimicrobial capabilities of these cells. The host, involving both innate and adaptive components of the immune system mounts a complex immune response that often sequesters the pathogen into granulomas, rendering the pathogen latent. The infection thus can again manifest as acute or chronic disease or may remain clinically asymptomatic with the potency to resurface later [170].

M. tuberculosis also possesses special mechanisms to counteract and survive the reactive oxygen species (ROS) and reactive nitrogen intermediates (RNIs) within a macrophage. Peptide, methionine sulfoxidereductase A (MsrA) is believed to repair the oxidative damage to methionine residues that occurs under these conditions. MsrB is also believed to reduce Met-O. Together, these proteins have been proposed to be the primary tools against oxidative stress in *Mycobacteria* and other pathogens. Disruption of MsrA in several pathogenic bacteria has been shown to result in the loss of the ability to colonize host cells [171].

M. tuberculosis, present a number of trial difficulties for the bacterial geneticist due to their slow growth, thick cell walls, and tendency to form clumps rather than single cell suspensions in culture. A considerable amount of information is now available concerning the genome structures of *M. tuberculosis* a major effort is on its way to determine their complete nucleotide sequences. A variety of systems are available for introducing genes into mycobacterium [51].A number of studies have been done on drug action and drug resistance. Specific enzyme cause inactivation of drugs and is a common mechanism with most genes encoding these enzymes being present on mobile genetic elements. Resistance can also be generated by specific point mutations or by target amplification. Decreased or increased permeability may also lead to changes in the intracellular concentration of the drug, rendering drug resistance [170].

there is a common mechanism with most of the genes encoding these enzymes being present on mobile genetic elements. Resistance can also be generated by specific point mutations or by target amplification. Decreased or increased permeability of the cell wall and the membrane systems may also lead to changes in the intracellular concentration of the drug, rendering drug resistance[170].

A major role in the control of tuberculosis is played by modern chemotherapy. Although tuberculosis still remains a leading infectious disease worldwide, largely because of the inadequacy of the current chemotherapeutic regimen and the latency of the organism. The increase in drug-resistant tuberculosis along with the HIV infection threatens disease control and highlights both the needs to develop new and more effective drugs and to understand how our current drugs work [170].

The current therapy, i.e., DOTS (directly observed therapy short course) is accepted worldwide which consists of two distinct phases: the initial phase of around 2months during which the patient is given four drugs, viz., isoniazid, rifampicin, pyrazinamide and ethambutanol to prevent the emergence of resistant mutants. These drugs constitute the first line drugs. The second line drugs are more potent but with a number of side effects and includes capreomycin, cycloserine, kanamycin, and fluoroquinolones[170].

The emergence of the multidrug-resistant TB (MDR-TB, resistant to at least two frontline drugs such as isoniazid and rifampicin), is particularly alarming. MDR-TB has already caused several fatal outbreaks and poses a significant threat to the treatment and control of the disease in some parts of the world, where the incidence of MDR-TB can be as high as 14 % [172].The standard TB therapy is ineffective in controlling MDR-TB. Fifty million people have already been reported to be infected with drug-resistant TB [172]. There is much concern that the situation may become even worse with the spread of HIV worldwide, a virus that weakens the host immune system and allows latent TB to reactivate and makes

the person more susceptible to re infection with either drug-susceptible or drug resistant strains. The lethal combination of drug-resistant TB and HIV infection is a growing challenge in effective TB control [170].

2.2 The search for new drugs

In recent times, emphasis is being given in introduction of new drugs as well as in the identification of new drug targets to treat TB. A few of the promising new drug candidates which are in different stages of drug trial and are discussed below [173]-

1)PA 824: It is a bicyclic nitroimidazo [2, 1-b] oxazine molecule exhibiting anti-TB activity against the non replicating *M. tuberculosis* inhibiting the cell wall lipid and protein synthesis. It did not exhibit any cross resistance to the present known first line drugs and is under the Phase III of drug trials [174].

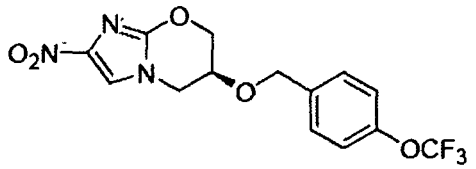

Fig2.1: The 2D structure of PA 824

2) **SQ 109**: It is a diamine analogue of ethambutol with unsaturated isoprenyl units and a bulky adamentyl unit. *In vitro* studies revealed its activity against both drug susceptible and resistant strains of *M. tuberculosis*. The putative target of this ethambutol analogue is the cell wall synthesis in *Mycobacteria*. SQ109 has exhibited synergistic activity upon administration with INH and RIF [175].

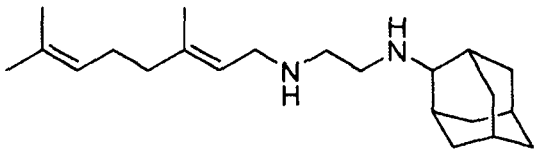

Fig2.2: The 2D structure of SQ 109

3) OPC 67683: It is a 6-nitro-2,3-dihydroimidazo[2,1-b] oxazole exhibiting *in vitro* activity against drug susceptible as well as drug resistant strains of *M. tuberculosis* It does not demonstrate any cross resistance to the presently available anti-TB drugs. It exhibits antimycobacterial activity by inhibiting the methoxy-mycolic acid and keto-mycolic acid synthesis of the cell wall [103, 104].

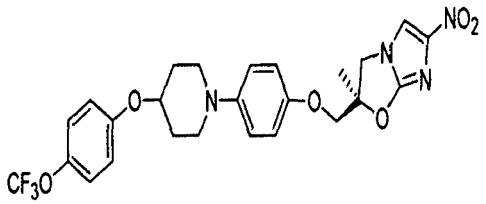

Fig2.3: The 2D structure of OPC 67683

4) TMC 207: This chemical entity has demonstrated a potent *in vitro* activity against drug susceptible, MDR and even XDR strains of *M. tuberculosis* by inhibiting the membrane bound ATP synthase. It belongs to the diarylquinolines (DARQs) class of molecules and didnot exhibit any cross resistance to any of the first line anti-TB drugs [83].

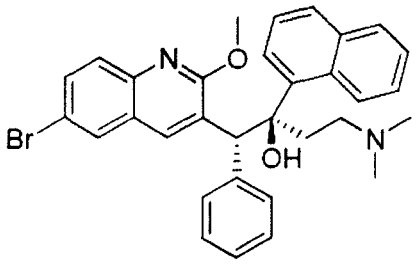

Fig2.4: The 2D structure of TMC 207

2.3 Medicinal plants as an alternative source of antimycobacterial molecules

Natural products including plants, animals and minerals have been the basis of treatment of many diseases. In fact medicinal history dates back to practically the very early existence of human civilization. The modern method of treatment, *i.e.*, allopathy developed over the years gradually, although its origin can be traced back to the traditional medicine and therapies. Thus ancient medicine has been an important base for the treatment of diseases and will remain as a source of development of allopathy in the future as well. The *Ayurveda*, which has been reported since 1000 BC, has a sound philosophical and experiential basis and is still practiced widely in India, Sri Lanka and other countries [176, 177].The Chinese medicine dates back to 500 BC and some of the formulae are still in use [178]. The vast wealth of 'Traditional Knowledge' (TK) of the different ethnic groups across the world provides an immense opportunity for discovering new drug molecules against TB.

The emergence of drug resistant pathogens and the side effects of the synthetic drugs have revived the interest in plants as a source of new active compounds. About 30% of the drugs which are being used today are of plant origin [178] and is worth around US $ 40 billion a year worldwide. Realizing the importance of traditional medicine, the WHO has developed strategies and guidelines for use of standardised botanical medicines [179] .

The aromatic secondary metabolites of plants are reported to have remarkable medicinal properties. These mostly include phenols and their oxygen substituted derivatives. The important subclasses are phenols, phenolic acids, flavonoids, flavones, tannins and coumarins which serve in plant defense mechanisms in response to microbial infections are often found as effective in vitro as antimicrobial agents [180].

The innovative potential of TK and its impact in drug discovery may be witnessed in the genesis of a number of useful drugs used extensively for treatment of many diseases. It has been estimated that almost 25% of all plant species posses some sort of medicinal use which means 40,000 to 70,000 plant species are used as medicines to treat various ailments[181]. A study on the use of plants in traditional medicine in Sitamata Wild life sanctuary in Rajasthan, India revealed the extensive use of 243 medicinal plants belonging to 76 different families [182]. The tribal practitioners of the Jaintia tribes inhabiting the North Cachar Hills district of Assam, India have been reported to use 39 medicinal plant species belonging to 35 genera and 27 families [183].The use of 65 different species of plants in traditional medicine in the state of Assam located in North East India has been reported [184]. The native inhabitants of Churu district in Rajasthan are known to be use various medicinal plants to treat a vast range of ailments by [185].The local inhabitants of Mozambique are reported to use 53 species of medicinal plants to treat a vast number of diseases [186].The plants used in traditional medicine in the Terai forest of Western Nepal belong to 66 species of 60 genera in 37 families of angiosperms. It has been reported that 41 species of these medicinal plants are used in treatment of gastro-intestinal disorders[187].

2.4 Antimycobacterial activity of Plant Natural Products

Natural products and their derivatives from plants have been reported to inhibit *Mycobacterial* species (180, 188). These generally belong to the secondary

metabolites and include coumarins, flavonoids, alkaloids, glycosides, lignans, steroids, sugars, terpenoids, etc. [189].

The flavonoids are commonly found in fruits, vegetables, nuts, seeds, stems, flowers, tea, wine, propolis and honey. Preparations containing flavonoids as the principal physiologically active constituents have been used to treat various human ailments [190].A brief review of the flavonoids exhibiting antimicrobial activity is reviwed below.

2.4.1 Flavonoids as antimycobacterials

The term "flavonoid" is generally used to elucidate a group of natural products that include a C_6-C_3-C_6 carbon framework (phenylbenzopyran functionality). Based on the position of the linkage of the aromatic ring to the benzopyrano (chromano) moiety, flavonoids can be divided into three classes:

- flavonoids (2-phenylbenzopyrans)
- isoflavonoids (3-benzopyrans)
- neoflavonoids (4-benzopyrans)

Flavonoides are synthesized in the plants from the common chalcone precursor and are responsible for the color of the flowers, fruits and sometimes of the leaves of plants [191]. Based on the differences in the molecular backbone structures, the flavonoids may be divided into six different major classes *viz.*, flavonols, flavanones, flavones, isoflavones, flavonols and anthocyanidins [192,193].

The flavones Nevadensin and Isothymusin isolated from *Limnophila geoffrayi* have exhibited inhibition activity against *M. tuberculosis* with equal MIC value of 200μg/ml [194]. The flavonoids, Isosakuranetin, 4'-hydroxy-5,6,7-trimethoxyflavanone, Acacetin and Luteolin extracted from the flowers of *Chromolaena odorata (Eupatorium odoratum)* exhibit moderate activity against *M*

tuberculosis H37Ra with the MIC values of 174.8μM , 606.0μM, 704.2μM and 699.3 μM, respectively [195].Three out of the four flavonoids extracted from the plant

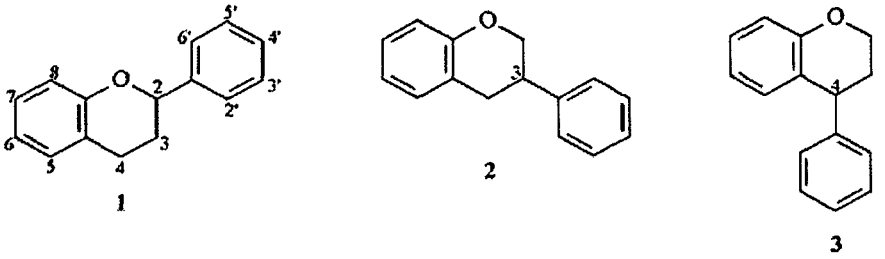

Fig2.5: The C6-C3-C6 carbon framework of the three classesof flavonoids : (1) the flavonoids (2-phenylbenzopyrans), (2)isoflavonoids (3-benzopyrans) ,and (3) the neoflavonoids (4-benzopyrans) .

Derris indica exhibited activity against *M. tuberculosis H37Ra*. The MIC of 3-Methoxy-(3″,4″-dihydro-3″,4″-diacetoxy)-2″,2″-dimethylpyrano-(7,8:5″,6″)-flavone,8,4′-Dimethoxy-7-O-c,c-dimethylallyliso-flavone and 3,4-Methylenedioxy-10-methoxy-7-oxo[2]benzopyrano[4,3-b]benzopyran were 25μg/ml, 100μg/ml and 6.25μg/ml respectively [196].The common acetyl derivative of Linaroside and Lantanoside, isolated from *Lantana camara,* exhibited 98% inhibition of *M. tuberculosis H37Rv* at 6.25μg/ml [197]. Butein, Isoliquirtigenin, 2,29,49-trihydroxychalcone and Fisetin have been reported to inhibit the growth of *M. bovis* BCG. Furthermore, *in vitro* inhibition of the mycolic-acid-producing fatty acid synthase II (FAS-II) of *M. smegmatis* suggests a mode of action analogous to those observed in *E. coli* and *Plasmodium falciparum* [198].These and other reports thus provide very strong indications about the possibility of discovering new plant based natural products as potential drug against *M. tuberculosis.*

The flavonoids *viz.*, Epicatechin, Isorhamnetin, Kaempferol, Luteolin, Myricetin, Quercetin, Rutin and Taxifolin were tested for their ability to modulate the susceptibility of different strains of fast-growing mycobacteria like *M. smegmatis*

(ATCC 14468), *M. smegmatis* mc2155 (ATCC 700084), *M. smegmatis* mc22700, *M. phlei* (ATCC 11758) and *M. fortuitum* (ATCC 6841) in combination with the first-line antituberculotic drug isoniazid (INH). The strongest synergistic effects were observed in *M. smegmatis* mc2155 followed by *M. phlei*. Myricetin, followed by quercetin, exhibited maximum intensification of INH susceptibility in all the tested strains decreasing the MIC of INH up to 64-fold at 16 μg/ml [199].

Three known flavonoids, (2S)-5,7,2'-trihydroxyflavanone, (E)-3,2',4'-trihydroxychalcone, and (E)-2',4'-dihydroxychalcone , and the new (E)-3,2',4'-trihydroxy-3'-methoxychalcone were isolated from the leaves of *Galenia africana.* (2S)-5,7,2'-trihydroxyflavanone and (E)-2',4'-dihydroxychalcone exhibited moderate antimycobacterial activity againt *M. tuberculosis.* A combination of (E)-3,2',4'-trihydroxy-3'-methoxychalcone and isoniazid, reduced their original MICs 4-fold, resulting in a fractional inhibitory concentration (FIC) of 0.50. The most pronounced effect was demonstrated by (2S)-5,7,2'-trihydroxyflavanone and isoniazid reducing their MICs 16-fold and resulting in an FIC of 0.12. [200]. The evaluation of the antimycobacterial activity of five flavonoids: Isobachalcone (IBC); Kanzanol C (KAN); 4-hydroxylonchocarpin (4-LCP); Stipulin (SPL) and Amentoflavone (AMF) from *Dortenia barteri* was performed using the Agar disc diffusion, broth microdilution, microplate alamar blue assay (MABA) and radiometric respiratory technique using BACTEC 460 system. The results showed that the crude extract and the flavonoids were able to prevent the growth of *M. tuberculosis* with isobachalcone exhibiting maximum activity with MIC < 10 μg/ml. The total inhibition effect on *M. tuberculosis* H37Rv strain was exhibited by isobachalcone and stipulin at day 9 when tested at 4× MIC [201].The flavonoids 5,4′-Dihydroxy-3,7,8,3′-tetramethoxyflavone and 5,4′-dihydroxy-3,7,8-trimethoxyflavone isolated and characterized from *Larrea tridentate exhibited* activity against *M. tuberculosis* MDR strains having MIC values of 25 and 25–50 μg/mL, respectively [202] Seven methoxy-flavones, namely, cirsimaritin , eupatilin , eupatorin , salvigenin , 3'-*O*-methyl-eupatorin, 3',7-dimethoxy-5,6,4'- trihydroxyflavone , and 7'-*O*-methylapigenin , and one triterpene-

oleanolic acid were isolated from the dichloromethane extract from *Lippia lacunosa* Mart. & Schauer, Verbenaceae. The compounds showed *in vitro* activity against *Mycobacterium tuberculosis* with MIC ranging from 25 to 200 μg/mL when studied using a redox bioassay [203]. Bioassay-guided fractionation of the active AcOEt-soluble layer led to the isolation the antimycobacterial flavonoids 3-Hydroxyxanthyletin , Genistein , Prunetin , and (*2S*)-Naringenin which showed antimycobacterial activities against *Mycobacterium tuberculosis* $H_{37}R_V$ with *MIC* values of 16, 35, 30, and ≤2.8 μg/ml, respectively [204]. The flavonoids isolated from flowers of *Butea monosperma* included one new dihydrochalcone, Dihydromonospermoside, with three known chalcones, Butein , Monospermoside and Isoliquiritigenin , one flavone, 7,3′,4′-trihydroxyflavone , four flavanones, (−)-Butin , (−)-Butrin, (+)-Isomonospermoside and (−)-Liquiritigenin , and three isoflavones, Formononetin, Afrormosin and Formononetin-7-*O*-β-D-glucopyranoside.of these compounds exhibited varying antimycobacterial activity where chalcone was found to be the most active compound (MIC 12.5 μg/ml [205]. Ermanin isolated from *Hapllopappus sonorensis* displayed 98% inhibition of *M. tuberculosis* at 100 μg/ml [206].Licochalcone A which was isolated from Chinese licorice root inhibited the growth of a range of clinical isolates of mycobacteria including *M. tuberculosis* (MIC 5–10 μg/ mL), *M. bovis* (MIC 10–20 μg/ mL) and *M. bovis* BCG (MIC 5–10 μg/ mL) [207].Licoisoflavanone isolated from the medicinal plant *Glycyrrhiza glabra* exhibited potent antimycobacterial activity with an MIC of 25 μg/mL against *M. tuberculosis* [208].The two flavonoids phaseollidin and erythrabyssin II from *Erythrina gibbosa*, inhibited the growth of *M. tuberculosis* with MIC values of 8–25 μg/ ml [208].

2.5 In silico studies

More innovative and openapproaches in place of the traditional closed-door and market driven approaches for drug discovery are required for diseases like tuberculosis and malaria as most patients suffering from these diseases have poor paying capacity [209]. *In silico* (computer aided) approaches in drug discovery have

gained immense popularity as these methods do not need animal models or enzymatic methods in comparison to *in vivo* and *in vitro* studies [210]. *In silico* approaches could expedite the process of drug development as simulation of every aspect of drug discovery and development has been made possible by the *in silico* approach.

2.5.1 Quantitative Structure Activity Relationship (QSAR)

Quantitative Structure Activity Relationship (QSAR) studies involve statistical analysis by tying various molecular descriptors to physical, chemical, and biological properties of a set of molecules to form a model which may be used to predict the antimycobacterial activity of a molecule. The public domain "C-QSAR" database, containing thousands of such models, has become a valuable resource for drug discovery [211]. QSAR studies was first reported by Hansch in 1963 [212].

QSAR studies can be one dimensional (1D) which focuses only on a single physico-chemical property for example, solubility, pKa value or by the biological effect of the molecule. Two dimensional 2D-QSAR, also known as local QSAR is an extension of Hammett's equation to biological systems (Hansch's analysis). The lead optimization step uses 2D-QSAR modeling by modifying the type and position of the small substituents on a large common chemical scaffold recognized to bear a specific bioactivity which include different effects/properties of the substituents (electronic, steric and lipophilicity) [152].The three dimensional (3D) QSAR studies include the length and width of the molecules. Comparative Molecular Field Analysis (CoMFA) which include the 3D structure of a molecule was first reported in 1988. The four dimensional (4D) QSAR studies involve the different conformations, orientations, stereo-isomers and tautomers of the molecules [213].3D QSAR studies have been reported on a set of pyrrole derivatives while investigating the correlation between the chemical structures of these compounds and the anti-TB activity exhibited by these molecules [214].QSAR studies involving multiparameter regression analysis was carried out on a set of isonicotinic acid hydrazide derivatives [215] . 3D QSAR studies involving CoMFA, Comparative Molecular Similarity

Indices Analysis (CoMSIA) and CoMFA alongwith the inclusion of Hydropathy field (HINT) analysis were performed on a set of anti-TB ring substituted quinoline derivatives [216]. 3D QSAR studies were also performed on a set of 24 compounds corresponding to 4 series of anti-TB ring substituted 2/4 quinolinecarbaldehyde [217]. QSAR studies were carried out for 25 chalcone molecules to analyze their anti-TB activity [218]. 8 QSAR models based on various descriptors were constructed using the compound libraries available online including PUBCHEM [219].A 3D QSAR study based on CoMFA and CoMSIA revealed the correlation between the chemical structures and their antimycobacterial activity[220].QSAR studies on a set of 104 flavonoid derivatives as p56lck protein tyrosine kinase inhibitors were carried out using hydration energy and logP as predictor parameters [221]. QSAR analysis of the interaction of set of flavones derivatives with the Benzodiazepine binding site of the $GABA_A$ receptor complex revealed the association of their binding to the negatively charged oxygen atom of the carbonyl group of the flavonoids and with the nature of the substituent in the position 3' [222]. An open-source program Open3DQSAR aimed at chemometric analysis of molecular interaction fields (MIFs) has been made available. MIFs can be generated by Open3DQSAR itself or imported from different sources (GRID, CoMFA/CoMSIA, quantum-mechanical electrostatic potential or electron density grids) [223].

2.5.2. Molecular docking studies

Molecular docking, widely used in the field of structure-based drug design, is an *in silico* computational technique which predicts the conformation and binding affinity of intermolecular complexes on the basis of the three-dimensional structures of individual molecules. The screening of compounds employing wet lab *in vitro* approaches is expensive and time-consuming process. Therefore to screen out the unlikely candidates, *in silico* fast molecular docking methods are gaining popularity [224, 225] .The availabity of large number of proteins and nucleic acids structures has increased the consideration of molecular docking for discovery of lead molecules. In case of mycobacterial pathogenesis molecular docking strategies

enabled identification of hits , elucidation of the drug target interaction and possible mechanism of drug inhibition [226,227].Ninety five potential molecules out of fifteen thousand four hundred and fifty two compounds were selected on the basis of their docking efficiencies for study against the chorismate dismutase protein of *M. tuberculosis*. Out of these hits, fifteen compounds were further screened using Flex X molecular docking software and subjected to biological study [228].Molecular docking studies of 27 different quinoline and amide derivatives against ATP synthase protein of *M. tuberculosis* were performed to study the ligand target interaction [229]. Molecular docking studies established the antimycobacterial activity of covalent hydrates of trifluoromethylated pyrazoles due to the inhibition of Riboflavin Synthase *M. tuberculosis* [230].Virtual screening was used to evaluate the antimycobacterial activity of a vast number of novel cyclic peptides in order to develop new drug molecules against *M. tuberculosis* [231].Screening of a virtual compound library containing one lakh fifty two thousand one hundred and two compounds against *M. tuberculosis* Inh A using the GOLD and DOCK software revealed five potent molecules on the basis of their docking scores [227]. Docking of phytochemicals from three different plants *Ficus religiosa, Saraca asoca* and *Tylophore indica* against PKs 18 and Acc D5 protein receptors in *M. tuberculosis* revealed phytol as an inhibitor [232]. *M*olecular docking studies of 2-methylheptyl isonicotinate as inhibitors of the DHDPS enzyme *M. tuberculosis* has been reported [233].

2.6 The search for new drug targets

Identification of the drug target and understanding the mechanism of drug – target interaction is a major component of the current research initiative for discovering new antitubercular agents. Out of many drug targets discovered for antituberculosis drug development, a few promising drug targets are as the follows: Isocitrate lyase [234] , Lumazine synthase [235] AccD5(an essential acyl-CoA carboxylase carboxyltransferase) [236] and mycobacterial translocase I enzyme [237]. An extensive review of research related to drug targets discovery has enlisted

many potential drug targets which include hyperphosphorylated guanine synthase I, sigma factors of *M.tuberculosis,* β-ketoacyl-acyl-carrier protein synthases- KasA and KasB, etc. [170].

2.6.1 Thy X as new drug target

The gene encoding the classical thymidylate synthase ThyA has been found to be absent from the genomes of a large number of nonsymbiotic microbes even though the deoxythymidylate cannot be provided directly by ribonucleotide reductase. This fact leads to the identification of ThyX (Thy1) proteins as a distinct class of thymidylate synthases the function of which were previously unknown. *ThyX* is present in microbial genomes lacking *thyA* and has a wide but sporadic phylogenetic distribution.The presence of Thy X in many pathogenic bacteria and absence in human make ThyX an attractive target for potential antibacterial drugs [238].Mechanistic studies of a FDTS from *Thermotoga maritima* (TM0449) reveal that the reaction proceeds via a ping-pong mechanism where nicotinamide binding and release precedes the oxidative halfreaction. It is primarily pro-*R* specific enzyme with regard to the nicotinamide (NADPH), the oxidation of which is the rate-limiting step of the whole catalytic cascade. An enzyme-bound flavin is reduced and exchanges protons with the solvent prior to the reduction of an intermediate methylene. The slow activity of the enzyme could be explained by the significant NADPH substrate inhibition and large rationalized K_M [239]. Biochemical and structural analyses also revealed the catalytic mechanism of the recently discovered flavin dependent thymidylate synthase ThyX from *Paramecium bursaria* chlorella virus-1 (PBCV-1). Several residues implicated in either NADPH oxidation or deprotonation activity of PBCV-1, ThyX were identified by site-directed mutagenesis [240].The investigation of the molecular mechanism of this enzyme revealed an unexpected substrate-dependent lag-phase found in the single turnover reduction of FDTS bound Flavin [239]. The catalytic mechanism of *Chlamydia trachomatis* ThyX has also been studied [241]. A report on the study of the oxidative half-reaction of the *thyX* gene product from *Campylobacter jejuni* established direct observation of the participation of flavin adenine dinucleotide(FAD) in the

stoichiometry of conversion of 2′-deoxyuridine monophosphate (dUMP) and 5,10-methylenetetrahydrofolate (CH2THF) into dTMP and tetrahydrofolate (THF). The study also established that flavin is oxidized after dUMP reacts with CH_2THF [242]. The *thyX* gene of te Lyme borreliosis (LB) agent *Borrelia burgdorferi* has been reported to be located in a 54-kb linear plasmid [243].Sequence revealed an open reading frame A674R that encodes ThyX. The mechanism of Thy X differs vastly from the traditional thymidylate synthase, ThyA, as Thy X uses methylenetetrahydrofolate (CH2H4folate) as both a source of the methylene group and the reductant, CH2H4folate only provides the methylene group in ThyX-catalyzed reactions. ThyX only catalyzes thymidylate (dTMP) formation in the presence of reduced pyridine nucleotides and oxidized FAD [244].Analysis of the *M. tuberculosis* ThyX enzyme revealed the presence of the short $RHRX_{7-8}S$ found in all *thy x* genes [245]. The cloning, over-expression, and purification of the ThyA and ThyX gene products were performed and the thymidylate-synthesizing ability was directly confirmed by HPLC analysis of reaction products and substrate saturation kinetics were established. 5-Fluoro-29-deoxyuridine 59-monophosphate (FdUMP) was identified as a potent inhibitor of both ThyA and ThyX, offering important clues to double-targeting strategies, however, the folate-based 1843U89 was a potent inhibitor of ThyA but not ThyX suggesting that it should be possible to find ThyX-specific antifolates [246]. Three series of compounds based on a thiazolidine core were synthesized to identify potent inhibitors of thymidylate synthase X. Two distinct classes of compounds that inhibit ThyX with submicromolar concentrations were identified on the basis of the evaluation of the catalytic activity of the enzyme in the presence of these molecules. After optimization this could lead to effective inhibitors with potential biomedical interest [247].

2.7 Nanocomposites as novel antimycobacetrial agents

The advent of nano-technology has enabled generation of nano-particles (1-100nm), as an alternative source of antibacterial agents. The high surface to volume ratio endows nanoparticles with an increased potential to interact with pathogens.

Recently, the antimicrobial activity of nanosized silver, zinc, and their compounds has been explored [248, 249]. The preparation and antimicrobial activity of four different types of chitosan-based nanocomposite films using a solvent-casting method by incorporation with four types of nanoparticles, that is, an unmodified montmorillonite (Na-MMT), an organically modified montmorillonite (Cloisite 30B), a Nano-silver, and a Ag-zeolite (Ag-Ion) [250].ZnO nanoparticles have been shown to posses antimicrobial activity [251] , on the other hand CNTs have been reported to be comparatively less dispersive, and can adopt different functionalities [252].Functionalization of MWCNT via covalent and non-covalent have been reported to be an apt strategy to the practical challenges of the chemical inertness of the graphitic network, poor dispersion and interfacial bonding with others and so on [253]. ZnO coated MWCNTs have been reported to exhibit higher antimicrobial activity in comparison to raw and purified MWCNTs [254].MWCNTs have been reported to possess less cytotoxicity than single-walled carbon nanotubes and functionalization of these MWCNTs with cationic amino acids could be a bene ficial approach [255].CNTs and PAni have been reported to posses inherent antimicrobial activity [167,257] .

Chapter III

MATERIALS AND METHODS

Materials

3.1 Bacterial strains

The bacterial strains used in this study are *Escherichia coli DH5α, Escherichia coli BL21(DE3)pLysS* , *Mycobacterium smegmatis* ATCC14468, *Mycobacterium smegmatis* mc2155, *Bacillus subtilis* MTCC441 , *Staphylococcus aureus* MTCC96, *Klepsiella pneumoniae* MTCC618. Stocks of all strains were made up in 20% glycerol and stored at -80°C.

3.2 Plasmids

The two plasmids used in this study are as the following:

i. **pTZ57R/T cloning vector** (Thermo Scientific): linearized and ddT tailed for direct use in cloning of PCR products, Phage f1 origin ,T7 promoter, MCS, Amp^r ,2.8 kb(Fig 3.1).

ii. ***pET32a(+) expression vector*** (Novagen) : protein over-expression vector, pBR322 origin, T7 promoter, T7 transcriptional start and terminator, His·Tag, MCS, Amp^r, 5. 9kb (Fig.3.2).

3.3 Media

3.3.1 *E. coli , B. subtilis, S.aureus and K. pneumoniae*

E. coli, B. subtilis, S. aureus and K. pneumoniae strains were cultured in Luria-Bertani broth (LB broth, HIMEDIA) and 1.5% Luria-Bertani agar (LB agar, HIMEDIA) as per the manufacturers' instructions with media supplements as described in section 3.4 and culture conditions as described in section 3.5. For antibacterial assays the strains were grown in Mueller Hinton Broth No.2 (MHB, HIMEDIA) and Mueller Hinton Agar as per the manufacturers' instructions . The

media was sterilized via autoclaving at 121°C for 15 minutes in an autoclave on a liquid cycle.

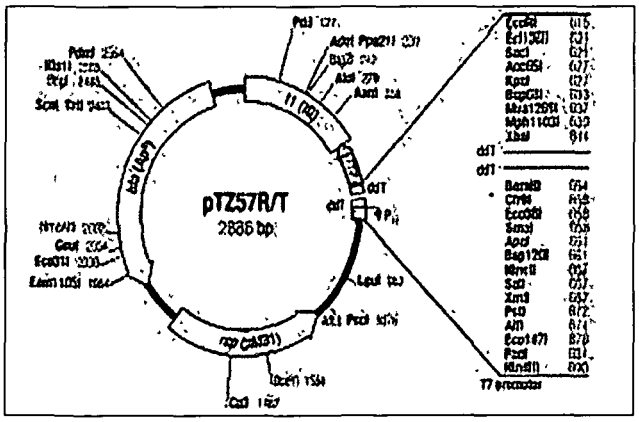

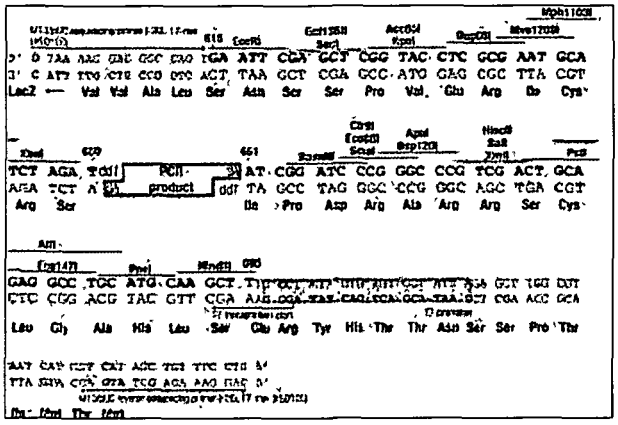

Fig.3.1. Map of the pTZ57R/T cloning vector and DNA sequence of MCS region.
(Source: InsTAclone™ PCR Cloning Kit, Thermo Scientific)

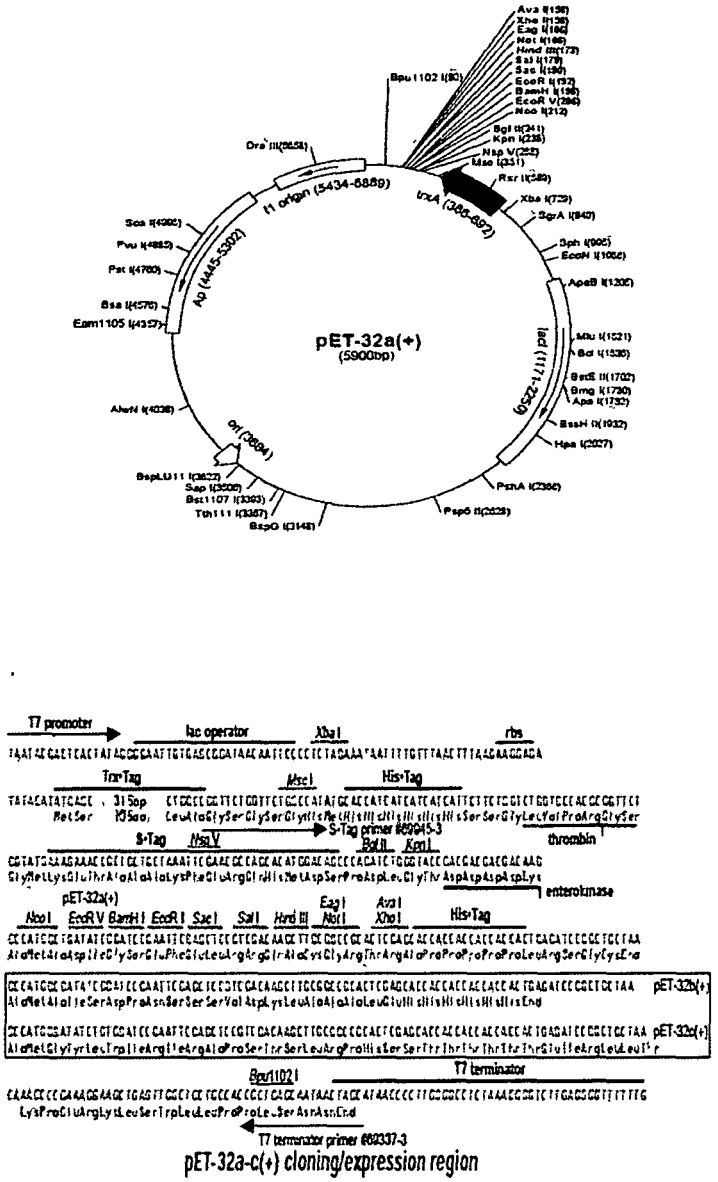

Fig.3.2. Map of the pET32a(+) cloning vector and DNA sequence of MCS region.

(Source: pET32a (+) vector map, NOVAGEN)

3.3.2 *M. smegmatis*

M. smegmatis strains were cultured in LB broth, 1.5% LB agar or Middle brook with media supplements as described in section32.2.4 and culture conditions as described in section 3.3.

3.4 Media supplements

Tween 80: 10% Stock solution of Tween 80 was made with deionized water and autoclaved at 121°C for 30 minutes in an autoclave on a liquid cycle. *M. smegmatis* culture media had a final concentration of 0.1% Tween 80.

Glycerol: 10%, 50% and 80% stocks of glycerol were made up to with deionized water and autoclaved at 121°C for 30 minutes in an autoclave on a liquid cycle.

Antibiotics: All antibiotic stocks were made with deionized water and filter-sterilized with a 0.22 μm Millipore filter and kept at -20°C. The final concentrations of all the antibiotics used are listed in Table 3.3.

Chemicals: Isopropyl-β-D-thiogalactopyranoside (IPTG, SIGMA) was prepared with deionized water and was filtered-sterilized with a 0.22 μm Millipore filter. 5-bromo-4-chloro-3-indolyl-β-D-galactopyranoside (X-gal,SIGMA) stock solution was made by dissolving X-gal in dimethylformamide(MERCK) at a concentration of 20 mg/ml solution. The polypropylene tube was wrapped in aluminum foil to prevent damage by light and store at -20°C. The final concentrations of all chemicals used are tabulated in Table 3.3.

Table 3.1: Antibiotics and chemicals used in this study

Antibiotics/ Chemicals	**Stocks**	**Working**
Ampicillin (Amp)	100 mg/mL	100 µg/mL
Streptomycin	100mg/ml	100 µg/mL
IPTG	100 mg/mL	100 µg/mL
X-gal	40 mg/mL	40 µg/mL

3.5 Culture Conditions

All the bacterial strains were cultured at 37°C. All agar plates were incubated in a stationary plate incubator and all liquid cultures in flasks, polypropylene tubes and 96 well plates (NUNC) were aerated with orbital shaking at 200 rpm.

3.6 Chemicals and Reagents

All chemicals and/or compounds were purchased from Sigma-Aldrich unless otherwise stated. Xgal, dNTPs, DNA ladder, DNA loading buffer, DNA Molecular Marker and Protein Molecular Marker were procured from Fermentas. The vector pTZ57R procured from Fermentas and the expression vector pET32a+ was procured from Novagen.

3.7 Enzymes

The restriction endonucleases were purchased from New England Biolab. T4 DNA ligase and Long PCR Enzyme Mix were procured from Fermentas. Proteinase K, lysozyme, RNase A, DNAse I and Enterokinase bovine recombinant expressed in *E.coli* were obtained from Sigma.

3.8 Oligonucleotides

Oligonucleotide primers were analyzed for restriction sites and designed using the softwares NEB Cutter V 2.0 and Generunner and were synthesized by Imperial Life Sciences(ILS). The sequences of the primers used in this study are shown in Table 3.4. Each primer was resuspended in nuclease free water as a stock solution at 100 μM and working stocks were made from these at 10 μM with nuclease free water .Table 3.2: Primers used in this study

Sl. No	Name	Primer sequence
1.	FPThx2	5`-GCCATGGCCGAGATCGCGCCGCTGCGCGTACAGCTGATC-3`
2.	RPThx2	5`- CCTCGAGTCACGCTTCTGTCGCCAGCGGGGAG -3`

3.9 Selection of medicinal plants:

The medicinal plants were selected on the basis of their use in traditional medicine. The plants were collected from Sonitpur District (Assam), East Khasi Hills District (Meghalaya).

Extracts of the plant samples were prepared using ethanol. The different parts of the plants which are used in traditional medicine were air dried to obtain a consistent weight. The powdered samples were extracted in ethanol by maceration for 72 hours and were passed through Whatman filter paper no.1.The filtrates obtained were dried *in vacuo* using rotatory vacuum evaporator and weighed to calculate the yield . The standard solution at the concentration of 20mg/ml were prepared in sterile 1% DMSO [298].The following plants were screened for their antimycobacterial properties.

3.9.1 *Binomial name: Cynodon dactylon* L.

Scientific Classification:

Kingdom: Plantae

Order: Poales

Family: Poaceae

Genus: *Cynodon*

Species: *C. dactylon*

The blades are rough edged and short with an average length of 2–15 cm. The color of the blades is grey-green. The stems are erect, flattened, often tinged purple in color and can grow 1–30 cm tall. *C. dactylon* can reproduce through seeds, runners, and rhizomes. The seed heads are produced at the top of the stem in a cluster of two to six spikes together. It possesses a deep root system and the grass creeps along the ground forming a dense mat wherever a node touches the ground. Optimum growth of the grass is between 24 and 37 °C .In winter, the grass becomes dormant and turns brown [257].

3.9.2 Binomial *name: Chromonaela odorata* L.

Scientific Classification:

Kingdom: Plantae

Order: Asterales

Family: Asteraceae

Genus: *Chromolaena*

Species: *C. odorata*

C. odorata is a multi-stemmed perennial herb with an average height of 2.5 m tall. It possesses soft stems , however, the base is woody. It becomes etiolated and behaves as a creeper in shady areas and can attain a height of 10 m. The plant is hirsute and glandular. The leaves are 4–10 cms long by 1–5 cms wide, opposite, triangular to elliptical with serrated edges and give off a pungent, aromatic odour . Petioles are 1–4 cms long. The inflorescences are panicle and consist of white to pale pink tubular 10 to 35 flowers at the ends of branches. The seeds are achenes and hairy

and mostly spread by the wind, but can also cling to fur, clothes and require light to germinate. A plant produces about 80000 to 90000 seeds. The plant can also regenerate from the roots.

Fig.3.3: Pictogram of the medicinal plants .

3.9.3 *Binomial name: Glycine max* L.

Scientific Classification:

Kingdom: Plantae

Order: Fabales

Family: Fabaceae

Subfamily: Faboideae

Genus: *Glycine*

Species: *G. max*

The height of the plant varies 0.2 to 2.0 m .The pods, stems, and leaves are hirsute. The leaves are trifoliolate, with three to four leaflets. The average size of the leaflets is 6–15 cm in length and 2–7 cm in breadth. The self-fertile flowers are white, pink or purple in color and borne in the axil of the leaf .The pod grows in clusters of three to five and is 3–8 cm long. It contains two to four seeds which are 5–11 mm in diameter [258].

3.9.4 *Binomial name: Lawsonia inermis* L.

Scientific Classification:

Kingdom: Plantae

Order: Myrtales

Family: Lythraceae

Genus: *Lawsonia*

Species: *L. inermis*

It is a tall shrub, with a height of 1.8 to 7.6 m. The plant is glabrous, multi-branched and have spine-tipped branchlets. The leaves are opposite, glabrous, sub-sessile, elliptical, and lanceolate with average dimensions of 1.5–5.0 cm x 0.5–2 cm. The flowers possess obvate petals with white or red flowers, four sepals, a 2 mm calyx tube, with 3 mm spread lobes. Fruits are have brownish capsules and are 4–8 mm in diameter and contain 32–49 seeds per fruit.

3.9.5 *Binomial name: Mimosa pudica L.*

Scientific Classification:

Kingdom: Plantae

Order: Fabales

Family: Fabaceae

Subfamily: Mimosoideae

Genus: *Mimosa*

Species: *M. pudica*

The plant has slender stem, branching, and sparsely to densely prickly and can grow to a length of 1.5 m . The leaves are bipinnately compound with one or two pinnae pairs and each pinna has about 10–26 leaflets. The pale pink or purple flower heads are pedunculate arising from the leaf axils and are globose to ovoid heads with a size varying from 8–10 mm in diameter (excluding the stamens). The fruit comprises of clusters of 2–8 pods which are 1–2 cm in length containing pale brown seeds some 2.5 mm long. The flowers are pollinated by the wind and insects.

3.9.6 *Binomial name: Potentilla fulgens* L.

Scientific Classification:

Kingdom: Plantae

Order: Fabales

Family: Rosaceae

Subfamily: Rosoideae

Tribe: Potentilleae

Genus: *Potentilla*

Species: *P. fulgens*

The perennial herb is erect with the average height of 15 to 75 cm. The leaves are pinnate and have both radical and cauline leaves. The radical leaves are 4-30cm in length , with serrated margins and have abaxial white surface The cauline leaves abaxially white with serrated margins. The flowers are yellow in color and 1-2 cm in diameter. The plant reproduces by rhizomes and seeds [259,260].

3.9.7 *Binomial name: Platycladus orientalis* L.

Scientific Classification:

Kingdom: Plantae

Order: Pinales

Family: Cupressaceae

Genus: *Platycladus*

Species: *P. orientalis*

It is a small tree with the height ranging between 15-20 ml and 0.5 m trunk diameter. It is a slow-growing tree. The scale-like leaves are 2-4 mm long and the green colored cones are 15-25 mm which become brown in color when ripe. The

cones have 6-12 thick scales arranged in opposite pairs and possess seeds with no wing and are 4-6 mm long [261].

Methods

3.10 Antibacterial assay

The assay was conducted by agar well diffusion method. The bacterial strains grown on MHB at 37°C for 18h were suspended in a saline solution (0.85% NaCl) and adjusted to a turbidity of 0.5 Mac farland standards (10^8CFU/ml). The suspension was used to inoculate 90mm diameter petri. Wells (6mm diameter) were punched in the agar and 50µL of 20mg/mL extracts or nanocomposites. The dissolution of the organic extracts (Ethanol) was aided by water, which did not affect the growth of microorganisms , in accordance with the control experiments. Plates were incubated in air at 37°C for 24h. Antibacterial activities were evaluated by measuring inhibition zone diameters. The experiments were conducted thrice. DMSO was taken as control for aqueous extracts.

3.11 MTT (3-(4,5-dimethylthiazol-2-yl)-2,5-diphenyltetrazolium bromide) Assay

MIC was determined using microdilution method .Bacterial strains were cultured in MHB2 media. Stock solution of the extract/nanocomposites were prepared at a concentration of 10 mg/ml. Various concentrations of the extract were prepared by serial dilution. 100 µL of extract/nanocomposites of each concentration was added to the respective wells serially followed by the inoculation of 100µL of the bacterial inoculum corresponding to 0.5 Mc Farland Standard into each well. Streptomycin was taken as the positive control while DMSO 1% was the negative control. The plates were then incubated at 37°C for 16hours. After the incubation period was over, 40 µL of MTT solution (0.2 mg/ml) was added into each well and further incubated at 37°C for 45 minutes for the formation of formazan. The

formazan complexes were dissolved using DMSO and the absorbance was recorded at 550nm [262].

3.12 Colony forming unit (CFU) count

The antibacterial assay of the prepared nanocomposites was assessed with standard Dynamic Shake Flask Method. The number of individual bacterial colonies growing on the samples inoculated with the nutrient agar and incubated at 37 °C was determined to find out the CFU. All the test strains were cultured in Mueller Hinton Broth media at 37° C for 18 h. The bacteria were then suspended in an isotonic solution of 0.85% NaCl to adjust the McFarland standard of the cells to a turbidity of 0.5 corresponding to approximately 1×10^8 CFU/mL. The prepared nanocomposites (50 mg/mL) were dissolved in DMSO (10% v/v), filter-sterilized through a 0.22-μm membrane filter and inoculated with bacterial suspension for 24 h at 37°C at 200rpm. The HBPEA film was used as the reference, while the bacterial inoculum without the films served as the experimental control. The reported results were averaged over a set of three independent experiments.

3.13 Total protein content

The total protein content of the bacteria that were adhered onto the film surface was estimated according to the method described by Bradford. 200 μL of (1 g/mL) bovine serum albumin (BSA) standard was mixed with 1.25 mL of Bradford reagent and the absorbance was measured at 595 nm. A standard curve of the absorbance at 595 nm versus protein concentration (mg/mL) with correlation coefficient (R^2=0.9997) was plotted and then the absorbance of the bacterial adhered film was also measured at the same wavelength. The total protein content was estimated using the following linear fit equation:

$$\mathbf{Y=0.2658X}$$

where Y is the absorbance and X is the protein concentration.

3.14 Nanocomposite-bacteria interaction.

The release of cytoplasmaic constituents, such as DNA and RNA of the microbial cells upon interaction of the same with the nanocomposites was monitored by their UV absorption at 260 nm. This study is represented as the optical density (OD) ratio of the tested bacterial suspension with nanocomposite to a bacterial suspension without the nanocomposites.

3.15 Reactive oxygen species (ROS) measurement.

The toxicity of the nanocomposites was evaluated by the ferric reducing ability of , FRAP, assay using ascorbic acid as the positive control. The specific conditions for this assay is as follows: 300 μL of FRAP reagent (acetate buffer+2,4,6-35 tripyridyl-s-triazine+FeCl3.6H2O) was added to 10 μL of nanocomposite followed by dilution with 30 μL of water. The change in the absorbance at 593 nm with and without nanocomposite quantifies the amount of quenched ROS.

3.16 Isolation and culturing of PBMC

The PBMC were separated from the goat blood by sedimentation technique (density gradient centrifugation) using histopaque. The blood was collected in sodium citrate and diluted in 1:1 ratio with phosphate buffer saline (PBS,Appendix) at pH 7.4. Differential migration of different cells in the blood during centrifugation resulted in the separation of the same into different layers. The blood was then layered with a Pastuer pipette on histopaque in 3:2 ratios in a wide transparent centrifuge tube. The bottom layer contained histopaque-aggregated red blood cells, followed by a diffuse layer containing granulocytes and unbound histopaque with PBMC fraction sandwiched at the interface between the unbound histopaque and uppermost plasma/platelet layer. The interface was collected after centrifugation at 400×g for 15 min and transferred to serum free DMEM (Dulbecco's Modified Eagle Medium). The diluted cell suspension was subjected to multiple washes in 20 mL serum free media at 70×g for 10 min. The final pellet of PBMC was resuspended in 2 mL of serum free medium. The PBMC were cultured for 2 h in RPMI-1640 medium supplemented with 10% fetal calf serum, antibiotic Penicillin-Streptomycin-

Neomycin solution and incubated in a humidified 95% O antibiotic Penicillin-Streptomycin-Neomycin solution and incubated in a humidified 95% O_2 with 5% CO_2 atmosphere at 37 °C.

3.17 *In vitro* biocompatibility assay

The biocompatibility of the pristine and nanocomposite films was evaluated using mammalian blood derived PBMC. The *in vitro* assessment of cell membrane integrity and proliferation of the PBMC onto the prepared films was determined by trypan blue exclusion assay by the following method. In this test, cells adhered onto the film surface were stained with 0.4% trypan blue solution in PBS (pH 7.4). The visual distinction between unstained viable cells and blue-stained nonviable cells was done using microscope at 20X magnification. The unstained cells as the viable cells were counted by help of a haemocytometer after an incubation period of 3 min. The percentage of viable cells was calculated using the following equation:

% of viable cells= (Number of unstained cells/total number of cells) × 100

3.18 Cytotoxicity assay

RAW264.7 were used for assaying the cytotoxicity of the plant extracts and PBMC were used for assaying the cytotoxicity of the nanocomposites . The cells were seeded onto 96-well microplates at the density of 1×10^4 cells/well and incubated at 37 °C under 5% CO_2 in water-saturated atmosphere and allowed to grow for 2 h. The metabolic activity of the viable cells was determined by using colorimetric MTT assay. The test samples were added into each microplate followed by incubation under the same conditions for 18 h. MTT was added to the seeded wells at different time intervals of 0, 1, 12, 24 and 48 h followed by 4 h incubation under the above conditions. The absorbance of the above cultured media was then recorded spectrophotometrically at 550 nm. The untreated cells were taken as the control and the experiments were performed in triplicates.

3.19 Scanning Electron Microscopy

Scanning electron microscopy was used to study the morphological changes induced in the cells by the plant extracts/nanocomposites at the MIC. The samples for the microscopy were prepared using the method of Roy et al.,2011[263]. In case of bacterialstrains the inoculum was adjusted to 0.5 Mc Farland standard and suspended into 4ml of sterile 10 mM sodium phosphate buffer, pH 7.4, followed by a treatment with the plant extract/ nanocomposites at MIC for 6 hours at 37°C. PBMCs grown on nanocomposite films and the bacteria were then fixed overnight at 4°C with 2.5 %(v/v) glutaraldehyde. After fixation the cells were mounted on coverslips using Poly-L-Lysine. The cells were rinsed with 10mM sodium phosphate buffer at pH7.4, and subjected to serial dehydration through an ethanol series for 15 min each .The samples were dried at room temperature and coated with10–15nmthickness of platinum using a JEOL1600 Auto Fine Coater. The samples were then examined under the SEM with an accelerating voltage of 10–15 kV (JEOL6390).

3.20. Ethidium bromide exclusion assay

0.2 μg of pET-32α(+) plasmid DNA (5.9 kB), isolated by standard protocol from *E. coli* DH5α and was treated with 0.1 μg, 0.8 μg, 1.3 μg and 1.4 μg of each of the samples. The complexes were allowed to interact for 1 h at 37 °C. The untreated plasmid DNA was taken as the control. The electrophoretic mobility shift (if any) of the plasmid DNA was analyzed by loading the complex mixtures in 1% agarose gel in TAE buffer containing ethidium bromide (EtBr). The gel was run for 90 min at 7 V/cm and photographed under UV light to check for EtBr exclusion.

3.21. Total phenols content assay

The total polyphenolic content of the plant extracts were determined using the modified Folin-Cioclateu method [264].An aliquot of the extract to a final

concentration of 0.1 mg/ml was added to diluted (1:10 v/v) 5 ml Folin-Ciocalteu reagent and 4 ml (7.5 %) of sodium carbonate. The tubes were vortexed and incubated for 30 minutes at 40°C. Absorbance was then measured at 765 nm using the (Cecil spectrophotometer). Total phenolic content was expressed as mg/g Gallic acid equivalent (GAE) using the following equation based on the calibration curve: **y=0.19 x, R^2=0.961,** where x is the absorbance and y is the gallic acid equivalent (mg/g).

3.22 Total flavonoids content assay

The total flavonoid assay was performed using quercitin as a standard [265]. 100µl of 1M potassium acetate and 100µl of 10% Aluminium nitrate was added to 1ml of the plant (1mg/ml) extracts. The total volume was made upto 5ml by addition of methanol and was incubated for 40mins at room temperature. The absorbance was recorded at 420 nm. Total flavonoid content was expressed as mg/g Quercitin equivalent (QE) using the following equation based on the calibration curve:

y=0 .01x, R^2=0.94,where x is the absorbance and y is the Quercitin equivalent (mg/g).

3.23 Hemocompatibility Test

Goat erythrocytes served as mammalian erythrocyte model for the assay haemolytic activity of the plant extract [266]. Goat blood was collected into heparinized tubes and centrifuged at 3000rpm for 20 mins at 4°C. The erythrocytes were washed in sterile 10mM Phosphate Buffer Saline (PBS) (pH 7.4) and centrifuged at 3000rpm for 10mins at 4°C. The packed erythrocytes were suspended with PBS to obtain a 5% haematocrit. Catalase activity was inhibited by addition of 1mM NaN_3 to the 5% haematocrit and incubation for 10 minutes at 37°C. 5mg/ml of stock solution of plant extract in sterile PBS was prepared and incubated with the haematocrit at the concentration of 0.039mg/ml to 1.25mg/ml and incubated for 60 mins at 37 °C. The cells were then centrifuged at 3000rpm for 10 mins at 4 °C.

Supernatants were used for determining haemoglobin concentration as a measure of haemolysis by taking absorbance at 540nm. Haemolysis caused by PBS and 1% (v/v) Triton X-100 were used as 0 and 100% controls respectively.

3.24 *In silico* investigation

3.24.1 Molecular Docking

Molegro Virtual Docker (MVD) 5.0 (Molegro ApS, Aarhus, Denmark) was used for the Molecular Docking studies. It is an integrated environment for studying and predicting how ligands interact with macromolecules. MVD performs a flexible ligand docking, therefore, the optimal geometry of the ligand is determined during the docking. The MolDock scoring function (MolDock Score) used by MVD is derived from the PLP . The MolDock scoring function further improves these scoring functions with a new hydrogen bonding term and new charge schemes. The docking scoring function, *E score*, is defined by the following energy terms:

$$E_{score} = E_{inter} + E_{intra}$$

The prediction of the binding affinities, different binding modes and orientation of the compounds in the active site(s) of the target proteins were determined by the scoring functions of the ligands and the H-bonds formed with the amino acids. The cavity detection algorithm in MVD was used for optimizing the potential binding site and water molecules were not taken into account for this study. A set of 100 runs was given for each docking study using 2000 interactions to calculate the Rerank score and the MolDock . The ligands were generated in CHEM OFFICE 2002.

3.24.2 Selection of the target proteins

The structure of the target protein (Thy X) was downloaded from the Protein Data Base (http://www.rcsb.org/pdb/explore/explore.do?structureId=2GQ2).

3.24.3 QSAR studies

DFT based Quantitative Structure Activity Relationship (QSAR) analysis using Multiple Linear Regression (MLR) has been attempted to relate the structural features of these chalcone molecules that may have an influence on their observed antimycobacterial activity.

3.24.3.1. Theoretical background

In theoretical chemistry, the chemical potential (μ) is identified as the negative of the electronegativity (χ) by Iczkowski and Margrave [267] and defined as:

$$\chi = -\mu = -\left(\frac{\partial E}{\partial N}\right)_{v(\vec{r})} \qquad (1)$$

The quantitative definition of hardness (η) of an N-electron system with total energy E and external potential $v(r)$ using density functional theory can be expressed as:

$$\eta = \frac{1}{2}\left(\frac{\partial^2 E}{\partial N^2}\right)_{v(\vec{r})} = \frac{1}{2}\left(\frac{\partial \mu}{\partial N}\right)_{v(\vec{r})} \qquad (2)$$

and the global electrophilicity index (ω) is expressed in terms of chemical potential and hardness as:

$$\omega = \frac{\mu^2}{2\eta} \qquad (3)$$

According to the finite difference approach, global hardness and chemical potential can be approximated as:

$$\mu = -\left(\frac{IP + EA}{2}\right) \tag{4}$$

$$\eta = \frac{IP - EA}{2} \tag{5}$$

where, IP and EA are the first vertical ionization potential and electron affinity, respectively, of the chemical system.

Further approximation using Koopmans' theorem [268], the above parameters can be expressed by taking IP and EA as negative of the HOMO and LUMO energies, respectively.

$$\mu = \frac{E_{LUMO} + E_{HOMO}}{2} \tag{6}$$

and

$$\eta = \frac{E_{LUMO} - E_{HOMO}}{2} \tag{7}$$

where, E_{LUMO} is the energy of the lowest unoccupied molecular orbital and E_{HOMO} is the energy of the highest occupied molecular orbital.

3.24.3.2 Computational details

Structures of all chalcone molecules are presented in Fig.3. 2. Full unconstrained geometry optimizations of these compounds were carried out using $DMol^3$ program [269]. The most widely used exchange-correlation functional suggested exchange potential by Becke [270] with gradient corrected correlation provided by Lee, Yang and Parr [271] (BLYP) was used in combination with double numerical with polarization (DNP) basis set to study chalcones derivatives. DNP is the double numerical with polarization basis set, size of which is comparable to 6-31G** basis of Hehre et al. [272].However, it is believed to be much more accurate than a Gaussian basis set of the

same size. Optimized geometries were verified by frequency calculations and characterized as minima (no imaginary frequency) in their potential energy surface. The reactivity descriptors electrophilicity index (ω), chemical potential (μ), and global hardness (η) were calculated for all systems using eqs.3, 6 and 7, respectively. The Conductor-like Screening Model (COSMO) [273] as incorporated into the $DMol^3$ program with dielectric constant of 78.4 was adopted to study the solvent (water) effect. In addition, the molar refractivity (MR), van der Waals surface area (SA), volume (V), mass (M) and lipophilicity index (logP) for whole molecule were calculated from the MM+ computations with Hyperchem software [274].

3.24.3.3 QSAR modeling

The analysis was performed selecting different descriptors such as, energy of highest occupied molecular orbital (E_{HOMO}), energy of lowest unoccupied molecular orbital (E_{LUMO}), energy of the next lowest unoccupied molecular orbital (E_{NL}), energy difference between LUMO and HOMO (Δ_{L-H}), dipole moments, electrophilicity (ω), hardness (η), etc. Molecular mechanics (MM) parameters such as van der Waals surface area (SA), molecular volume (V), hydrophobicity, polarizibility, molar refractivity were also calculated. Subdivision of the flavonoid molecules into submolecular fragments have been suggested [275] for a more informative approach relationship model.

In QSAR modeling based on the reports that different moieties of flavonoid scaffold being responsible for antioxidant activity and inhibition of Reactive Oxygen Species (ROS) production in enzymatic and whole cell system [276, 277]. Therefore, we also subdivided the chalcone molecules into Ring A and Ring B to calculate the molar refractivity of the groups at the carbon position 4 and Carbon position 4′ of Ring A and Ring B, respectively.

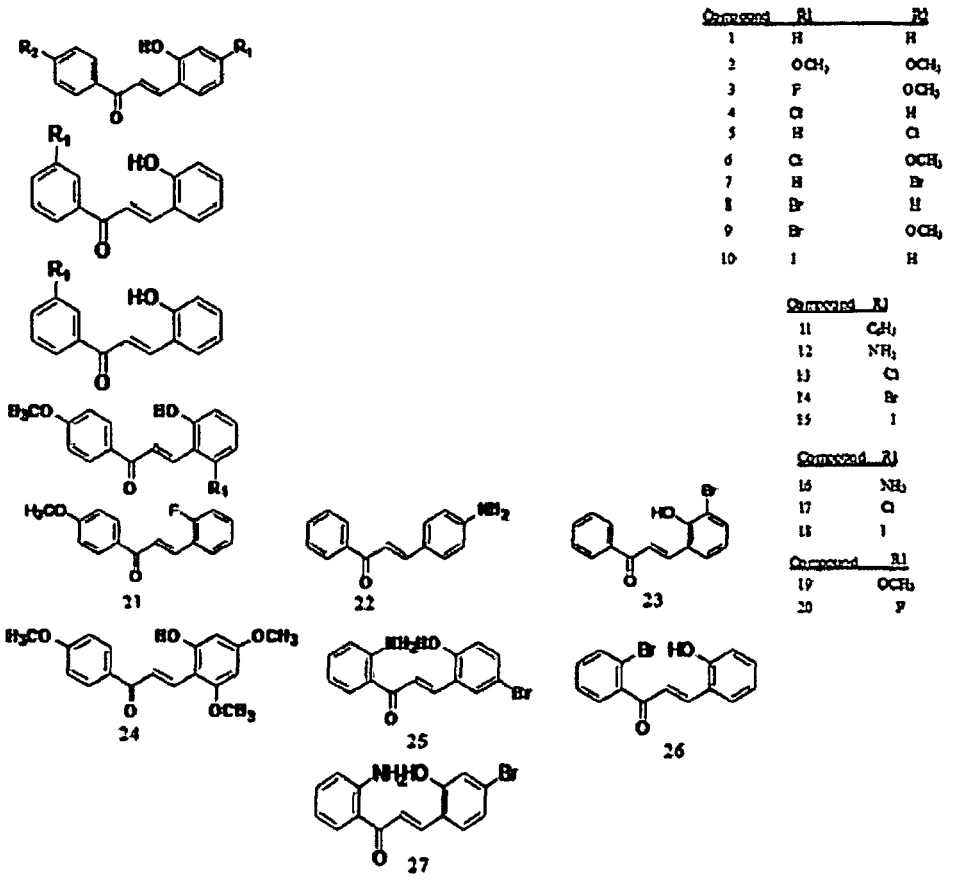

Fig 3.4: Sketch of the chalcones used tobuild quantitative structure–activity

The antimycobacterial activity data of the chalcone molecules 1-27 against *Mycobacterium tuberculosis H37Rv* determined by BACTEC method were taken from the results reported by Lin et al., 2002 [278]. The analyses of the 27 molecules were performed in both gas phase and solvent phase. Multi-linear Regression was performed by those descriptors which showed greater correlation to the % inhibition of *M. tuberculosis H37Rv* at a concentration of 12.5μg/ml and smaller autocorrelation were selected out. Four parameter QSAR was performed using the least square error estimation [279] to calculate and compare bioactivity of the molecules. The quality and predictability of the QSAR models were determined using the "leave one out" (LOO) cross validation method.

3.25 DNA Isolation, Purification and Quantification

The chromosomal DNA of *Mycobacterium smegmatis* was performed using MB545 Mycobacterium tuberculosis DNA Extraction Kit (HIMEDIA).5 ml of the culture media was inoculated and incubated for 16 hours at 37°C. The culture was centrifuged for 3 minutes at 4,000x g. The culture medium was removed and discarded. The pellet was resuspended thoroughly in 250 µl of Lysis Solution (AL) (DS0015) and incubated in 80°C oven for 60 minutes . The Mycobacterium spp. suspension was added to the HiBead Tube (DBCA04) provided and mixed by vortexing. The tubes were centrifuged at 13,000 x g for 1 minute at room temperature. The supernatant was transferred to a new 2.0 ml collection tube and 25 mg of Lysozyme (MB098) and 25 µl of the Proteinase K solution (20 mg/ml) (MB086) was added.The sample was mixed and incubated for 2 hours at 37°C followed by the addition 20 µl of RNase A solution (DS0003) and incubate, vortexed thoroughly (about 15 seconds), and incubated at 70°C for 10 minutes. 200 µl of ethanol (95-100%) was added to the lysate ,mixed thoroughly by vortexing for 15 seconds. The lysate obtained was transferred into HiElute Miniprep Spin column and centrifuged at 6,500 x g for 1 minute. The flow-through liquid was discarded and the spin column was placed in a new 2.0 ml collection tube. 500 µl of Prewash Solution was added to the HiElute Miniprep Spin column and centrifuged at 6,500 x g for 1 minute. The flow-through liquid was discarded and 500 µl of Wash Solution added to the column followed by centrifugation for 3 minutes at maximum speed 13,000 x g. 100 µl of the Elution Buffer (ET) (DS0040) was directly added into the column without spilling and incubate for 1 minute at room temperature. The DNA was eluted by centrifugation at 6,500 x g .

3.26 Purification of plasmid DNA

Two methods were used for the isolation of plasmid DNA in this study; phenol/chloroform extraction (section 3.20.1) and QIAGEN Plasmid Miniprep Kit (QIAGEN, section 3.20.2).

3.26.1 Phenol/chloroform extraction

Single colonies were picked from LB agar plates and inoculated in 2 mL LB broth in 15 mL polypropylene tubes with ampicillicin (Table 2.3) and cultured overnight (section 2.3). A 1.5 mL of the overnight culture was transferred to microfuge tubes and centrifuged at 13, 000 x g for 30 seconds (all subsequent centrifugation steps were carried out at 13, 000 x g). The pellets was resuspended in 100 µL cold Alkaline Lysis Solution I (Appendix) by vigorous vortexing. Approximately 200 µL of freshly prepared Alkaline Lysis Solution II (Appendix) was added to the bacterial suspensions and mixed via inverting the tube. 150 µL of cold Alkaline Lysis Solution III (Appendix) was added to the lysate, mixed via inverting the tubes, incubated on ice for 3 minutes and centrifuged for 5 minutes. One volume of phenol: chloroform (1:1) was added to the supernatant, mixed via vortexing then centrifuged for 2 minutes. This step was repeated with chloroform. The aqueous layer was transferred to fresh microfuge tubes and 2.5 volumes of cold 99% ethanol was added to these. The solution was mixed via vortexing and allowed to stand at room temperature for 2 minutes before it was centrifuged for 5 minutes. The supernatant was removed and all drops of fluid were removed by inverting the tubes on a Kimwipe. About 200 µL of cold 70% ethanol was added to the pellets, inverted several times and centrifuged for 2 minutes. The supernatant was removed and the tubes were stored at room temperature until all the ethanol evaporated. The nucleic acid was resuspended in 50 µL TE buffer (Appendix) and stored at -20°C.

3.26.2 QIAGEN Plasmid Miniprep Kit

QIAGEN Plasmid Miniprep Kit was used to isolate plasmids following the

manufacturer's instruction. A single colony from a freshly streaked selective plate was inoculated as a starter culture of 5ml LB medium containing 50ug/ml .Ampicillin was used as the selective antibiotic. The culture was then incubated for approximately 8h at 37°C in an orbital shaker (Scigenics) at 300rpm.The starter culture was diluted to 1/500 to 1/1000 into 3 ml selective LB medium and incubated at 37°C for 12–16h in an orbital shaker at 300rpm.The bacterial cells were harvested by centrifugation at 6000xg for 15 min at 4°C. The bacterial cells were resuspended in 0.3ml of Buffer P1 followed by the addition of 0.3 ml of Buffer P2 and mixing thoroughly by vigorously inverting the sealed tube 4–6times. The tubes were incubated at room temperature (15–25°C) for 5min. 0.3 ml of chilled Buffer P3 was added to the tubes and mixed immediately and thoroughly by vigorously inverting4–6times, and incubated on ice for 5min. The tubes were centrifuged at maximum speed in a microcentrifuge for 10min followed by the prompt removal of the supernatant containing plasmid DNA. The QIAGEN-tip20 was equilibrated by applying 1ml Buffer QBT, and allowing the column to empty by gravity flow. The supernatant was applied to the QIAGEN-tip 20 and allowed to enter the resin by gravity flow. The QIAGEN-tip20 was washed twice by 2ml of Buffer QC and the DNA was eluted with 0.8ml Buffer QF. The eluted plasmid DNA was precipitated by adding 0.7 volumes (0.56 ml per 0.8 ml of elution volume) of room-temperature isopropanol followed by mixing and centrifugation immediately at 15,000xg for 30 min in a microcentrifuge. The supernatant was decanted. The plasmid DNA pellet was the washed with 1ml of 70%ethanol and centrifuged at 15,000xg for10min. The pellet was air-dried for 5–10min, redissolved in 50 ul of TEbuffer,pH8.0 and stored at -20°C for further use.

3.27 PCR Purification

PCR purification was done using QIAGEN PCR Purification Kit. 5 volumes of Buffer PB was added to 1volume of the PCR sample and mix. The sample was applied to the QIAquick spin column placed in a 2 ml collection tube and centrifuged for 1min at 10,000xg. The flow-through was discarded and placed in the QIAquick column back into the same tube. To wash 0.75 ml Buffer PE was added to

the QIAquick column and centrifuge for 1min and the flow-through was discarded. The QIAquick spin column was centrifuged for an additional 1 min. The QIAquick column was placed in a fresh 1.5 ml microcentrifuge tube and the DNA was eluted by addition of 50 µl Buffer EB (10 mM Tris·Cl, pH 8.5) and centrifuging the column for 1min. The purified DNA was stored at -20°C for further use.

3.28 Gel purification of DNA

The DNA fragment was purified from gel using QIAGEN Gel Purification Kit. The DNA band was excised from the agarose gel with a clean, sharp scalpel and weighed. 3 volumes of Buffer QG was added to 1 volume of gel and incubated at 50°C for 10 min . 1 gel volume of isopropanol was added to the sample and mixed. A QIAquick spin column was placed in the provided 2 ml collection tube and the sample was applied to the QIAquick column, and centrifuge for 1 min at 10,000rpm. The flow-through was discarded and the QIAquick column was placed back in the same collection tube. To wash , 0.75 ml of Buffer PE was added to the QIAquick column and centrifuge for 1 min. The flow-through was discarded followed by centrifugation for an additional1min at 17,900 x g (13,000 rpm).

The QIAquick column was placed into a clean 1.5 ml microcentrifuge tube and 50µl of Buffer EB(10mMTris·Cl,pH8.5) was added to the center of the QIAquick membrane and centrifuged the column for 1 min to elute the DNA. The purified DNA was analyzed on a gel and the rest was stored at -20°C for further use.

3.29 DNA quantification

All nucleic acid was quantified using THERMO Spectrophotometer (THERMO). Deionized water was used as blank. The solution. DNA was dissolved in deionized water .

3.30 Genetic Manipulation

3.30.1 Polymerase Chain Reaction (PCR)

PCRs were performed using GeneAmp* PCR system 9700 (Applied Biosystems) in PCR tubes. To isolate the *thy x* gene from *M. smegmatis* , primers were designed to bind specifically to the 5′ and 3′ ends of the *MSMEG_2683* gene. The forward primer (2p1) contains an *NcoI* site and the reverse primer (2p2) an *Xho I* site, both of which are just 5′ of the respective *thy x* binding sequences. The *M. smegmatis thy x* gene was then isolated by PCR amplification from the genomic DNA. PCR conditions involved an initial denaturation step at 95°C for 3 min, then 35 cycles of denaturation at 94°C for 15 s, annealing at 60°C for 20 s, extension at 68°C for 1.5 min,and a final extension of 68 °C for 10 min. The PCR product was gel-purified using the Gel Purification Kit indicated above.

Table 3.3: Reagents and concentrations used with Taq DNA Polymerase /Reagent

Reagents	Stock conc.	Final conc.
Primer_ FPThx2	10 µM	0.4 µM
Primer_ RPThx2	10 µM	0.4 µM
Buffer	10x	1x
Long Taq	250 U	1U
$MgCl_2$	25 mM	1.5 mM
DNA Template	200 ng/uL	40 – 80 pg

3.30.2 DNA ligations

T4 DNA ligase was used in this study. TA cloning of PCR fragments was carried out using the T4 DNA ligase supplied with the InsTA clone PCR Cloning Kit . Ligation reaction in case of cohesive end ligations (Table 3.4), were carried out using T4 DNA ligase purchased from Thermo Scientific . The negative control with

no vector were run for both TA ligation reactions and cohesive end ligation reactions. To identify the percentage of false positives in the transformations, cohesive end ligation reactions had control with the digested but unligated vector .

Table 3.4: Reagents and concentrations used for ligation

Reagents	Stock conc.	Final conc.
T4 DNA Ligase	10 U/µL	0.5 U/µL
Primer_ RPThx2	10 µM	0.4 µM
Ligation Buffer	10x	1x
ATP solution	10 x	1 x
Vector	10 – 20 ng/µL	10 ng
Insert	50 – 200 ng/µL	90 ng

3.30.3 Transformations into *E. coli*

E. coli was transformed with vectors and ligation reactions into calcium competent cells (section 3.24.3.1) with heat-shock (section 3.24.3.2).

3.30.3.1 Preparation of calcium competent cells

Single colony of the strains *E. coli* DH5α and *E. coli BL21(DE3)pLysS* from the overnight plates were inoculated into 10 mL LB broth in 50 mL culture tubes and cultured overnight . The overnight cultures were sub-cultured in 100 mL LB broth and incubated in an orbital shaker at 200 rpm until the optical density at 600 nm (OD600) reached ~ 0.5. The OD600 of the cultures were measured in 1cm path length cuvettes using a Thermo Spectrophotometer. The cells were incubated in ice for 30 minutes. The cells were harvested by centrifugation at 4, 000 x g for 10 minutes at 4°C (all subsequent centrifugation steps were carried out at 4, 000 x g for 10 minutes at 4°C). The supernatant was discarded and the pellet was resuspended in 50 mL cold sterile 0.1 M $CaCl_2$ The cells were incubated on ice for 20 minutes and

recovered by centrifugation and resuspended in 2 mL cold sterile 0.1 M CaCl2 with 14% glycerol. 50 µL aliquots of the cells were stored into 1.5 ml microfuge tubes and were used for heatshock transformations (section 3.24.3.2)

3.30.3.2 Heat-shock transformation

150 µL cold sterile 0.1 M CaCl2 was added to the cells and 10 µL of the ligation reactions or 50 ng/µL of purified plasmid DNA were added to the calcium competent cells , incubated on ice for 20 minutes and heat-shocked at 42°C on a preheated 42°C circulating water bath for 90 seconds. After heat-shock the tubes were further incubated on ice for 5 minutes and 800 µL LB broth were added to the cells. The tubes were incubated at 37°C for 60 minutes in a stationary incubator. After 60 minutes, the cells were harvested at 13, 000 x g for 30 seconds, the supernatant was discarded and the pellet was resuspended in 100 µL media and plated on LB agar plates with ampicillin, IPTG and XGAL (Table 3.1).

3.30.4 Identification of recombinant clones

Colony PCR was used to identify the recombinants clones initially (section 3.24.1). The confirmed clones with the correct inserts were cultured overnight (section 3.3) in LB with ampicillin and the recombinant plasmids were isolated.

3.30.4.1 Colony PCR

The white colonies were used as templates in the PCR reactions with the primers (Table 3.3) following the PCR protocols shown in section (3.3) and the amplified products were analyzed on 1% agarose gels . The presence of the PCR product corresponding to the *thy x gene* verified that the insert was present in the colony. The verified clones with inserts were prepared using the protocols in section 3.24.4.2 for further analysis.

3.30.4.2 Restriction digests

Restriction digestion were performed with the enymes *NcoI* and *XhoI* along with the buffer 4 supplied with the enzyme for double digestion as per manufacturer's

instruction [Double Digest Finder, NEB (http://www.neb.com/nebecomm/doubledigestcalculator.asp)]. 1x BSA was added to the digestion mixture as recommended by the manufacturer. The restriction digestion (Table 3.5) for the analysis of insertions into vectors was made up to a total volume of 10 µL with ddH2O and incubated 1 hour at 37°C. The digested DNA was analysed on an 1% agarose gel .

The restriction digestion performed to extract DNA fragments from TPZ vector and pET32a+ was made up to a total volume of 10 µL with Nuclease free water and incubated 1 hour at 37°C and run on a 1% agarose gel (section 3.25) to separate the extracted DNA fragment from the plasmid DNA before being gel purified (section 3.22).

Table 3.5: Reagents and concentrations used for restriction digests

Reagents	Stock conc.	Final conc.
Restriction Enzyme	10,000 U/µL	0.5 U/µL
NE Buffer 4	10x	1x
BSA	10 x	1 x
Vector	50 – 200 ng/µL	25-100 ng

3.31 Agarose gel electrophoresis

25mL of 1% agarose gels were prepared in 1 x TAE buffer (Appendix) via heating and was mixed with 0.5ug/ml ethidium bromide. It was poured into a gel cast with combs and set at RT for 30 minutes. 5 µL of DNA ladder and DNA with 5x DNA loading buffer (1: 4) were loaded on the gel and ran at 7 V/cm for 90 minutes. Gels were visualized using a High Performance UV transilluminator and recorded.

3.32 DNA sequencing

DNA sequencing was performed by ABI3730xl DNA analyzer (Applied Biosystems). 300 ng of plasmid DNA, 3.2 pmol of the primers and nuclease free

water wasused to make the reaction up to 15µL. The chromatograms received from the sequencing reactions were analyzed using 3730/3730xl Analyzer Data Collection and GeneMapper Software (Applied Biosystems).

3.33 Protein Over-expression, Purification and Quantification

Protein over-expressions were carried out in *E. coli* BL21 (DE3)pLysS with the pET-32a(+) vector. The vectors was cloned with the thyx gene from *M. smegmatis ATCC14468* under the transcriptional control of the T7 promoter for the pET-32a(+) vector .

3.33.1 Expression of recombinant protein in *E. coli* BL21

Single colonies of BL21(DE3)pLysS transformed with recombinant pET-32a(+) cells were picked and inoculated in 5ml LB broth containing Amp and incubated in an orbital shaker at 200rpm at 37°C overnight. The starter culture was then inoculated in 50 ml LB with Amp and grown at 37°C with shaking till O.D at 600 nm reached 0.6-0.7. BL21(DE3)pLysS transformed with pET-32a(+) was taken as control. IPTG was added to the culture to a final concentration of 1 mM and incubated at 37°C. Before addition of IPTG, 2ml of the culture was kept aside which served as uninduced cells. 1 ml of the induced cells were pelleted down at 0, 1, 2, 3, 4 and 5 hours respectively at 5000 rpm for 10 min. The pelleted down cells were lysed with 100 µl of sample buffer (1X SDS gel-loading dye) and run on 12.5% SDS-PAGE gel to confirm overexpression of the recombinant protein.

3.33.2 Protein Over-expression, Purification and Quantification

3.33.2.1 Purification of recombinant protein

Ni-NTA Magnetic Agarose Beads

Cell lysis under native conditions:

The culture was lysed by sonication in presence of lysis buffer(Appendix) .Lysozyme was added at the concentration of 1 mg/ml to the lysate and incubated on ice for 30 min. The lysate was centrifuged at 10,000 x g for 30 min at 4°C.The

supernatant was collected. The Ni-NTA Magnetic Agarose Beads were resuspended by vortexing for 2 s. Immediately 10 µl of the 5% Ni-NTA Magnetic Agarose Beads suspension was added to 200 µl of the 6xHis-tagged protein solution in each well of a 96-well microplate and mixed for 45 min to 1 h. 20 µl 1% Tween 20 was added to each well and mixed for 15 min. The 96-well microplate was placed on the 96-Well Magnet for 1 min and the supernatant was removed with a pipet. 200 µl of Interaction Buffer was added to each well, mixed, placed for 1 min on the 96-Well Magnet. The buffer was removed. 50 µl of Elution Buffer was added to each well, mixed and incubated for 1 min. The microplate was placed on on the 96-Well Magnet for 1 min and the eluate was collected. The crudely purified protein was subjected to dialysis against 10 mM Tris HCl (pH 7.2), 50 mM NaCl, and 2 m M DTT, and then bound to a Q Sepharose Fast Flow column.

3.33.2.2 Protein quantification

All protein was quantified using the method of Lowry et al,1951[280] . 1mg/ml BSA was taken as the protein standard. Different concentration of BSA was taken in test tubes and the volume was made up to 1ml using distilled water. The test tube with 1 ml distilled water served as blank. 4.5 ml of Reagent I (Appendix)was added and incubated for 10 minutes. After incubation 0.5 ml of reagent II (Appendix) was added and incubated for 30 minutes. The absorbance was measured at 660 nm and the standard graph was plotted . The amount of protein present in the given sample was estimated from the standard graph.

3.33.2.3 SDS-PAGE

About 4.5 mL of 12% resolving gel (Appendix) was casted between gel plates (GE-Lifesciences), covered with 1mL dH_2O and set at RT for 40 minutes. After 40 minutes the dH_2O was decanted off and 4% stacking gel (Appendix) was poured on top of the resolving gel, the comb was put in the stacking gel and allowed to set at RT for 45 minutes. The comb was removed and the wells were washed with dH_2O to remove unpolymerized acrylamide and the gel plates were placed in the gel

tank (GE-Life sciences) and filled with running buffer (Appendix).

1 mL bacterial pellets were resuspended into 100 µL of SDS loading buffer (Appendix) in case of the induction of the recombinant protein and 20 µL of the purified protein was added to 10 µL 3x sample buffer (2:1) () and boiled at 95°C 10 minutes before being loaded onto the gel. 20 µL of samples were loaded in the wells with 5 µL protein molecular weight marker and run at 12 V/cm until the bromophenol blue ran off the end of the gel.

At the end of the run the gel was removed from between the glass plates and stained for 2 hours in coomassie stain (Appendix) on a rocking platform at RT. After staining the gel was destained (Appendix) for 4 hours with one change of destaining solution after every hour. The gel was destained overnight in water and the gel were recorded for analysis.

3.33.2.4 Ion exchange Chromatography

To further purify the recombinant protein HiTrap Q FF prepacked 1mL column (GE Health care) was used for ion exchange chromatography was used. The column was equilibrated with Tris-Cl buffer.The elution was performed by using elution buffer (Appendix). The flow rate was maintained at 1 min/ml and 1.0 ml fractions were collected just after loading the proteins. The fractions containing ThyX were pooled and subjected to dialysis against 50 mM Tris HCl (pH 7.5), 200 mM NaCl, and 10% glycerol.

3.33.2.5 RP-HPLC

The enriched fraction was subjected to purification by HPLC. HPLC was performed on Waters HPLC system with a binary 515 Pump system and a 2489 UV-VIS detector. The semi-preparative reverse phase HPLC column Symmetry C18 (7.8µ x 7), 250mm in length was used for the purification using isocratic elution. The flow rate was maintained at 1 ml/min using mobile phase acetonitrile and water (90: 10, v/v) 10 µl sample was injected at a time and chromatogram was recorded at 278nm.

3.33.2.6 Enterokinase Digestion

The concentration of the fusion protein solution was adjusted to 1.5 mg/ml (pH between 7.0–8.0) with 500 mM Tris-HCl, pH 8.0, 2.0 mM $CaCl_2$, and 1% TWEEN20. Enterokinase was added to fusion protein solution at a ratio of ~0.02 units per 1 mg of fusion protein and mixed. The reaction mixture was incubated at 25°C for 16 hours.

3.33.2.8 TMP synthesis

Approximately 3 µg of ThyX, was added to a mixture of 60 µL mTHF (final 20 mM), 15µL o f 140 µM ,dUMP, 3 µL o f 350 µM FAD , and 1 µL o f 35 µM NADPH and water to give reaction volume of 105 mL. The reaction times varied from 30 to 120 minutes. To isolate the products, the reaction mixture was spun through a Microcon YM-10 centrifugal filter (MWCO = 10,000) at 13,0006g for 5 minutes. An additional 100 Microcon YM-10 centrifugal filter µL o f water was added and the spin was repeated. The deproteinized reaction mixture was run on an HPLC using a HPLC column Symmetry C_{18} with isocratic flow with 5 mM potassium phosphate (pH 7.0), 5 mM tetrabutylammonium dihydrogen phosphate, and 5% (v/v) acetonitrile, while monitoring elution at 260 nm. To assign the elution positions of reactants and products standard solutions of dUMP, TMP, and mTHF were also run.

3.33.2.9 Enzyme Assay (NADPH oxidation assay)

Assay reactions were performed with a final volume of 200 µl, consisted of 200 µM NADPH, 5µM CH_2H_4folate, 5 µM dUMP, 1 mM MgCl, 1 % glycerol, 62.5 µM FAD and 12.5 µ M o f ThyX. The reactions were initiated by addition of NADPH to each well of the Microtiter 96-well clear flat-bottom plate, followed by rapid shaking of the microplate. ThyX activity was determined by following the decrease of A_{340} (due to oxidation of NADPH) that was measured with a reading interval of 30s for duration of 15 min. All assays were recorded by multilabel microplate reader .The primary screen was performed with the ligands dissolved in DMSO, including DMSO alone as low-activity control. The concentration of

screened compounds was 20 μM. All screening reactions were performed in triplicates.

The plots of the reaction velocity (v) versus the substrate concentration (A and/or B) were fit to the Michaelis-Menten equation for a sequential mechanism:

$$v = (Vmax[A][B])/([A][B]+Km^{A}[B]+Km^{B}[A]+Km^{B}Ks^{A}).$$

Ackermann-Potter plots using the equation, Slope= (kcat[S])/([S]+Km) were used to determine the k_{cat} value.

3.33..2.7 Mass Spectrometric Analysis

The methylation of *M. smegmatis* ThyX was determined following the method of Griffin et al., 2005 [241]. A thymidylate synthesizing half reaction which included all the substrates except dUMP was set up. The reaction was incubated for 5 min at 37 °C, followed by the addition of SDS sample buffer. The sample was run on a 10% SDS-polyacrylamide gel and the protein band was excised mechanically and subjected to in-gel trypsin digest. The peptides were extracted following the standard protocol and were analyzed by electrospray ion trap time-of-flight mass spectrometry (LC/MS/TOF) using a Q-Star Pulsar *i* (Applied Biosystems).

ChapterIV

Results and Discussion

4.1. QSAR studies

Flavonoids constitute the largest class of polyphenols and are ubiquitous in plants. They posses the common structure of diphenylpropanes (C6-C3-C6), consisting of two aromatic rings linked through three carbons. Chalcones are the important precursors of flavonoids and isoflavonoids [192] and, recently, have been subjected to great interest for their valuable pharmacological activities, including antioxidant [281], antibacterial [282], antitrypanosomal [283], antileishmanial [284], anticancer, cytotoxic[285] , antidiabetic [286] and anti-inflammatory [287] activities protective against cardiovascular disease [288]. The presence of a reactive α,β-unsaturated keto function in chalcones is found to be responsible for their antimicrobial activity, which may be altered depending on the type and position of the substituent on the aromatic rings [282]. In this work we attempt to identify antimycobacterial flavonoid molecules present in traditionally used medicinal plants of North East India to treat tuberculosis. We have also attempted to establish these flavonoid molecules as inhibitors of mycobacterial Flavin Dependent Thymidylate Synthase (Thy X). In order to identify the molecule descriptors responsible for the antimycobacterial activity of selected chalcone molecules we performed a QSAR study.

QSAR is an in silico method which is being frequently used in the discovery and optimization of novel molecules with affinity toward a target as well as physicochemical characterization of the potential drug molecules [289].The molecular descriptors are used to define the electronic properties of a molecule owing

to the presence of limitations of fundamental physical and chemical laws in direct quantification of biological activity. In this study, we found that DFT-derived descriptors chemical hardness (η), E_{HOMO} and MM+ descriptor, namely molar refractivity (MR), correlates with the antituberculosis activity of the chalcone molecules remarkably in both gas and solvent phases.

		Gas phase					Solvent phase				
No.	% inhibition at 12.5 mg/ml	η	E_{HOMO}	MR_{A-4}	MR_{B-F}	r_J^2	η	E_{HOMO}	MR_{A-4}	MR_{B-F}	r_J^2
1	61	1.255	-5.665	0.89	0.89	0.7459	1.2035	-5.593	0.89	0.89	0.8116
2	32	1.22	-5.205	7.32	7.32	0.7264	1.161	-5.25	7.32	7.32	0.8043
3	63	1.3	-5.635	7.32	0.8	0.7424	1.258	-5.569	7.32	0.8	0.8084
4	89	1.249	-5.782	0.89	5.39	0.7508	1.226	-5.676	0.89	5.39	0.8222
5	67	1.231	-5.746	5.39	0.89	0.7285	1.87	-5.599	5.39	0.89	0.8112
6	57	1.278	-5.648	7.32	5.39	0.7297	1.2365	-5.572	7.32	5.39	0.8051
7	70	1.224	-5.754	8.21	0.89	0.7267	1.2025	-5.588	8.21	0.89	0.8033
8	57	1.252	-5.799	0.89	8.21	0.7306	1.219	-5.644	0.89	8.21	0.8053
9	25	1.275	-5.655	7.32	8.21	0.7449	1.2425	-5.545	7.32	8.21	0.8271
10	21	1.227	-5.752	0.89	12.99	0.7194	1.178	-5.558	0.89	12.99	0.807
11	68	1.128	-5.422	0.89	0.89	0.7488	1.085	-5.366	0.89	0.89	0.8147
12	6	0.905	-4.842	0.89	0.89	0.7309	0.817	-4.754	0.89	0.89	0.7834
13	67	1.192	-5.705	0.89	0.89	0.7275	1.1615	-5.582	0.89	0.89	0.8046
14	68	1.18	-5.693	0.89	0.89	0.7274	1.165	-5.546	0.89	0.89	0.8031
15	51	1.142	-5.614	0.89	0.89	0.7312	1.106	-5.437	0.89	0.89	0.8086
16	11	1.074	-5.189	0.89	0.89	0.7267	0.9785	-5.078	0.89	0.89	0.8039
17	90	1.222	-5.762	0.89	0.89	0.7231	1.192	-5.631	0.89	0.89	0.8024
18	92	1.225	-5.771	0.89	0.89	0.723	1.207	-5.652	0.89	0.89	0.8013
19	75	1.282	-5.365	7.32	0.89	0.7278	1.2015	-5.415	7.32	0.89	0.8169
20	66	1.291	-5.642	7.32	0.89	0.7344	1.252	-5.63	7.32	0.89	0.8102
21	5	1.141	-4.948	0.89	4.22	0.7208	0.9905	-4.868	0.89	4.22	0.7819
22	82	1.271	-5.487	7.32	0.89	0.7291	1.2675	-5.639	7.32	0.89	0.7981
23	79	1.255	-5.824	0.89	0.89	0.7219	1.2455	-5.745	0.89	0.89	0.8013
24	40	1.222	-5.081	7.32	7.32	0.7499	1.1545	-5.21	7.32	7.32	0.8258
25	8	1:103	-5.402	0.89	0.89	0.7692	1.027	-5.144	0.89	0.89	0.8225
26	83	1.234	-5.645	0.89	0.89	0.7225	1.1955	-5.626	0.89	0.89	0.7994
27	12	1.11	-5.383	0.89	8.21	0.705	1.038	-5.147	0.89	8.21	0.787

Table 4.1: Parameters used to build the QSAR models with the jackknife results for gas and solvent phases against *M. tuberculosis*.

The calculated DFT-based parameters such as ω, E_{NL}, E_{LUMO} for the derivation of the QSAR models were analyzed and found that the equations derived by considering the percentage of inhibition at 12.5 μg / mL as a dependent variable

and hardness (η), energy of the HOMO orbital (E_{HOMO}), MR of the group at position 4 of Ring A (MR_{A-4}), and MR of the position 4' of Ring B ($MR_{B-4'}$) as independent variables gave the best correlation in the gas phase and the solvent phase. The gas-phase and solvent-phase models are presented as equations 4.1and 4.2. The descriptors used to build theQSAR model for both gas and solvent phases are presented in Table 4.1.

Gas phase:

$$\textbf{Activity} = -321.01 + 181.44\eta - 31.00\, E_{HOMO} - 1.10\, MR_{A-4} - 3.94\, MR_{B-4'} \quad \text{(Eq:4.1)}$$

$$n=27,\ r^2=0.73,\ F=14.85,\ p<0.05,\ r^2_{cv}=0.56$$

Solvent phase:

$$\textbf{Activity} = -416.84 - 7.01\eta - 89.45E_{HOMO} + 0.02\, MR_{A-4} - 3.01\, MR_{B-4'} \quad \text{(Eq:4.2)}$$

$$n=27,\ r^2=0.81,\ F=22.72,\ p<0.05,\ r^2_{cv}=0.50$$

In the QSAR equations, n is the number of data points, r^2 is square of the correlation coefficient and represents the goodness of fit, r^2cv is the LOO cross-validated r^2 (a measure of the quality of the QSAR model). F is the overall F-statistics for the addition of each successive term, and p is the p values using the F statistics. We have found that the gas-phase r^2 value (0.73) increases (0.81) when calculated in the solvent phase; however, the r^2 cv value is 0.56 in the gas phase and decreases to 0.50 in the solvent phase. The errors of regression coefficients are also found to be less in solvent phase than that of gas phase. These regression models are significant as depicted by the p value <0.05 using the F statistics [290]. The QSAR models had to be further improved as general statistical standards requires $r^2 > 0.80$ [291] and r^2cv > 0.60 [292] for a regression model to be acceptable. Therefore, to improve the overall quality of the regression models, we applied the scheme suggested by Dietrich

et al., 1980 [293]and Cornish- Bowden and Wang ,1978 [294]. In this scheme, a compound is considered as an outlier if its corresponding r^2, called jackknife r^2 (r^2 cv) value obtained from the regression analysis after deleting the compound, is comparatively higher than the other r^2 cv values. Table 1 presents the r^2cv values calculated in gas phase and solvent phase. Although the independent variables are same in both gas and solvent phases, the r^2cv values differed in case of each molecule. In gas phase, it was observed that molecules 4, 11, 24, and 25 possessed higher r^2cv values (0.751, 0.749, 0.750, and 0.769, respectively), whereas in solvent phase, molecules 4, 9, 24, and 25 exhibited high r 2 cv values (0.822, 0.827, 0.826, and 0.823, respectively). These molecules were
considered as outliers, and it was observed that deleting these molecules from the data set lead to the improvement of the statistical parameters in the QSAR models. The QSAR equations after deleting these outliers (4, 11, 24, and 25in gas phase) and (4, 9, 24, and 25 in solvent phase) are as follows:

Gas phase:

$$\textbf{Activity} = -323.18 + 131.62\eta - 42.05\, E_{HOMO} - 0.63MR_{A\text{-}4} - 4.46MR_{B\text{-}4'}$$

$$n=23,\ r^2=0.84,\ F=23.46,\ p<0.05,\ r^2_{cv}=0.70 \qquad \text{(Eq:4.3)}$$

Solvent phase:

$$\%\ \textbf{Inhibition} = -391.68 - 8.82\eta - 85.37\, E_{HOMO} + 0.31MR_{A\text{-}4} - 3.34MR_{B\text{-}4'}$$

$$n=23,\ r^2=0.88,\ F=33.0,\ p<0.05,\ r^2_{cv}=0.67 \qquad \text{(Eq:4.4)}$$

It was observed that the r^2 value increased from 0.73 to 0.84 and 0.81 to 0.88 in gas phase and solvent phase, respectively. The r^2cv value increased from 0.56 to 0.70 in the gas phase and 0.50 to 0.67 in the solvent phase; however, the r^2cv value remained lower in solvent phase as compared to the gas phase. The error of regression coefficient was found to decrease for both gas- and solvent-phase model calculated using jackknife scheme. However, the error of regression coefficient significantly decreases for independent variable, E_{HOMO}, in solvent phase. The t- and

p-values for all the regression coefficients for all the equations were also calculated and are provided in Table 4.2. Although both the QSAR models are significant, the solvent phase was observed to be better than the gas phase–derived model based on the r^2 values. The correlation plots between the experimental and calculated bioactivity values of the chalcones molecules derived from the two QSAR models are shown in Figure 4.1. The plots indicate that these descriptors can be effectively used in the prediction of the bioactivity of the chalcone molecules.

The QSAR models predict that in both gas phase and solvent phase, lower values of E_{HOMO} and MRB-4' relate to greater inhibition of *M. tuberculosis*. However, difference was observed in the dependence of antimycobacterial activity of the chalcone molecules on hardness and MRA-4 when calculated in gas and solvent phases. In gas phase, the antimycobacterial activity increased with the higher values of hardness and lower values of MRA-4 of the molecules as shown by the equations 4.1 and 4.2 The equations 4.3 and 4.4 depicting the antimycobacterial activity of the chalcone molecules in solvent phase, however, predict that decrease in the hardness and increase in MRA-4 of these molecules increase their antimycobacterial activity. The frontier orbital theory states that the energy of the HOMO and LUMO is the important factors that determine the reactivity of a molecule. The QSAR models generated in both gas and solvent phase predict that decrease in the energy of HOMO increased the inhibition activity of the chalcone molecules. It was observed that the presence of a halogen in one of the two rings, irrespective of the position, increased the antimycobacterial activity of the chalcones. This could be attributed to the electronegativity of the halogens which decrease the energy of HOMO by removing the electron density from the r space of the benzene rings [295].The very low values of antimycobacterial inhibitions can be similarly explained by the presence of an electron donating group such as an amino group(-NH2). The lone pair of electrons of nitrogen atom delocalize into the p space of the benzene ring and increase the E_{HOMO} of the molecule [296]. Table 4.1 shows that in both gas and solvent phases, the presence of the amino group in the B ring of the chalcone molecules increases the

E_{HOMO} more as compared to the presence of the amino group in Ring A. However, no such discrete increase in E_{HOMO} was observed owing to the presence of halogens in Ring A or Ring B. Sivakumar et al. [297]] reported the QSAR study of 33 chalcones using robust statistical technique such as genetic function approximation. Their analysis also indicates the importance of hydrogen bond donor and HOMO in the determination of antituberculosis activity of chalcones. The correlation plots between experimental and calculated activity values in gas and solvent media presented in Figure 4.1 indicated that the selected parameters can predict the antimycobacterial activity of the set chalcone molecules with greater predictability in the solvent phase. Thus, designing new chalcone molecules with electron withdrawing substituent on the ring may increase the antimycobacterial activity.

Table 4.2: Statistical t- and p-values for all the regression coefficients for all the equations

n		η		E_{HOMO}		MRA-4		MRB-4'	
	Phase	t-Value	p-Value	t-Value	p-Value	t-Value	p-Value	t-Value	p-Value
27	Gas phase	2.5943	0.0166	-1.6574	0.11164	-0.7729	0.4478	-4.2062	0.0004
27	Solvent phase	-0.3242	0.7489	-6.5668	1.32E-06	0.2236	0.8251	-3.8779	0.0008
23	Gas phase	2.3386	0.0311	-2.6958	0.01478	-0.5618	0.5812	-5.9341	1.00E-05
23	Solvent phase	-0.5285	0.6036	-7.7234	4E-07	0.4053	0.6900	-5.0311	9.00E-05

MR, molar refractivity

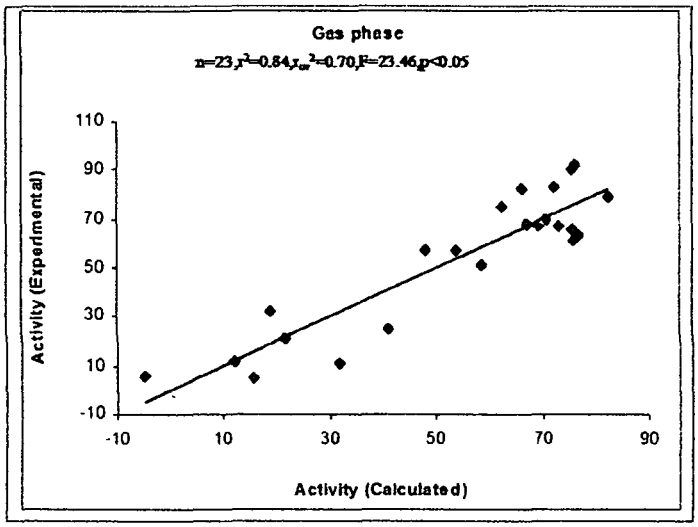

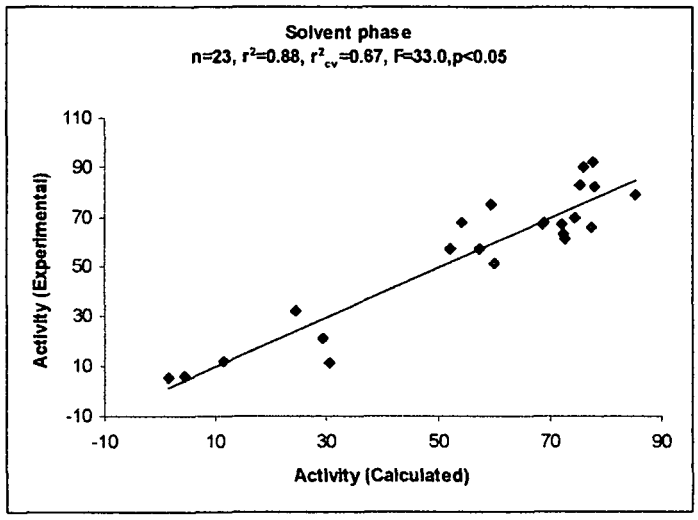

Fig. 4.1 :Plots of experimental versus calculated values of bioactivity for the two models

4.2. Screening of Medicinal plants and biochemical investigation of the important plant metabolites

4.2.1. Plant samples

Subsequently, on identification of the molecular descriptors , plants which are traditionally used in North East India to treat tuberculosis were screened for their amtimycobacterial activity. The plants were collected during field trips from Sonitpur

and Jorhat Districts of Assam and from East Khasi Hills District of Meghalaya after interviewing Viadyas and Ojhas (traditional healers) .

4.2.2.Plant extract yield

The yield of the ethanol extract of the respective plant plants are presented in the Table4.3.The yield was observed to be higher in case of leaves.

Table 4.3 : Yield of the various plant extracts.

Sl. No.	Plant	Part used	Yield (%)
1	*C.odorata*	Buds	28.7
2	*C.dactylon*	Leaves	42.06
3	*G.max*	Leaves	45.43
4	*L. inermis*	Leaves	51.03
5	*M.pudica*	Root	19.2
6	*P.fulgens*	Root	32.02
7	*P.orientalis*	Leaves	49.08

4.2.3.Antibacterial Assay

The antimycobacterial activity of the plant extracts was assessed using agar well diffusion assay against *Mycobacterium smegmatis ATCC* 14468 as the model . The antibacterial activity of the plant extracts was also assessed against *E. coli* and *K.pnuemoniae* (gram negative) and *S. aureus* and *B. subtilis* (gram positive). From the result of the agar well diffusion assay presented in Table 4.4, it can be inferred that the root extract of *L. inermis* possess the highest antibacterial activity in comparison to the other six extracts tested.

Table4.4: Antibacterial activity of various plant extracts

Sl. No	Plant	Part used	Solvent	Inhibition zone *M. smegmatis* (mm)	Inhibition zone *S. aureus* (mm)	Inhibition zone *B.subtilis* (mm)	Inhibition zone *K.pnuemoniae* (mm)
1	*C. odorata*	Buds	Ethanol	10	10	12	11
2	*C.dactylon*	Leaves	Ethanol	7	10	8	11
3	*G. max*	Leaves	Ethanol	9	13	10	8
4	*L. inermis*	Leaves	Ethanol	17	11	14	12
5	*M.pudica*	Root	Ethanol	13	11	14	11
6	*P.fulgens*	Root	Ethanol	14	12	15	13
7	*P. orientalis*	Leaves	Ethanol	11	12	11	13

4.2.4. Assay of Minimum Inhibition Concentration of the various plant extracts

MIC activity was calculated using the MTT (3-(4,5-dimethylthiazol-2-yl)-2,5-diphenyl tetrazolium bromide) Assay. MTT is a water soluble dye which is yellow in color and is transformed into purple colored formazan crystals when reduced by the dehydrogenase system of live cells. Formazan crystal formation indicated bacterial growth which was measured by the absorbance at 550nm. From the Table 4.5 it can be inferred that *L. inermis* leaf extract possess the highest antibacterial activity as it eixhibited the lowest MIC.

Table4.5: Minimum Inhibition Concentration of the various plant extracts

Sl. No	*Plant*	*Part used*	*Solvent*	*M. smegmatis MIC(µg/µl)*	*S. aureus MIC(µg/µl)*	*B.subtilis MIC(µg/µl)*	*K.pnuemoniae MIC(µg/µl)*
1	*C. odorata*	*Buds*	*Ethanol*	*12.5*	*12.5*	*3.125*	*12.5*
2	*C.dactylon*	*Leaves*	*Ethanol*	*12.5*	*6.25*	*6.25*	*12.5*
3	*G. max*	*Leaves*	*Ethanol*	*12.5*	*12.5*	*6.25*	*12.5*
4	*L.inermis*	*Leaves*	*Ethanol*	*0.9*	*0.9*	*0.9*	*1.87*
5	*M.pudica*	*Root*	*Ethanol*	*1.25*	*1.25*	*2.5*	*3.125*
6	*P.fulgens*	*Root*	*Ethanol*	*1.0*	*0.78*	*3.125*	*1.56*
7	*P.orientalis*	*Leaves*	*Ethanol*	*12.5*	*12.5*	*6.25*	*12.5*

4.2.5.Scanning Electron Microscopy

The morphological changes induced in the mycobacterial cells by the plant extracts at their respective MIC values was studied by the Scanning Electron

Microsopy. Comparative morphological changes were observed in the mycobacterial cells upon treatment with the plant extracts as seen in the Fig4.2.

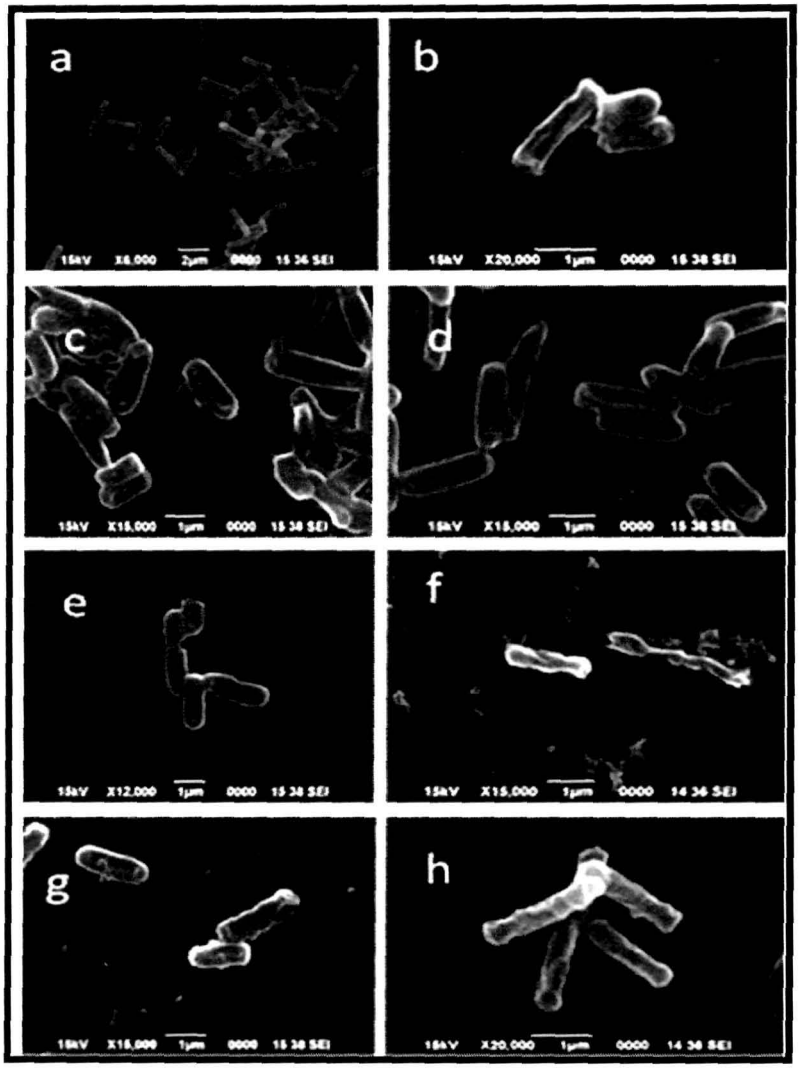

Fig4.2: Scanning electron micrographs of *M. smegmatis* a) without treatment of plant extracts (control), morphological changes induced upon treatment with the plant extracts of b) *C. odorata* , c) *C. dactylon* d) *G.max* e) *L. inermis* f) *M. pudica* g) *P. fulgens* and h) *P. orientalis* .

From the representative micrographs shown in Fig. 4.2 (b),(d),(e) and (f) cell lysis and wrinking was observed when the cells were treated with plant extracts of *C. odorata*, *G. max*, *L. inermis*, *M. pudica*. The cells treated with *C. dactylon* and *P. fulgens extracts* showed shortening of the cell length as observed from Fig 4.2(c) and (g). Wrinkling of the cell wall was observed in *P. orientalis* as seen in Fig 4.2 (h).

4.2.6. Total polyphenolic content

The total polyphenolic content of the positive plant extracts was determined. Total phenolic content was expressed as mg/g Gallic acid equivalent (GAE) using the calibration curve: **y=0.17 x, R^2=0.954**,where x is the absorbance and y is the Gallic acid equivalent (mg/g). It was found that both the *L. inermis* and *P. fulgens* had high amount of phenolic content followed by *C. odorata*, T. *orientalis* possessed the lowest total polyphenolic content.

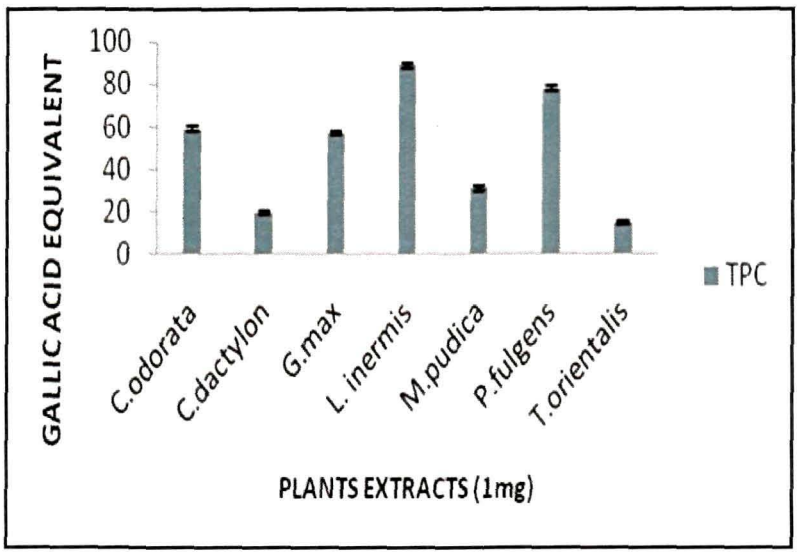

Fig4.3: Total phenolic content of the plant extracts expressed as mg/g Gallic acid equivalent (GAE).

4.2.7 Total Flavonoid Content

The total flavonoid content was carried out to determine the amount of flavonoid content in the crude extracts (Fig 4.4). The absorbance was recorded at 420 nm. Total flavonoid content was expressed as mg/g Quercitin equivalent (QE) using the following calibration curve: **y=0 .008x, R^2=0.937,**where x is the absorbance and y is the Quercitin equivalent (mg/g). It has been found that both the *L. inermis* and *P. fulgens* had high amount of flavonoid content followed by *C. odorata, T. orientalis* possessed the lowest total flavonoid content. The high amount of polyphenolics and flavonoids correlate with the low MIC values of the plant crude extracts. This provided an inkling of the natural products present in the plant extracts that endow the antimycobacterial activity to the respective plant extracts.

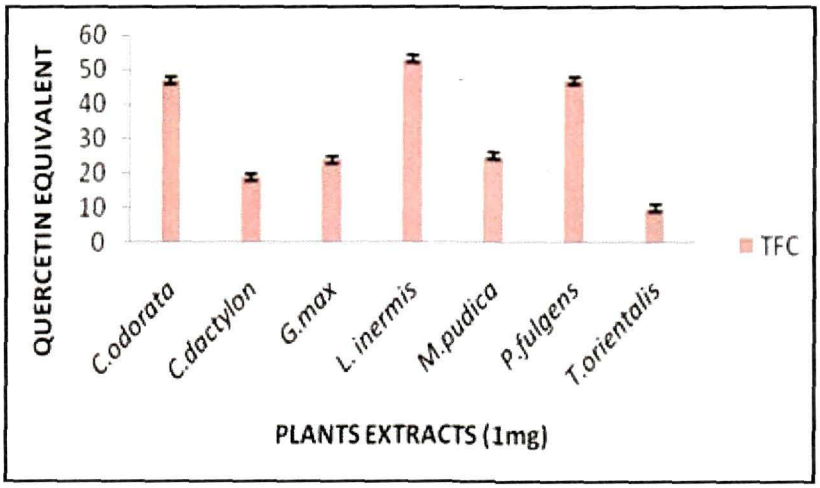

Fig4.4: Total phenolic content of the plant extracts expressed as mg/g Quercitin equivalent (QE) .

4.2.8 Cytotoxicity Assay

The plant extracts were assayed at the concentration of their respective MIC, 10XMIC, 50XMIC and 100XMIC. The viability of the RAW264.7, same as in the control post 48 h incubation showed that the plant extracts exhibited no cytotoxic effect on the cells.

4.3 Molecular Docking studies

Literature survey was then performed to identify the flavonoids present in the above mentioned seven plants which exhibited antimycobacterial activity. The chalcone molecules after the QSAR study were subjected to docking against the protein Thy X to establish it as a putative target of the chalcones. After the analysis of the docking results of the chalcone molecules and the flavonoids molecules of the plants exhibiting antimycobacterial activity were also subjected to a virtual screen against the target *M.tuberculosis* Thy X.

Molegro Virtual Docker (MVD) 5.0 (Molegro ApS, Aarhus, Denmark) was used for the Molecular Docking studies. Molecular docking was carried out and the top ranking ligands were further analyzed visually to exclude structure with improbable docking orientation. The docking score and H-Bond energies are shown in Table 4.6 which indicates that there is a strong interaction between the ligands and the receptor indicating a binding affinity.

Table 4.6. Docking Score of the plant derived flavonoids against *M. tuberculosis* Thy X enzyme.

SL .NO.	COMMON NAME	IUPAC NAME	MOLDOCK SCORE	RERANK SCORE	H-BOND
1	Fisetin	2-(3,4-dihydroxyphenyl)-3,7-dihydroxychromen-4-one	-82.1957	-69.2189	-2 5
2	Quercetin	2-(3,4-dihydroxyphenyl)-3,5,7-trihydroxychromen-4-one	-83.5485	-75.9531	-5.46533
3	Kaempferol	3,5,7-trihydroxy-2-(4-hydroxyphenyl)chromen-4-one	-74.2173	-45.2306	-10.258

4	Rutin	2-(3,4-dihydroxyphenyl)-5,7-dihydroxy-3-[(2S,3R,4S.5S,6R)-3,4,5-trihydroxy-6-[[(2R,3R,4R,5R,6S)-3,4,5-trihydroxy-6-methyloxan-2-yl]oxymethyl]oxan-2-yl]oxychromen-4-one	-96 7286	-87 8667	-17 9934
5	Epigallocatechin gallate	[(2R,3R)-5,7-dihydroxy-2-(3,4,5-trihydroxyphenyl)-3,4-dihydro-2H-chromen-3-yl] 3,4,5-trihydroxybenzoate	-100 498	- 72 8734	-13 3435
6	Butein	(E)-1-(2,4-dihydroxyphenyl)-3-(3,4-dihydroxyphenyl)prop-2-en-1-one	-96 9071	-85 2024	-4 7157
7	Apiin	7-[(2S,3R,4S,5S,6R)-3-[(2S,3R,4R)-3,4-dihydroxy-4-(hydroxymethyl)oxolan-2-yl]oxy-4,5-dihydroxy-6-(hydroxymethyl)oxan-2-yl]oxy-5-hydroxy-2-(4-hydroxyphenyl)chromen-4-one	-111 053	-108 533	-20 5082
8	Acacetin	5,7-dihydroxy-2-(4-methoxyphenyl)chromen-4-one	-109 507	-91 7063	-5
9	Daidzein	7-hydroxy-3-(4-hydroxyphenyl)chromen-4-one	-107 01	-86 0845	-4 14654
10	Gossypentin 8 rhamnoside	2-(3,4-dihydroxyphenyl)-3,5,7-trihydroxy-8-[(2S,5R,6S)-3,4,5-trihydroxy-6-methyloxan-2-yl]oxychromen-4-one	-80 8798	-60 2466	-18 1686
11	Taxifolin	(2R,3R)-2-(3,4-dihydroxyphenyl)-3,5,7-trihydroxy-2,3-dihydrochromen-4-one	-83 6282	-68 1427	-10 9553
12	Apigenin	5,7-dihydroxy-2-(4-hydroxyphenyl)chromen-4-one	-78 2139	-57 1441	-3 27871
13	Genistein	5,7-dihydroxy-3-(4-hydroxyphenyl)chromen-4-one	-81 2082	-64 4444	-3 23097
14	Luteolin	2-(3,4-dihydroxyphenyl)-5,7-dihydroxychromen-4-one	-102 447	-88 0168	-4 92109
15	Baicalein	5,6,7-trihydroxy-2-phenylchromen-4-one	-65 5542	-62 8541	-13 0018
16	Myricetin	3,5,7-trihydroxy-2-(3,4,5-trihydroxyphenyl)chromen-4-one	-95 6148	-84 7355	-21 7226

It was observed that the flavonoids docked into the active site of Thy X (shown in Figure 4.5.a). The docking results show that out of the 16 flavonoids Apiin bound tightly at the active site of Thy X. The ligands were found lying deep into the binding site exhibiting molecular interactions such as hydrogen bonding, electrostatic interactions (Figure 4.5.b) and hydrophobic interaction (Figure 4.5c). The docking analysis also showed the interactions with seven amino acid residues Arg190(A), His194(B), Arg199(B), Ser201(B), His203(B), Arg95(B), Arg97(B), present in the active site of *M. tuberculosis* Thy X (shown in Figure 4.5.a) The MolDock docking score was used in the present study. The MolDock scoring function (MolDock Score) in MVD

5.0 derived from the PLP scoring functions originally proposed by Gehlhaar *et al.* 1998.[299] and later extended by Yang et al., 2004 [300]. The MolDock scoring function further improves these scoring functions with a new hydrogen bonding term and new charge schemes. The docking scoring function, E_{score}, is defined by the following energy terms:

$$E_{score}=E_{inter}+E_{intra}$$

where E_{inter} is the ligand protein interaction energy.

The detailed analysis of docking in terms of protein-ligand interaction energy including ligand- protein interaction energy analysis (both electrostatic and H-bond) was calculated in order to get a better understanding of the variations between the binding mode. Table 4.7 enlists the protein-ligand interaction energy calculation including the interacting residues , the protein-ligand interaction distances and H-bond energy. These 16 flavonoid molecules with good docking orientations were then chosen for biological testing.

Table 4.7: Protein-ligand interaction energy calculation presenting the interacting residues , the protein-ligand interaction distances and H-bond energy.

SL. NO.	NAME	INTERACTING AMINO ACID	H-BOND ENERGY	DISTANCE
1	Fisetin	His96(B) Arg97(B) Arg97(B) Arg190(A)	-0.332573 -0.698702 -0.18251 -0.358469	3.39218 3.18471 3.45688 3.56885
2	Quercetin	Arg190(A) His98(A) Asn198(A) Arg97(B) His98(B)	-2.5 -.0569377 -2.12306 -0.136657 -1.7764	2.9809 2.82163 2.55477 3.1959 2.65343
3	Kaempferol	His98(A) Arg97(B) His194(B) His98(B)	-2.5 -2.29836 -2.5 -2.5	2.60021 3.14033 2.61906 3.09998

4	Rutin	Ser71(A) Ser71(A) Ser71(A) Tyr44(A) Gly68(A) Phe70(A) Gly68(A) Arg95(B) Arg199(B) Arg95(B) Arg95(B) Arg95(B) His96(B) Glu92(B) Arg95(B) Gln103(C) Gln103(C)	-0.315465 -2.04203 -2.5 -2.24762 -2.35563 -0.103013 -2.5 -1.93924 -0.406315 -0.00136683 -0.00436841 -0.12287 -0.0321357 -2.5 -2.5 -0.0986245 -2.5	3.53691 3.19159 2.99877 3.15048 3.12887 3.49592 2.93262 3.21215 3.18268 3.57506 2.3087 3.54558 3.49462 3.09892 3.05907 2.8583 2.8211
5	Epigallocatechin gallate	Glu74(A) His194(B) His96(B) Arg97(B) Arg97(B) His96(B) Arg199(B) Arg199(B) Ser201(B) Ala197(B) Ser201(B)	-2.5 -1.95002 -1.27405 -0.563414 -1.74058 -0.262532 -0.180583 -0.139752 -0.0902595 -2.5 -2.5	3.03379 2.80719 3.31054 3.48732 3.25188 2.68372 2.54413 2.575598 3.58195 2.75591 3.05147
6	Butein	Arg190(A) Arg190(A) Arg199(B) Arg94(B) Arg97(B) Arg97(B) Ala191(B)	-1.32158 -0.645843 -0.714438 -2.5 -0.469226 -0.416274 -2.18809	2.45859 3.35867 2.90229 2.83914 2.93588 2.94651 3.16238
7	Apiin	Arg190(A) Arg190(A) His194(B) His194(B) Arg199(B) Arg199(B) Ser201(B) His203(B) His194(B) Arg199(B) Arg199(B) Arg95(B) Arg97(B) Arg97(B) His194(B) Arg97(B)	-0.256345 -0.773451 -0.340732 -2.29109 -0.426749 -2.48898 -1.92968 -2.5 -1.11623 -2.49124 -0.33222 -2.5 -2.22763 -0.279329 -1.39809 -0.988423	2.6806 3.16945 3.13566 3.04363 3.51465 2.59868 3.21406 2.90468 3.37675 2.77017 3.15323 2.88459 3.017 3.51053 3.09088 3.52587

8	Acacetin	Asn188(A) Arg97(B) His96(B)	-2.5 -0.581426 -2.2521	3.07017 3.48371 3.14958
9	Daidzein	His(C) His98(A) Phe99(C)	-1.55193 -0.236697 -0.243747	2.48623 3.47752 3.48281
10	Gossypentin 8 rhamnoside	Tyr44(A) His69(A) Arg95(B) Arg95(B) Glu92(B) Ser105(C) Arg87(C) Arg87(C) Arg87(C) Gln103(C)	-0.433347 -0.726745 -0.63145 -1.45804 -2.5 -1.13918 -1.71659 -2.5 -2.19156 -1.35669	2.352 2.76001 2.70992 2.88233 2.6216 3.37216 2.61267 2.94981 3.0769 3.32866
11	Taxifolin	Glu74(A) His96(B) His194(B) Arg97(B) Ser100(C)	-2.14323 -1.29079 -1.09413 -1.41372 -2.5	3.17135 3.2425 2.65455 3.31726 -3.06988
12	Apigenin	His96(B) Asn188(A) Asn188(A)	-2.24733 -0.0293033 -0.503443	3.15053 3.53125 3.49931
13	Genistein	Arg190(A) Arg190(A) Arg190(A) Asn188(A) Arg97(B)	-1.88074 -0.120066 -0.140274 -1.5986 -2.27887	3.03789 3.39005 3.40521 2.49183 3.14423
14	Luteolin	Arg190(A) Glu74(A) Arg97(B) Arg97(B) Ala191(B)	-2.39578 -2.49435 -0.106161 -0.0266119 -0.679836	2.58749 3.10068 3.14962 3.47179 3.46403
15	Baicalein	His91(B) Glu92(B) Arg87(C) Arg87(C) Gln103(C) Arg87(C) Gln106(C)	-0.582338 -2.48802 -2.02117 -1.84542 -2.5 -2.02639 -2.5	3.11389 2.59856 3.19577 3.11422 2.60983 2.63319 3.01107
16	Myricetin	Tyr44(A) Ser71(A) Tyr44(A) Arg87(C) Gln103(C) Leu104(C)	-2.5 -2.5 -0.240772 -2.49974 -2.5 -2.5	2.98624 2.82364 3.55185 3.10005 2.91516 2.92214

		Arg87(C) Arg87(C) Ser105(C) Tyr101(C) Ser102(C) Ser105(C)	-0.528879 -2.49945 -2.16036 -1.44525 -1.73192 -2.05926	3.49422 2.59993 2.55924 3.31095 3.25362 2.54711

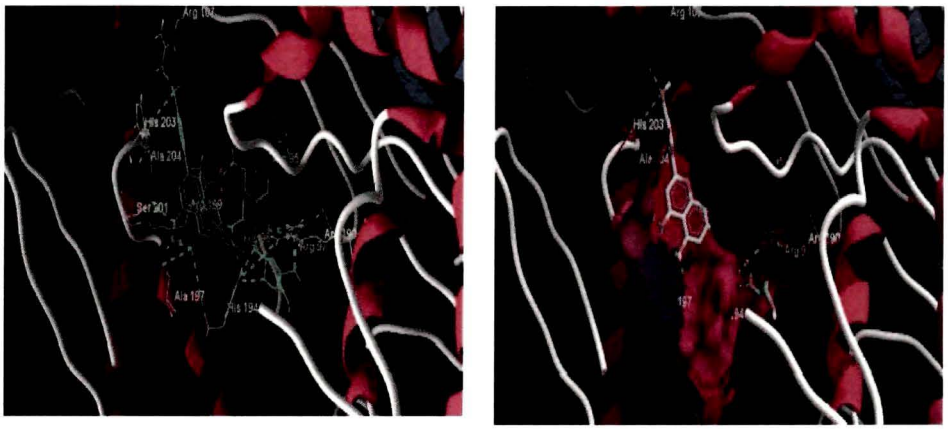

(a) **(b)**

(c)

Fig 4.5: Docking study of Apiin. (a) Predicted bonded interactions (green dashed lines) between ligands (green) and mycobacterial Thy X , (b) predicted non bonded electrostatic interaction between ligands (green) and the residues at the active site and (c) predicted non bonded hydrophobic interaction between ligands (green) and the residues at the active site

4.4 Minimum Inhibition Concentration of the Flavonoids

The intrinsic tolerance of *M.tuberculosis* to most of the commercially available antibiotics which has limited the chemotherapy to a small number of antibiotics [96] can be attributed to the failure of the antibiotics to reach the cytoplasmic membrane[301]. Therefore, before performing the study of the inhibitory effects of the flavonoids on the mycobacterial Thy X we performed the well diffusion assay as well as the MTT assay to confirm the antimycobacterial activity of the flavonoids. The 2D structure of the flavonoids is presented in Fig4.6.

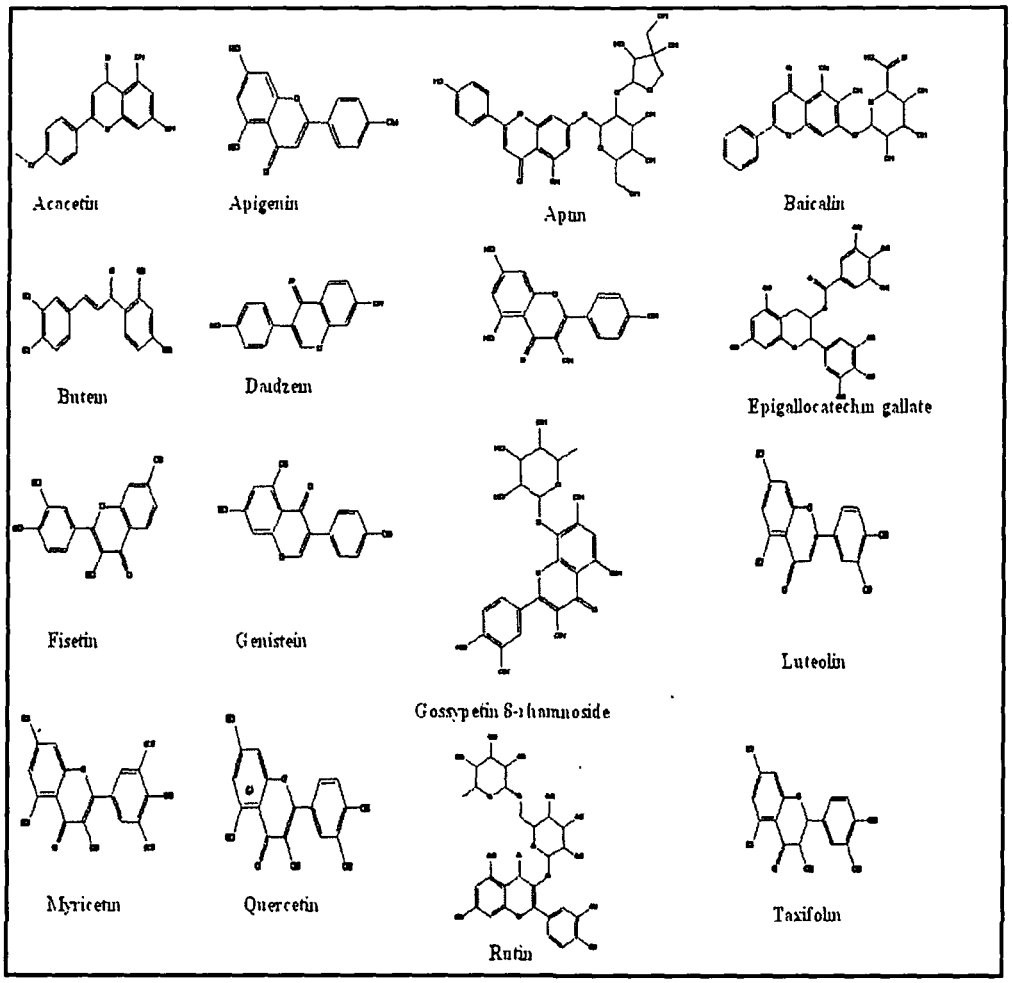

Fig4.6: 2D Structure of the sixteen flavonoid molecules

The potency of the flavonoid molecules against *M. smegmatis ATCC 14468* was assessed quantitatively by determining the minimum inhibitory concentration (MIC) using MTT assay. MTT [3-(4,5-dimethylthiazol-2-yl)-2,5-diphenyltetrazolium bromide] is a pale yellow water soluble substrate which forms water-insoluble purple formazan crystals upon reduction by the dehydrogenase system of active living cells and forms the basis of this assay used to estimate the cell viability. Dead cells do not reduce MTT [302].The MIC of the flavonoids is provided in Table4.8.

4.5. QSAR study of the flavonoids

In this QSAR study, we found that DFT-derived descriptors, chemical potential (μ) and E_{NL} descriptor correlated with the antimycobacterial activity of the flavonoid molecules remarkably in both gas and solvent phases. In both Gas phase and Solvent phase decrease in chemical potential and increase in E_{NL} correlated with the antimycobacterial activity.

Gas phase:

$$1471.182\ (\pm 268.3639) + 13328.14\ (\pm 2281.242)\ \mu - 10540.5\ (\pm 2069.893) E_{NL}$$

$$R^2=0.803023,\ SE=43.0175,\ F=18.34536,\ p<0.05$$

Solvent phase:

$$1542.12\ (\pm 382.7402) + 13496.05\ (\pm 3025.485)\ \mu - 10008.6\ (\pm 2300.821)\ E_{NL}$$

$$R^2= 0.733099,\ SE= 50.07406,\ F= 12.3602,\ p<0.05$$

Table 4.8: Minimum Inhibition Concentration of the flavonoid molecules.

SL.NO.	Name	Physical Properties	XLogP3	Molecular Formula	Molecular Weight[g/mol]	MIC (µg/µl)
1	Acacetin	Compound ID: 5280442	XLogP3: 2.1 H-Bond Donor: 2 H-Bond Acceptor: 5	$C_{16}H_{12}O_5$	284.26348	100
2	Apigenin	Compound ID: 5280443	XLogP3: 1.7 H-Bond Donor: 3 H-Bond Acceptor: 5	$C_{15}H_{10}O_5$	270.2369	240
3	Apiin	Compound ID: 5280746	XLogP3-AA: -0.4 H-Bond Donor: 8 H-Bond Acceptor: 14	$C_{26}H_{28}O_{14}$	564.49212	250
4	Baicalein	Compound ID: 5281605	XLogP3: 1.7 H-Bond Donor: 3 H-Bond Acceptor: 5	$C_{15}H_{10}O_5$	270.2369	70
5	Butein	Compound ID: 5281222	XLogP3-AA: 2.8 H-Bond Donor: 4 H-Bond Acceptor: 5	$C_{15}H_{12}O_5$	272.25278	50
6	Daidzein	Compound ID: 5281708	XLogP3-AA: 2.5 H-Bond Donor: 2 H-Bond Acceptor: 4	$C_{15}H_{10}O_4$	254.2375	255
7	Epigallocatechin gallate	Compound ID: 65064	XLogP3: 1.2 H-Bond Donor: 8 H-Bond Acceptor: 11	$C_{22}H_{18}O_{11}$	458.37172	100
8	Fisetin	Compound ID: 5281614	XLogP3: 2 H-Bond Donor: 4 H-Bond Acceptor: 6	$C_{15}H_{10}O_6$	286.2363	150
9	Genistein	Compound ID: 5280961	XLogP3-AA: 2.7 H-Bond Donor: 3 H-Bond Acceptor: 5	$C_{15}H_{10}O_5$	270.2369	270
10	Gossypentin-8, rhamnoside	Compound ID: 44259993	XLogP3-AA: 0.5 H-Bond Donor: 8 H-Bond Acceptor: 12	$C_{21}H_{20}O_{13}$	464.3763	250
11	Kaempferol	Compound ID: 5280863	XLogP3: 1.9 H-Bond Donor: 4 H-Bond Acceptor: 6	$C_{15}H_{10}O_6$	286.2363	130
12	Luteolin	Compound ID: 5280445	XLogP3: 1.4 H-Bond Donor: 4 H-Bond Acceptor: 6	$C_{15}H_{10}O_6$	286.2363	40
13	Myricetin	Compound ID: 5281672	XLogP3: 1.2 H-Bond Donor: 6 H-Bond Acceptor: 8	$C_{15}H_{10}O_8$	318.2351	60
14	Quercetin	Compound ID: 5280343	XLogP3: 1.5 H-Bond Donor: 5 H-Bond Acceptor: 7	$C_{15}H_{10}O_7$	302.2357	125
15	Rutin	Compound ID: 5280805	XLogP3-AA: -1.3 H-Bond Donor: 10 H-Bond Acceptor: 16	$C_{27}H_{30}O_{16}$	610.5175	120
16	Taxifolin	Compound ID: 439533	XLogP3-AA: 1.5 H-Bond Donor: 5 H-Bond Acceptor: 7	$C_{15}H_{12}O_7$	304.25158	130
17	Isoniazid	Compound ID: 3767	XLogP3: -0.7 H-Bond Donor: 2 H-Bond Acceptor: 3	$C_6H_7N_3O$	137.13928	1

Table 4.9: Parameters used to build the QSAR models with the jackknife results for gas phase against *M. smegmatis*

Gas phase	SA	HE	LogP	MR	Pol	homo	lumo	μ	η	ω	E_{ec}	E_{nomo-1}	MIC(μg/ml)
Acacetin	407.72	-19.85	4.51	21.69	29.1	-0.197	-0.099	-0.148	0.049	0.222	-0.063	-0.209	100
Apigenin	363.42	-25.16	4.57	16.65	27.27	-0.203	-0.106	-0.155	0.048	0.248	-0.069	-0.22	240
Apiin	641.01	-43.51	1.83	76.03	51.64	-0.199	-0.1	-0.15	0.05	0.226	-0.067	-0.214	250
Baicalein	345.76	-22.94	4.57	16.65	27.27	-0.194	-0.107	-0.151	0.043	0.262	-0.067	-0.212	70
Butein	412.77	-29.96	4.9	18.21	28.04	-0.195	-0.11	-0.152	0.043	0.274	-0.058	-0.204	50
Diadzein	356.93	-20.22	4.26	15.21	26.63	-0.192	-0.089	-0.14	0.051	0.192	-0.062	-0.204	255
Epigallocatechin_gallate	526.33	-52.67	5.09	40.32	42.78	-0.189	-0.077	-0.133	0.056	0.158	-0.037	-0.192	100
Fisetin	367.22	-28.72	4.4	18.04	27.9	-0.184	-0.099	-0.142	0.042	0.237	-0.057	-0.214	150
Genistein	356.5	-25.6	4.09	16.59	27.27	-0.194	-0.093	-0.144	0.05	0.205	-0.067	-0.211	270
Gossypentin_8_r	473.35	-41.02	3.27	51.96	41.96	-0.186	-0.101	-0.143	0.042	0.247	-0.059	-0.201	250
Isoniazid	249.78	-16.69	1.57	13.98	14.35	-0.227	-0.099	-0.163	0.064	0.207	-0.064	-0.232	1
Kaempferol	363.23	-28.59	4.4	18.04	27.9	-0.189	-0.102	-0.145	0.044	0.242	-0.06	-0.212	130
Luteolin	365.88	-30.62	4.4	18.04	27.9	-0.199	-0.103	-0.151	0.048	0.236	-0.063	-0.209	40
Myricetin	373.62	-39.25	4.05	20.81	29.18	-0.189	-0.103	-0.146	0.043	0.248	-0.06	-0.208	60
Quercetin	367.45	-34.14	4.22	19.42	28.54	-0.188	-0.103	-0.145	0.042	0.25	-0.06	-0.209	125
Rutin	590.58	-50.78	2.23	82.99	54.75	-0.201	-0.108	-0.155	0.047	0.256	-0.07	-0.211	120
Taxifolin	376.86	-33.08	3.51	26.51	28.73	-0.208	-0.102	-0.155	0.053	0.226	-0.052	-0.21	130

Table 4.10: Parameters used to build the QSAR models with the jackknife results for solvent phase against *M. smegmatis.*

Solvent phase	SA	HE	LogP	MR	Pol	homo	lumo	μ	η	ω	E_{ad}	$E_{protein-L}$	MIC(μg/μl)
Acacetin	407.72	-19.85	4.51	21.69	29.1	-0.198	-0.101	-0.15	0.049	0.229	-0.063	-0.208	100
Apigenin	363.42	-25.16	4.57	16.65	27.27	-0.2	-0.101	-0.15	0.049	0.229	-0.064	-0.21	240
Apiin	641.01	-43.51	1.83	76.03	51.64	-0.201	-0.102	-0.152	0.05	0.233	-0.068	-0.211	250
Baicalein	345.76	-22.94	4.57	16.65	27.27	-0.194	-0.105	-0.149	0.044	0.252	-0.065	-0.21	70
Butein	412.77	-29.96	4.9	18.21	28.04	-0.191	-0.112	-0.152	0.04	0.291	-0.058	-0.207	50
Diadzein	356.93	-20.22	4.26	15.21	26.63	-0.194	-0.091	-0.143	0.052	0.197	-0.06	-0.213	255
Epigallocatechin_gallate	526.33	-52.67	5.09	40.32	42.78	-0.191	-0.08	-0.135	0.056	0.164	-0.036	-0.191	100
Fisetin	367.22	-28.72	4.4	18.04	27.9	-0.185	-0.101	-0.143	0.042	0.241	-0.055	-0.211	150
Genistein	356.5	-25.6	4.09	16.59	27.27	-0.193	-0.094	-0.143	0.05	0.206	-0.064	-0.211	270
Gossypentin 8 Rr	473.35	-41.02	3.27	51.96	41.96	-0.185	-0.102	-0.144	0.042	0.248	-0.059	-0.2	250
Isoniazid	-249.78	-16.69	1.57	13.98	14.35	-0.226	-0.092	-0.159	0.067	0.189	-0.057	-0.228	1
Kaempferol	363.23	-28.59	4.4	18.04	27.9	-0.188	-0.101	-0.145	0.043	0.242	-0.058	-0.21	130
Luteolin	365.88	-30.62	4.4	18.04	27.9	-0.195	-0.102	-0.148	0.047	0.236	-0.063	-0.207	40
Myricetin	373.62	-39.25	4.05	20.81	29.18	-0.186	-0.102	-0.144	0.042	0.248	-0.058	-0.204	60
Quercetin	367.45	-34.14	4.22	19.42	28.54	-0.186	-0.102	-0.144	0.042	0.248	-0.057	-0.206	125
Rutin	590.58	-50.78	2.23	82.99	54.75	-0.193	-0.103	-0.148	0.045	0.245	-0.064	-0.206	120
Taxifolin	376.86	-33.08	3.51	26.51	28.73	-0.203	-0.1	-0.151	0.052	0.221	-0.051	-0.208	130

4.6 PCR of the *thy x* gene *from M. smegmatis*

The mycobacterial genomic DNA was isolated using the MB545 *Mycobacterium tuberculosis* DNA Extraction Kit (HIMEDIA) Fig4.7.In order to clone *thy x of M. smegmatis ATCC16648* specific primers were designed to amplify

out the *x* gene. The resulting nucleic acid product was run on a 1% agarose gel. The product matched the expected length of 753 base pairs.

Fig4.7: Gel (0.8%) showing Genomic DNA isolated from *Mycobacterium smegmatis* ATCC 14468. Lane 1& 2 : Genomic DNA. Lane 3: 1Kb Gene Ruler

Fig4.8: Gel showing the amplified product. Lane 1: Amplified product & Lane 2:Gene ruler

4.7 Cloning of the *thy x gene* into pTZ57R/T vector

For ease of reproduction and amplification as well as for simplicity in sequence verification, the PCR product was ligated pTZ57R/T vector according to the InsTAclone™ PCR Cloning Kit protocol. The ligated PCR product was used to transform *E.coli* DH5α cells using heat shock method. Transformed cells were plated and positive selection was based on light blue colonies Fig4.9 Colony PCR was

performed to screen the positive colonies Fig4.10..Nonspecific amplification was observed in case of colony PCR. The plasmids were isolated Fig4.11, submitted to the National Institute of Plant Genome Research, New Delhi and the sequence was verified Fig4.12.

(a) (b)

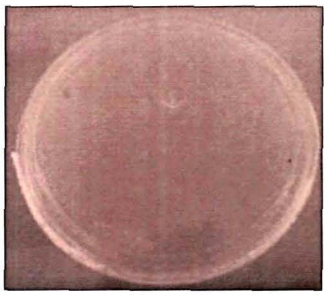

(c)

Fig4.9: Plate containing Transformed Cells. (i) Plate with Control DNA 1 (with out insert) . Blue Colonies Observed, Plate containing Transformed Cells with Control DNA 2 (with insert) . White Colonies Observed. Plate containing Transformed Cells with pTZ57R/T plasmid containing the insert *(thyx gene).*

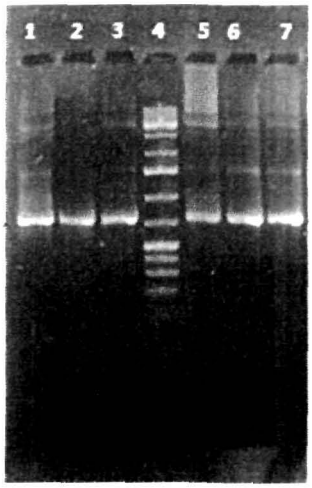

Fig.4.10: Gel showing the amplified products of the colony pcr . Lane 1, 2, 3, 5, 6 &7 amplified products, band of 761bps present. Lane 4 :gene ruler

Fig.4.11: Gel showing the plasmid isolated from the white colony . Lane 1:Gene ruler and Lane 2: pTZ57R/T plasmid containing the insert

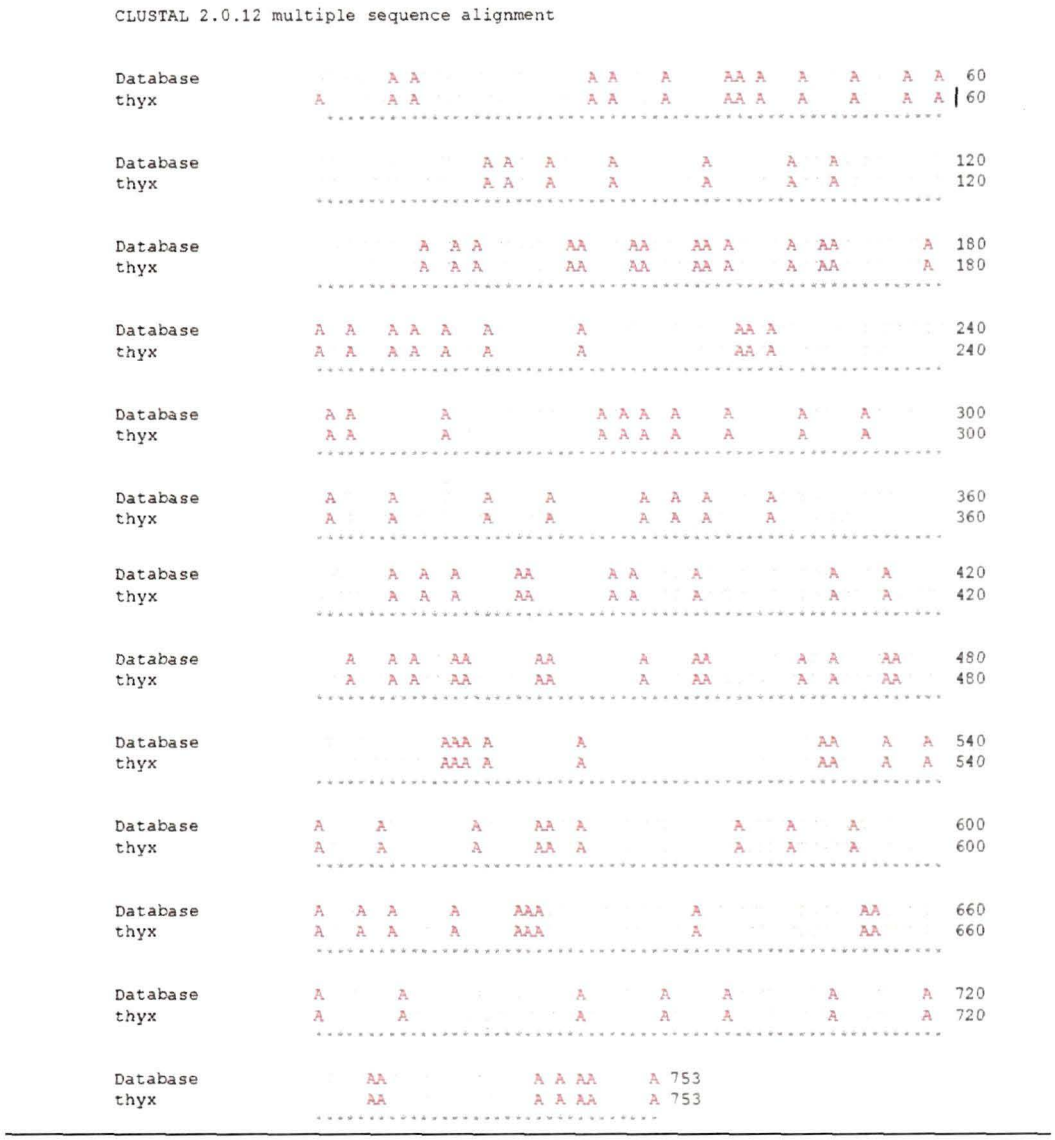

Fig.4.12: Nucleic acid sequence alignment

4.8 Cloning into the pET 32a+ expression vector

pET vector was used for the benefit of expressing the protein with the addition of an N-terminal or C-terminal His tag. Restriction enzymes from New England Biolabs were used to cut the *thy x* insert from the TA vector. Individual restriction enzyme digests with *NcoI* and *XhoI* were performed on both *thy x* -TA vector and pET32a + expression vector. Initial digest with *NcoI* was performed and the resulting product was purified with Qiagen PCR purification kit. The second digestion reaction was performed with *XhoI* and the resulting product was gel purified and concentrated (Fig. 4.13). The expression vector was similarly digested, with purification of both restriction enzyme reactions using the Qiagen PCR purification kit.

Fig4.13: Gel showing the Restriction digestion by *Nco I* and *Xho I* product . Lane 1: Restriction digestion product, two bands of 761bps and 2886 present. Lane 2 : Gene ruler

Digested *thy x* and pET32a+ were ligated together using T4 ligase from Thermo Scientific and were used to transform *E.coli* DH5α cells. Transformed cells were selected on ampicillin plates and positive selection was based on light blue colonies. Again, plasmid was isolated and submitted for sequence verification.

4.9. Overexpression and purification of the Thy X protein

4.9.1 Induction by IPTG

The plasmids were then used to transform *E.coli BL21 DE-3 pLysS* cells, with positive transformants selected on ampicillin plates. Expression in *BL21 DE-3* cells was induced with isopropyl-beta-D-thiogalactopyranoside (IPTG). Cells were harvested five hours post-IPTG induction by centrifugation. Cell pellets were lysed and resuspended in protein sample buffer containing fresh DTT. Cell lysates were run on 12% glycine gel and stained. Positive induction was seen as a band at 42.5 kDaltons in lane 2 Fig.4.14.

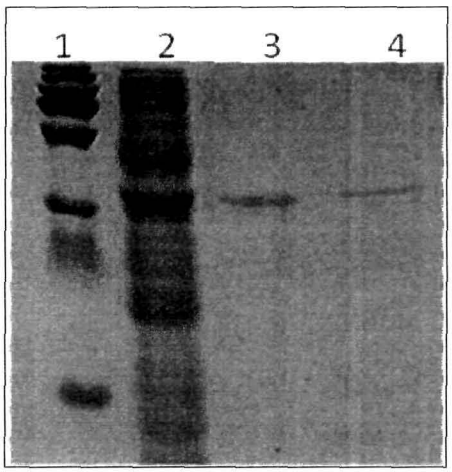

Fig.4.14:Purification Analysis of *M. smegmatis* ThyX by SDS-PAGE. Lanes: 1, Molecular weight marker,Lane 2 Soluble cell lysate fraction from ThyX expression. Lane 3: Recombinant Thy X with fusion tag after Ni-NTA Magnetic Agarose . Lane 4: Recombinant Thy X with fusion tag after Q-Sepharose column.

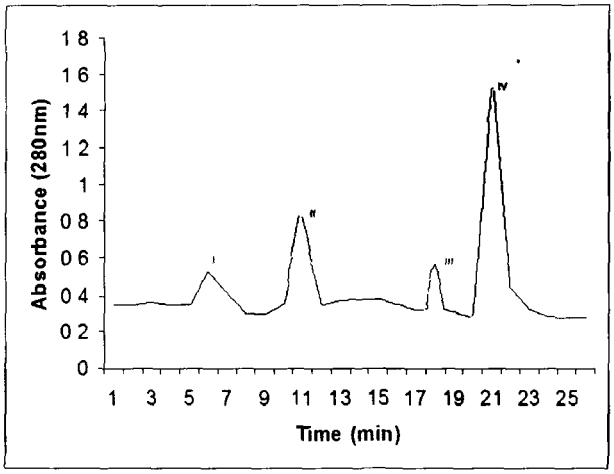

Fig4.15: Ion exchange chromatography of Recombinant Thy X . The elution profile was monitored at 280nm, Peak 4 was of Recombinant Thy X containing solution.

4.9.2 Purification by Affinity Chromatography

Initial isolation of the recombinant Thy x protein was attempted using Ni-NTA Magnetic Agarose beads (Fig. 4.14,Lane 3) following the manufacturer's instructions.

4.9.3 Purification by Ion-exchange Chromatography

The Q-Sepharose captured Recombinant Thy X protein was eluted with 50mM Tris-Cl (pH-7.3) containing 50mM to 500mM NaCl (pH 7.5) successively. The eluates were collected and the factions were measured for the following spectroscopic features. PeakI probably some unbound proteins; Peak II colorless solution was of some protein impurities; Peak III colorless solution containing some protein impurities and Recombinant Thy x protein; Peak IV yellow colored solution containing Recombinant Thy x protein . The Recombinant Thy X protein rich fraction was pooled and subjected to RP-HPLC for further purification.

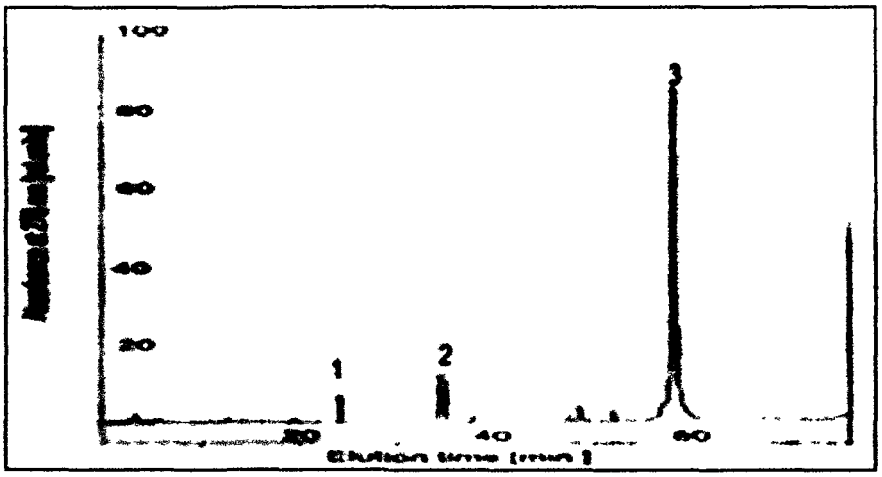

Fig4.16: Reversed phase HPLC profile

4.9.4 RP-HPLC

RP-HPLC method coupled to a UV-Vis detector was used to purify the protein. Elution of 150 μg protein was performed at 1 ml/min with using mobile phase Acetonitrile and Water (90: 10, v/v) and monitored online at 273 nm. Recombinant Thy x was eluted as yellow colored solution of Peak 3 s at 58 min(Fig. 4.16). Peak 1 and Peak 2 were protein impurities which were obtained as colorless solutions.

4.9.5 Enterokinase digestion

The His tag was cleaved from the purified protein by Enterokinase digestion (Fig4.17, Lane 4.) . The expected band of 27.59 kD could be observed in the SDS-PAGE.

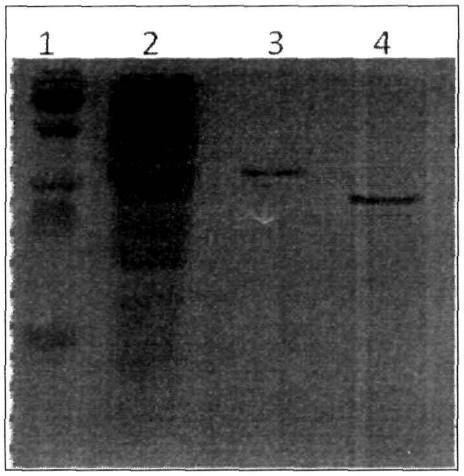

Fig4.17: Analysis of *M. smegmatis* ThyX by SDS-PAGE.Lanes: 1, Molecular weight marker,Lane 2 Soluble cell lysate fraction from ThyX expression. Lane 3: Purified Recombinant Thy X with fusion tag.Lane 4: ThyX after cleavage of the fusion tag.

Table 4.11.Purification of M. smegmatis ThyX

Purification step	Total amount of protein (mg)	Total activity	Specific activity	Purification factor	Yield%
Cell lysate	325	754	2.32	1	100
HPLC Purified protein	6	51	8.5	3.6	6.76

The amino acid sequence for this construct was aligned to sequence of *Mycobacerium smegmatis* Thy X protein (Fig.4.18).

Fig4.18 *Mycobacerium smegmatis* Thy X protein sequence (ThyX) aligned with the protein sequence of the overexpressed protein of Thy X(Thy X2) of *Mycobacterium smegmatis* expressed in *E.coli*

4.10 TMP synthesis

The thymidylate-synthesizing ability of *M. smegmatis* ThyX was investigated by reversed phase HPLC (Fig.4.19). The products of the enzymatic reactions were loaded onto a HPLC column Symmetry C_{18}. The decrease in dUMP and increase in TMP were confirmed using known standards. On the basis of the absorbance at 260 nm, the peak corresponding to dUMP (tr = 8.5 min) decreases while the peak corresponding to TMP (tr = 11 min) increases over a 120 minute time course (0, 30, 60, and 120 minute time points) thus confirming the synthesis of TMP synnthesis. However, difference in the retention time of UMP and TMP has been observed when compared to the retention time reported by Hunter et al, 2008[246]. This difference

in the retention time may be attributed to the difference in the HPLC columns used during the experiment.

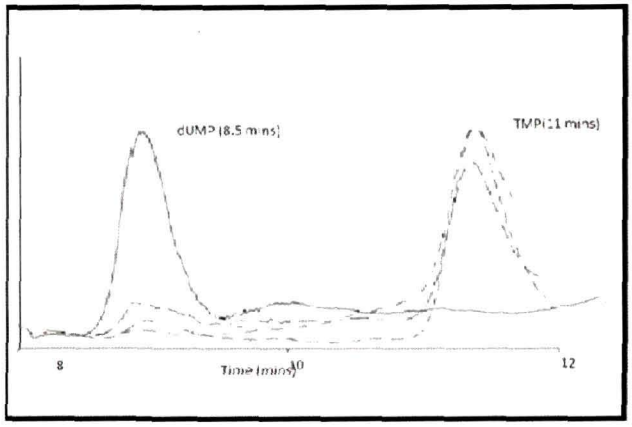

Figure 4.19. The HPLC analysis of *M. smegmatis* ThyX products to ensure TMP synthesis.

ThyX activity was examined by NADPH oxidation assay. The purified enzyme was assayed with various concentrations of the substrate dUMP or with varying concentrations of the substrate(mTHF). The enzyme displayed a standard Michaelis-Menten curve (Fig.4.20).

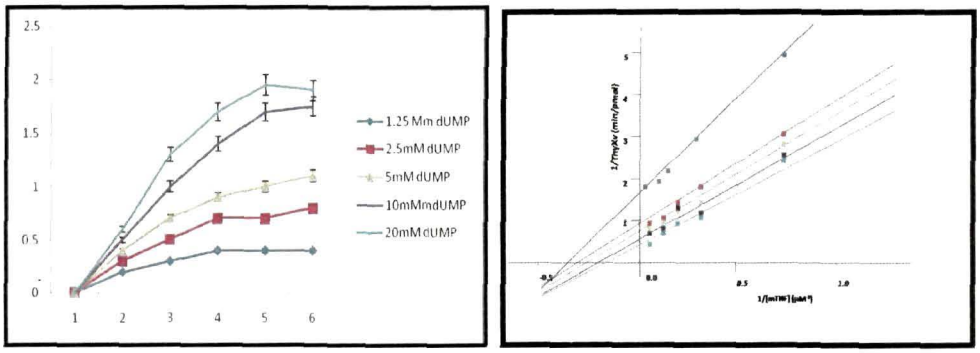

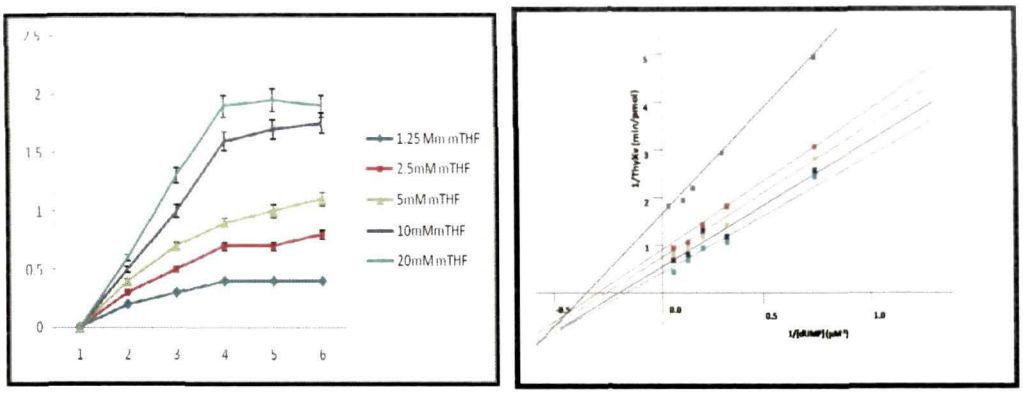

Fig.4.20: The kinetics of *M. smegmatis* Thy X. (i) Titrations of mTHF (1.25, 2.5, 5, 10, 20 mM) with varying concentrations of dUMP 1.25 mM; 2.5 mM; 5 mM; 10 mM; 20 mM). (ii) Double reciprocal plot of data from plot (i) showing a sequential reaction mechanism. (iii)Titrations of dUMP (1.25, 2.5, 5, 10, 20 mM) with varying concentrations of mTHF (1.25 mM; 2.5 mM; 5 mM; 10 mM; 20 mM). (iv) Double reciprocal plot of data from plot (iii) showing a sequential reaction mechanism. Lines in (i) and (iii) depict the Michaelis-Menten curve with calculated constants. Lines in (ii) and (iv) are the linear regressions.

Fitting of the data to the appropriate equation revealed K_m values for *M. smegmatis* ThyX were 4±0.6 μM for dUMP and 5.0±0.8 μM for mTHF.

These values are higher in comparison to the experimentally determined values for the *M. tuberculosis* ThyX enzyme by Hunter et al., 2008. The experimentally determined values for the ThyX enzymes of other prokaryotes , 6–65 μM for dUMP and 20–24 μM for mTHF [239, 240,244, 303]. The value of k_{cat} of *M. semgmatis* Thy X is 0.5 min^{-1}

4.11 Inhibition studies

The screening of the flavonoids as inhibitors of *M. smegmatis* ThyX revealed Apiin as a promising candidate. The NADPH oxidation assay was used to determine the K_i value of the flavonoid Apiin as an inhibitor for the ThyX enzyme. Apiin and the corresponding substrate dUMP concentrations were varied as listed in the legends of Fig. 4.21.The data was fitted in double reciprocal plots that yielded linear regression lines.

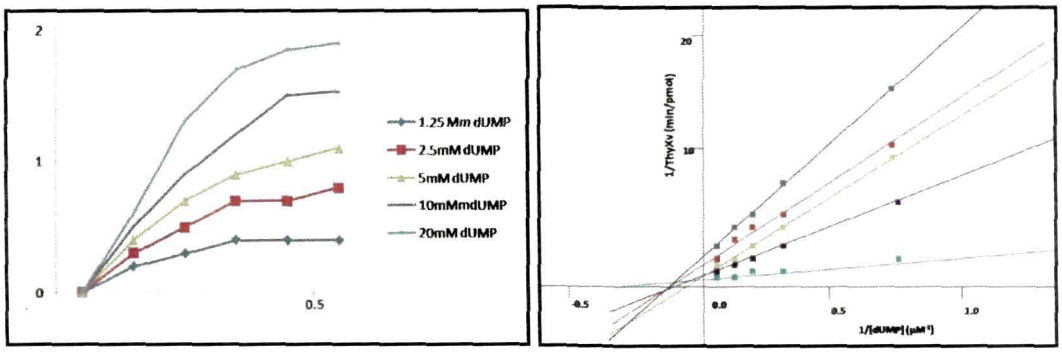

Fig4.21: Inhibition of *M. smegmatis* Thy X by Apiin . (i) Titrations of dUMP (1.25, 2.5, 5, 10,20 μM) with varying concentrations of Apiin (0 nM;250 nM;500 nM; 750 nM; 1000 nM) in the presence of 8 μM mTHF. (ii) Double reciprocal plot of data from plot (i) showing a mixed inhibition mechanism. Lines in (i) are plots of Michaelis-Menten equations with calculated constants. Lines in (ii) are linear regressions.Error bars are propagation of standard deviations.

M. smegmatis ThyX was inhibited by Apiin with the K_i of 200nM±15. The double reciprocal plot of the data showed a mixed inhibition mechanism (Fig4.21.ii).

The K_i value of Apiin is comparatively higher than the *M. tuberculosis* Thy X inhibitor FdUMP with the K_i of 100nM as reported by Hunter et al., 2008[246], however, it constitutes a promising starting point for optimized inhibitors of Thy X.

4.12 Mass Spectrometric Analysis

Mass spectrometry was used to elucidate the peptide fragment that harbours the methyl group. MALDI-TOF was carried out on trypsin digested protein which revealed a peptide corresponding to amino acid residues 173-182 (**AVLPNATETR**), exhibited a mass shift of 14 atomic mass units following the methyl-donating half-reaction (Fig.4.22 , peak 1085.181) thus, identifiying Arg 182 as the amino acid residue in the peptide that can accept a methyl .

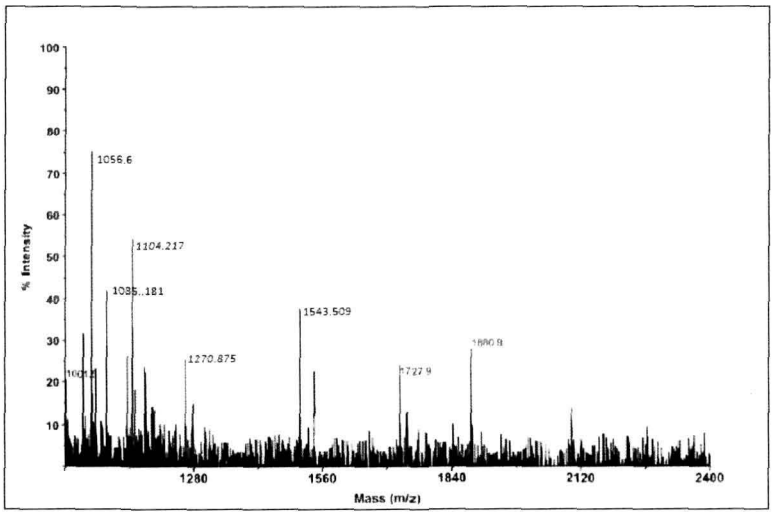

Fig4.22:MALDI-TOF mass spectrometric analysis of purified recombinant *M.smegmatis* ThyX following the Thymidylate synthesizing half-reaction. Peaks with a mass between 1000 and 2400 are shown . Peptide 1085.181 represents residues 173-182 (AVLPNATETR) which shows an increase of 14 atomic mass units in calculated mass as compared with the expected mass.

4.13 Antimycobacterial activity of hyperbranched poly(ester amide)/MWCNT nanocomposites

4.13.1 Antibacterial assay of hyperbranched poly (ester amide)/MWCNT

In the present investigation, therapeutic potential of the novel nanocomposites, as implant materials, has been examined for its antibacterial and

antimycobacterial activity.This study was performed in collaboration with the laboratory of Professor N. Karak, Department of Chemical Sciences , Tezpur University where the novel nanocomposites were prepared. Antimicrobial activity of nanocomposites termed HBPEA, HBPEAM1, HBPEAM2.5 and HBPEAM5 towards (a) *B. subtilis*, (b) *S. aureus*, (c) *E. coli*, (d) *K. pneumonia*, (e) *M. smegmatis* mc2 155, and (f) *M. smegmatis* ATCC14468 was studied using Well Diffusion assay. From the result of the agar well diffusion assay presented in the following Table4.11 it can be inferred that the nanocomposites possess antimicrobial activity.

Table4.12: Antibacterial activity of the nanocomposites

Sl. No	Nanocomposite	Inhibition zone *M. smegmatis mc2 155* (mm)	Inhibition zone *M. smegmatis ATCC14468* (mm)	Inhibition zone *Staphylococcus aureus* (mm)	Inhibition zone *Bacillus subtilis* (mm)	Inhibition zone *Escherichia coli* (mm)	Inhibition zone *Klepsiella pnuemoniae MTCC618* (mm)
1	HBPEA	NA	NA	NA	NA	NA	NA
2	HBPEAM1	9	9	10	8	NA	NA
3	HBPEAM2.5	11	11	13	10	8	8
4	HBPEAM5	15	17	14	14	10	9

NA: No Activity

Table4.13: MIC of the nanocomposites against the sixbacterial strains.

Sl. No	Nanocomposite	*M. smegmatis mc2 155* MIC(μg/μl)	*M. smegmatis ATCC14468* MIC(μg/μl)	*Staphylococcus aureus* MIC(μg/μl)	*Bacillus subtilis* MIC(μg/μl)	*Escherichia coli* MIC(μg/μl)	*Klepsiella pnuemoniae* MIC(μg/μl)
1	HBPEAM1	10.0	10.0	7.5	7.5	25	25

2	HBPEAM2.5	5.0	5.0	3.12	3.12	15.0	15.0
3	HBPEAM5	3.125	3.125	1.56	1.56	12.5	12.5

4.13.2 Enumeration of CFU count

The antibacterial effect of the prepared nanocomposites by the incorporation of *f*-MWCNT in the HBPEA on bacterial growth was assessed by culturing the bacteria with the nanocomposites a concentration lower than MIC value. Enumeration of the colony forming units (CFU) revealed a substantial reduction in the attachment of the Gram positive and acid fast bacterial species. (Fig. 4.23.b). Pronounced antibacterial efficacy was exhibited by the nanocomposites against *B. subtilis* (Fig. 4.23.a) and *S. aureus* (Fig. 4.23.b), as compared to *E. coli* (Fig. 4.23.c) and *K. pneumonia* (Fig. 4.23.d). Significantly less number of bacterial colonies was observed on the nanocomposite films with respect to pristine HBPEA implying the superior antibacterial activity over of the same. The results show that the nanocomposites were more effective against Gram-positive bacteria as compared to the Gram-negative ones, showing differential interaction of the same with the surface moieties of the two different bacterial strains. The basic differences between the cell wall structures in Gram-positive bacteria and Gram-negative ones strains may play a key role in determination of their antibacterial activities. The *M. smegmatis* mc2 155 (Fig. 4.23.e) (ampicillin resistant) and *M. smegmatis* ATCC14468 (Fig. 423.f) exhibited low colonization onto the nanocomposites as compared to the pristine HBPEA (Fig.4.24.a).

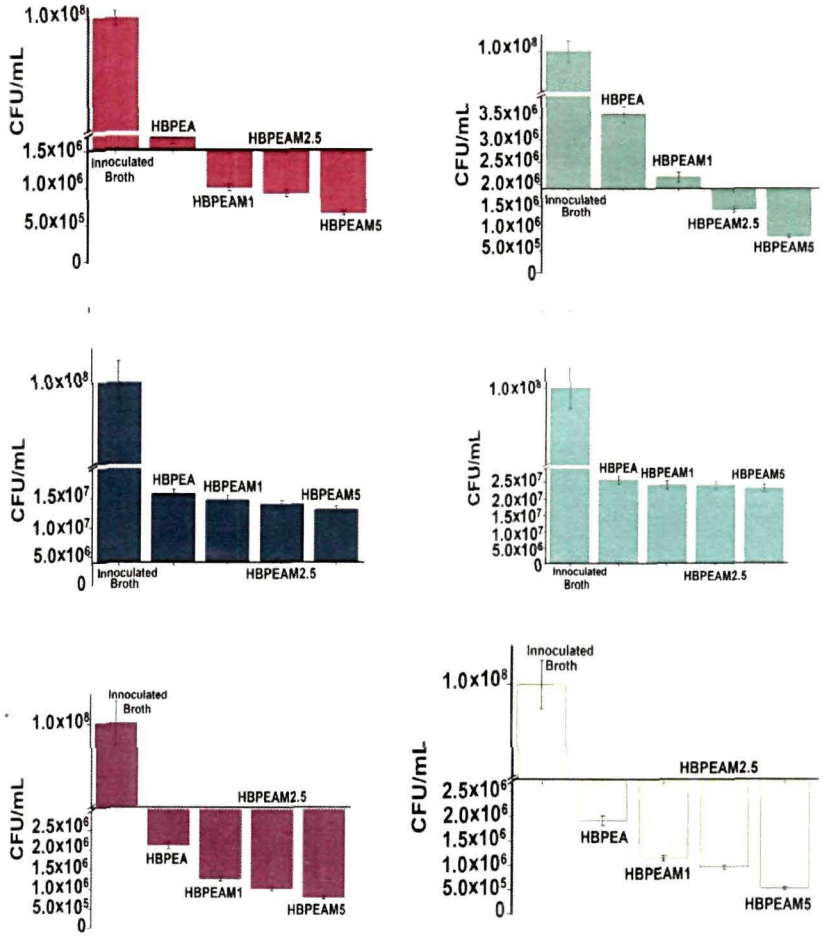

Fig. 4.23: Antimicrobial activity of HBPEA, HBPEAM1, HBPEAM2.5 and HBPEAM5 towards (a) *B. subtilis*, (b) *S. aureus*, (c) *E. coli*, (d) *K. pneumonia*, (e) *M. smegmatis* mc2 155, and (f) *M. smegmatis* ATCC14468. The CFU results are compared with the control sample of inoculated broth.

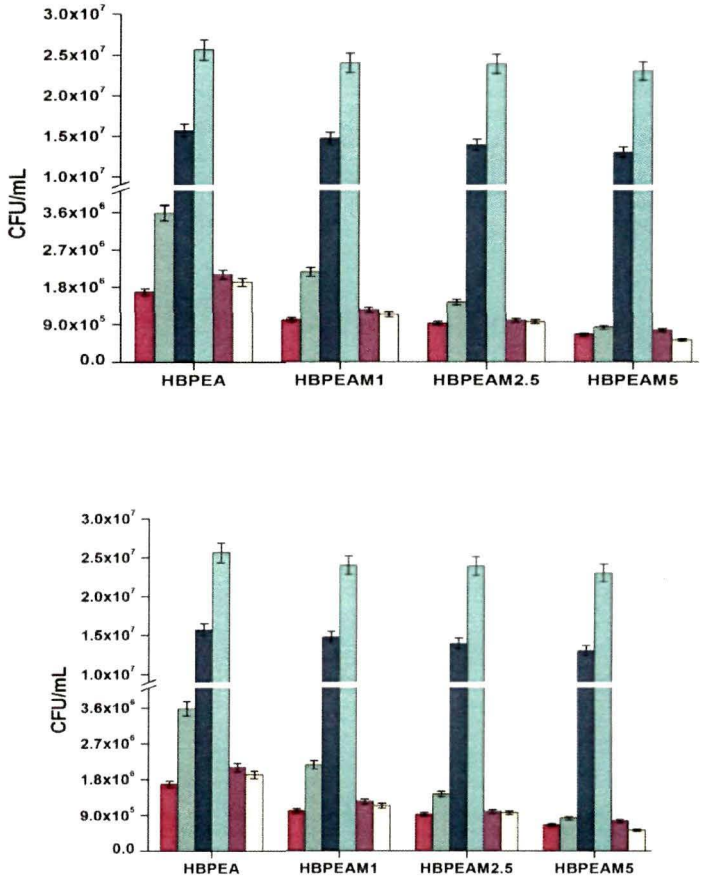

Fig. 4.24: Comparative antibacterial study in terms of (a) Colony-forming units enumerated from, and (b) protein adsorbed on the HBPEA, HBPEAM1, HBPEAM2.5 and HBPEAM5 towards *B. subtilis* (colored in red), *S. aureus* (colored in green), *E. coli* (colored in blue), *K. pneumonia* (colored in cyan), *M. smegmatis* mc2 155 (colored in purple) and *M. smegmatis* ATCC14468 (colored in yellow).

4.13.4 Total protein content from bacterial adhesion

The reduction in the protein adsorbed on the nanocomposite films was observed for the bacterial strains (Fig. 4.24.b). The adhesion of the bacteria onto the films decreased with the increase of *f*-MWCNT content, with the lowest adhesion

onto the HBPEAM5. This was attributed due to the synergism of antibacterial effect of MWCNT and the presence of emeraldine salt form of PAni nanofiber (the key structural unit having similarity with that of the active antibacterial tetracyclines) wrapped onto the MWCNT. The protein concentration increased similarly with increasing CFU count (Fig. 4.24.a). The proteins concentration of *B. subtilis* decreased by 80.6%, which is more than five-fold decrease as compared to *K. pneumoniae* upon culturing on the HBPEAM5 matrix. The decrease of protein content may arise from the *f*-MWCNT that retarded the bacterial cell growth result in decreased proliferation rates. The selective antibacterial potency of the nanocomposites, as estimated by the total protein content correlated well with the CFU study.

4.13.5 Interaction of the nanocomposite with the bacteria

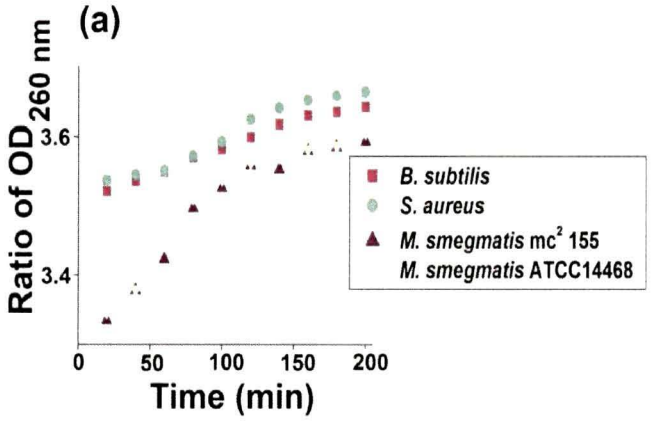

Fig.4.25: Release of 260 nm absorbing materials from Gram positive and acid fast positive bacterial strains.

The plausible mechanism of cytotoxicity of the prepared nanocomposites on the tested bacterial species is presented underneath. The release of intracellular components (having UV absorption at 260 nm) is indicative of loss of cell membrane integrity. The absorbance at 260 nm thus provided a mechanistic study of the

interaction of the bacterial cells with the nanocomposites (Fig. 4.25). It was observed that the release of the cytoplasmic constituents from the Gram positive bacterial strains attained to a level of saturation within 120 min of incubation, though the curve reached almost plateau, post 220 min incubation with the 20 μg/mL of nanocomposite at 37 °C. However, the mycobacterial strains exhibited a monotonic increase of the cytoplasmic constituents release over time. The release of these 260 nm absorbing materials from the bacterial cytoplasm is attributed to the disruption of the cell wall and cell membrane in the bacterial strains, which allowed the influx of the nanocomposites. The differential UV absorption pattern of the Gram positive and mycobacterial strains is attributed to the presence of a characteristic mycolic acid rich cell wall in the *M. smegmatis* which may have played an important role in a slow release profile.

Further the SEM study showed a distinct difference in cellular morphologies of the bacterial cells after treatment with the nanocomposite. The *B. subtilis* are elongated and evenly shaped cells, which became corrugated with ruptured cell surface upon interaction with the tested material (Fig. 4.26.b). The cell wrinkling and shortening together with the formation of craters were also observed. Upon interaction with the nanocomposite, deformation and disintegration of the cells were observed from round and proliferating cells with intact and well-defined membranes of the control *S. aureus* (Fig. 4.26.c). The *M. smegmatis* bacterial strains have uniform cylindrical-shape morphology (Fig. 4.26.d). The cells ruptured, becoming flattened together with compromising their cellular integrity (Fig. 4.26.e). The different morphological observations of two tested bacterial strains indicated their difference in the strain susceptibility towards the nanocomposite. Thus on the basis of the above study, it can be inferred that there exists a positive correlation of loss of cellular integrity and release of cytoplasmic constituents from the bacterial cells.

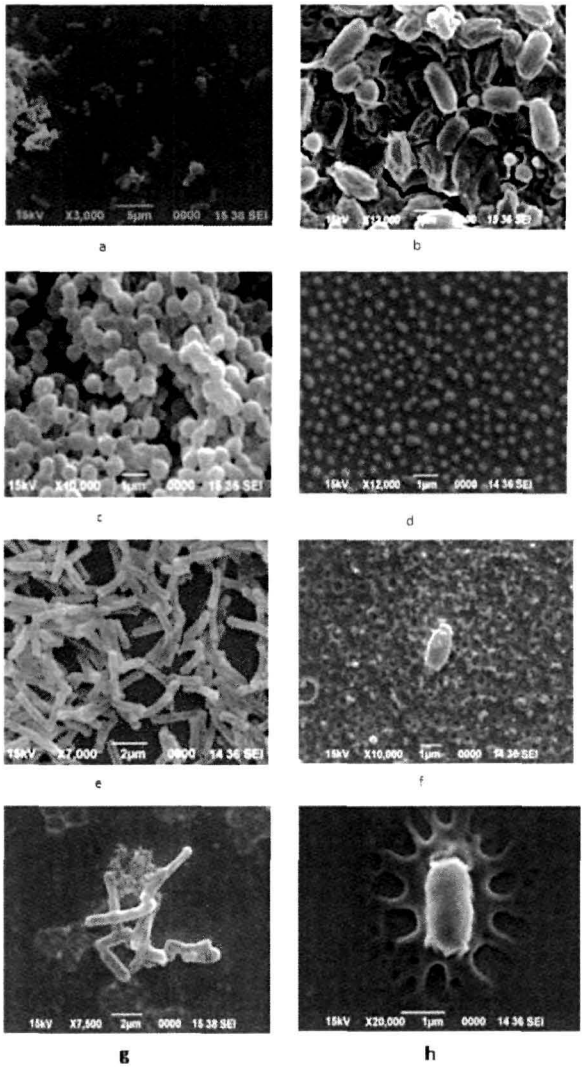

FIG4.26: Scanning electron micrographs of (a) *B.* subtilis without treatment, (b) *B.* subtilis upon interaction with the HBPEAM5 (c) *S. aureus* without treatment, (d) *S. aureus* upon interaction with the HBPEAM5 (e) *M. smegmatis* mc2 155 without treatment, (f) *M. smegmatis* mc2 155 upon interaction with the HBPEAM5 (g) *M. smegmatis* ATCC14468 without treatment (h) *M. smegmatis* ATCC14468 upon interaction with the HBPEAM5.

4.13.6 Trypan blue exclusion assay

The prepared nanocomposites were examined for their biocompatibility with PBMC by trypan blue exclusion assay. The PBMC-matrix adhesion was evident from the Fig. 4.27. It was observed that the nanocomposite films supported more cells as compared to the pristine polymer, indicating that *f*-MWCNT is the key player. The dose-dependent increment of cell viability of the nanocomposites is attributed to the presence of *f*-MWCNT as the cell adhesion and proliferation is influenced by the matrix on which it grows [304].

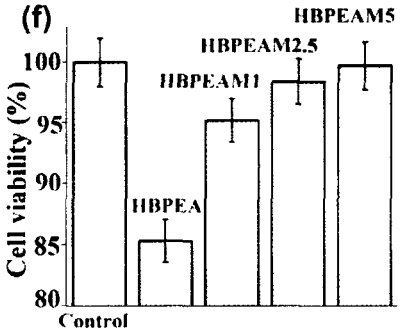

Fig. 4.27: Representative picture of cell viability using the trypan blue exclusion assay after 48 h of incubation of PBMC onto (a) control, (b) HBPEA, (c) HBPEAM1, (d) HBPEAM2.5, (e) HBPEAM5, and (f) % cell viability.

4.13.7 MTT assay

The biocompatibility of the prepared nanocomposites with PBMC was further examined by the colorimetric MTT assay. The spectroscopic measurement of the solubilized formazan crystals (an indirect measurement of the activity of the mitochondrial dehydrogenase) in MTT assay is directly related to the number of viable cells [305]. Fig. 4.28. showed a time- and dose-dependent increment in cell viability of the nanocomposites. The viability of the PBMC, same as in the control post 48 h incubation showed that the nanocomposite films exhibited no cytotoxic effect on the cells. The cell viability increased with the incubation time, imparting a

superior biocompatibility with time. The Janus-like properties of the MWCNT has been reported , wherein the pristine nanotubes are found to be cytotoxic to the cells, unless surface functionalized owing to the lowering of their surface activity. Thus the adhering of PGMA and PAni nanofiber onto the *f*-MWCNT together with their dispersion in between the HBPEA chains altered their cytotoxicity, thereby imparting biocompatibility with the PBMC.

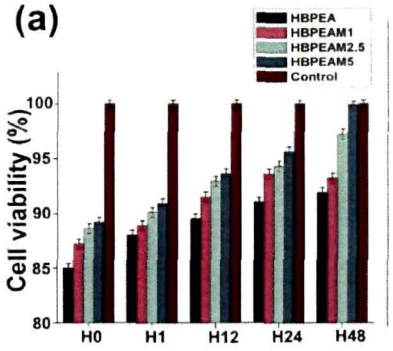

Fig. 4.28. The cell viability of PBMC in terms of absorbance at 540 nm at different time intervals of 0, 1, 12, 24 and 48.

4.13.8 PBMC adhesion and proliferation studies

The SEM was conducted to assess the seeding of PBMC, particularly to probe into the cell adhesion and proliferation onto the nanocomposite films. The SEM micrographs were found to be consistent with the proliferation of PBMC with *f*-MWCNT content, as indicated by an apparent increase in the magnitude of the adhered cells. Fig. 4.29 show the attachment and interaction of PBMC with porous HBPEA as well as the nanocomposite films. The presence of both macro- and micro-pores of diameter ranging from 10-230 nm (Fig. 4.29b) proved to be effective as anchoring points in the attachment and proliferation of the PBMC, as evident from Fig. 4.29.c. The 3D interconnected porous structure improve cell attachment and growth [306]. The low shrinkage of the films (due to their optimum crosslinking density) promoted cell adhesion and good biocompatible properties, which is further supported by Fernandes et al., 2010 [307]. The surface of the porous films exhibited

an interconnected structure of PBMC at the loading of 2.5 wt% *f*-MWCNT in the nanocomposite (appearing to mimic mesocarp of a watermelon pepo). However the PBMC were well-adhered and proliferated to form a continuous layer of cells covering the HBPEAM5. In other words, the surface of porous HBPEAM5 film exhibited a mat-like conformation (appearing to mimic a graphene sheet), with the pores of the film being completely masked by the continuous mesh of PBMC (Fig.

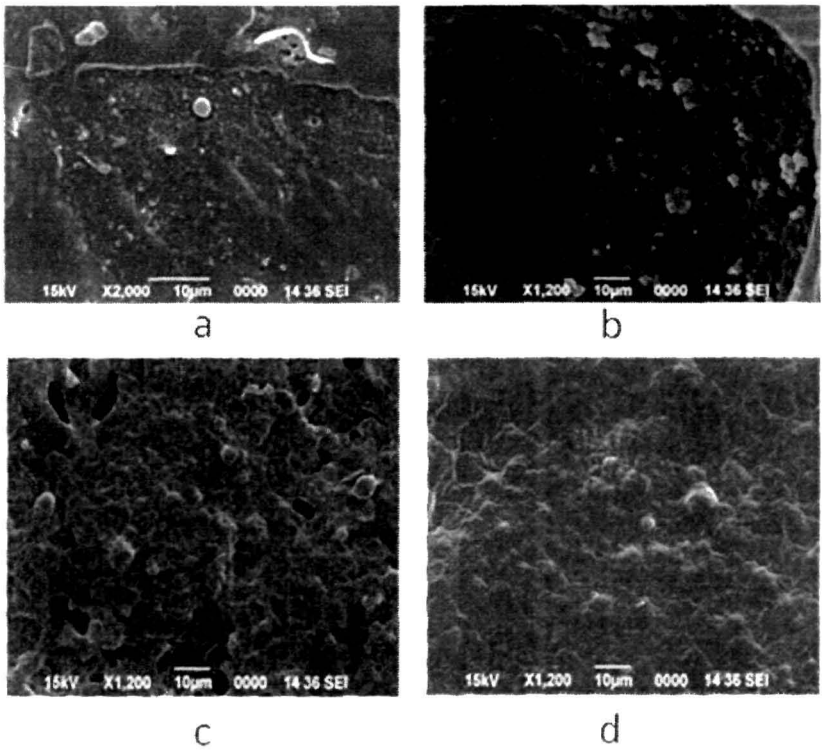

Fig4.29: SEM images showing adhesion and proliferation of PBMC after seeding on the surfaces of (a) HBPEA, (b) HBPEAM1, (c) HBPEAM2.5, and (d) HBPEAM5.

4.29.d). The porosity of the films allowed gas exchange (O2 uptake and CO2 release) together with passage of cell signaling of the PBMC .Thus the above results indicated the porous nanocomposite films support attachment and well proliferation of the PBMC. The hyperbranched architecture is exemplified with indispensable biological perspectives due to their unique 3D structure and presence of multitude of

functional groups at the periphery, imparting biocompatibility of the matrix via cellular interactions with PBMC. Rajaraman and his coworkers documented that spreading behaviour of the PBMC is governed by the factors like the available surface area, number and density of adhesion sites and other receptors of the substrate [304] .The SEM micrographs suggested that the biocompatibility was further augmented by increasing *f*-MWCNT content in the HBPEA matrix. It is essentially a surface phenomenon epitomized by cell-cell and cell-matrix interactions. Thus the masking of the MWCNT with PAni nanofiber and their dispersion in the HBPEA matrix impart tissue tolerance and cellular interactions [308] .The presence of carbonyl group on the surface of *f*-MWCNT also plays a key role in enhancing the biocompatibility owing to the decreased activation of mitochondria mediated apoptotic pathway [309] .Thus the SEM study corroborated well with the results obtained from trypan blue exclusion assay and MTT assay.

4.13.9 Measurement of reactive oxygen species (ROS)

The potential of the nanomaterials to penetrate the healthy cells due to their quantum size effect has triggered the exploration of the toxicity of the prepared nanocomposites. The production of ROS is a two-edged sword which acts as a boon in cell signaling, gene expression and in maintaining homeostasis in human, while as a bane by damaging cellular proteins, lipids and DNA that subsequently lead to carcinogenesis under oxidative stress condition [309]. It is primordial to know that production of ROS is one of the health hazards related to the exposure of MWCNT [310]. A decrease in the membrane integrity of the PBMC leads to the leakage of ROS outside the cell leading to cell apoptosis. Therefore, FRAP assay ,based on the reduction of ferric-tripyridyltriazine (FeIII-TPTZ) to an intense blue colored ferrous form (FeII), was performed [311]. The ROS production or reducing ability of the nanocomposites is directly proportional to the amount of ferrous product formed which can be quantified photometrically at 593 nm. The dose-response characteristics of the prepared nanocomposites showed a linear behavior Fig. 4.30. It was evident

from the FRAP assay that the ascorbic acid (control) showed an absorbance of 0.68, the prepared nanocomposites exhibited the absorbance of 0.5 post 10 min interaction with FeIII-TPTZ. The MWCNT on one hand showed no absorbance at 593 nm indicating their pronounced oxidative nature, while the *f*-MWCNT on the other hand showed meagre absorbance (0.09). The masking of MWCNT with large number of –OH groups residing at the periphery of the HBPEA, rendered the prepared nanocomposites with significantly low toxicity as compared to MWCNT. This study showed that the prepared nanocomposites attenuated the quenching of ROS as compared to the *f*-MWCNT.

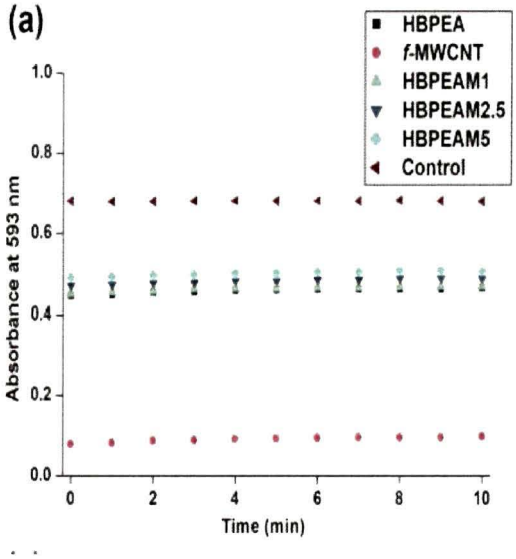

Fig. 4.30.ROS reaction kinetics

4.13.10 Hemocompatibility assay

The hemocompatibility is an important aspect of biocompatibility because of the direct/indirect contact of the samples with blood. The hemolytic assay results showed that the optical density at 540 nm observed for the pristine and the nanocomposites were equivalent as that of PBS, the negative control [266].Thus the samples showed no lysis of the red blood cells, implying their compatibility with the cells. Thus, in vitro cell response studies showed that the adhesion and proliferation rate of

the PBMC increased with increasing f-MWCNT content, without having any hemolysis activity or production of reactive oxygen species. In this context, both 3D porous interconnected network structure and presence of f-80 MWCNT proved to be the prime factors in harboring cell growth.

4.14.Antimycobacterial activity of poly(glycidyl methacrylate)-functionalized multiwall carbon nanotubes with a 'tendrillar' nanofibrous polyaniline wrapping

4.14.1.Minimum Inhibition Concentration

The antimycobacterial activity of the poly(glycidyl methacrylate)-functionalized multiwall carbon nanotubes with a nanofibrous polyaniline wrapping synthesized in the lab of Professor N. Karak, Department of Chemical Sciences , Tezpur University was also studied. MWCNTs sonicated in THF solvent was termed as S1,PGMA-f-MWCNTs was termed as S2, PAni nanofiber was termed S3 and PAni nanofiber wrapped around PGMA-f-MWCNTs was ermed asS4.The minimum inhibitory concentration of the nanocomposites required to inhibit the mycobacterial growth was found to be 8μg/mL for both S1 and S2 while S3 and S4 exhibited antimycobacterial activity at the higher concentration of 10 μg/mL. The toxicity of MWCNTs and PAni nanofiber in bacterial cells was found to be higher as compared to the functionalized nanotubes. This efficiency may be attributed to the larger surface area of the former available for interaction with the bacterial cell surface which in turn facilitated the penetration of the nanomaterials into the bacteria. The larger surface area facilitated the partitioning and partial penetration of nanotubes into the bacterial cell wall and thereby caused cell membrane damage and subsequent cell death by oxidative stress.

4.14.2 EtBr exclusion assay

Plasmids being critical for the survival of bacteria may be one of the possible targets of various antibacterial nanomaterials [312] and can be also used as a model to study the effect of antimicrobials on the DNA. To study the MWCNTs mediated antimicrobial activity plasmid DNA was incubated with the prepared samples and run on gel electrophoresis. The migration of the pristine and functionalized MWCNT-

plasmid DNA complex (for the concentration of 0.8 μg/mL of S1, S2, S3 and S4) in 1% agarose gel electrophoresis and the degree of plasmid DNA condensation by EtBr exclusion are shown in Fig.4.31.

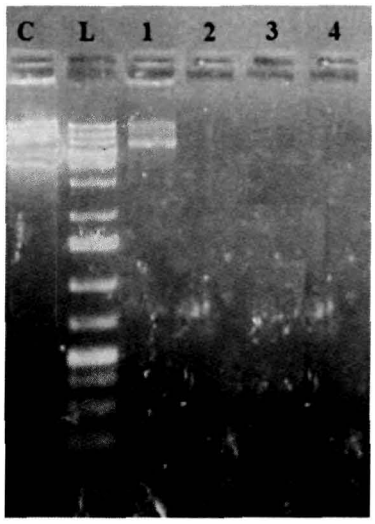

Fig 4.31: Agarose gel(0.8%) showing electrophoretic motility of the complexes of S1, S2, S3, and S4 with the plasmid DNA

Chapter V

Conclusion and Future Work

The multifaceted approaches of drug discovery from medicinal plants involving the combination of botanical, phytochemical, biological, computational and molecular techniques continue to provide new and important lead molecules against various pharmacological targets including cancer, HIV/AIDS and TB. The emergence of new resistant forms of infectious diseases has lead to the need for discovering new drugs. In the current scenario, each of the chemotherapeutic drugs of TB contains at least one resistant strain against it. Plants are a known source various phytochemicals and have been the corner stone of medicinal therapies for thousands of years, thus, forwarding a very important source for the discovery of new drug molecules.

As the study of the mechanisms of a large number of plant natural products by means of traditional assay based methods is a costly and time-consuming process due to the difficulty in extraction, synthesis, and activity testing, *in silico* virtual screening approach is fast emerging as an alternative strategy of choice for low-cost and rapid analysis of the plant derived natural products and efficient search for their targets.In the present study DFT-based QSAR studies were performed on a set of twenty seven chalcone molecules in order to identify the molecular descriptors responsible for their antimycobacerial activity. It was observed that the reliability of the QSAR model is higher in the case of the model built in the Solvent phase and the antimycobacterial activity of the chalcone molecules increased with the decrease in the descriptors of chemical hardness, Energy of Highest Occupied Molecular Orbital and Molar Refractivity of the group present in position 4'of Ring B of the chalcone molecules. The activity of the chalcone molecules decreased with the increase in the

Molar Refractivity of the group present in position 4 of Ring A of the chalcone molecules .

After the identification of the molecular descriptors , seven plants *viz.*, *Cynodon dactylon* L., *Chromonaela odorata* L. , *Glycine max* L., *Lawsonia inermis* L., *Mimosa pudica L., Potentilla fulgens* L. and Platycladus orientalis L. which are traditionally used in North East India to treat tuberculosis were screened for their amtimycobacterial activity. As chalcone are the common precursors of flavonoids synthesis, the antimycobacterial activity of flavonoid rich ethanolic extracts of seven plants which are traditionally known to be used for the treatment of TB were tested.

All the plant extracts were also assayed for their phenolics and flavonoid contents to ascertain the class of compounds present. *L. inermis* and *P. fulgens* had high phenolic and flavonoid contents followed by *C. odorata. P. orientalis* possessed the lowest total phenolic as well as flavonoid contents. The high amounts of phenolics and flavonoids correlate with the low MIC values of the plant crude extracts thus, providing an cue to the nature of the range of plant compounds with antimycobacterial properties.

A virtual screen of the chalcone and the flavonoids molecules of the seven plants which were identified by a literature survey was performed against the Thy X protein of *M. tuberculosis* . The molecular docking studies identified sixteen flavonoid molecules, *viz.*, Fisetin, Quercetin, Kaempferol, Rutin, Epigallocatechin gallate, Butein, Apiin, Acacetin, Daidzein, Gossypentin, 8- rhamnoside, Taxifolin, Apigenin, Genistein, Luteolin, Baicalein and Myricetin as putative inhibitors of Thy X. The maximum antimycobacterial activity was found to be in Luteolin which acted with the lowest MIC of 50 μg/μl.

In order to confirm the *in silico* driven hypothesis, the *thy x gene* of *M. smegmatis* was cloned, over expressed and purified. The inhibition of the activity of the Thy X by the flavonoid molecules was studied using the NADPH-oxidation

assay. The flavonoid molecule Apiin (IUPAC:7-[(2S,3R,4S,5S,6R)-3-[(2S,3R,4R)-3,4-dihydroxy-4-(hydroxymethyl)oxolan-2-yl]oxy-4,5-dihydroxy-6-(hydroxymethyl)oxan-2-yl]oxy-5-hydroxy-2-(4-hydroxyphenyl)chromen-4-one) was identified as a potent inhibitor of the Thy X enzyme. This is the first report of both cloning , over-expression of *thy x gene* of *M. smegmatis* as well as flavonoids as inhibitors of Thy X.

The antimycobacterial activity of the novel nanocomposites was studied .The multifunctional bio-based HBPEA/*f*-MWCNT nanocomposites nanocomposites exhibited antibacterial activity by triggering the release of a significant amount of cytoplasmic constituents of Gram positive bacteria as well as *M. smegmatis.* MTT assay established the biocompatibility of the nanocomposites with PBMC, further vouched by significant PBMC attachment and proliferation in response to varied *f*-MWCNT content of the nanocomposites and exposure time. Thus, this study opens up promising avenues for biomedical applications of the novel nanocomposites.

Investigation of the antimycobacterial activity functionalized nanotubes exhibited anti-mycobacterial activity at the higher concentration as compared to that of the pristine nanotubes due to the reduction of active surface area upon functionalization. The ethidium bromide exclusion assay indicated the complexation of the plasmid DNA with the nanomaterials as a possible mode of anti-bacterial action by the latter.

Future Work:
The future work includes the following:

1. Lead optimization of the Apiin molecule.
2. Animal toxicity studies of the optimized lead molecule.
3. Co-crystallization of the Thy X protein with Apiin.

References

1. Brosch, R., et al. A new evolutionary scenario for the *Mycobacterium tuberculosis* complex, *Proc. Natl. Acad. Sci.* **99**, 3684--89, 2002.
2. Niemann, S., et al. *Mycobacterium africanum* subtype II is associated with two distinct genotypes and is a major cause of human tuberculosis in Kampala, Uganda, *J. Clin. Microbiol* **40**, 3398--405, 2002.
3. Hart, P.D., & Sutherland, I. BCG and vole bacillus vaccines in the prevention of tuberculosis in adolescence and early adult life, *Br. Med. J.* **2**, 293--95. 1977.
4. Bloom, B.R., & Murray, C.J.L. Tuberculosis: Commentary on a Reemergent Killer, *Science* **257**, 1055--1064, 1992.
5. Dannenberg, A.M. Jr. Immunopathogenesis of pulmonary tuberculosis, *Hosp. Pract.* **28**, 51--58, 1993.
6. Ernst, J.D. Macrophage receptors for Mycobacterium tuberculosis, *Infect. Immun.* **66**, 1277--81, 1998.
7. Rajagopalan, M., et al. Mycobacterium smegmatis dnaA region and autonomous replication activity, *J. Bacteriol.* **177**(22), 6527--6535, 1995.
8. Lustgarten, S. Ueber spezifische Bacillen in syphilitischen Krankheitsprodukten. *Wiener Medizinische Wochenschrift* **1**, 1884.
9. Alvarez, E. & Tavel, E. Recherches sur le bacille de Lustgarten, *Arch Physiol Normal Pathol* **6**, 303--321, 1885.
10. Gupta, S. Stress Responses in Mycobacteria, *IUBMB Life* **57**(3), 149--159, 2005.
11. Dick, T., et al.Oxygen depletion induced dormancy in Mycobacterium smegmatis. *FEMS Microbiol. Lett.* **163**, 159-164,1998.
12. Bagchi, M., et al. Molecular analysis of the dormancy response in *Mycobacterium smegmatis*: expression analysis of genes encoding the DevR-DevS two-component system, Rv3134c and chaperone alpha-crystallin homologues. *FEMS Microbiol Lett* .**211**, 231-237,2002.

13. O'Toole, R., et al. A two component regulator of universal stress protein expression and adaptation to oxygen starvation in *Mycobacterium smegmatis*. *J. Bacteriol* .**185**,1543-1554,2003.
14. Altaf, M., et al. Evaluation of the *Mycobacterium smegmatis* and BCG models for the discovery of *Mycobacterium tuberculosis* inhibitors. *Tuberculosis* **90,** 333-337,2010.
15. Andries, K, et al. A diarylquinoline drug active on the ATP synthase of *Mycobacterium tuberculosis*. *Science.* **307**,223-227, 2005.
16. Chaturvedi, V., et al. Evaluation of Mycobacterium smegmatis as a possible surrogate screen for selecting molecules active against multidrug resistant *Mycobacterium tuberculosis, J Gen Appl Microbiol* **53**(6), 333--337, 2007.
17. Tyagi, J.S., & Sharma, D. *Mycobacterium smegmatis* and *tuberculosis. TrendsMicrobiol* **10**(2), 68--69, 2002.
18. Reyrat, J.M., & Kahn, D. *Mycobacterium smegmatis*: an absurd model for tuberculosis? *Trends Microbiol* **9**(10), 472--473, 2001.
19. Hershkovitz, I., et al. Detection and Molecular Characterization of 9000-Year Old Mycobacterium tuberculosis from a Neolithic Settlement in the Eastern Mediterranean, *PLoS One* **3** (10), 1--6, 2008.
20. Andersen, P., et al. The prognosis of latent tuberculosis: can disease be predicted? *Trends Mol Med* **13**(5), 175--182, 2007.
21. Ducati, R.G., et al. The resumption of consumption -- a review on tuberculosis, *Mem Inst Oswaldo Cruz* **101**(7), 697--714, 2006.
22. Donoghue, H.D. Human tuberculosis - an ancient disease, as elucidated by ancient microbial biomolecules, *Microbes Infect* **11**(14-15), 1156--116, 2009.
23. Chew, C.H., & Hu, P.Y. BCG Programme in the Republic of Singapore, *Singapore Medical Journal* **15**, 241—245, 1974.
24. World Health Organization. The World Health Organization Global Tuberculosis Program. 2003.
25. World Health Organization: Global Tuberculosis Control Epidemiology Strategy Financing, 2012.

26. Kunst, F., et al. The complete genome sequence of the gram-positive bacterium Bacillus subtilis, *Nature* **390**(6657), 249--256, 1997.
27. Cole, S.T., et al. Deciphering the biology of *Mycobacterium tuberculosis* from the complete genome sequence, *Nature* **393**, 537--544, 1998.
28. Cole, S.T. Learning from the genome sequence of *Mycobacterium tuberculosis* H37Rv. *FEBS Lett* **452**, 7--10, 1999.
29. Mostowy, S., et al. Genomic deletions suggest a phylogeny for the *Mycobacterium tuberculosis* complex, *J. Infect. Dis.* **186**, 74--80, 2002.
30. Kapur, V., et al. Is *Mycobacterium tuberculosis* 15,000 years old? *J. Infect. Dis.* **170**, 1348--49, 1994.
31. Stead, W.W., et al. When did *Mycobacterium tuberculosis* infection first occur in the New World? An important question with public health implications, *Am. J. Respir. Crit. Care Med.* **151**, 1267--68, 1995.
32. Comas, I. et al. Out-of-Africa and Neolithic coexpansion of Mycobacterium tuberculosis with modern humans.*Nat. Genet.* **45**, 1176–1182 ,2013.
33. Pepperell, C.S. et al. *The role of selection in shaping diversity of natural M. tuberculosis populations.PLoS Pathog.* **9**, 1-14 ,2013.
34. Warner, D. F. & Mizrahi, V. Complex genetics of drug resistance in *Mycobacterium tuberculosis. Nat. Genet.* **45** (10), 1107-1108,2013.
35. Kato-Maeda, M., et al. Comparing genomes within the species *Mycobacterium tuberculosis*, *Genome Res.* **11**, 547--54, 2001.
36. Fleischmann, R.D., et al. Whole-genome comparison of *Mycobacterium tuberculosis* clinical and laboratory strains, *J. Bacteriol.* **184**, 5479--90, 2002.
37. Russell, D.G. *Mycobacterium tuberculosis*: here today, and here tomorrow, *Nat. Rev. Mol. Cell Biol.* **2**,569--77, 2001.
38. Sibley, L.D., et al. Phagosome acidification blocked by intracellular Toxoplasma gondii, *Nature* **315**, 416--419, 1985.
39. Sibley, L.D., et al. Toxoplasma modifies phagosomes by secretion of a vesicular network rich in surface proteins, *J. Cell Biol.* **103**,867--874, 1986.

40. Joiner, K.A., et al. *Toxoplasma gondii*: fusion competence of parasitophorous vacuoles in Fc receptor-transfected fibroblasts, *Science.* **249**,641--646, 1990.

41. Hart, P.D., et al. Ultrastructural study of the behavior of macrophages to ward parasitic mycobacteria, *Infect. Immun.* **5**, 803--807, 1972.

42. Kim, K., et al. The isolation and purification of a specific "protector" protein which inhibits enzyme in activation by a thiol/Fe(III)/02 mixed-function oxidation system, *J. Biol. Chem.* **263**, 4704--4711, 1988.

43. Fields, P.I., et al. A Salmonella locus that controls resistance to microbicidal proteins from phagocytic cells, *Science.* **243**, 1059--1062, 1989.

44. Sansonetti, P.J., et al. Multiplication of Shigella flexneri within HeLa cells: lysis of the phagocytic vacuole and plasmid-mediated contacthemolysis, *Infect.Immun.* **51**, 461--469, 1986.

45. Portnoy, D.A., et al. Role of hemolysin for the intracellular growth of *Listeria monocytogenes*, *J.Exp.Med.***167**, 1459--1471, 1988.

46. Russell, D.G., et al. Foamy macrophages and the progression of the human tuberculosis granuloma, *Nat Immunol* **10**, 943-- 948, 2009.

47. Bishburg, E., et al. Central Nervous System Tuberculosis with the Acquired Immunodeficiency Syndrome and Its Related Complex, *Ann. Intern. Med.* 105(2), 210--3, 1986.

48. Rasool, M.N., et al. Cystic tuberculosis of bone in children, *J Bone Joint Surg Br* 76 (1), 113--117, 1994.

49. Kaufmann, S.H. Immune response to tuberculosis: experimental animal models, *Tuberculosis* **83**, 107--11, 2003.

50. North, R.J., & Jung, Y.J. Immunity to tuberculosis, *Annu. Rev. Immunol.* **22**,599--623, 2004.

51. Raghuvanshi, S., et al. *Mycobacterium tuberculosis* evades host immunity by recruiting mesenchymal stem cells, *Proc. Natl. Acad. Sci* **107** (50), 21653--21658, 2010.

52. Alcais, A., et al. Tuberculosis in children and adults: two distinct genetic diseases, *J. Exp. Med.* **202**, 1617--21, 2005.

53. Stewart, J.N., et al. Increased pathology in lungs of mice after infection with an alpha-crystallin mutant of *Mycobacterium tuberculosis*: changes in cathepsin proteases and certain cytokines, *Microbiol* 152(1), 233--44, 2006.

54. Schatz, A.B., et al. Streptomycin, a substance exhibiting antibiotic activity against gram-positive and gram-negative bacteria, *Proc. Soc. Exp. Biol. Med.* **55**, 66--69, 1944.

55. Chorine, V. Action de l'amide nicotiniquesurles bacillesdugenre Mycobacterium. *C. R. Acad. Sci.* 220:150–51, 1945.

56. Malone, L., et al. The effect of pyrazinamide (Aldinamide) on experimental tuberculosis in mice, *Am. Rev. Tuberc.* **65**, 511--18, 1952.

57. Liebermann, D., et al. Sur la preparation de nouveaux thioamides pyridiniques acitifs dans la tuberculose experimentale, *C. R. Acad. Sci.* **242**, 2409--12, 1956.

58. Thomas, J.P., et al. A new synthetic compound with antituberculous activity in mice: ethambutol (dextro-2, 2 -(ethylenediimino)-di-butanol), *Am. Rev. Respir. Dis.* **83**, 891--93, 1961.

59. Kurosawa, H. Studies on the antibiotic substances from actinomyces. The isolation of an antibiotic produced by a strain of Streptomyces "K 30", *J. Antibiot. Ser. B* **5**, 682--88, 1952.

60. Umezawa, H., et al. Production and isolation of a new antibiotic, kanamycin, *J. Antibiot. Jpn. Ser. A* **10**,181--88, 1957.

61. Bartz, Q.R., et al. Viomycin, a new tuberculostatic antibiotic, *Am. Rev. Tuberc.* **63**, 4--6, 1951.

62. Herr, E.B. Jr., et al. Isolation and characterization of a new peptide antibiotic, *Proc. Indiana Acad. Sci.* **69**,134, 1960.

63. Sensi, P., et al. Rifomycin, a new antibiotic. Preliminary report, *Farmaco. Sci.* **14**, 146--47, 1959.

64. Maggi, N., et al. Rifampicin: a new orally active rifamycin, *Farmaco. Sci.* **21**, 68--75, 1966.

65. Tsunekawa, H.M.T., et al. Therapeutic effect of ofloxacin on 'treatment failure' pulmonary tuberculosis, *Kekkaku* **62**,435--39, 1987.
66. Yew, W.W., et al. *In-vitro* activity of ofloxacin against *Mycobacterium tuberculosis* and its clinical efficacy in multiply resistant pulmonary tuberculosis, *J. Antimicrob. Chemother.* **26**, 227--36, 1990.
67. Chan, E.D., & Iseman, M.D. Current medical treatment for tuberculosis, *BMJ* **325**(7375), 1282--1286, 2002.
68. Frieden, T.R., et al. Tuberculosis, *The Lancet* **362**(9387), 887--899, 2003.
69. Onyebujoh, P., et al. Treatment of tuberculosis: present status and future prospects, *Bulletin of the World Health Organization* **83**, 857--865, 2005.
70. Spigelman, M.K. New Tuberculosis Therapeutics: A Growing Pipeline, *J. Infect. Dis.* **196**(1), 28--34, 2007.
71. Guy, E.S., & Mallampalli, A. Review: Managing TB in the 21st century: existing and novel drug therapies, *Ther Adv Respir Dis.* **2**(6), 401--408, 2008.
72. Chan, E.D., & Iseman, M.D. Current medical treatment for tuberculosis, *BMJ,* **325**(7375), 1282--1286, 2002.
73. Zhang, Y., & Mitchison, D.A. The curious characteristics of pyrazinamide: a review, *Int. J. Tuberc. Lung Dis.* **7**, 6--21, 2003.
74. Deng, L., et al. Recognition of multiple effects of ethambutol on metabolism of mycobacterial cell envelope, *Antimicrob Agents Chemother* **39**, 694--701, 1995.
75. Belanger, A., et al. The embAB genes of Mycobacterium avium encode an arabinosyl transferase involved in cell-wall arabinan biosynthesis that is the target for the antimycobacterial drug ethambutol, *Proc Natl Acad Sci* **93**, 11919--24, 1996.
76. Vilcheze, C., et al. Transfer of a point mutation in MT inhA resolves the target for isoniazid, *Nat Med* **12**, 1027--9, 2006.
77. Boshoff, H., et al. Effects of pyrazinamide on fatty acid synthesis by whole mycobacterial cells and purified fatty acid synthase I, *J Bacteriol* **184**, 2167--72, 2002.

78. Zhang, Y., et al. Mode of action of pyrazinamide: disruption of Mycobacterium tuberculosis membrane transport and energetics by pyrazinoic acid, *J Antimicrob Chemother* **52**, 790--5, 2003.

79. Wade, M., & Zhang, Y. Anaerobic incubation conditions enhance pyrazinamide activity against Mycobacterium tuberculosis, *J Med Microbiol* **53**, 769--73, 2004.

80. Wade, M., & Zhang, Y. Effects of weak acids, UV and proton motive force inhibitors on pyrazinamide activity against Mycobacterium tuberculosis in vitro, *J Antimicrob Chemother* **58**, 936--41, 2006.

81. Wehrli, W., et al. Interaction of rifamycin with bacterial RNA polymerase, *Proc Natl Acad Sci* **61**, 667--73, 1968.

82. Davies, A., et al. Comparison of phenotypic and genotypic methods for pyrazinamide susceptibility, *J Clin Microbiol* **38**, 3686--8, 2000.

83. Huitric, E., et al. Resistance levels and rpoB gene mutations among in vitro - selected rifampin-resistant *Mycobacterium tuberculosis* mutants, *Antimicrob Agents Chemother* **50**, 2860--2, 2006.

84. Perri, G.D., & Bonora, S. Which agents should we use for the treatment of multidrug-resistant *Mycobacterium tuberculosis*? *J. Antimicrob. Chemother.* **54**(3), 593--602, 2004.

85. Sharma, S.K., & Mohan, A. Multidrug-Resistant Tuberculosis, *Chest*, **130**(1), 261--272, 2006.

86. Wing W. Y., Management of multidrug-resistant tuberculosis: Update 2007, *Respirology*, **13**(1), 21--46, 2008.

87. Deitz, W.H., et al. Froelich EJ. In vitro antibacterial properties of nalidixic acid, a new drug active against gram-negative organisms, *Antimicrob. Agents Chemother.* **161**, 583--87, 1963.

88. Andersson, M.I., & MacGowan, A.P. Development of the quinolones, *J. Antimicrob. Chemother.* **51**(1), 1--11, 2003.

89. Jacobs, M. Activity of quinolones against mycobacteria, *Drugs* **58**(2), 19--22, 1999.

90. Grimaldo, E.R., et al. Increased resistance to ciprofloxacin and ofloxacin in multidrug-resistant *Mycobacterium tuberculosis* isolates from patients seen at a tertiary hospital in the Philippines, *Int. J. Tuberc. Lung Dis.* **5**,546--50, 2001.

91. Takiff, H.E., et al. Cloning and nucleotide sequence of *Mycobacterium tuberculosis gyrA* and *gyrB* genes and detection of quinolone resistance mutations, *Antimicrob. Agents Chemother.* **38**, 773--80, 1994.

92. Kocagoz, T., et al. Gyrase mutations in laboratory selected, fluoroquinolone-resistant mutants of *Mycobacteriumtuberculosis* H37Ra, *Antimicrob Agents Chemother.* **40**, 1768--74, 1996.

93. Gardner, C, A., et al. The Global Alliance for Tuberculosis Drug Development--Accomplishments and Future Directions, *Clinics in Chest Medicine* **26**(2), 341--347, 2005.

94. Dye, C. Doomsday postponed? Preventing and reversing epidemics of drug-resistant tuberculosis, *Nat Rev Micro* 7(1), 81--87, 2009.

95. Velayati, A. A., et al. Emergence of new forms of totally drug-resistant tuberculosis bacilli: super extensively drug-resistant tuberculosis or totally drug-resistant strains in Iran, *Chest* **136**(2), 420--425, 2009.

96. Nguyen, L., & Pieters, J. Mycobacterial Subversion of Chemotherapeutic Reagents and Host Defense Tactics: Challenges in Tuberculosis Drug Development, *Annu. Rev..Pharmacol. .Toxicol.* **49**, 427--53, 2009.

97. Gillespie, S.H. Evolution of Drug Resistance in *Mycobacterium tuberculosis*: Clinical and Molecular Perspective, *Antimicrob. Agents Chemother.* **46**(2), 267--274, 2002.

98. Nguyen, L., & Thompson, C.J. Foundations of antibiotic resistance in bacterial physiology: the mycobacterial paradigm, *Trends Microbiol.* **14**(7), 304--312, 2006.

99. Chalker, A.F., & Lunsford, R.D. Rational identification of new antibacterial drug targets that are essential for viability using a genomics based approach, *Pharmacol Ther* **95**(1), 1--20, 2002.

100. World Health Organization. Global Tuberculosis Control; Surveillance, Planning, Financing. 2008.

101. Guillemont, L., & Lounis N.. New anti-tuberculosis drugs in clinical development: an overview, *Curr Bioact Compd* **5**(2), 137--154, 2009.

102. Zhao D., et al. Advance in the research of new anti-tuberculosis drugs in clinical trials, Journal of New Drugs, 2009.

103. Sasaki, H., et al. Synthesis and Antituberculosis Activity of a Novel Series of Optically Active 6-Nitro-2, 3-dihydroimidazo[2,1-*b*]oxazoles, *J. Med. Chem* **49**(26), 7854--7860, 2006.

104. Matsumoto, M., et al. OPC-67683, a Nitro-Dihydro-Imidazooxazole Derivative with Promising Action against Tuberculosis In Vitro and In Mice, *PLoS Med* **3**(11), 2131--2144, 2006.

105. Mdluli, K., & Ma, Z. *Mycobacterium tuberculosis* DNA gyrase as a target for drug discovery, *Infect Disord Drug Targets* 7(2), 159 --168. 2007.

106. Von Groll, A., et al., Fluoroquinolone resistance in *Mycobacterium tuberculosis* and mutations in gyrA and gyrB. *Antimicrob Agents Chemother.* **53**(10), 4498--500, 2009.

107. Walubo, A. The role of cytochrome P450 in antiretroviral drug interactions, *Expert Opin Drug Metab Toxicol* **3**(4), 583--598. 2007.

108. Dover, L.G., & Coxon, G.D. Current Status and Research Strategies in Tuberculosis Drug Development, *Journal of Medicinal Chemistry* **54**, 6157 -- 6165, 2011.

109. Philips, J.A., & Ernst, J.D. Tuberculosis Pathogenesis and Immunity, *Annu. Rev. Pathol. Mech. Dis.* 7, 353--84, 2012.

110. Boshoff, H.I., et al. The transcriptional responses of M. tuberculosis to inhibitors of metabolism: Novel insights into drug mechanisms of action, *J. Biol. Chem.*196-200. 2004

111. Tatusov, R.L., et al. A Genomic Perspective on Protein Families, *Science* **278**(5338), 631--637, 1997.

112. Pathania, R.& Brown, E.D Small and lethal: searching for new antibacterial compounds with novel modes of action, *Biochem Cell Biol* **86**(2), 111-115, 2008.

113. Hughes, D. Exploiting genomics, genetics and chemistry to combat antibiotic resistance, *Nat Rev Genet* **4**(6), 432--441, 2003.

114. Moir, D.T., et al. Genomics and Antimicrobial Drug Discovery, *Antimicrob. Agents Chemother.* **43**(3), 439--446, 1999.

115. Sampathkumar, P., et al. Structure of the *Mycobacterium tuberculosis* flavin dependent thymidylate synthase (Mtb ThyX) at 2.0A resolution, *J Mol Biol* **352**, 1091--1104. 2005.

116. Carreras, C.W., & Santi, D.V. The catalytic mechanism and structure of thymidylate synthase, *Annu Rev Biochem* **64**, 721--762. 1995.

117. Myllykallio, H., et al. An alternative flavin dependent mechanism for thymidylate synthesis, *Science* **297**, 105--107, 2002.

118. Mathews, I. I., et al. Functional analysis of substrate and cofactor complex structures of a thymidylate synthase-complementing protein, *Structure (Camb)* **11**, 677--690. 2003.

119. Myllykallio, H., et al. Life without dihydrofolate reductase FolA. *Trends Microbiol.* **11**, 220--223, 2003.

120. Sampathkumar, P., et al. $NADP^+$ Expels both the Co-factor and a Substrate Analog from the *Mycobacterium tuberculosis* ThyX Active Site: Opportunities for Anti-bacterial Drug Design, *J. Mol. Biol.* **360**, 1--6, 2006.

121. Sassetti, C.M., et al. Genes required for mycobacter ial growth defined by high density mutagenesis, *Mol M icrobiol* **48**, 77--84, 2003.

122. Sassetti, C.M., & Rubin, E.J. Genetic requirements for mycobacterial survival during infection, *Proc Natl Acad Sci* **100**, 12989--12994, 2003.

123. Rengarajan, J., et al. Genome-wide requirements for *Mycobacterium tuberculosis* adaptation and survival in macrophages, *Proc. Natl Acad. Sci.* **102**, 8327--8332, 2005.

124. Hardy, L. W, et al. Atomic structure of thymidylate synthase: target for rational drug design. *Science* 235, 448--455. 1987.

125. Murzin, A. G. DNA building block reinvented, *Science 297, 61--62,* 2002.

126. Kuhn, P., et al. Crystal structure of thy1, a thymidylate synthase complementing protein from*Thermotoga maritima* at 2.25 A resolution, *Proteins* **49**, 142--145. 2002.

127. Donadio, S., et al. Targets and assays for discovering novel antibacterial agents. *J Biotechnol* **99**(3), 175--185. 2002.

128. Loferer, H., et al. Integrated bacterial genomics for the discovery of novel antimicrobials, *DDT* **5**(3), 107--114, 2000.

129. Balganesh, T.S., et al. Rising standards for tuberculosis drug development, *Trends Pharmacoll Sci* **29**(11), 576--581, 2008.

130. Gautam, R., et al. Indian medicinal plants as source of antimycobacterial agents, *J Ethnopharmacol* **110**, 200--234, 2007.

131. Baker, J.T., et al. Natural product drug discovery and development new perspectives on international collaboration, *J Nat Prod* **58**, 1325--1357, 1995.

132. Shrestha, P.M., & Dhillion, S.S. Medicinal plant diversity and use in the highlands of Dolakha district, Nepal, *J Ethnopharmacol* **86**, 81--96, 2003.

133. Gadgil, M., & Rao, P.R.S. Nurturing biodiversity: an Indian agenda. Centre for Environment Education, Ahmedabad, India., 1998.

134. Dutta, B.K., & Dutta, P.K. Potential of ethnobotanical studies in Norht East India: An Overview, *IJTK* **4**, 7--14, 2005.

135. Mao, A.A., et al. Plant wealth of Northeast India with reference to ethnobotany, *IJTK* **8**, 96--103, 2009.

136. Duffy, B.C., et al. Early phase drug discovery: Cheminformatics and computational techniques in identifying lead series, *Bioorg. Med. Chem.***20,** 5324--5342, 2012.

137. Hardy, L.W., & Malikayil, A. The impact of structure-guided drug design on clinical agents *Curr. Drug. Discov.* **15**,15-20,2003.

138. Maryanoff, B. E. Inhibitors of serine proteases as potential therapeutic agents: the road from thrombin to tryptase to cathepsin G. *J. Med. Chem.*, **47**, 769-787, 2004.

139. Acharya, C., et al.. Recent advances inligand-based drug design: relevance and utility of the conformationally sampled pharmacophore approach. *Curr Comput Aided Drug Des.* 7,10-22,2011.

140. Ou-Yang S., et al. Computational drug discovery. *Acta Pharm. Sinic.***33**, 1131–1140,2012.

141. Tang, Y., et al. New technologies in computer aided drug design: Toward target identification and new chemical entity discovery. *DDTT* **3**,307-313, 2006.

142. Wang, F., et al. Computational screening for active compounds targeting protein sequences: methodology and experimental validation. *J. Chem.Inf. Model.***51**,2821–28,2011.

143. Schneider, G. Virtual screening: an endless staircase? *Nat. Rev. Drug Discov.* **9**, 273 – 276,201 0.

144. Gozalbes, R., et al. Development and experimental validation of a docking strategy for the generation o f kinase-targeted libraries, *J Med Chem.* **51**, 3124--32, 2008.

145. Deng, X.Q., et al. Pharmacophore modelling and virtual screening for identification of new Aurora-A kinase inhibitors, *Chem Biol Drug Des* **71**, 533--9, 2008.

146. Deanda, F., et al. Kinase-targeted library design through the application of the PharmPrint methodology, *J Chem Inf Model* **48**, 2395--403, 2008.

147. Briem, H., & Gunther, J. Classifying "kinase inhibitor-likeness" by using machine-learning methods, *Chembiochem* **6**, 558--66, 2005.

148. Gundla, R., et al. Discovery of novel small-molecule inhibitors of human epidermal growth factor receptor-2: combined ligand and targetbased approach, *J Med Chem* **51**, 3367--77, 2008.

149. Ma, X.H., et al. Evaluation of virtual screening performance o f support vector machines trained by sparsely distributed active compounds, *J Chem Inf Model* **48**(6),1227--37, 2008.

150. Moroy, G., et al.Toward *in silico* structure-based ADMET prediction in drug discovery, *DDT* **17** (1-2), 44-- 55, 2012.

151. Barua, N., et al. DFT-based QSAR Models to Predict the Antimycobacterial Activity of Chalcones, *CBDD.* **79**, 553--559, 2012.

152. Benedetti, P. G. D., & Fanelli F.. Computational quantum chemistry and adaptive ligand modeling in mechanistic QSAR. *D.D.T.* **15**,19-20, 2010.

153. Agrafiotis, D.K. et al. Recent advances in chemoinformatics. *J. Chem. Inf.Model.* **47**, 1279–1293, 2007.

154. Baker-Austin, C. et al. Co-selection of antibiotic and metal resistance. *Trends. Microbiol.* **14**, 176–182,2006.

155. Huh, A.J. & Kwon, Y.J. "Nanoantibiotics": a new paradigm for treating infectious diseases using nanomaterials in the antibiotics resistant era. *J. Control. Release* .**156**, 128–145,2011.

156. Whitesides, G.M. Nanoscience, nanotechnology, and chemistry. **1**, 172–179,2005.

157. Hajipour, M. J., et al. Antibacterial properties of nanoparticles *Trends. Biotech.***30**,(10),1-1, 2012.

158. Dankovich, T.A. & Gray, D.G. Bactericidal paper impregnated with silver nanoparticles for point-of-use water treatment..*Environ. Sci. Technol.* **45**, 1992–1998, 2011.

159. Abdullayev, E., et al. Natural Tubule Clay Template Synthesis of Silver Nanorods for Antibacterial Composite Coating ACS *Appl. Mater. Interfaces* **3**, 4040–4046, 2011.

160. Zhang, N., et al. Preparation and characterization of core–shell structure of SiO2@Cu antibacterial agent. *Colloids Surf. B Biointerfaces* .**81** (1),537–543,2010.

161. Sui , M., et al. Synthesis of ZnO coated multi-walled carbon nanotubes and their antibacterial activities. *Sci Total Environ* **452,** 148–154,2013.

162. Krishna, V., et al. Photocatalytic disinfection with titanium dioxide coated muti-wall carbon nanotubes. *Process .Saf. Environ .Prot.* **83**(B4),393-397,2005.

163. Li, Q., et al. Antimicrobial nanomaterials for water disinfection and microbial control: potential applications and implications. *Water Res* **42,** 4591–4602,2008.

164. Lukhele, L.P., et al. Water disinfection using novel cyclodextrin polyurethanes containing silver nanoparticles supported on carbon nanotubes. *J. Appl. Sci.***10**(1)65-70, 2010.

165. Upadhyayula, V.K.K., et al., . Application of carbon nanotube technology for removal of contaminants in drinking water: a review. *Sci. Total. Environ.***408,**1-13,2009.

166. Kang, S., et al. Single-walled carbon nanotubes exhibit strong antimicrobial activity. *Langmuir* **23**,8670-8673,2007..

167. Kang, S., et al. Antibacterial Effects of Carbon Nanotubes: Size Does Matter! *Langmuir.***24** , 6409–6413,2008.

168. Kang S., et al. Microbial cytotoxicity of carbon-based nanomaterials: implications for river water and wastewater effluent. *Environ. Sci. Technol.* **43,** 2648–2653,2009.

169. Tiruviluamala, P. & Reichman, L. B. Tuberculosis. *Annu. Rev. Public Health* .**23**, 403-426,2002.

170. Zhang Y. The magic bullets and tuberculosis drug targets. *Annu Rev Pharmacol Toxicol.* **45**,529–564,2005.

171. Smith, C.& Sacchettini, J.. *Mycobacterium tuberculosis*: a model system for structural genomic. *Curr. Opinion. Struct.Biol.* .**13**, 658–664,2003.

172. World Health Organization. Global Tuberculosis Control Epidemiology Strategy Financing, 2011.

173. Rivers, E.C.,& Mancera, R.L. New anti-tuberculosis drugs in clinical trials with novel mechanisms of action,*DDT* **13**, 1090--1098, 2008.

174. Stover, C.K., et al. A small-molecule nitroimidazopyran drug candidate for the treatment of tuberculosis, *Nature* **405**, 962--966, 2000.

175. Protopopova, M., et al. Identification of a new antitubercular drug candidate, SQ109, from a combinatorial library of 1,2-thylenediamines, J. *Antimicrob.Chemother* .**56**(5), 968--974, 2005.

176. Dahanukar, S. & Thatte, U., *Ayurveda Revisited*, Popular Prakashan, Mumbai, 2000, 3rd edn.

177. Chopra, A., & Doiphode, V., Ayurvedic medicine: Core concept, therapeutic principles, and current relevance. *Med. Clin. North Am.***86,** 75– 8, 2002.

178. Grabley, S.,& Thiericke, R. Drug Discovery from Nature.*Springer*,1999.

179. Dutta, B.K.,& Dutta, P.K.. Potential of ethnobotanical studies in NE India: An Overview. IJTK.**4**(1), 7-14, 2005.

180. Copp, B.R., & Pearce A.N. Natural product growth inhibitors of *Mycobacterium tuberculosis Nat. Prod. Rep.* **24**, 278–297,2007.

181. Schippmann, U., et al. Plants as source of medicines: new perspectives. Bogers RJ, Craker LE, Lange D (eds) Medicinal and Aromatic Plants – Agricultural, Commercial, Ecological, Legal, Pharmacological and Social Aspects. *Springer*, Dordrecht,75,2006.

182. Jain, A., et al. Medicinal plant diversity of Sitamata wildlife sanctuary, Rajasthan, India, *J.Ethnopharmacol.* **102**(2), 143--57, 2005.

183. Sajem, A. L., & Gosai, K. Traditional use of medicinal plants by the Jaintia tribes in North Cachar Hills district of Assam, northeast India, *J Ethnobiol Ethnomed.* 2, 33--39, 2006.

184. Purakayastha, J., & Nath, S. C. Biological activities of ethnomedicinal claims of some plant species of Assam, *IJ T K.* **5**(2), 229--236, 2006.

185. Parveen, et al. Traditional uses of medicinal plants among the rural communities of Churu district in the Thar Desert, India, *J Ethnopharmacol* 113 (3), 387--399, 2007.

186. Ribeiro, A., et al. Ethnobotanical survey in Canhane village, district of Massingir, Mozambique: medicinal plants and traditional knowledge, *J Ethnobiol Ethnomed.* 6, 33, 2010.

187. Singh, A. G., et al. An ethnobotanical survey of medicinal plants used in Terai forest of western Nepal, *J of Ethnobiol and Ethnomedicine* 8, 19--33, 2012.

188. Copp BR.. Antimycobacterial natural products. *Nat. Prod. Rep.* 2003 535-557.

189. Samuelsson , G. Drugs o f Nat ural Origin: A Textbook of Pha rmacognosy . 4th Revised Edition . *Swedish Pharmaceutical Press*, Stockholm , Sweden , 1999.

190. Cushnie,T.P. T., & Lamb A, J. Antimicrobial activity of flavonoids. *Int J Antimicrob Ag* .**26,** 343–356,2005

191. Grotewold, E. The Science of flavonoids. *Springer* . 1-2, 2006.

192. Harborne, J.B., et al. *The Flavonoids*, London, Chapman and Hall, 1974.

193. Beecher, G.R. Overview of Dietary Flavonoids: Nomenclature, Occurrence and Intake. *J Nutr*, **133** , 3248-3254,2003.

194. Suksamram A., et al. Antimycobacetrial and antioxidant flavones from *Limnophila geoffrayi. Arch. Pharm. Res.* **26**(10),816-820, 2003.

195. Suksamram A., et al. Antimycobacterial activity and cytotoxicity of flavonoids from the flowers of *Chromolaena odorata. Arch. Pharm. Res.* **27** (5), 507-511, 2004.

196. Koysomboon S., etal. Antimycobacterial flavonoids from *Derris indica. Phytochemistry.* **67**,1034–1040, 2006.

197. Begum S., et al. 2008. Antimycobacterial activity of flavonoids from *Lantana camara Linn. Nat. Prod. Res.* **22**(6):467-470.

198. Brown A.K., et al. Flavonoid inhibitors as novel antimycobacterial agents targeting *Rv0636*, a putative dehydratase enzyme involved in *Mycobacterium tuberculosis* fatty acid synthase II. *Microbioogyl.***153,**3314–3322, 2007.

199. Lechner D., et al.Modulation of isoniazid susceptibility by flavonoids in Mycobacterium. *Phytochem. Lett.* **1** ,2008.

200. Mativandlela, S.P., et al. Antimycobacterial flavonoids from the leaf extract of *Galenia africana.J Nat Prod.* **72**(12), 2169-71,2009.

201. Kuetea, V., et al. Evaluation of flavonoids from *Dorstenia barteri* for their antimycobacterial, antigonorrheal and anti-reverse transcriptase activities . *Acta Tropica.* **116**(1), 100–104,2010.

202. Favela-Hernández, J. M. J., et al.Antibacterial and Antimycobacterial Lignans and Flavonoids from *Larrea tridentate. Phytother. Res.* **26**(12), 1957–1960,2012.

203. Castellar, A., et al. The activity of flavones and oleanolic acid from *Lippia lacunosa* against susceptible and resistant *Mycobacterium tuberculosis* strains. *Rev.bras.farmacogn.* **21**(5), 835-840, 2011.

204. Chen, L.W., et al. Secondary Metabolites and Antimycobacterial Activities from the Roots of *Ficus nervosa.* Chem Biodivers. 7(7), 1814–1821, 2010.

205. Chokchaisiri, R., et al. Bioactive Flavonoids of the Flowers of *Butea monosperma* . Chemical and Pharmaceutical Bulletin Vol. 57 (2009) No. 4 P 428-432

206. Murillo, J.I., et al. Antimycobacterial flavones from *Haplopappus sonorensis, Fitoterapia* **74** (3), 226--230, 2003.

207. Friis-Møller, et al., In vitro antimycobacterial and antilegionella activity of licochalcone A from Chinese licorice roots. *Planta Med.*, **68**, 416-419, 2002.

208. Mitscher ,L. A. & Baker, W. R.. A search for novel chemotherapy against tuberculosis amongst natural products. *Pure Appl. Chem.*, 1998, 70,365-371.

209. Bhardwaj, A., et al. Open source drug discoverye A new paradigm of collaborative researchin tuberculosis drug development. *Tuberculosis* .**91,** 479-486 ,2011.

210. Jennings, A., & Tennet, M. Discovery strategies in a biopharmaceutical startup : Maximising your chances of success using computational filters:Computer aided drug design. *Curr. Pharm. Des.* **11,**335-344,2005.

211. Shekhar, C. In Silico P harmacology: Computer-Aided Methods Could Transform Drug Development. *Chemistry & Biology* .***15,*** 13-14,2008.

212. Hansch, C., et al. The Correlation of Biological Activity of Plant Growth Regulators and Chloromycetin Derivatives with Hammett Constants and Partition Coefficients, *J Am Chem Soc* **85**, 2817--2824, 1963.

213. Lill, M.A., et al. Multi-dimensional QSAR in drug discovery , *DDT* **12**(23), 1013--1017, 2007.

214. Ragno, R., et al. Antimycobacterial pyrroles: synthesis, anti-*Mycobacterium tuberculosis* activity and QSAR studies, *Bioorg Med Chem* 8(6) 1423--32,2000.

215. Bagchi, M.C., et al. QSAR of anti tuberculosis drugs of INH type using graphical invariants, *J of Mol Struct: THEOCHEM* .**679**(3), 179--186, 2004.

216. Nayyar, A.,et al. Synthesis, anti-tuberculosis activity, and 3D-QSAR study of ring-substituted-2/4-quinolinecarbaldehyde derivatives, *Bioorgc & Medl Chem* .**14**, 7302--7310, 2006.

217. Nayyar, A., et al. 3D-QSAR study of ring-substituted quinoline class of antituberculosis agents, *Bioorg Med Chem.* **14**(3), 847--56, 2006.

218. Sivakumar, P.M., et al. QSAR Studies on Chalcones and Flavonoids as Antituberculosis Agents Using Genetic Function Approximation (GFA) Method, *Chem and Pharm Bull.* **55**(1), 44--49, 2007.

219. Kovalishyn, V., et al. QSAR modeling of antitubercular activity of diverse organic compounds, *Chem and Intell Lab Sys.* **107**(1), 69--74, 2011.

220. Khunt, R.C., et al. Synthesis, antitubercular evaluation and 3D-QSAR study of *N*-phenyl-3-(4-fluorophenyl)-4-substituted pyrazole derivatives, *Bioorganic& Medl Chem Lett* . **22**(1), 666--678, 2012.

221. Thakur, A., et al. QSAR study of flavonoid derivatives as p56lck tyrosinkinase Inhibitors. *Bioorg. Med. Chem.* **12,** 1209–1214,2004.

222. Marder, M., et al. Molecular Modelling and QSAR analysis of the interaction of flavones derivatives with the Benzodiazepine binding site of the $GABA_A$ receptor complex. *Bioorg. Med. Chem.***9**, 323-335,2001.

223. Tosco, P.,& Balle, T.Open3DQSAR: a new open source software aimedat high-throughput chemometric analysis of molecular interaction fields. *J Mol Model.* **17**,201–208,2011.

224. Lengauer, T. & Rarey, M.. Computational methods for biomolecular docking. *Curr. Opin. Struct. Biol.*, **6**(3):402–406, 1996.

225. Kitchen, D. B., et al. Docking and scoring in virtual screening for drug discovery: methodsand applications. *Nature. Rev. Drug. Discov.* **3**(11),935–949, 2004.

226. Kolb, P., et al. Docking and chemoinformatic screens for new ligands and targets, *Curr Opin Biotech* **20**(4), 429--436, 2009.

227. Izumizono, Y., et al. Identification of novel potential antibiotics fortuberculosis by in silico structure – based screening. *Eur J of Med Chem* **46**,1849--1856, 2011.

228. Agrawal, H., et al. Ligand based virtual screening and biological evaluation ofinhibitors of chorismatemutase (Rv1885c) from *Mycobacterium tuberculosis*H37Rv, *Bioorg & Med Chem Lett.* **17**(11), 3053-3058, 2007.

229. Upadhayaya, R.S., et al. Design, synthesis, biological evaluation andmolecular modelling studies of novel quinoline derivatives against *Mycobacterium tuberculosis*, *Bioorg Med Chem* **17**, 2830--2841, 2009.

230. Zhao, Y., et al. Discovery and Development of the Covalent Hydrates of Trifluoromethylated Pyrazoles as Riboflavin Synthase Inhibitors with Antibiotic Activity Against *Mycobacterium tuberculosis*. J. Org. Chem. **74**, 5297–5303, 2009.

231. Chandra, K., et al. Design, synthesis and inhibition activity of novel cyclic peptides against protein tyrosine phosphatase A from *Mycobacterium tuberculosis* , *Bioorg & Med Chem* .**18**(23), 8365--8373,2010.

232. Devi, C. A. Docking study on *Mycobacterium tuberculosis* receptors AccD5 and PKS18 with selected phytochemicals. *J of Pharm and Biol Sc* **4**(3), 1--4, 2012.

233. Singh, S.P., et al. Molecular docking and in silico studies on analogues of 2-methylheptyl isonicotinate with DHDPS enzyme of *Mycobacterium tuberculosis, Med Chem Res*. **22**(10), 4755-4765, 2013.

234. McKinney J. D., et al. Persistance of *Mycobacterium tuberculosis* in macrophages and mice requires the glyoxalate shunt enzyme ioscitrate lyase. *Nature*.**406,**735-738, 2000.

235. Morqunova, E., et al. 2005. Crystal structure of Lumazine synthase from *Mycobacterium tuberculosis* as a target for rational drug design: binding mode of new class of purinetrione inhibitors. *Biochemistry*. **44**(8):2746-2758.

236. Lin, T., et al. Structure-based inhibitor design of AccD5, an essential acyl-CoA carboxyltransferase domain of *Mycobacterium tuberculosis. PNAS*.**103**,3072-3077. 2006.

237. Reddy, V.M, et al. In vitro antimycobacterial activities of Capuramycin analogues: Characterization of. *Antimicrob. Agents Chemother.* 52(2),719-721,2008.

238. Liu, X.Q. & Yang, J. Bacterial Thymidylate Synthase with Intein, Group II Intron, and Distinctive ThyX Motifs. *J Bacteriol.* **186**(18), 6316–6319, 2004.

239. Agrawal, N. et al. Mechanistic Studies of a Flavin-Dependent Thymidylate Synthase.*Biochemistry*. **43** (32) , 10295-10301,2004.

240. Graziani, S., et al.Catalytic Mechanism and Structure of Viral Flavin-dependentThymidylate Synthase ThyX. *J .Biol .Chem.* **281**(33), 24048–24057,2006.

241. Griffin, J., et al. Catalytic Mechanism of *Chlamydia trachomatis* Flavin-dependent Thymidylate Synthase. *J. Biol. Chem* . **280**(7) ,5456–5467, 2005.

242. Gattis, S. G., & Palfey, B. A. Direct Observation of the Participation of Flavin in Product Formation by thyX-Encoded Thymidylate Synthase and *J. Am. Chem. Soc.* **127**, 832-833,2005.

243. Zhong, J., et al. Function and Evolution of Plasmid-Borne Genes for Pyrimidine Biosynthesis in *Borrelia* spp.. *J. Bacteriol.* **188**(3) ,909–918 , 2006.

244. Graziani, S., et al. Functional Analysis of FAD-dependent Thymidylate Synthase ThyX from *Paramecium bursaria* Chlorella Virus-1. *J .Biol. Chem.* **279**(52), 54340–54347, 2004.

245. Ulmer, J.E., et al. Functional analysis of the *Mycobacterium tuberculosis* FAD-dependent 2 thymidylate synthase, ThyX, reveals new amino acid residues contributing to 3 an extended ThyX .**190** (6), 2056–2064, 2008 .

246. Hunter, J.H., et al. Kinetics and Ligand-Binding Preferences of *Mycobacterium tuberculosis* Thymidylate Synthases, ThyA and ThyX. *PLoS ONE.* **3**(5), 1-10,2008.

247. Önen, F. E . et al. Design, synthesis and evaluation of potent thymidylate synthase X inhibitors .*Bioorg. Med. Chem. Lett.***18,** 3628–3631,2008.

248. Huang, Z., et al. Toxicological effect of ZnO nanoparticles based on bacteria, *Langmuir* .**24** (8), 4140 –4144,2008.

249. Mühling, M., et al. An investigation into the effects of silver nanoparticles on antibiotic resistance of naturally occurring bacteria in an estuarine sediment. *Mar. Environ. Res.* **68**, 278 –283,2009.

250. Rhim , J.W., et al. Preparation and Characterization of Chitosan-Based Nanocomposite Films with Antimicrobial Activity. *J. Agric. Food Chem.* , **54** , 5814-5822,2006.

251. Roy, S. et al. Study of ZnO nanoparticles: antibacterial property and light depolarization property using light scattering tool. *JQSRT* .**118,** 8–13.2013.

252. Zhou, J. et al. Multi-walled carbon nanotubes/epilson–polylysine nanocomposite with enhanced antibacterial activity, *Lett. Appl. Microbiol.* 52, 76–83, 2011.

253. Pramanik, S., et al. Microwave-assisted poly(glycidyl methacrylate)-functionalized multiwall carbonnanotubes with a 'tendrillar' nanofibrous polyaniline wrapping and theirinteraction at bio-interface. *Carbon.* **55**, 34-43, 2013.

254. Sui, M. Synthesis of ZnO coated multi-walled carbon nanotubes and their antibacterial activities, *Sci. Total. Environ.***452-453**,148—154, 2013.

255. Zardini, H.Z., et al. Enhanced antibacterial activity of amino acids-functionalized multi walled carbon nanotubes by a simple method, *Colloids Surf.,* B **92**,196—202, 2012.

256. Gizdavic, M.R.N. et al.Broad spectrum antimicrobial activity of functionalized polyanilines. *Acta. Biomater.* 7(12),4204-09, 2011.

257. Walker, K. et al. *Bidgee bush :* an identification guide to common native plant species of the south western slopes of New South Wales. Yarralumla, Australian Capital Territory: Greening Australia, 2010.

258. Blackman, S. A., et al.Maturation Proteins and Sugars in Desiccation Tolerance of Developing Soybean Seeds *Plant Physiology.* **100** (1), 225–230,1992.

259. Chaoluan, L. et al. *Potentilla linnaues.* Flora of China. **2003**, 9, 291-327.

260. Kaul, K, et al. Review on pharmaceutical properties and conservation measuresof *Potentilla fulgens* Wall. ex Hook- A medicinal endangered herb of higher Himalaya. *IJNPR.* **2**(3), 298-306, 2011.

261. Harrison, L. *RHS Latin for gardeners.* United Kingdom: Mitchell Beazley. 2012.

262. Wang, H.et al. An improved 3-(4,5-dimethylthiazol-2-yl)-2,5-diphenyl tetrazolium bromide (MTT) reduction assay for evaluating the viability of Escherichia coli cells. **Journal of Microbiological Methods. 82 ,** 330–333. 2010.

263. Roy, S., et al. Monitoring of pathogen carrying air-borne tea dust particles by light scattering. JQSR. **112** ,1784–1791, 2011.

264. Wolfe, K. et al. . Antioxidant activity of apple peels. *J. Agricult. Food Chem.* **51**,609-614, 2003.

265. Sarikurkcu, C., et al. Studies on the antioxidant activity of the essential oil and methanol extract of *Marrubium* globosum subsp. globosum (lamiaceae) by three different chemical assays. *Bioresource Technology* **99**, 4239-46, 2008.

266. Nair, D.G., et al. Antimicrobial activity of omwaprin, a new member of the waprin family of snake venom proteins. *Biochemical J.* **402**, 93–104, 2007.

267. Iczkowski, R.P., & Margrave, J.L. Electronegativity. *J.Am. Chem. Soc.* **83**,3547–3551,1961.

268. Koopmans, T.A. Ordering of Wave Functions and Energies to the Individual Electrons of an Atom. *Physica.* **1**,104-113,1933.

269. Delley, B. An All-Electron Numerical Method for Solving the Local Density Functional for Polyatomic Molecules. *J. Chem. Phys.* 92:508–517,1990.

270. Becke, A.D. Density-functional exchange-energy approximation with correct asymptotic behavior. *Phys. Rev. A.* **38**,3098-3100, 1988.

271. Lee, C., et al. Development of the Colle-Salvetti conelation energy formula into a functional of the electron density. *Phys. Rev.* **37**,785-789,1988.

272. Hehre, W.J., et al. *Ab Initio* Molecular Orbital Theory, Wiley, New York. 1986.

273. Andzelm, J., et al. Incorporation of solvent effects into density functional calculations of molecular energies and geometries. *J. Chem. Phys.* **103**,9312-9320, 1995.

274. HyperChem; Release 7; Hypercube; http://www.hyper.com/, 2002.

275. Khlebnikov, A.I., et al. Improved quantitative structure-activity relationship models to predict antioxidant activity of flavonoids in chemical, enzymatic, and cellular systems. *Bioorgan. Med. Chem.* **15**(4),1749-1770, 2007.

276. Cos, P., et al. Structure-Activity Relationship and Classification of Flavonoids as Inhibitors of Xanthine Oxidase and Superoxide Scavengers. *J. Nat.Prod.* **61**,71-76, 1998.

277. Varga, Z., et al. Structure prerequisite for antioxidant activity of silybin in different biochemical systems *in vitro*. *Phytochemistry* .**13**,85-93,2006.

278. Lin ,Y.M., et al. Chalcones and flavonoids as anti-tuberculosis agents. *Bioorg. Med. Chem.* **10**(8):2795-2802,2002.

279. Penrose, R. A generalized inverse for matrices. *Proc. Cambridge Philos. Soc.* **52**,406-413,1995.

280. Lowry, O.H. Protein measurement with the folin phenol reagent . *J. Biol. Chem.* 193:265-275,1951.

281. Kozlowski, D., et al. Density functional theory study of the conformational, electronic, and antioxidant properties of natural chalcones. *J Phys Chem.***111**,1138–1145,2007.

282. Prasad Y.R., et al. QSAR studies on chalcone deivatives as antibacterial agents against *Bacillus pumilis*. *ARKIVOC.***11**,266–276, 2008.

283. Aponte, J.C., et al. Synthesis, cytotoxicity, and anti-*Trypanosoma cruzi* acitivity of new chalcones. *J Med Chem,***51**,6230–6234,2008.

284. Nielsen, S.F., et al. Antileishmanial chalcones: statistical design, synthesis, and three-dimensional quantitative structure-activity relationship analysis. *J Med Chem.***41**,4819–4832,1998.

285. Dimmock, J.R., et al. Bioactivities of chalcones. *Curr Med Chem.* **6**,1125–1149,1999.

286. Enoki, T., et al. Antidiabetic activities of chalcones isolated from Japanese Herb, *Angelica keiskei*. *J Agric Food Chem.***55**,6013–6017,2007.

287. Saydama, G., et al. Cytotoxic and inhibitory effects of 4,4-dihydroxy chalcone (RVC-588) on proliferation of human leukemic HL-60 cells. *Leuk Res.***27**,57–64, 2003.

288. Ness, A. R.,& Powles, J. W., , Fruit and vegetables, and cardiovascular disease: a review, *Int J Epidemiol*, **26**, 1-13, 1997.

289. Ekins, S., et al. In silico pharmacology for drug discovery: methods for virtual ligand screening and profiling. *Br J Pharmocol.***152**,21–37, 2007.

290. Cho, D.H., et al. Quantitative structure activity relationship (qsar) study of new fluorovinyloxyacetamides. *Bull Korean Chem Soc.* **22**,388–394,2001.

291. Yao, S.W., et al. Synthesis and QSAR study of the anticancer activity of some novel indane carbocyclic nucleosides. *Bioorg Med Chem.***11**, 4999–5006, 2003.

292. Wold, S. Validation of QSAR's quantum. *Struc-Act. Relat.* **10**,191–193, 1991.

293. Dietrich, S.W., et al. Confidence interval estimators for parameters associated with quantitative structure-activity relationships. *J Med Chem.***23,** 1201–1205,1980.

294. Cornish-Bowden, A., & Wong, J.T. Evaluation of rate constants for enzyme-catalysed reactions by the jackknife technique. *Biochem J.* **175**, 969–976,1978.

295. Venkataraman, L., et al. Electronics and chemistry: varying single-molecule junction conductance using chemical substituents. *Nano Lett.*7,502–506,2007.

296. Sarmah, P.,& Deka, R.C. Anticancer activity of nucleoside analogues: a density functional theory based QSAR study. *J MolModel.***16**,411–418, 2010.

297. Sivakumar, P.M., et al. QSAR studies on chalcones and flavonoids as anti-tuberculosis agents using genetic function approximation (GFA) method. *Chem Pharm Bull.* **55**,44–49,2007.

298. Nyila, M.A., et al. Activity of South African medicinal plants against *Listeria monocytogenes* biofilms, and isolation of active compounds from *Acacia karroo. S. Afri. J Bot.* **78**, 220 – 227. 2012.

299. Gehlhaar, D. K et al. Fully automated and rapid flexible docking of inhibitors cova-lently bound to serine proteases. *Proceedings of the Sev-enth International Conference on Evolutionary Pro-gramming*, Morgan Kaufmann, San Mateo, 449-461,1998.

300. Yang, J.M. & Chen, C.C. Gemdock: A generic evolutionary method for molecular docking. *Proteins*, **55**, 288-304,2004.

301. David, H.L. Basis of lack of drug susceptibility of a typical mycobacteria. *Rev Infect Dis.* **3**(5)-878-84, 1981.

302. Morgan, D.M. Tetrazolium (MTT) assay for cellular viability and activity. *Methods Mol. Bio.* 79,179–183, 1998.

303. Leduc, D, et al. Functional evidence for active site location of tetrameric thymidylate synthase X at the interphase of three monomers. *PNAS.* **101**, 7252–7257, 2004.

304. Rajaraman, R., et al. Adhesion and spreading behavior of human peripheral blood mononuclear cells (PBMC) in vitro. *Exp. Cell Res.* **107**, 179-190, 1977.

305. Konwarh, R., et al. Biomimetic preparation of polymer-supported free radical scavenging , cytocompatible and antimicrobial :green" silver nanoparticles using aqueous extract of *Citrus sinensis* peel.*Colloids Surf., B* **84** (2), 338-345, 2011.

306. Das, B. et al. Bio-based biodegradable and biocompatible Hyperbranched Polyurethane:A scaffold for tissue engineering .*Macromol. Biosci.* **1**, 126-139, 2012.

307. Fernandes, E. G. R., et al. Electrospinning of Hyperbranched Poly-L-Lysine/Polyaniline nanofibers for application in cardiac tissue engineering. *J. Macromol. Sci. A* .**47**, 1203–1207, 2010.

308. Huang, S. & Ingber D. E. Shape-dependent control of cell growth , differentiation, and apoptosis: Switching between attractors in cell regulatorynetworks.*Exp. Cell Res.* **261**, 91-103, 2000.

309. Liu Z., et al.Antibacterial property expressedby anovel calcium phosphate glass *J. Biomed. Mater. Res. A.* 34729, 2013,

310. Jacobsen, N. R. et al. Genotoxicity, cytotoxicity, and reactive oxygen species induced by single walled carbon nanoubes and c(60) fullrenes in the FE-1 Mutatrade markMouse lung epithelial cells. *Environ. Mol. Mutagen.* **49**, 476-487, 2008.

311. Benzie, I. F. F. & Strain, J. J.The ferric reducing ability of plasma (FRAP) as a measure of "antioxidant power" : the FRAP assay. *Annal. Biochem.* **239**, 70-76. 1996.

312. Morones, JR, et al. The bactericidal effect of silver nanoparticles.Nanotech. **16**(10), 2346-2353, 2005.

Media and Solutions

Solutions

Proteinase K

1 mg lyophilized powder was dissolved in 1 mM Tris (pH 8.0) and 1.5 mM calcium acetate and stored at -20°C.

Alkaline Lysis Solution I

1 M Glucose 5 mL
1 M Tris-Cl (pH 8.0) 2.5 mL
0.5 M EDTA (pH 8.0) 2 mL

Alkaline Lysis Solution I was made up to 100 mL with deionized water, autoclaved for 15 minutes at 121°C on a liquid cycle and stored at 4°C.

Alkaline Lysis Solution II

0.2 M NaOH

1% SDS (w/v)

Alkaline Lysis Solution II was freshly prepared before use.

Alkaline Lysis Solution III

5 M Potassium acetate 60.0 mL
Glacial Acetic Acid 11.5 mL
H_2O 28.5 mL

Alkaline Lysis Solution III was stored at 4°C.

Coomassie Stain

It was made up to 400 mL with deionized water and stored at RT.

Coomassie Brilliant Blue 1.25 g
Methanol 223 mL
Acetic acid 45 mL

Destain was made up to 1 L with with deionized water and stored at RT

Methanol 400 mL
Acetic acid 100 mL

Buffers

1 M Tris-HCl

Tris base 121.1 g

Tris base was dissolved in 800 mL deionized water, the pH was adjusted by adding concentrated HCl and the volume made up to 1 L.

0.5 M EDTA (pH 8.0)

EDTA 186. 2 g

EDTA was dissolved in 800 mL deionized water, the pH was adjusted with 10 M NaOH with vigorous stirring with a magnetic stirrer and the volume made up to 1 L.

50x TAE buffer

Tris base 242 g
Glacial acetic acid 57.1 mL

10x Phosphate-buffered Saline (PBS)

NaCl 80 g
KCl 2 g
Na_2HPO_4 14.4 g
KH_2PO_4 2.4 g

These were dissolved in 800 mL water and the pH was adjusted to 7.4 by adding HCl. The volume was then made up to 1 L. The solution was sterilized by autoclaving for 15 minutes at 121°C on a liquid cycle.

10x SDS Running buffer

Tris base 0.2 g
Glycine 44g
SDS 1 g

This was made up to 1 L with distilled water and stored at RT.

2X Sample Buffer

0.5 M Tris-HCl (pH 6.8) 2.5 mL
Glycerol 2 mL
10% SDS (w/v) 4 mL
2-mercaptoethanol 1 mL

1.5% Bromophenol Blue 1 mL

This was made up to 20 mL with distilled water. The solution was mixed and stored at -20°C as 1 mL aliquots.

SDS gels
12% separating gel (50 mL)

40% acrylamide 14.6 mL
2% bis-acrylamide 8 mL
1.5 M Tris-HCl pH 8.8 12.5mL
10% SDS (w/v) 0.5 mL
ddH_20 14.15 mL

for 5 mL:

10% APS 0.05 mL
TEMED 0.006 mL

4% stacking gel (makes 25 mL)

40% acrylamide 2.4 mL
2% bis-acrylamide 1.3 mL
1 M Tris-HCl pH 6.8 3.15 mL
10% SDS (w/v) 2.5 mL
ddH_20 15.4 mL

for 2.5 mL

10% APS 0.025 mL
TEMED 0.0042 mL

APS and TEMED were added just before the gels were poured.

Elution Buffer

50mM Tris-Cl, pH-7.3
50mM to 500mM NaCl, pH 7.5

50mMTris buffer

50 mM Tris-Cl, pH-7.3

LIST OF PUBLICATIONS

N. Barua, P. Sarmah, I.Hussain, R. C. Deka and A. K. Buragohain. DFT-based QSAR Models to Predict the Antimycobacterial Activity of Chalcones. Research Letter in the Journal of Chemical Biology and Drug Design. Volume 79, Issue 4, pages 553–559, April 2012 .

S. Pramanik,R.Konwarh, **N. Barua**, A. K. Buragohain and N. Karak. Bio-based hyperbranched poly(ester amide)–MWCNT nanocomposites: multimodalities at the biointerface. BiomaterialsScience (Accepted)

S. Roy, R. Mahatta, **N. Barua**, A.K. Buragohain and G.A.Ahmed,Monitoring of pathogen carrying air- borne Camellia sinensis dust particles by light scattering. *Journal of Quantitative Spectroscopy & Radiative Transfer.* 112 (2011) 1784–1791 .

S. Roy, **N. Barua**, A. K. Buragohain and G. A. Ahmed A Light scattering study of ZnO nanoparticles for the application of its anti-*bacterial property.* AAPP j Atti della Accademia Peloritana dei Pericolanti Classe di Scienze Fisiche, M atematiche e Naturali. Vol. 89, Suppl. No. 1, C1V89S1P001 (2011).

S. Pramanik,R. Konwarh,R. C. Deka,L. Aidew, **N. Barua**, A.K. Buragohain, D. Mohanta,N.Karak.Microwave-assisted poly(glycidyl methacrylate)-functionalized multiwall carbon nanotubes with a 'tendrillar' nanofibrous polyaniline wrapping and their interaction at bio- interface. Carbon. Volume55, Pages 34-43, April 2013.

Sanchita Roy, Nilakshi Barua, Alak K. Buragohain, Gazi A. Ahmed. Study of ZnO nanoparticles:Antibacterial property and light depolarization property using light scattering tool. *Journal of Quantitative Spectroscopy & Radiative Transfer.* 118 (2013) 8–13 .

PUBLICATIONS IN CONFERENCE/PROCEEDINGS/SYMPOSIUMS

1. **Nilakshi Barua** , Ranjan Dutta Kalita , Md Imran Ullaha Farooqui, Lipika Aidew and Alak Kumar Buragohain. ***A Study on the Antimicrobial Activity of Some Locally. Available Medicinal Plants Against Staphylococcus aureus.*** Indian National Science Academy Platinum Jubilee International Symposium on Research in Molecular. Medicine Based on Natural Resources and Traditional Knowledge, National Chemical Laboratory, Pune, India, November 21-23, 2009.
2. Ranjan Dutta Kalita ,**Nilakshi Barua** ,Lipika Aidew and Alak Kumar Buragohain, ***Antimycobacterial activity of the methanol extract of latex from Jatropha curcus.*** Indian National Science Academy Platinum Jubilee International Symposium on Research in Molecular Medicine Based on Natural Resources and Traditional Knowledge, National Chemical Laboratory, Pune, India, November 21-23, 2009.
3. S. Roy, R. Mahatta, **N. Barua,** A.K. Buragohain and G.A. Ahmed, ***Monitoring of pathogen carrying air-borne Camellia sinensis dust particles by light scattering***, XII International Conference on Electromagnetic and Light Scattering, University of Helsinki, Finland, June 28- July 2, 2010.
4. **Nilakshi Barua**, Lipika Aidew, Ranjan Dutta Kalita and Alak Kumar Buragohain, ***Antimycobacterial Activity of Cannabis sativa L.*** National Seminar on Medicinal Plant and Microbe Diversity and Their Pharmaceuticals", Tezpur University, Tezpur, India, December 19-21, 2010.
5. Lipika Aidew, Ranjan Dutta Kalita , **Nilakshi Barua** , and Alak Kumar Buragohain.***Antibacterial and Antioxidant Properties of Sapindus Mukorossi Gaertn. (Sapindaceae).*** National Seminar on Medicinal Plant and Microbe Diversity and Their Pharmaceuticals", Tezpur University, Tezpur, India, December 19-21, 2010.
6. Ranjan Dutta Kalita ,**Nilakshi Barua** , Lipika Aidew, and Alak Kumar Buragohain. ***Evaluation of the Antimycobacterial potential of Xanthium strumarium.*** National Seminar on Medicinal Plant and Microbe Diversity and Their

Pharmaceuticals", Tezpur University, Tezpur, India, December 19-21, 2010.

7. Nilakshi Barua, Saurov Mahanta and Alak Kumar Buragohain. ***Flavin-Dependent Thymidylate Synthase (ThyX) of Mycobacterium tuberculosis is a potential target for Isoniazid and Paclitaxel*** .T he Fourth Congress of European Microbiologists, Federation of European Microbiological Societies,Geneva,Switzerland.June26-30,2011.
8. Nilakshi Barua, Atlanta Borah and Alak K Buragohain. **Modulation of Akt/ Protein Kinase B (PKB) activation by Mycobacterial Lipoarabinomannan in Macrophage and antimycobacterial activity by an indigenous plant of North East India.** International Symposium on "Molecular Signaling" ,Visva-Bharati, Shantiniketan, India, February 18-20, 2013.
9. Bhaskarjyoti Gogoi, Lipika Aidew, Nilakshi Barua and Alak K Buragohain. ***In silico*** **investigation of new inhibitor(s) of Protein Tyrosine Phosphatase 1B (PTB 1B) and Toll Like Receptor 4 (TLR4): the therapeutic targets of type 2 Diabetes mellitus.** International Symposium on "Molecular Signaling" ,Visva-Bharati, Shantiniketan, India, February 18-20, 2013.
10. Nilakshi Barua, Lipika Aidew and Alak K Buragohain. ***In silico*** **investigation of new inhibitor(s) of Enoyl-ACP Reductase InhA : A Therapeutic target of Mycobacterium tuberculosis.** National seminar cum workshop on "Recent advances in microbial biotechnology and molecular evolution", Tezpur University, Tezpur, India, March 01-04, 2013.
11. Lipika Aidew, Nilakshi Barua and Alak K Buragohain. **Identification of potent antimycobacterial agents from indigenous plants of Assam.** National seminar cum workshop on "Recent advances in microbial biotechnology and molecular evolution", Tezpur University, Tezpur, India, March 01-04, 2013.

Chem Biol Drug Des 2012; **79:** 553–559

Research Letter

doi: 10.1111/j.1747-0285.2011.01289.x

DFT-based QSAR Models to Predict the Antimycobacterial Activity of Chalcones

Nilakshi Barua[1], Pubalee Sarmah[2], Iftikar Hussain[2], Ramesh C. Deka[2,*] and Alak K. Buragohain[1]

[1]*Department of Molecular Biology and Biotechnology, Tezpur University, Assam 784028, India*

[2]*Department of Chemical Sciences, Tezpur University, Tezpur, Assam 784028, India*

**Corresponding author: Ramesh C. Deka, ramesh@tezu.ernet.in*

In this study, antimycobacterial activity of a set of *synthesized chalcone derivatives against Mycobacterium tuberculosis H37Rv* was investigated by quantitative structure–activity relationship (QSAR) analysis using density functional theory (DFT) and molecular mechanics (MM+)-based descriptors in both gas and solvent phases. The best molecular descriptors identified were hardness, E_{HOMO}, MR_{A-4} and MR_{B-4}, that contributed to the antimycobacterial activity of the chalcones as independent factors. The correlation of these four descriptors with their antimycobacterial activity increases with the inclusion of solvent medium, indicating their importance in studying biological activity. QSAR models revealed that in gas phase, lower values of E_{HOMO}, MR_{A-4} and MR_{B-4}, increase the antimycobacterial activity of the chalcone molecules. However, in solvent phase, lower values of E_{HOMO} and MR_{B-4}, and higher values of MR_{A-4} increase their activity.

Key words: antimycobacterial activity, chalcones, density functional theory, quantitative structure-activity relationships, solvent effect

Received 25 May 2010, revised 15 October 2011 and accepted for publication 29 November 2011

Introduction

The battle between humankind and *Mycobacterium tuberculosis*, the etiological agent of tuberculosis (TB), dates back to antiquity. Although in 1950s, TB incidences were reduced by the introduction of antimycobacterial chemotherapy and the widespread use of BCG vaccine (1), TB still remains a major international health problem, which is likely to become even more alarming in the coming years due partly to TB deaths in HIV-infected patients and partly to the emergence of multidrug resistant strains of the *Mycobacterium tuberculosis* (2). TB was declared as a global emergency by the World Health Organization (WHO) in the year 1993. The prolonged therapy and the significant toxicity of the current TB drugs make patient compliance to therapy very difficult, giving rise to selection for drug-resistant TB bacteria (3). This is also responsible for the emergence of the threats from the phenomena of multidrug resistance and extensive drug resistance against the conventional first line and second line of drugs. The rapid spread of TB worldwide has intensified the need for more efficient antimycobacterial agents to combat this disease.

Chalcones, or 1, 3-diaryl-2-propen-1-ones (Figure 1), are a group of natural or synthetic compounds (4), consisting of open-chain flavonoids in which the two aromatic rings are joined by a three-carbon α, β-unsaturated carbonyl system (5). Chalcones are important precursors of flavonoids and isoflavonoids (6) and, recently, have been subjected to great interest for their valuable pharmacological activities, including antioxidant (7), antibacterial (8), antitrypanosomal (9), antileishmanial (10), anticancer, cytotoxic (11), antidiabetic (12) and anti-inflammatory (13) activities. The presence of a reactive α, β-unsaturated keto function in chalcones is found to be responsible for their antimicrobial activity, which may be altered depending on the type and position of the substituent on the aromatic rings (8).

In silico virtual screening is fast emerging to be a potentially useful tool in search of targets of natural products. This approach is inexpensive as it is effective and fast. *In silico* methods are being increasingly applied in generating hypothesis relating to the possible mechanism of drug target interactions. This approach implicates databases, quantitative structure-activity relationships (QSAR), similarity searching, pharmocophores, homology models and other molecular modeling, machine learning, data mining, network analysis tools, and data analysis tools. *In silico* methods have been frequently used in the discovery and optimization of novel molecules with affinity toward a target, the clarification of absorption and in studying the distribution, metabolism, excretion, and toxicity properties as well as physicochemical characterization of the potential drug molecules (14). QSAR is fast emerging as a useful tool in modern chemistry, biology, and drug discovery (15,16). A QSAR model is a mathematical equation that correlates the biological, chemical, or physical activity of a molecular system to its geometric and chemical characteristics. The molecular descriptors are used to define the electronic properties of a molecule owing to the presence of limitations of fundamental physical and chemical laws in direct quantification of biological activity. The quantum chemical descriptors computed by density functional theory (DFT) and semi-empirical methods have found increasing use in modern QSAR analysis (16).

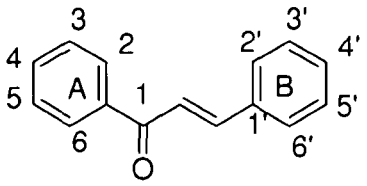

Figure 1: Basic structure of chalcone

In this study, we have found that DFT-derived descriptors chemical hardness (η), E_{HOMO} and MM+ descriptor, namely molar refractivity (MR), correlates with the antituberculosis activity of the chalcone molecules remarkably in both gas and solvent phases

Methods

Theoretical background

In theoretical chemistry, the chemical potential (μ) is identified as the negative of the electronegativity (χ) by Iczkowski and Margrave (17) and defined as

$$\chi = -\mu = -\left(\frac{\partial E}{\partial N}\right)_{v(r)} \tag{1}$$

The quantitative definition of hardness (η) of an N-electron system with total energy E and external potential $v(r)$ using DFT can be expressed as

$$\eta = \frac{1}{2}\left(\frac{\partial^2 E}{\partial N^2}\right)_{v(r)} = \frac{1}{2}\left(\frac{\partial \mu}{\partial N}\right)_{v(r)} \tag{2}$$

and the global electrophilicity index (ω) is expressed in terms of chemical potential and hardness as

$$\omega = \frac{\mu^2}{2\eta} \tag{3}$$

According to the finite difference approach, global hardness and chemical potential can be approximated as

$$\mu = -\left(\frac{IP + EA}{2}\right) \tag{4}$$

$$\eta = \frac{IP - EA}{2} \tag{5}$$

where IP and EA are the first vertical ionization potential and electron affinity, respectively, of the chemical system

Further approximation using Koopmans' theorem (18), the above parameters can be expressed by taking IP and EA as negative of the HOMO and LUMO energies, respectively

$$\mu = \frac{E_{LUMO} + E_{HOMO}}{2} \tag{6}$$

and

$$\eta = \frac{E_{LUMO} - E_{HOMO}}{2} \tag{7}$$

where E_{LUMO} is the energy of the lowest unoccupied molecular orbital and E_{HOMO} is the energy of the highest occupied molecular orbital

Computational details

Structures of all chalcone molecules are presented in Figure 2 Full unconstrained geometry optimizations of these compounds were carried out using DMol^3 program (19) The most widely used exchange-correlation functional suggested exchange potential by Becke (20) with gradient-corrected correlation provided by Lee Yang and Parr (21) (BLYP) was used in combination with double numerical with polarization (DNP) basis set to study chalcones derivatives DNP is the double numerical with polarization basis set, size of which is comparable with 6-31G** basis of Hehre *et al* (22) However, it is believed to be much more accurate than a Gaussian basis set of the same size Optimized geometries were verified by frequency calculations and characterized as minima (no imaginary frequency) in their potential energy surface The reactivity descriptors electrophilicity index (ω), chemical potential (μ), and global hardness (η) were calculated for all systems using eqns 3, 6 and 7, respectively The conductor-like screening model (COSMO) (23) as incorporated into the DMol^3 program with dielectric constant of 78 4 was adopted to study the solvent (water) effect In addition, the MR, van der Waals surface area (SA), volume (V), mass (M), and lipophilicity index (logP) for whole molecule were calculated from the MM+ computations with Hyperchem software ([a])

QSAR modeling

Quantitative structure-activity relationship (QSAR) analysis using multiple linear regression has been attempted to relate the structural features of these chalcone molecules that may have an influence on their observed antimycobacterial activity

The analysis was performed selecting different descriptors such as, energy of highest occupied molecular orbital (E_{HOMO}), energy of lowest unoccupied molecular orbital (E_{LUMO}), energy of the next lowest unoccupied molecular orbital (E_{NL}), energy difference between LUMO and HOMO ($\Delta_{L\,H}$), dipole moments, electrophilicity (ω), and hardness (η) Molecular mechanics (MM) parameters such as van der Waals surface area (SA), molecular volume (V), hydrophobicity, polarizibility, and MR were also calculated Subdivision of the flavonoid molecules into submolecular fragments has been suggested (24) for a more informative approach in QSAR modeling based on the reports that different moieties of flavonoid scaffold being responsible for antioxidant activity and inhibition of reactive oxygen species production in enzymatic and whole cell system (25,26) Therefore, we also subdivided the chalcone molecules into Ring A and Ring B to calculate the MR of the groups at the carbon position 4 and carbon position 4′ of Ring A and Ring B, respectively

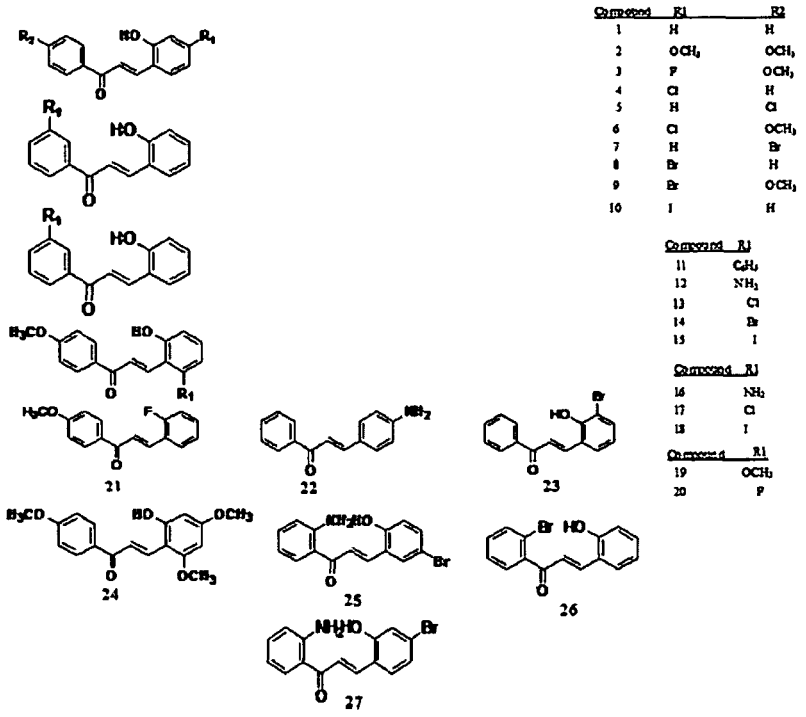

Figure 2: *Sketch of the chalcones used to build quantitative structure–activity relationship model*

The antimycobacterial activity data of the chalcone molecules 1–27 against *Mycobacterium tuberculosis H37Rv* determined by BACTEC method were taken from the results reported by Lin *et al* (27) We have randomly selected these 27 molecules of the reported 47 chalcones (27) However, we have excluded some molecules for this study as they are ineffective with inhibitory activity value zero The analyses of the 27 molecules were performed in both gas phase and solvent phase Multi-linear regression was performed by those descriptors which showed greater correlation to the percentage of inhibition of *M tuberculosis H37Rv* at a concentration of 12 5 μg/mL and smaller autocorrelation were selected out Four-parameter QSAR was performed using the least square error estimation (28) to calculate and compare bioactivity of the molecules The quality and predictability of the QSAR models were determined using the 'leave one out' (LOO) cross-validation method

Results and Discussion

We analyzed all the calculated DFT-based parameters such as ω, E_{NL}, E_{LUMO} for the derivation of the QSAR models and found that the equations derived by considering the percentage of inhibition at 12 5 μg/mL as a dependent variable and hardness (η), energy of the HOMO orbital (E_{HOMO}), MR of the group at position 4 of Ring A ($MR_{A\,4}$), and MR of the position 4′ of Ring B ($MR_{B\text{-}4'}$) as independent variables gave the best correlation in the gas phase and the solvent phase The gas-phase and solvent-phase models are presented as eqns 8 and 9 The descriptors used to build the QSAR model for both gas and solvent phases are presented in Table 1

Gas phase

$$\text{Activity} = -321\,01(\pm 64\,301) + 181\,42(\pm 69\,929)\eta - 31\,07(\pm 18\,748)E_{HOMO} - 1\,104(\pm 1\,429)MR_{A-4} - 3\,94(\pm 0\,937)MR_{B-4'} \quad (8)$$

$n = 27$, $r^2 = 0\,73$, $F = 14\,86$, $p < 0\,05$, $r^2_{cv} = 0\,56$

Solvent phase

$$\text{Activity} = -416\,87(\pm 61\,492) - 7\,03(\pm 21\,689)\eta - 89\,47(\pm 13\,624)E_{HOMO} + 0\,21(\pm 0\,931)MR_{A-4} - 3\,02(\pm 0\,778)MR_{B-4'} \quad (9)$$

$n = 27$, $r^2 = 0\,81$, $F = 22\,73$, $p < 0\,05$, $r^2_{cv} = 0\,50$

In the QSAR equations, n is the number of data points, r^2 is square of the correlation coefficient and represents the goodness of fit, r^2_{cv} is the LOO cross-validated r^2 (a measure of the quality of the QSAR model) F is the overall F-statistics for the addition of each successive term, and p is the p values using the F statistics We have found that the gas-phase r^2 value (0 73) increases (0 81) when calculated in the solvent phase, however, the r^2_{cv} value is 0 56 in the gas phase and decreases to 0 50 in the solvent phase The errors of regression coefficients are also found to be less in solvent phase than that of gas phase

These regression models are significant as depicted by the p value <0 05 using the F statistics (29) The QSAR models had to be

Table 1: Parameters used to build the quantitative structure–activity relationship models with the jackknife results for gas and solvent phases against *M tuberculosis*

	Gas phase						Solvent phase				
Compounds	Percentage of inhibition at 12 5 mg/mL	η	E_{HOMO}	MR_{A-4}	$MR_{B-4'}$	r_j^2	η	E_{HOMO}	MR_{A-4}	MR_{B-4}	r_j^2
1	61	1 255	−5 665	0 89	0 89	0 7459	1 203	−5 593	0 89	0 89	0 8116
2	32	1 22	−5 205	7 32	7 32	0 7264	1 161	−5 25	7 32	7 32	0 8043
3	63	1 3	−5 635	7 32	0 8	0 7424	1 258	−5 569	7 32	0 8	0 8084
4	89	1 249	−5 782	0 89	5 39	**0.7508**	1 226	−5 676	0 89	5 39	**0.8222**
5	67	1 231	−5 746	5 39	0 89	0 7285	1 187	−5 599	5 39	0 89	0 8112
6	57	1 278	−5 648	7 32	5 39	0 7297	1 236	−5 572	7 32	5 39	0 8051
7	70	1 224	−5 754	8 21	0 89	0 7267	1 202	−5 588	8 21	0 89	0 8033
8	57	1 252	−5 799	0 89	8 21	0 7306	1 219	−5 644	0 89	8 21	0 8053
9	25	1 275	−5 655	7 32	8 21	0 7449	1 242	−5 545	7 32	8 21	**0.8271**
10	21	1 227	−5 752	0 89	12 99	0 7194	1 178	−5 558	0 89	12 99	0 807
11	68	1 128	−5 422	0 89	0 89	**0.7488**	1 085	−5 366	0 89	0 89	0 8147
12	6	0 905	−4 842	0 89	0 89	0 7309	0 817	−4 754	0 89	0 89	0 7834
13	67	1 192	−5 705	0 89	0 89	0 7275	1 161	−5 582	0 89	0 89	0 8046
14	68	1 18	−5 693	0 89	0 89	0 7274	1 165	−5 546	0 89	0 89	0 8031
15	51	1 142	−5 614	0 89	0 89	0 7312	1 106	−5 437	0 89	0 89	0 8086
16	11	1 074	−5 189	0 89	0 89	0 7267	0 978	−5 078	0 89	0 89	0 8039
17	90	1 222	−5 762	0 89	0 89	0 7231	1 192	−5 631	0 89	0 89	0 8024
18	92	1 225	−5 771	0 89	0 89	0 723	1 207	−5 652	0 89	0 89	0 8013
19	75	1 282	−5 365	7 32	0 89	0 7278	1 201	−5 415	7 32	0 89	0 8169
20	66	1 291	−5 642	7 32	0 89	0 7344	1 252	−5 630	7 32	0 89	0 8102
21	5	1 141	−4 948	0 89	4 22	0 7208	0 990	−4 868	0 89	4 22	0 7819
22	82	1 271	−5 487	7 32	0 89	0 7291	1 267	−5 639	7 32	0 89	0 7981
23	79	1 255	−5 824	0 89	0 89	0 7219	1 245	−5 745	0 89	0 89	0 8013
24	40	1 222	−5 081	7 32	7 32	**0.7499**	1 154	−5 210	7 32	7 32	**0.8258**
25	8	1 103	−5 402	0 89	0 89	**0.7692**	1 027	−5 144	0 89	0 89	**0.8225**
26	83	1 234	−5 645	0 89	0 89	0 7225	1 195	−5 626	0 89	0 89	0 7994
27	12	1 11	−5 383	0 89	8 21	0 705	1 038	−5 147	0 89	8 21	0 787

MR, molar refractivity

The bold values in Table were selected and subjected to the LOO method with an intention to increase the correlation coefficient

further improved as general statistical standards requires $r^2 > 0\,80$ (30) and $r_{cv}^2 > 0\,60$ (31) for a regression model to be acceptable Therefore, to improve the overall quality of the regression models, we applied the scheme suggested by Dietrich *et al* (32) and Cornish-Bowden and Wang (33) as we have applied in our recent paper (34,35) In this scheme, a compound is considered as an outlier if its corresponding r^2, called jackknife r^2 (r_{cv}^2) value obtained from the regression analysis after deleting the compound, is comparatively higher than the other r_{cv}^2 values Table 1 presents the r_{cv}^2 values calculated in gas phase and solvent phase Although the independent variables are same in both gas and solvent phases, the r_{cv}^2 values differed in case of each molecule In gas phase, it was observed that molecules 4, 11, 24, and 25 possessed higher r_{cv}^2 values (0 751, 0 749, 0 750, and 0 769, respectively), whereas in solvent phase, molecules 4, 9, 24, and 25 exhibited high r_{cv}^2 values (0 822, 0 827, 0 826, and 0 823, respectively) These molecules were considered as outliers, and it was observed that deleting these molecules from the data set lead to the improvement of the statistical parameters in the QSAR models

The QSAR equations after deleting these outliers (4, 11, 24, and 25 in gas phase) and (4, 9, 24, and 25 in solvent phase) are as follows

Gas phase

$$\text{Activity} = -323\,24(\pm54\,0887) + 131\,53(\pm56\,246)\eta - 42\,08(\pm15\,610)E_{HOMO} - 0\,63(\pm1\,127)MR_{A-4} - 4\,46(\pm0\,752)MR_{B-4'} \quad (10)$$

$n = 23$, $r^2 = 0\,84$, $F = 23\,46$, $p < 0\,05$, $r_{cv}^2 = 0\,70$

Solvent phase

$$\text{Activity} = -391\,63(\pm50\,827) - 8\,85(\pm16\,737)\eta - 85\,38(\pm11\,055)E_{HOMO} + 0\,31(\pm0\,788)MR_{A-4} - 3\,35(\pm0\,666)MR_{B-4'} \quad (11)$$

$n = 23$, $r^2 = 0\,88$, $F = 33\,0$, $p < 0\,05$, $r_{cv}^2 = 0\,67$

We have observed that the r^2 value increased from 0 73 to 0 84 and 0 81 to 0 88 in gas phase and solvent phase, respectively The r_{cv}^2 value increased from 0 56 to 0 70 in the gas phase and 0 50 to 0 67 in the solvent phase, however, the r_{cv}^2 value remained lower in solvent phase as compared to the gas phase We have found that the error of regression coefficient decreases for both gas- and

solvent-phase model calculated using jackknife scheme However, the error of regression coefficient significantly decreases for independent variable, E_{HOMO}, in solvent phase We have also calculated the *t*- and p-values for all the regression coefficients for all the equations and provided in Table 2 Although both the QSAR models are significant, we found solvent phase to be better than the gas phase–derived model based on the r^2 values The correlation plots between the experimental and calculated bioactivity values of the chalcones molecules derived from the two QSAR models are shown in Figure 3 The plots indicate that these descriptors can be effectively used in the prediction of the bioactivity of the chalcone molecules

The QSAR models predict that in both gas phase and solvent phase, lower values of E_{HOMO} and $MR_{B-4'}$ relate to greater inhibition of *M tuberculosis* However, difference was observed in the dependence of antimycobacterial activity of the chalcone molecules on hardness and MR_{A-4} when calculated in/gas and solvent phases In gas phase, the antimycobacterial activity increased with the higher values of hardness and lower values of MR_{A-4} of the molecules as shown by the eqs 8 and 10 The eqs 9 and 11 depicting the antimycobacterial activity of the chalcone molecules in solvent phase, however, predict that decrease in the hardness and increase in MR_{A-4} of these molecules increase their antimycobacterial activity

The frontier orbital theory states that the energy of the HOMO and LUMO is the important factors that determine the reactivity of a molecule The QSAR models generated in both gas and solvent phase predict that decrease in the energy of HOMO increased the inhibition activity of the chalcone molecules It was observed that the presence of a halogen in one of the two rings, irrespective of the position, increased the antimycobacterial activity of the chalcones This could be attributed to the electronegativity of the halogens which decrease the energy of HOMO by removing the electron density from the σ space of the benzene rings (36) The very low values of antimycobacterial inhibitions can be similarly explained by the presence of an electron donating group such as an amino group($-NH_2$) The lone pair of electrons of nitrogen atom delocalize into the π space of the benzene ring and increase the E_{HOMO} of the molecule (35) Table 1 shows that in both gas and solvent phases, the presence of the amino group in the B ring of the chalcone molecules increases the E_{HOMO} more as compared to the presence of the amino group in Ring A However, no such discrete increase in E_{HOMO} was observed owing to the presence of halogens in Ring A or Ring B Sivakumar *et al* (37) reported the QSAR study of 33 chalcones using robust statistical technique such as genetic function approximation Their analysis also indicates the importance of hydrogen bond donor and HOMO in the determination of antituberculosis activity of chalcones

The correlation plots between experimental and calculated activity values in gas and solvent media presented in Figure 3 indicated that the selected parameters can predict the antimycobacterial activity of the set chalcone molecules with greater predictability in the solvent phase Thus, designing new chalcone molecules with electron withdrawing substituent on the ring may increase the antimycobacterial activity

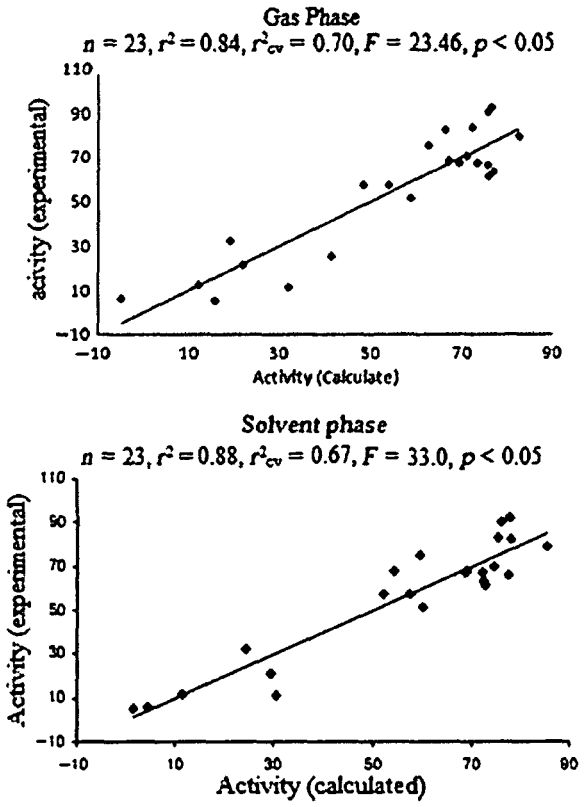

Figure 3: Plot of experimental versus calculated values of bioactivity for the two models

Table 2: Statistical *t*- and p-values for all the regression coefficients for all the equations

		η		E_{HOMO}		MR_{A-4}		$MR_{B-4'}$	
n	Phase	*t*-Value	p-Value	*t*-Value	p-Value	*t*-Value	p-Value	*t*-Value	p-Value
27	Gas phase	2 5943	0 0166	−1 6574	0 11164	−0 7729	0 4478	−4 2062	0 0004
27	Solvent phase	−0 3242	0 7489	−6 5668	1 32E−06	0 2236	0 8251	−3 8779	0 0008
23	Gas phase	2 3386	0 0311	−2 6958	0 01478	−0 5618	0 5812	−5 9341	1 00E−05
23	Solvent phase	−0 5285	0 6036	−7 7234	4E−07	0 4053	0 6900	−5 0311	9 00E−05

MR, molar refractivity

Conclusions

The QSAR equations developed with the four parameters hardness (η), E_{HOMO}, $MR_{A\text{-}4}$ and $MR_{B\text{-}4'}$ provide regression models to predict the activity of the set of chalcone molecules against *Mycobacterium tuberculosis H37Rv* The statistical quality of the regression models in both gas and solvent phases was improved by applying the jackknife test Increase in correlation coefficient (r^2 = 0 88) by the inclusion of solvent medium depicts the importance of the solvent effect and the selected parameters These regression models reveal that in gas phase, higher values of hardness and lower values of E_{HOMO}, $MR_{A\,4}$ and $MR_{B\text{-}4'}$ of chalcones increase their inhibitory activities against *M tuberculosis H37Rv* In solvent phase, lower values of hardness, E_{HOMO} and MRB-4′ and higher value of MRA-4 increase the antimycobacterial activity of the chalcones The QSAR models also show that the descriptors derived from DFT and MM+ methods can successfully be utilized to predict the antimycobacterial activity of the chalcone molecules

Acknowledgment

The authors thank the Department of Science and Technology (DST), New Delhi, for financial support

References

1 Chew C H, Hu P Y (1974) BCG Programme in the Republic of Singapore Singapore Med J,15 241–245
2 WHO Report (2009) Global Tuberculosis Control Epidemiology Strategy Financing
3 Zhang Y (2005) The magic bullets and tuberculosis drug targets Annu Rev Pharmacol Toxicol,45 529–564
4 Dong X, Liu T, Chen J, Ying H, Hu Y (2009) Microwave-assisted Mannich reaction of 2-hydroxy-chalcones Synth Commun,139 733–742
5 Lunardi F, Guzela M, Rodrigues A T, Corrêa R, Eger-Mangrich I, Steinde M, Grisad E C, Assreuy J, Calixto J B, Santos A R S (2003) Trypanocidal and leishmanicidal properties of substitution-containing chalcones Antimicrob Agents Chemother,47 1449–1451
6 Harborne J B, Mabry T J (1982) The Flavonoids Advances in Research London Chapman and Hall, p 313
7 Kozlowski D, Trouillas P, Calliste C, Marsal P, Lazzaroni R, Duroux J L (2007) Density functional theory study of the conformational, electronic, and antioxidant properties of natural chalcones J Phys Chem,111 1138–1145
8 Prasad Y R, Kumar P R, Smiles J, Babu A (2008) QSAR studies on chalcone derivatives as antibacterial agents against *Bacillus pumilis* ARKIVOC,11 266–276
9 Aponte J C, Verástegui M, Málaga E, Zimic M, Quiliano M, Vaisberg A J, Gilman R H, Hammond G B (2008) Synthesis, cytotoxicity, and anti-*Trypanosoma cruzi* acitivity of new chalcones J Med Chem,51 6230–6234
10 Nielsen S F, Christensen S B, Cruciani G, Kharazmi A, Liljefors T (1998) Antileishmanial chalcones statistical design, synthesis, and three-dimensional quantitative structure-activity relationship analysis J Med Chem,41 4819–4832
11 Dimmock J R, Elias D W, Beazely M A, Kandepu N M (1999) Bioactivities of chalcones Curr Med Chem,6 1125–1149
12 Enoki T, Ohnogi H, Nagamine K, Kudo Y, Sugiyama K, Tanabe M, Kobayashi E, Sagawa H, Kato I (2007) Antidiabetic activities of chalcones isolated from Japanese Herb, *Angelica keiskei* J Agric Food Chem,55 6013–6017
13 Saydama G, Aydin H H, Sahin F, Kucukoglu O, Erciyas E, Terzioglu E, Buyukkececi F, Omaya S B (2003) Cytotoxic and inhibitory effects of 4,4′-dihydroxy chalcone (RVC-588) on proliferation of human leukemic HL-60 cells Leuk Res,27 57–64
14 Ekins S, Mestres J, Testa B (2007) *In silico* pharmacology for *drug discovery methods for virtual ligand screening and profiling* Br J Pharmocol,152 21–37
15 Hansch C, Leo A (1995) Exploring QSAR Fundamentals and Applications in Chemistry and Biology Washington, DC American Chemical Society
16 Cherkasov A (2005) Inductive descriptors 10 successful years in QSAR Curr Comput Aided Drug Des,1 21–42
17 Iczkowski R P, Margrave J L (1961) Electronegativity J Am Chem Soc,83 3547–3551
18 Koopmans T A (1933) Ordering of wave functions and energies to the individual electrons of an atom Physica,1 104–113
19 Delley B (1990) An all-electron numerical method for solving the local density functional for polyatomic molecules J Chem Phys,92 508–517
20 Becke A D (1988) Density-functional exchange-energy approximation with correct asymptotic behavior Phys Rev A,38 3098–3100
21 Lee C, Yang W, Parr R G (1988) Development of the Colle-Salvetti correlation energy formula into a functional of the electron density Phys Rev,37 785–789
22 Hehre W J, Radom L, Schlyer P R, Pople J A (1986) *Ab Initio* Molecular Orbital Theory New York Wiley
23 Andzelm J, Koelmel C, Klamt A (1995) Incorporation of solvent effects into density functional calculations of molecular energies and geometries J Chem Phys,103 9312–9320
24 Khlebnikov A I, Schepetkin I A, Domina N G, Kerpotina L N, Quinn M (2007) Improved quantitative structure-activity relationship models to predict antioxidant activity of flavonoids in chemical, enzymatic, and cellular systems Bioorg Med Chem,15 1749–1770
25 Cos P, Ying L, Calomme M, Hu J P, Cimanga K, Van P B, Pieters L, Vlietinek A J, Vanden B D (1998) Structure-activity relationship and classification of flavonoids as inhibitors of xanthine oxidase and superoxide scavengers J Nat Prod,61 71–76
26 Varga Z, Seres I, Nagy E, Ujhelyi L, Balla G, Balla J, Antus S (2006) Structure prerequisite for antioxidant activity of silybin in different biochemical systems *in vitro* Phytochemistry,13 85–93
27 Lin Y M, Zhou Y, Flavin M T, Zhou L M, Nie W, Chen F C (2002) Chalcones and flavonoids as anti-tuberculosis agents Bioorg Med Chem,10 2795–2802
28 Penrose R (1995) A generalized inverse for matrices Proc Cambridge Philos Soc,52 406–413
29 Cho D H, Lee S K, Kim B T, No K T (2001) Quantitative structure-activity relationship (qsar) study of new fluorovinyloxyacetamides Bull Korean Chem Soc,22 388–394
30 Yao S W, Lopes V H C, Fernández F, García-Mera X, Morales M, Rodríguez-Borges J E, Cordeiroa M N D S (2003) Synthesis and QSAR study of the anticancer activity of some novel indane carbocyclic nucleosides Bioorg Med Chem,11 4999–5006

31 Wold S (1991) Validation of QSAR's quantum Struc-Act Relat,10 191–193
32 Dietrich S W, Dreyer N D, Hansch C, Bently D (1980) Confidence interval estimators for parameters associated with quantitative structure-activity relationships J Med Chem,23 1201–1205
33 Cornish-Bowden A, Wong J T (1978) Evaluation of rate constants for enzyme-catalysed reactions by the jackknife technique Biochem J,175 969–976
34 Sarmah P, Deka R C (2009) DFT-based QSAR and QSPR Models of several *cis*-platinum complexes solvent effect J Comput Aided Mol Des,23 343–354
35 Sarmah P, Deka R C (2010) Anticancer activity of nucleoside analogues a density functional theory based QSAR study J Mol Model,16 411–418
36 Venkataraman L, Park Y S, Whalley A C, Nuckolls C, Hybertsen M S, Steigerwald M L (2007) Electronics and chemistry varying single-molecule junction conductance using chemical substituents Nano Lett,7 502–506
37 Sivakumar P M, Babu S K G, Mukesh D (2007) QSAR studies on chalcones and flavonoids as anti-tuberculosis agents using genetic function approximation (GFA) method Chem Pharm Bull,55 44–49

Note

[a]HyperChem, Release 7, Hypercube, http //www hyper com/, 2002

Biomaterials Science

RSC Publishing

PAPER

View Article Online
View Journal

Bio-based hyperbranched poly(ester amide)–MWCNT nanocomposites: multimodalities at the biointerface†

Cite this: DOI: 10.1039/c3bm60170f

Sujata Pramanik,[a] Rocktotpal Konwarh,[a] Nilakshi Barua,[b] Alak K. Buragohain[b] and Niranjan Karak*[a]

There has been a growing interest in the use of nanomaterials featuring potent biocompatibility and biodegradability together with the added facet of antibacterial activity, particularly against drug-resistant bacterial species. Addressing these three features at the biointerface, we report the fabrication of multimodal bio-based hyperbranched poly(ester amide) (HBPEA)–microwave functionalized multiwalled carbon nanotube (*f*-MWCNT) nanocomposites by incorporation of various weight percentages (1, 2.5, and 5 wt%) of the *f*-MWCNTs into HBPEA by using an *ex situ* polymerization technique. Fourier transform infrared spectroscopy confirmed the structural changes upon interaction of the *f*-MWCNTs with HBPEA. The formation of thermosetting nanocomposites resulted in an acceptable improvement of the desired properties including their mechanical properties (~170%), instrumental for providing mechanical integrity in cultured cells. The nanocomposite films were found to be biocompatible substrates for the *in vitro* adhesion and proliferation of peripheral blood mononuclear cells (PBMC) with enhanced cell viability correlating with the increase of the *f*-MWCNT content. The antibacterial results, monitored by a CFU count and the protein concentration, demonstrated that the prepared nanocomposites were more toxic towards Gram positive bacteria and *Mycobacterium smegmatis* than the Gram negative ones. The damage of bacterial cells upon interaction with the nanocomposites was validated by UV-visible spectroscopy and a SEM study. The antibacterial and biocompatibility studies suggested that these microporous nanocomposite films (3D interconnected porous structures with pore diameters of 5–105 μm and a porosity of 39.90%) possess concurrent long-term lethal activity against the bacterial cells and biocompatibility with PBMC. Thus, the prepared nanocomposites may find potential bio-medical applications, particularly as antimicrobial dressing materials for infected burn wounds.

Received 11th July 2013,
Accepted 13th August 2013

DOI: 10.1039/c3bm60170f

www.rsc.org/biomaterialsscience

1. Introduction

The steep augmentation in deadly infections associated with infected wounds including burns has posed a serious nuisance in the realm of medical sciences. The prevalence of community-associated and hospital-acquired infections has increased abruptly in the last 20 years, particularly with the methicillin-resistant *Staphylococcus aureus* (MRSA) and the drug resistant *Mycobacterium smegmatis* and so on, accompanied by a rise in antibiotic-resistant strains.[1,2] These multi-drug resistant opportunistic bacteria, ubiquitous in distribution, are recognized as deadly pathogens which require a foreign body such as sutures or burn wounds to invade tissues. The loss of skin, availability of bacterial nutrients in the burn locale and destruction of the vascular system near the burned region lead to immune-suppression, thereby making burn wounds susceptible to infection.[3] Such bacterial colonization near the periphery of the injury region causes sepsis.[4] The prevailing scenario of the infection susceptibility of burn patients by drug-resistant bacterial species has caused a global need for antibacterial dressing materials. Thus, a major drive to search for suitable antimicrobial materials is underway.

In this vein, a nanotechnology-based approach can be effective in addressing the aforementioned challenges. Amidst the genre of nanomaterials, polyaniline (PAni) nanofibers[5] and multiwalled carbon nanotubes (MWCNTs)[6] have carved a unique niche of their own as potent antibacterial materials in the biomedical field. The functionalization of MWCNTs *via* covalent and non-covalent approaches is an apt strategy to address the practical challenges of the chemical inertness of the graphitic network, poor dispersion, interfacial bonding with others, and so on.[7] The microwave (MW) assisted functionalization of MWCNTs, covalently with poly(glycidyl

[a]Department of Chemical Sciences, Tezpur University, Tezpur-784028, India. E-mail: karakniranjan@yahoo.com
[b]Department of Molecular Biology and Biotechnology, Tezpur University, Tezpur-784028, India

†Electronic supplementary information (ESI) available. See DOI: 10.1039/c3bm60170f

methacrylate) (PGMA) and non-covalently with PAni nanofibers in a single pot, proved to be an efficient technique amongst all others, particularly in the context of green chemistry.[7] Thus, in the present study, MW-assisted PGMA and PAni nanofiber functionalized MWCNTs (*f*-MWCNT) will be employed as efficient antibacterial materials. The effects of functionalization and synergism of MWCNTs and PAni nanofibers as the single nanohybrid in the antibacterial efficacy against a spectrum of bacterial species will be delved into. Further, the potential toxicity of these nanomaterials implies an urgent need for the development of biocompatible nanomaterials.

However, the rapid advancement of nanotechnology in the realm of bio-medical science over the past few decades has resulted in growing concern regarding the biosafety of these nanomaterials to human health, particularly the immunologic toxicity. The conventional antibacterial materials including antibiotics, metal ions, and quaternary ammonium compounds used in the domain of bioscience suffer from limitations such as short-term efficacy, a poor release profile together with cumulative toxicity, and subsequently, microbe resistance.[8] The unison of nanotechnology and polymer science may be imperative in amalgamating the biocompatibility together with antibacterial efficacy to address the above problems. The inclusion of a small wt% of *f*-MWCNTs into a biocompatible polymeric matrix holds potential in reducing the cytotoxicity of the nanotubes. The blood compatibility is one of the key problems that limit the applications of these materials in blood-contacting environments such as in the cardiovascular system.[9] The peripheral blood mononuclear cells (PBMC) are of immunological importance, and particularly help in the healing of wounds and in controlling the response of the host matrix towards a foreign body.[10] The response of the prepared nanocomposites towards the same is dictated by the adhesion and proliferation of PBMC onto the host matrix, making the interaction imperative in evaluating the biocompatibility. The rationale behind the adherence and proliferation of PBMC is for the practical utility of the nanocomposites as antibacterial dressing materials for infected burn wounds. The lipid protein layer (LPC) produced in the skin after the burning accident inhibits the immune response and the production of interleukin 2 (IL2), a cytokine.[11] PBMCs stimulate the release of IL2, essential for the growth of IL2-dependent lymphocytes in the periphery of the infected burn wound region.[12] Thus, the current focus remains on scrutinizing the compatibility of the *f*-MWCNTs with the polymer along with its interaction with the PBMC for their potent application as antibacterial dressing materials for infected burn wounds.

Again, the biodegradability of the polymeric materials is of paramount importance because this provides long term biocompatibility as well as leaving room for tissue regeneration.[13] In addition to the above, no post-healing treatment is required in the context of the biodegradable dressing material. Thus, there has been a paradigm shift from non-degradable to biodegradable polymeric materials for applications in the arena of bio-medical science. This is attested to by the latter's inherent amenability for tailorable degradation kinetics, which is useful for various applications.[14] In this milieu, bio-based hyperbranched poly(ester amide) (HBPEA) is an important proposition as the global scientific community thrusts to opt for renewable bioresources endowing green credentials.[15] The unison of ester and amide moieties in the hyperbranched architecture bequeaths the resin with the synergism of high functionality, adequate mechanical strength and flexibility together with improving the biocompatibility and biodegradability of the same.[16] It is pertinent to mention that non-edible castor oil containing more than 90–95% ricinoleic acid is a good candidate for the preparation of HBPEA.[17]

Thus, the judicious inclusion of the antibacterial *f*-MWCNTs into a bio-based HBPEA matrix constitutes an interesting strategy for the fabrication of novel antibacterial, biocompatible and biodegradable materials. A perusal of the literature has shown that the preparation of bio-based HBPEA–MWCNT nanocomposites having antimicrobial properties, biocompatibility and biodegradability under the biological conditions of stimulated human body fluid has never been attempted, which encouraged us to initiate the present study. Thus, in continuation of our exploration of *f*-MWCNTs,[7] we herein wish to report the fabrication of castor oil based HBPEA–*f*-MWCNT nanocomposites. The response of these nanocomposites towards a number of bacteria including drug resistant bacterial species was investigated. The UV absorption at 260 nm and SEM studies were done to gain insight into the antibacterial action of the nanocomposites. Further, the potential of the same to support the attachment and proliferation of PBMC, and the biodegradability in simulated body fluid was also delved into.

2. Materials and methods

2.1 Materials

Castor oil (Sigma Aldrich, India), diethanol amine (Merck, India), phthalic anhydride (Merck, India) and isophthalic acid (Sisco Research Laboratory Pvt. Ltd, India) were used after being dried under vacuum at 50 °C overnight. Maleic anhydride (Merck, Germany) was used after being dried in a vacuum desiccator for 2 days. The MWCNTs (purity ~95 wt%, external diameter of about 10–15 nm) were purchased from Hanwha Nanotech Corp., Korea. Glycidyl methacrylate (GMA), 2,2′-azobis-(isobutyronitrile) (AIBN), ammonium peroxydisulfate (APS) and hydrochloric acid (HCl) (36.46 g mol^{-1}, 11.6 N) were obtained from Merck, India, and used as received. Aniline (Merck, India) was purified by vacuum distillation in the presence of zinc dust (SD Fine-Chem Limited, India, atomic weight 65.37 g mol^{-1}) and stored at 4 °C prior to use. The solvents such as benzene, methanol, tetrahydrofuran (THF), dimethyl acetamide (DMAc) and dimethyl sulfoxide (DMSO) were obtained from Merck, India, and distilled before use. The bisphenol-A-based epoxy resin (Araldite GY 250) (epoxy equivalent: 180–190 g per equiv. and density: 1.16 g cc^{-1} at 25 °C) and poly(amido amine) hardener ((HY 840) Hindustan Ciba Geigy Ltd, India) were used as received.

Histopaque (density 1.077 g mL^{-1}) was obtained from Sigma Aldrich. Sodium citrate was obtained from Merck, India, and phosphate buffer saline from HIMEDIA. All other chemicals and bacterial strains used in the biological study were procured from the Department of Molecular Biology and Biotechnology, Tezpur University.

2.2 Characterization of the nanocomposites

The interaction of the *f*-MWCNT and HBPEA matrix was confirmed by Fourier transform infrared (FTIR) spectroscopy using a Nicolet Impact-410 FTIR spectrophotometer. The spectral studies were conducted in transmission mode within the wavenumber range of 500–4000 cm^{-1} using KBr pellets. The prepared nanocomposites were exposed to MW irradiation using a Catalyst Scientific microwave system at 30% power of 210 W at 60–80 °C for 2 min in pulsed mode. The crystallinity of the prepared nanocomposites was evaluated by a Rigaku Miniflex X-ray diffraction (XRD) system using CuKα radiation with a wavelength (λ) of 1.5406 Å in the range of 2–70°. The dispersion of the *f*-MWCNT in the HBPEA matrix was done using a standard sonotrode of 3 mm tip-diameter in a Hielscher UP200S high intensity ultrasonic processor at a 60% amplitude and 0.5 cycles. The thermal stability of the nanocomposites was determined by thermogravimetric analysis (TGA) using a Shimazdu TGA 50 thermal analyzer at a nitrogen flow rate of 30 mL min^{-1} and at the heating rate of 10 °C min^{-1} within the temperature range of 25 to 700 °C. The mechanical performance of the cured thermosets (as per the ASTM D 412-51 T)[18] was determined using a Zwick Z010 universal testing machine (UTM) with a load cell of 10 kN and at a 40 mm min^{-1} jaw separation speed. The results were averaged over three replicates. The gloss, scratch hardness and impact resistance of the cured films were measured as per the standard methods.[19] The absorbance for the MTT assay was measured by ultraviolet (UV)-visible spectroscopy using a UV-1700 PharmaSpec spectrophotometer. The surface morphology of the thermosets was studied by high-resolution transmission electron microscopy (HRTEM) using a JEOL 2100X electron microscope at an operating voltage of 200 kV after casting on carbon coated copper grids. The adhesion of the PBMC onto the thermosets and the antibacterial interaction of the used bacterial strains with the nanocomposites was assessed by scanning electron microscopy (SEM) using a JEOL JSM-6390LV microscope after platinum coating on their surface.

3. Results and discussion

3.1 Fabrication of the nanocomposites

A solution technique was adopted to fabricate the HBPEA–*f*-MWCNT nanocomposites. Firstly, the MWCNTs were functionalized with PGMA and PAni nanofibers, wherein the functionalization occurred at the defects – the prime sites present on the nanotube edges and on the sidewalls.[20] The epoxy groups and benzenoid-quinoid moieties generated by the MW-assisted functionalization inferred interfacial adhesion and wettability of the same with the HBPEA. The interaction of the MWCNTs with the PGMA and PAni nanofibers dictated the dispersion of the debundled nanotubes in the HBPEA matrix. The preparative layout of the HBPEA–*f*-MWCNT nanocomposites is shown in Scheme 1.

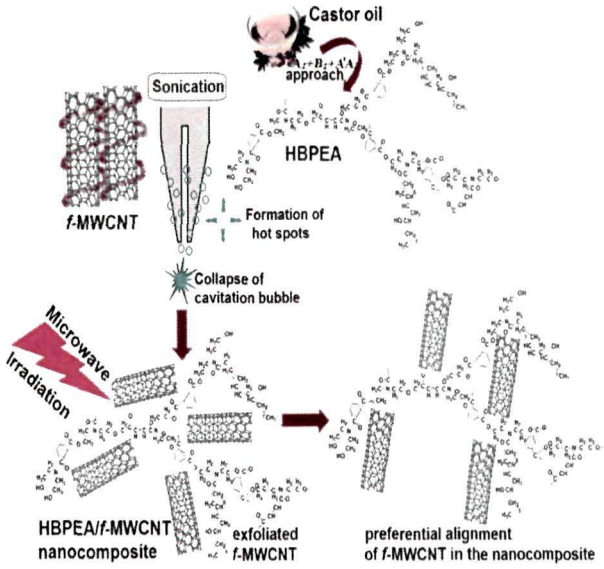

Scheme 1 Preparation of the bio-based HBPEA–*f*-MWCNT nanocomposites by the synergism of ultrasonication and MW irradiation.

3.2 Possible mechanism of the formation of the nanocomposites

The ultrasonic waves as well as the MW irradiation played vital roles in the formation of the HBPEA–*f*-MWCNT nanocomposites with a preferred directionality, as evident from the HRTEM study. Pulsed ultrasound was reported to be effective in the exfoliation and dispersion of MWCNT agglomerates in the HBPEA matrix.[21] The effects of the ultrasound are associated with the rapid collapse of cavitation bubbles on a microsecond time scale, creating microscopic domains of high temperature and pressure, which opened up the non-covalently wrapped PAni nanofibers from the nanotube surface. The formation of microjets of energy or hot spots caused enhanced exfoliation of the *f*-MWCNTs,[22] thereby allowing a greater surface area of the same to interact with the HBPEA chains. Dictated by previous reports on the active MW absorption by the MWCNTs,[23] the prepared nanocomposites were exposed to MW radiation for 2 min (divided into six cycles, each cycle containing an irradiation of 10 s succeeded with an interval of 10 s) to assist in the dispersion of the *f*-MWCNTs in the HBPEA matrix. The strong MW absorption is ascribed to the presence of free π-electrons moving out of the graphitic framework of the *f*-MWCNTs with a simultaneous volume expansion of the nanotubes.[24] The MW absorption by the MWCNTs at a relatively low temperature caused a thermal expansion of the nanotube layers, thereby facilitating the formation of

Table 1 *Performance and domain length of the HBPEA, HBPEAM1, HBPEAM2.5 and HBPEAM5 thermosets*

Physico-mechanical property	HBPEA	HBPEAM1	HBPEAM2.5	HBPEAM5
Curing time (h)	10	1.5	1.2	1
Gel fraction (%)	77.2	78.4	79.7	80.2
Scratch hardness (kg)	8.5	9.5	10	>10
Impact resistance[a] (cm)	>100	>100	>100	>100
Tensile strength (MPa)	7.2	9.5	12.7	16.7
Elongation at break (%)	88.1	83.3	77.5	70.3
Domain length (Å)	—	9.7	12.4	16.2

[a] The maximum limit of the instrument is 100 cm.

interfacial interactions between the MWCNTs and the polymer matrix.[24] The MW irradiation induced the localized heating of the *f*-MWCNTs at the nanotube–HBPEA interface such that the nanotubes aligned in a preferred direction within the matrix.[23] The alignment of the *f*-MWCNTs in the HBPEA is supported by the morphological study and the presence of long-range order by the XRD study (ESI† and Table 1). Upon direct MW irradiation, the static temperature gradients resulted in well oriented and aligned nanotubic arrays in the HBPEA matrix.

3.3 Morphology of the nanocomposites

The stable and uniform dispersion of the *f*-MWCNTs in the HBPEAM5, as evident from the HRTEM study, is instrumental in comprehending the enhancement of the structural and thermal properties of the nanocomposites. The HRTEM image (Fig. 1a) shows that the pristine MWCNTs have an average external diameter of ~15 nm. A representative HRTEM micrograph (Fig. 1b) shows the anchoring of a PGMA layer onto a MWCNT (having a diameter of ~35 nm). A reconstruction of the wall-to-wall distance of *f*-MWCNTs was observed in the MW treated nanocomposites as compared to the untreated *f*-MWCNTs. The wall-to-wall distance of the untreated *f*-MWCNTs was ~0.37 nm, which increased to ~0.4 nm in the case of MW irradiated *f*-MWCNTs dispersed in the HBPEA nanocomposite (inset Fig. 1b).[24] This change in the intertubular distance of the *f*-MWCNTs is indicative of the high temperature and pressure encountered by the nanotubes during MW irradiation. The dispersion of the PAni nanofibers in the nanocomposite was observed in Fig. 1c. The MW irradiation suffices for the appearance of a furrowed-like architecture of the nanocomposite (Fig. 1d). This is further confirmed by the presence of long range order in the XRD study (Table 1).

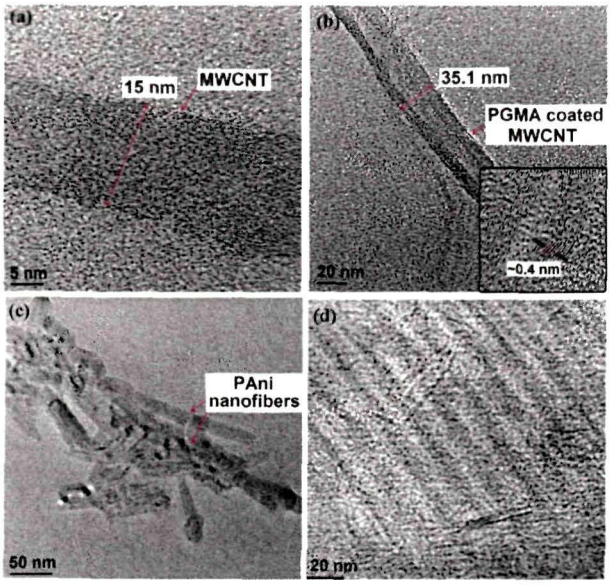

Fig. 1 High-resolution TEM images of (a) a pristine MWCNT, (b) a *f*-MWCNT based nanocomposite with the inset of an enlarged wall-to-wall distance of the *f*-MWCNT, (c) a dispersion of PAni nanofibers in HBPEAM5, and (d) a dispersion scenario of *f*-MWCNTs in HBPEAM5.

3.4 Performance of the nanocomposites

The performance of the epoxy-poly(amido amine) cured thermosetting nanocomposites effectively changed with the incorporation of *f*-MWCNTs. Table 1 lists properties such as the curing time, gel fraction, scratch hardness, impact resistance, gloss, tensile strength and elongation at break of the nanocomposites. It is evident from Table 1 that the curing time of the epoxy-poly(amido amine) cured HBPEA and its nanocomposites baked at 150 °C decreased significantly with the increase of the *f*-MWCNT content. This was attributed to the presence of the N-atom of the benzenoid ring and the oxirane ring (adhered to the *f*-MWCNTs) which aided the crosslinking reaction of HBPEA. In other words, the covalent bonding between the epoxide groups adhered to the *f*-MWCNTs and –OH groups present in the periphery of the HBPEA backbone resulted in a strong interfacial adhesion between the nanotubes and the polymer matrix.[25] The preferred orientation of the *f*-MWCNTs in the HBPEA matrix, as evident from the HRTEM study, also helped in decreasing the curing time. The increment in the gloss with the *f*-MWCNT content in the nanocomposites indicated that the cured thermosets possessed a good dimensional stability and smooth surface morphology. The increment in scratch hardness of the nanocomposites with the *f*-MWCNT content was attributed to the enhanced strength of the nano-reinforcing functionalized nanotubes and flexibility of the HBPEA chains. The high impact resistance of the thermosets reflected optimum crosslinking and flexibility of the long hydrocarbon chains of the fatty acid part of the HBPEA. The pristine HBPEA thermoset possessed a tensile strength of 7.2 MPa which increased from 9.5 to 16.2 MPa with the incorporation of *f*-MWCNTs from 1 to 5 wt%. The increment in the magnitude of the tensile strength of the HBPEA nanocomposites to ~170% as compared to the pristine one further supports the presence of strong *f*-MWCNT–HBPEA interfacial interactions. The interactions between *f*-MWCNTs and HBPEA, as evident from the FTIR study, enhanced the dispersion of the *f*-MWCNTs in the matrix and hence led to the formation of dense crosslinked structures, which hindered the mobility of the HBPEA chains, thereby improving the mechanical properties.[26] In other words, the incorporation of the

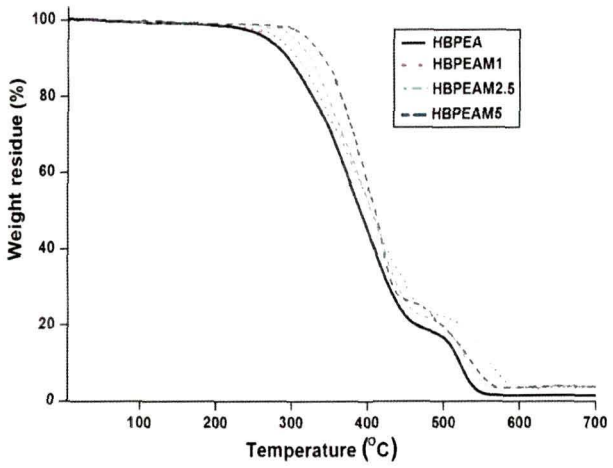

Fig. 2 Thermogravimetric analysis of HBPEA, HBPEAM1, HBPEAM2.5 and HBPEAM5.

f-MWCNTs in the HBPEA imparted a nano-reinforcing effect, which is responsible for providing mechanical integrity to the PBMC. The restricted mobility of the long fatty acid chains due to the incorporation of *f*-MWCNTs justified the decrease (20.2%) in the elongation at break of the nanocomposites. The minimal decrement in the elongation at break also reflects sufficient flexibility of the nanocomposite films for being suitable for a number of applications including wound dressing materials.

The thermal stability and degradation pattern of the HBPEA and its nanocomposites were assessed by thermogravimetry (Fig. 2). The HBPEA thermoset exhibited a two-step degradation profile, with an initial and final degradation at around 277 °C (weight loss due to ester groups) and 521 °C (weight loss due to amide groups), respectively.[15] The HBPEA nanocomposites also presented a two-step degradation pattern with a dose-dependent increment of thermal stability. The increase (277–325 °C) of the initial degradation temperature of the nanocomposites with increasing *f*-MWCNT content is attributed to the nano-mechanical interlocking of the *f*-MWCNTs within the HBPEA matrix *via* the adherence of functionalities onto the nanotube surface. An increment in the weight residue of the nanocomposites (~2–3% as compared to the HBPEA) observed at 800 °C reflects the presence of thermo-stable *f*-MWCNTs.

3.5 Antibacterial activity of the nanocomposites

3.5.1 Enumeration of the CFU count. This study investigated the antibacterial effect of the prepared nanocomposites against bacterial strains, which cause a host of infections from localized skin eruptions to life-threatening conditions such as bacteraemia, endocarditis and pneumonia.

The effect of the incorporation of *f*-MWCNTs in the HBPEA on bacterial growth was assessed by inoculating the nanocomposite films with the test strains. A substantial reduction in the attachment of the Gram positive and acid fast bacterial

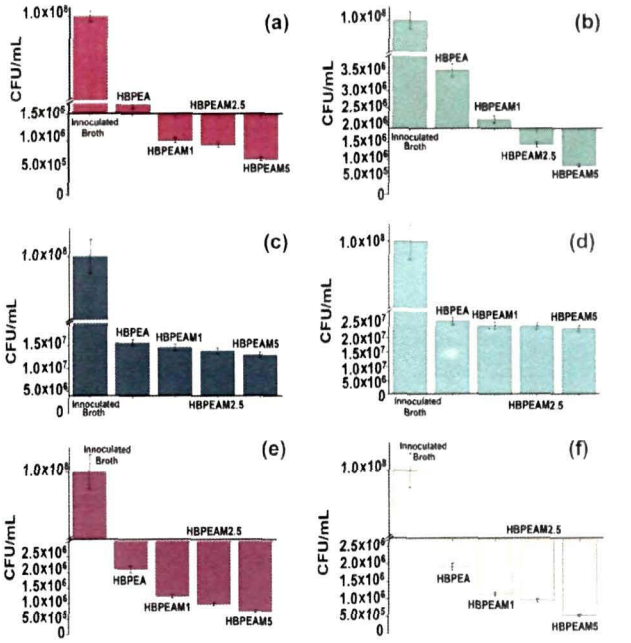

Fig. 3 Antimicrobial activity of HBPEA, HBPEAM1, HBPEAM2.5 and HBPEAM5 towards (a) *B. subtilis*, (b) *S. aureus*, (c) *E. coli*, (d) *K. pneumonia*, (e) *M. smegmatis* mc^2 155, and (f) *M. smegmatis* ATCC14468. The CFU results are compared with the control sample of inoculated broth.

species was observed as assessed through enumeration of the colony forming units (CFU) (Fig. 3). The nanocomposites exhibited pronounced antibacterial efficacy against *B. subtilis* (Fig. 3a) and *S. aureus* (Fig. 3b), as compared to *E. coli* (Fig. 3c) and *K. pneumonia* (Fig. 3d). A significantly lower number of bacterial colonies was observed on the nanocomposites, implying the superior antibacterial activity of the same over the pristine HBPEA. It can thus be inferred from the above observations that the nanocomposites were more effective against Gram positive bacteria as compared to the Gram negative ones, showing differential interaction of the same with the surface moieties of the two different bacterial strains. The basic architectural differences between the cell wall structures in these bacterial strains may play a key role in the determination of their antibacterial activities.[27] The *M. smegmatis* mc^2 155 (Fig. 3e) (conventionally available, antibiotic ampicillin resistant) and *M. smegmatis* ATCC14468 (Fig. 3f) exhibited low colonization onto the nanocomposites as compared to the pristine HBPEA (Fig. 4a).

3.5.2 Total protein content from bacterial adhesion. In line with the above result, the reduction in the protein adsorbed on the nanocomposite films was observed for the tested bacterial species (Fig. 4b). The adhesion of the bacteria onto the films decreased with the increase in the *f*-MWCNT content, with the lowest adhesion onto HBPEAM5. This was attributed to the synergism of antibacterial effect of the MWCNTs and the presence of the emeraldine salt form of the PAni nanofibers (the key structural unit having similarity with that of the active antibacterial tetracyclines)[28] wrapped onto

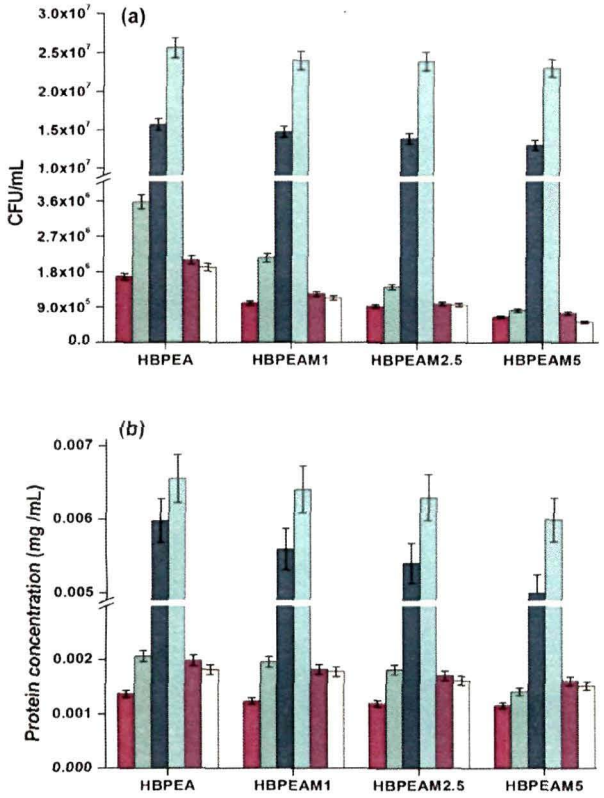

Fig. 4 Comparative antibacterial study in terms of (a) colony-forming units enumerated from, and (b) protein adsorbed on HBPEA, HBPEAM1, HBPEAM2.5 and HBPEAM5 towards *B. subtilis* (colored in red), *S. aureus* (colored in green), *E. coli* (colored in blue), *K. pneumonia* (colored in cyan), *M. smegmatis* mc^2 155 (colored in purple) and *M. smegmatis* ATCC14468 (colored in yellow).

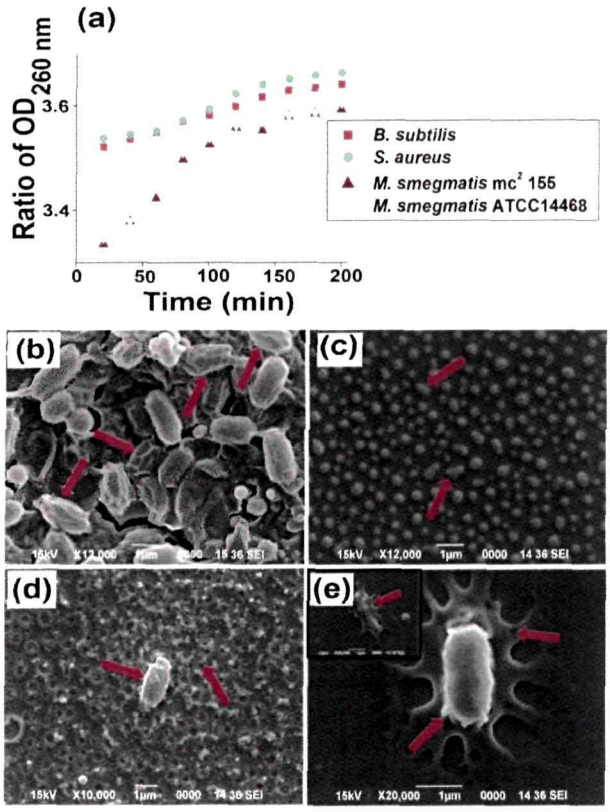

Fig. 5 (a) Release of 260 nm absorbing materials from Gram positive and acid fast positive bacterial strains. SEM images of (b) *B. subtilis*, (c) *S. aureus*, (d) *M. smegmatis* mc^2 155, (e) *M. smegmatis* ATCC14468 upon interaction with HBPEAM5.

the MWCNTs. The *f*-MWCNTs are dispersed throughout the HBPEA matrix, so the nanotubes are present both on the surface as well as in the bulk. Although the HBPEA does not possess antibacterial activity, the presence of dispersed *f*-MWCNTs in the HBPEA matrix is responsible for the antibacterial action of the nanocomposites. This is supported by the work of Liu *et al.*, which reported that the large surface area and the strong adsorption of bacteria by the nanotubes present in the dispersed state in the polymer matrix account for the pronounced antibacterial activity.[29] The protein concentration decreased similarly with decreasing CFU count (Fig. 4a). The excretion of extra-cellular components such as proteins by *B. subtilis* decreased by 80.6%, which is a more than five-fold decrease as compared to *K. pneumoniae* upon culturing on the HBPEAM5 matrix. The decrease in protein content may arise from the *f*-MWCNTs that retarded the bacterial cell growth, resulting in decreased proliferation rates instead of the death of the cells. The selective antibacterial potency of the nanocomposites, as estimated by the total protein content correlated well with the CFU study.

3.5.3 Interaction of a nanocomposite with bacteria. The plausible mechanism of cytotoxicity of the HBPEAM5 on the tested bacterial species is presented below. The release of intracellular components, particularly nucleotides such as DNA and RNA (having a strong UV absorption at 260 nm), is indicative of the loss of cell membrane integrity.[30] The absorbance at 260 nm thus provided a basis for the mechanistic study of the interaction of the bacterial cells with the nanocomposite (Fig. 5a). It was observed that the release of the cytoplasmic constituents from the Gram positive bacterial species attained a level of saturation within 120 min of incubation, though the curve almost reached a plateau after 220 min of incubation with 20 μg mL^{-1} of the nanocomposite at 37 °C. However, the 'acid fast positive species' exhibited a monotonic increase of the cytoplasmic constituents released over time. The release of these 260 nm absorbing materials from the bacterial cytoplasm is attributed to the absence of the outer cell membrane in both bacterial strains, which allowed the influx of the nanocomposite. The differential in the UV absorption pattern of the Gram positive and acid fast positive bacterial species is attributed to the presence of a characteristic mycolic acid rich cell wall in *M. smegmatis* which caused a slow release profile.

Further, the SEM study showed a distinct difference in cellular morphology of the bacterial cells after treatment with HBPEAM5. The *B. subtilis* are elongated and evenly shaped cells, which became corrugated with a ruptured cell surface

upon interaction with the tested material (Fig. 5b). The cell wrinkling and shortening together with the formation of craters were also observed. Upon interaction with the nanocomposite, the deformation and disintegration of the cells were observed from round and proliferating cells with intact and well-defined membranes of the control *S. aureus* (Fig. 5c). The *M. smegmatis* bacterial strains have a uniform cylindrical-shape morphology. These cells exhibited cell lesions together with the formation of mycothiol for survival under hostile oxidative stress conditions, upon interaction with the nanocomposite (Fig. 5d). In other words, the cells ruptured, becoming flattened together with compromising their cellular integrity while remaining embedded in the mycothiol (Fig. 5e).[31] The different morphological observations of the two tested bacterial strains indicated different strain susceptibility towards the nanocomposite. Thus, on the basis of the above study, it can be inferred that there exists a positive correlation of the loss of cellular integrity and the release of cytoplasmic constituents from the bacterial cells. These results confirmed the interaction between the nanocomposite and the bacterial cells. This is due to the fact that the cells are damaged upon interaction with the nanocomposite, which is clearly seen from the SEM micrographs. The nano-biointeraction is further supported by the UV-visible results, as the peak at 260 nm confirmed the release of DNA and RNA from the bacterial cytoplasm (absorbance at 260 nm).

3.6 *In vitro* biocompatibility of the nanocomposites

3.6.1 Trypan blue exclusion assay. The prepared nanocomposites were examined for their biocompatibility with PBMC by a trypan blue exclusion assay.[32] The PBMC–matrix adhesion is evident from Fig. 6. It was observed that the nanocomposite films supported more healthy cells as compared to the pristine polymer, indicating that the *f*-MWCNTs are the key players. The dose-dependent increment of cell viability of the nanocomposites is attributed to the presence of *f*-MWCNTs, as the cell adhesion and proliferation is influenced by the matrix on which it grows.[33]

3.6.2 MTT assay. The biocompatibility of the prepared nanocomposites with PBMC was further examined in terms of the former's effect on the latter's proliferation by the colorimetric MTT assay. The spectroscopic measurement of the solubilized formazan crystals (an indirect measurement of the activity of mitochondrial dehydrogenase) in the MTT assay is directly related to the number of viable cells.[27] Fig. 7a showed a time- and dose-dependent increment in cell viability of the nanocomposites. The viability of the PBMC compared to the control after 48 h of incubation showed that the nanocomposite films exhibited no cytotoxic effect on the cells. The cell viability ≥85% at 0, 1, and 2 h is attributed to the acclimatization of the cells to the matrix. The cell viability increased with the incubation time, imparting a superior biocompatibility with time. Shvedova *et al.* reported the Janus-like properties of the MWCNTs, wherein the pristine nanotubes were found to be cytotoxic to the cells, unless surface-functionalized owing to the lowering of their surface activity.[34] In other words, the non-cytotoxic *f*-MWCNTs enhanced the proliferation of the PBMC. Thus, the adhering of PGMA and PAni nanofibers onto the *f*-MWCNTs together with their dispersion in between the HBPEA chains altered their cytotoxicity, thereby imparting biocompatibility with the PBMC.

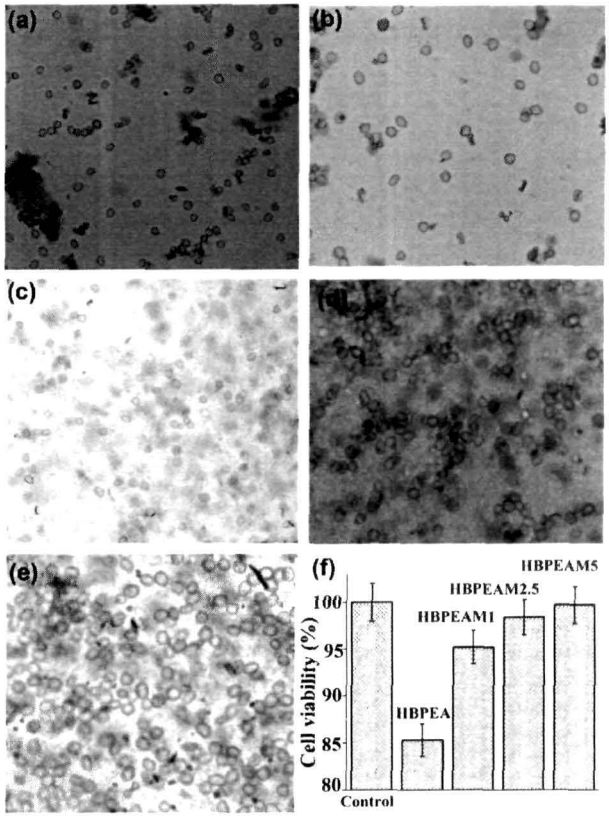

Fig. 6 Representative pictures of cell viability using the trypan blue exclusion assay after 48 h of incubation of PBMC with (a) control, (b) HBPEA, (c) HBPEAM1, (d) HBPEAM2.5, (e) HBPEAM5. (f) % Cell viability.

3.6.3 PBMC adhesion and proliferation studies. The SEM analysis was conducted for PBMC seeding assessment, particularly to probe the cell adhesion and spreading onto the nanocomposite films. The SEM micrographs were found to be consistent with the proliferation of PBMC with increasing *f*-MWCNT content, as indicated by an apparent increase in the number of the adhered cells. Fig. 7(c–f) showed the attachment and interaction of PBMC with porous HBPEA as well as the nanocomposite films. The presence of both macro- and micro-pores of a diameter ranging from 5–105 μm and 39.90% porosity (Fig. 7b) proved to be effective as anchoring points in the attachment and proliferation of the PBMC, as evident from Fig. 7c. The 3D interconnected porous structure appeared to resemble the elements of an extra-cellular matrix, thereby improving cell attachment and growth.[13] The low shrinkage of the films (due to their optimum crosslinking density) promoted cell adhesion and good biocompatibility, which was further supported by Fernandes *et al.*[35] The surface of the porous films exhibited an interconnected structure of PBMC at

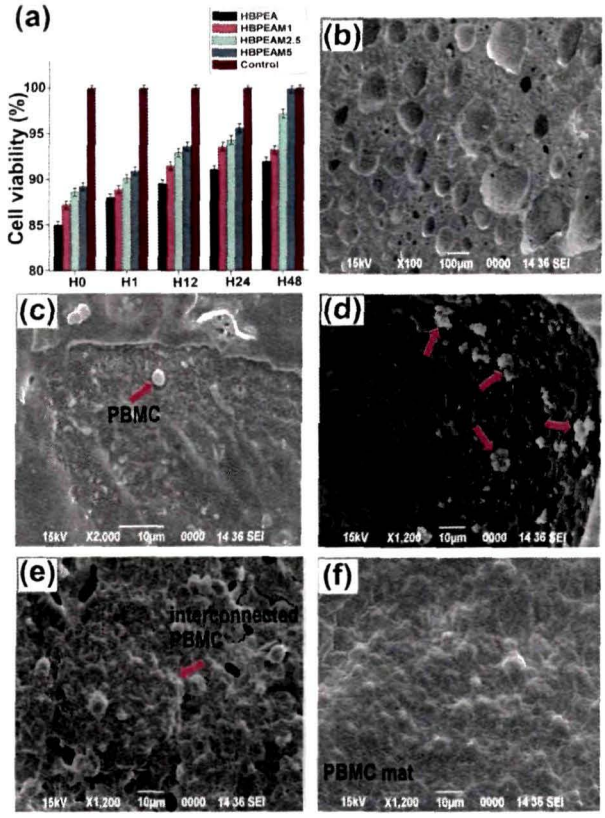

Fig. 7 (a) The cell viability of PBMC in terms of absorbance at 540 nm at different time intervals of 0, 1, 12, 24 and 48 h. SEM images showing the adhesion and proliferation of PBMC after seeding on the surfaces of (b) HBPEA, (c) HBPEAM1, (d) HBPEAM2.5, and (e) HBPEAM5.

the loading of 2.5 wt% *f*-MWCNTs in the HBPEA (appearing to mimic the mesocarp of a watermelon pepo). However, the PBMC were well-adhered, and proliferated to form a continuous layer of cells covering the HBPEAM5. In other words, the surface of the porous HBPEAM5 film exhibited a mat-like conformation (appearing to mimic a graphene sheet), with the pores of the film being completely masked by the continuous mesh of PBMC (Fig. 7f). Although PBMC consists of a mixed population, the PBMC isolation protocol supports the adherence of ~90% of the non-specific esterase-positive cells (rich in macrophages) on the nanocomposite surface.[36] The porosity of the films allowed gas exchange (O_2 uptake and CO_2 release) together with the passage of cell signaling molecules such as hemokinins in the PBMC.[37] Thus, the above results indicate that the porous nanocomposite films support the attachment and good proliferation of the PBMC. The hyperbranched architecture, when viewed from a biological perspective, has a unique 3D structure and the presence of a multitude of functional groups at the periphery imparts the biocompatibility of the matrix *via* cellular interactions with PBMC. Rajaraman and his coworkers documented that the spreading behaviour of the PBMC is governed by factors such as the available surface area, number and density of adhesion sites and other receptors of the substrate.[33] The SEM micrographs suggest that the biocompatibility was further augmented by increasing the *f*-MWCNT content in the HBPEA matrix. It is essentially a surface phenomenon epitomized by cell–cell and cell–matrix interactions. Thus, the masking of the MWCNTs with PAni nanofibers and their dispersion in the HBPEA matrix impart tissue tolerance and cellular interactions.[38] The presence of carbonyl groups on the surface of *f*-MWCNTs also plays a key role in enhancing the biocompatibility owing to the decreased activation of a mitochondria mediated apoptotic pathway.[39] Thus, the SEM study corroborated well the results obtained from the trypan blue exclusion assay and the MTT assay.

3.6.4 Measurement of reactive oxygen species (ROS). The potential of the nanomaterials to penetrate healthy cells due to their quantum size effect triggered the exploration of the toxicity of the prepared nanocomposites. The production of ROS is a two-edged sword which acts as a boon in cell signaling, gene expression and in maintaining homeostasis in man, while as a bane by damaging cellular proteins, lipids and DNA which subsequently leads to carcinogenesis under oxidative stress conditions.[39] It has long been known that the production of ROS is one of the health hazards related to the exposure of MWCNTs.[40] A decrease in the membrane integrity of the PBMC leads to the leakage of ROS outside the cell, leading to cell apoptosis. The FRAP assay is based on the reduction of ferric-tripyridyltriazine (Fe^{III}-TPTZ) to an intense blue colored ferrous form (Fe^{II}).[21] The ROS production or reducing ability of the nanocomposites is directly proportional to the amount of ferrous product formed, which can be quantified photometrically at 593 nm.[41] The dose–response characteristics of the prepared nanocomposites showed a linear behavior (Fig. 8a). It was evident from the FRAP assay[41] (Fig. 7d) that ascorbic acid showed an absorbance of 0.68, the prepared nanocomposites exhibited an absorbance of 0.5 after 10 min of interaction with Fe^{III}-TPTZ. The MWCNTs on one hand showed no absorbance at 593 nm, indicating their pronounced oxidative nature, while the *f*-MWCNTs on the other hand showed meagre absorbance (0.09). The masking of the MWCNTs with a large number of –OH groups residing at the periphery of the HBPEA rendered the prepared nanocomposites with significantly low toxicity as compared to MWCNTs. This study showed that the prepared nanocomposites attenuated the quenching of ROS as compared to the *f*-MWCNTs.

3.6.5 Hemocompatibility assay. Hemocompatibility is an important aspect of biocompatibility because of the direct/indirect contact of the samples with blood. The hemolytic assay results showed that the optical density at 540 nm observed for the pristine MWCNTs and the nanocomposites were almost equivalent to that of PBS, the negative control.[18] Thus, the samples showed no lysis of the red blood cells, implying their compatibility with the cells.

Thus, the *in vitro* cell response studies showed that the adhesion and proliferation rate of the PBMC increased with increasing *f*-MWCNT content, without having any hemolysis activity or without inducing any production of ROS. In this

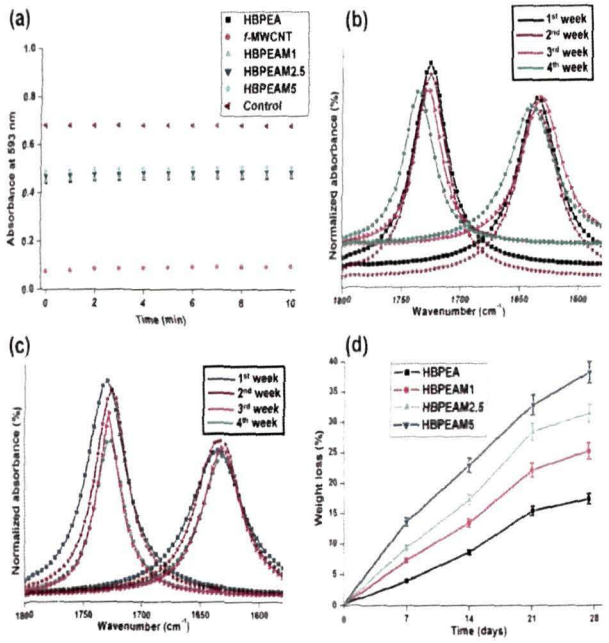

Fig. 8 (a) ROS reaction kinetics, and deconvoluted I_{ester}/I_{amide} FTIR peaks of (b) HBPEA, and (c) HBPEAM5. (d) Weight loss profile of HBPEA and its nanocomposites.

context, both the 3D porous interconnected network structure and the presence of *f*-MWCNTs proved to be the prime factors in promoting cell growth.[8]

3.7 *In vitro* biodegradation of the nanocomposites

The *in vitro* biodegradation of pristine MWCNTs and HBPEA–*f*-MWCNT nanocomposites was studied by subjecting the films to the degrading action of a lipase–phosphate buffer solution, which mimics the pseudo-chemical environment of simulated animal body fluid.[42] The biodegradation of the pristine and nanocomposite films occurred as an extracellular process in PBS catalyzed by lipase *via* an enzymatic oxidative mechanism. Lipase, interfacially activated at the water–polymer interface, assists in the enzymatic hydrolysis of the ester moieties present in the polymeric backbone.[43] The enzyme contains buried catalytic sites and their activation occurs as a result of a conformational change induced upon binding to the polymer substrate. In aqueous media, the α-helical lid covers the active site of the enzyme and blocks its access to the substrate. Upon contact with the hydrophobic polymeric substrate, the lid rolls back and the active site becomes accessible, and thus, the enzyme gets in its active conformation.[43,44] Firstly, the inclusion of water into the polymer matrix occur *via* attack of the polar groups, followed by bond scission catalyzed by the enzyme. Thus, the bulk degradation takes place by the uptake of water, followed by surface erosion at the interfacial region between the polymeric surfaces and the aqueous media. The increase in the *f*-MWCNT content in the HBPEA matrix directly correlates with the increase in the degradability of the fabricated films.

Table 2 Deconvolution of the ester and amide band of HBPEA and HBPEAM5

	I_{ester}/I_{amide}			
Sample	1st week	2nd week	3rd week	4th week
HBPEA	1.12	1.05	0.92	0.89
HBPEAM5	1.11	0.89	0.75	0.61

The FTIR spectroscopic analysis of the ester to amide ratio (I_{ester}/I_{amide}) of the nanocomposite films before and after biodegradation provided a mechanistic understanding of its enzymatic degradation. The scission kinetics of the ester bond of the biodegraded films was investigated from the FTIR spectrum. The pristine HBPEA exhibited an absorption peak at around 1730 cm^{-1}, corresponding to the C=O stretching. The integrated intensity of I_{ester}/I_{amide} was analyzed by fitting with a Lorentzian profile. The enzymatic hydrolysis of ester moieties of the pristine MWCNTs (Fig. 8b) and the HBPEA nanocomposites (Fig. 8c) by lipase is evident from the decrement in integrated intensity of I_{ester}/I_{amide} (Table 2) for the biodegraded films.

The degradation by a surface erosion mechanism, characterized by the loss of material from the surface, is evident from the mass loss profile of the films (Fig. 8d). With the increase in *f*-MWCNT content, a considerable decrement in the mass of the films (17.09, 25.04, 31.16 and 38.19% mass loss for HBPEAM1, HBPEAM2.5 and HBPEAM5, respectively) was observed. Thus, the hydrolysis of the ester bonds in HBPEA and its nanocomposites has been postulated as the mechanism of its biodegradation.[15] Further, the observed dose-dependent biodegradation is attributed to the increasing *f*-MWCNT content. The increment of the degradation of the nanocomposites with the *f*-MWCNT content is attributed to the presence of polar moieties on the *f*-MWCNTs, such as epoxy, carbonyl and PAni nanofibers. These groups aided in the enhancement of the wettability and hydrolytic degradation of the nanocomposites by sorption and penetration of water into the polymer matrix. The penetrated water molecules promoted the accessibility of the polymer chains towards lipase, thereby enhancing chain scission, which hence resulted in good biodegradation.

However, upon degradation of the nanocomposites in due course of time, the *f*-MWCNTs may be released from the polymer matrix, although the rate of degradation slows down with time. The fate of the released MWCNTs in the body yields concern regarding their cytotoxicity. In such a situation, the nanotubes are catalytically biodegraded by the radical intermediates generated inside the biofluids in the body, such as myeloperoxidase and hypochlorite, resulting in the release of carbon dioxide without generating any inflammatory response.[45]

3.8 Antibacterial efficacy of the biodegraded nanocomposites

The long-term antibacterial potency of the biodegraded films was investigated by inoculating the biodegraded

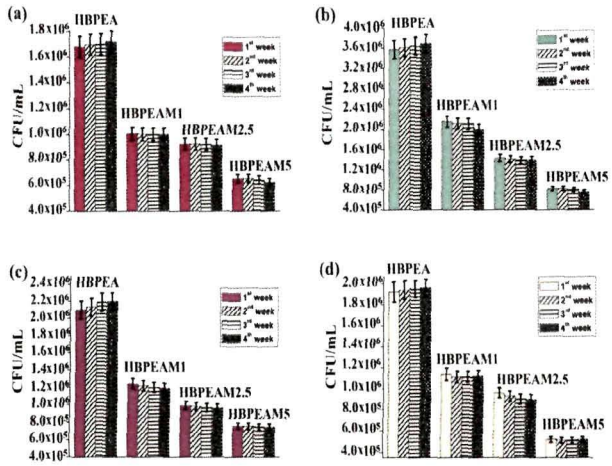

Fig. 9 Antimicrobial activity (CFU count) of HBPEA, HBPEAM1, HBPEAM2.5 and HBPEAM5 towards (a) *B. subtilis*, (b) *S. aureus*, (c) *M. smegmatis* mc^2 155, and (d) *M. smegmatis* ATCC14468.

nanocomposites with the tested bacterial strains and calculating the CFU count. It was clearly evident from Fig. 9 that there is a slight increment in the CFU count with time on HBPEA. The increase in the CFU count on the film is illustrative of the enhancement of the bacterial adhesion onto HBPEA with time. This may be attributed to the increase in oligomeric products with degradation time. These low-molecular-weight HBPEAs may increase the accessibility of the film towards bacteria by serving as the carbon source for their growth. However, the antibacterial activity of the degraded nanocomposites was fairly constant with degradation time. In other words, the inhibition of bacterial growth on the biodegraded nanocomposites was similar to that of the non-biodegraded ones (Fig. 9). This is attributed to the presence of *f*-MWCNTs – the prime factor for antibacterial activity in the degraded nanocomposites. Also the *in vitro* biodegradation study of the HBPEAM5 (the maximum biodegraded nanocomposite) showed that it required four weeks to degrade 38.19 wt% with a gradual decrease in the rate of degradation with exposure time. Moreover, the above degradation accounted for the polar moieties such as esters. The nanotubes remained intact for longer (more than four weeks). Thus, these results indicate that the nanocomposite retained the antibacterial efficacy for a longer time period.

4. Conclusions

The present study highlighted the fabrication of multifunctional bio-based HBPEA–*f*-MWCNT nanocomposites. The antibacterial nanocomposites triggered the release of a significant amount of cytoplasmic constituents of Gram positive bacteria and *M. smegmatis*. The mitochondrial enzyme activity assay established the biocompatibility of the nanocomposites with PBMC, further confirmed by the significant PBMC attachment and proliferation in response to a varied *f*-MWCNT content of the nanocomposites and exposure time. The time-course dependent biodegradation of the nanocomposites augmented in line with the increase in the *f*-MWCNT content. Thus, the study opens up the promising application of bio-based HBPEA–*f*-MWCNT nanocomposites as antibacterial dressing materials for infected burn wounds, where a decrease in the bacterial colonization onto the wound surface is favorable for the reduction in the infection rate of burn wounds. However, before the practical utilization of these microporous nanocomposites as wound dressing materials for burn infections, further *in vivo* studies need to be performed. The authors are happy to announce that the study of the prepared nanocomposites as prospective scaffold materials for facilitating the proliferation of epithelial cells, an integral part of the wound healing process, is in progress, and the preliminary results are very encouraging.

Acknowledgements

The authors express their gratitude and thanks to the research project assistant given by DRL, India, through the grant no. DRL/1047/TC, dated 2nd March, 2011, SAP (UGC), India, through the grant no. F.3-30/2009(SAP-II) and FIST program-2009 (DST), India, through the grant no. SR/FST/CSI-203/209/1 dated 06.05.2010. Mr Joston P. Nongkynrih and SAIF, NEHU, Shillong are gratefully acknowledged for TEM imaging. R. Konwarh acknowledges the receipt of his senior research fellowship from the Department of Biotechnology, Government of India. N. Barua thankfully acknowledges the receipt of a senior research fellowship from the CSIR, Government of India.

References

1 L. Broxmeyer, D. Sosnowska, E. Miltner, O. Chacon, D. Wagner, J. McGarvey, R. G. Barletta and L. E. Bermudez, *J. Infect. Dis.*, 2002, **186**, 1155–1160.
2 B. R. Copp and A. N. Pearce, *Nat. Prod. Rep.*, 2007, **24**, 278–297.
3 T. Dai, Y. Y. Huang, S. K. Sharma, J. T. Hashmi, B. D. Kurup and M. R. Hamblin, *Recent Pat. Anti-Infect. Drug Discovery*, 2010, **5**, 124–151.
4 J. P. Barret and D. N. Herndon, *Plast. Reconstr. Surg.*, 2003, **111**, 744–750.
5 S. Kang, M. Herzberg, D. F. Rodrigues and M. Elimelech, *Langmuir*, 2008, **24**, 6409–6413.
6 M. R. N. Gizdavic, J. R. Bennett, S. Swift, A. J. Easteal and M. Ambrose, *Acta Biomater.*, 2011, **7**, 4204–4209.
7 S. Pramanik, R. Konwarh, R. C. Deka, L. Aidew, N. Barua, A. K. Buragohain, D. Mohanta and N. Karak, *Carbon*, 2013, **55**, 34–43.
8 S. C. M. Fernandes, P. Sadocco, A. Alonso-Varona, T. Palomares, A. Eceiza, A. J. D. Silvestre, I. Mondragon and

C. S. R. Freire, *ACS Appl. Mater. Interfaces*, 2013, **5**, 3290–3297.
9 E. K. Yim, I. C. Liao and K. W. Leong, *Tissue Eng.*, 2007, **13**, 423–433.
10 R. Abe, S. C. Donnelly, T. Peng, R. Bucala and C. N. Metz, *J. Immunol.*, 2001, **166**, 7556–7562.
11 B. G. Sparkes, *Vaccine*, 1993, **11**, 504–510.
12 B. G. Sparkes, *Burns*, 1991, **17**, 128–135.
13 B. Das, P. Chattapadhyay, M. Mandal, B. Voit and N. Karak, *Macromol. Biosci.*, 2012, **1**, 126–139.
14 P. A. Gunatillake and R. Adhikari, *Eur. Cells Mater.*, 2003, **5**, 1–16.
15 S. Pramanik, R. Konwarh, K. Sagar, B. K. Konwar and N. Karak, *Prog. Org. Coat.*, 2013, **76**, 689–697.
16 M. Deng, J. Wu, C. A. Reinhart-King and C. C. Chu, *Biomacromolecules*, 2009, **10**, 3037–3047.
17 S. Pramanik, K. Sagar, B. K. Konwar and N. Karak, *Prog. Org. Coat.*, 2012, **75**, 569–578.
18 D. G. Nair, B. G. Fry, P. Alewood, P. P. Kumar and R. M. Kini, *Biochem. J.*, 2007, **402**, 93–104.
19 Oil and Colour Chemist's Association of Australia, *Surface Coatings*, Chapman & Hall, Methuen, New York, 1st edn, 1986, vol. **1**, p. 139.
20 M. A. Hamon, H. Hu, P. Bhowmik, S. Niyogi, B. Zhao, M. E. Itkis and R. C. Haddon, *Chem. Phys. Lett.*, 2001, **347**, 8–12.
21 F. H. Gojny, M. H. G. Wichmann, U. Kopke, B. Fiedler and K. Schulte, *Compos. Sci. Technol.*, 2004, **64**, 2363–2371.
22 R. Konwarh, S. Pramanik, D. Kalita, C. L. Mahanta and N. Karak, *Ultrason. Sonochem.*, 2012, **19**, 292–299.
23 J. Chang, G. Liang, A. Gu, S. Cai and L. Yuan, *Carbon*, 2012, **50**, 689–698.
24 H. Hu, Z. Zhao, Q. Zhou, Y. Gogotsi and J. Qiu, *Carbon*, 2012, **50**, 3267–3273.
25 S. Pramanik, J. Hazarika, A. Kumar and N. Karak, *Ind. Eng. Chem. Res.*, 2013, **52**, 5700–5707.
26 W. Yuan and M. B. Chan-Park, *ACS Appl. Mater. Interfaces*, 2012, **4**, 2065–2073.
27 R. Konwarh, B. Gogoi, R. Philip, M. A. Laskar and N. Karak, *Colloids Surf., B*, 2011, **84**, 338–345.
28 C. Sun, D. K. Hunt, R. B. Clark, D. Lofland, W. J. O. Brien, L. Plamondon and X. Y. Xiao, *J. Med. Chem.*, 2011, **54**, 3704–3731.
29 S. Liu, L. Wei, L. Hao, N. Fang, M. W. Chang, R. Xu, Y. Yang and Y. Chen, *ACS Nano*, 2009, **3**, 3891–3902.
30 S. Liu, L. Wei, L. Hao, N. Fang, M. W. Chang, R. Xu, Y. Yang and Y. Chen, *ACS Nano*, 2009, **3**, 3891–3902.
31 C. C. Miller, M. Rawat, T. Johnson and Y. A. Gay, *Antimicrob. Agents Chemother.*, 2007, **51**, 3364–3366.
32 X. Sun, L. Zhang, Z. Cao, Y. Deng, L. Liu, H. Fong and Y. Sun, *ACS Appl. Mater. Interfaces*, 2010, **2**, 952–956.
33 R. Rajaraman, R. A. Fox, V. G. Vethamany, L. A. Fernandez and J. M. Macsweene, *Exp. Cell Res.*, 1977, **107**, 179–190.
34 A. A. Shvedova, E. R. Kisin, D. Porter, P. Schulte, V. E. Kagan, B. Fadeel and V. Castranova, *Pharmacol. Ther.*, 2009, **121**, 192–204.
35 E. G. R. Fernandes, V. Zucolotto and A. A. A. D. Queiroz, *J. Macromol. Sci., Part A: Pure Appl. Chem.*, 2010, **47**, 1203–1207.
36 W. Lew, J. J. Oppenheim and K. Matsushima, *J. Immunol.*, 1988, **140**, 1895–1902.
37 S. Hofmanna, H. Hagenmüllera, A. M. Kocha, R. Müllerb, G. V. Novakovicc, D. L. Kaplane, H. P. Merklea and L. Meinel, *Biomaterials*, 2007, **28**, 1152–1162.
38 S. Huang and D. E. Ingber, *Exp. Cell Res.*, 2000, **261**, 91–103.
39 Z. Liu, X. Dong, L. Song, H. Zhang, L. Liu, D. Zhu, C. Song and X. Leng, *J. Biomed. Mater. Res., Part A*, 2013, DOI: 10.1002/jbm.a.34729.
40 N. R. Jacobsen, G. Pojana, P. White, P. Møller, C. A. Cohn, K. S. Korsholm, U. Vogel, A. Marcomini, S. Loft and H. Wallin, *Environ. Mol. Mutagen.*, 2008, **49**, 476–487.
41 I. F. F. Benzie and J. J. Strain, *Anal. Biochem.*, 1996, **239**, 70–76.
42 R. R. Mitry, R. D. Hughes, M. M. Aw, C. Terry, G. Mieli-Vergani, R. Girlanda, P. Muiesan, M. Rela, N. D. Heaton and A. Dhawan, *Cell Transplant.*, 2003, **12**, 69–74.
43 A. M. Brzozowski, U. Derewenda, Z. S. Derewenda, G. G. Dodson, D. M. Lawson, J. P. Turkenburg, F. Bjorkling, B. H. Jensen, S. A. Patkar and L. Thim, *Nature*, 1991, **351**, 491–494.
44 N. K. Singh, B. D. Purkayastha, J. K. Roy, R. M. Banik, M. Yashpal, G. Singh, S. Malik and P. Maiti, *ACS Appl. Mater. Interfaces*, 2010, **2**, 69–81.
45 V. E. Kagan, N. V. Konduru, W. Feng, B. t. Allen, J. Conroy, Y. Volkov, I. I. Vlasova, N. A. Belikova, N. Yanamala, A. Kapralov, Y. Y. Tyurina, J. Shi, E. R. Kisin, A. R. Murray, J. Franks, D. Stolz, P. Gou, j. K. Seetharaman, B. Fadeel, A. Star and A. A. Shvedova, *Nat. Nanotechnol.*, 2010, **5**, 354–359.